

Gas Permeability of Bentonite
Samples of the FEBEX
Dismantling Project
(FEBEX-DP)

M^a. V. Villar
B. Carbonell
P. L. Martín
C. Gutiérrez-Álvarez
J. M. Barcala



Gas Permeability of Bentonite Samples
of the FEBEX Dismantling Project
(FEBEX-DP)

M^a. V. Villar
B. Carbonell
P. L. Martín
C. Gutiérrez-Álvarez
J. M. Barcala

Toda correspondencia en relación con este trabajo debe dirigirse al Servicio de Información y Documentación, Centro de Investigaciones Energéticas, Medioambientales y Tecnológicas, Ciudad Universitaria, 28040-MADRID, ESPAÑA.

Las solicitudes de ejemplares deben dirigirse a este mismo Servicio.

Los descriptores se han seleccionado del Thesaurus del DOE para describir las materias que contiene este informe con vistas a su recuperación. La catalogación se ha hecho utilizando el documento DOE/TIC-4602 (Rev. 1) Descriptive Cataloguing On-Line, y la clasificación de acuerdo con el documento DOE/TIC.4584-R7 Subject Categories and Scope publicados por el Office of Scientific and Technical Information del Departamento de Energía de los Estados Unidos.

Se autoriza la reproducción de los resúmenes analíticos que aparecen en esta publicación.

Catálogo general de publicaciones oficiales

<http://www.060.es>

Depósito Legal: M-26385-2011

ISSN: 1135-9420

NIPO: 058-18-011-1

“Publicación incluida en el programa editorial del suprimido Ministerio de Economía, Industria y Competitividad, y editada por el Ministerio de Ciencia, Innovación y Universidades, (de acuerdo con la reestructuración ministerial establecida por Real Decreto 355/2018, de 6 de junio)”.

Editorial CIEMAT

CLASIFICACIÓN DOE Y DESCRIPTORES

S58

GASES; PERMEABILITY; POROSITY; BENTONITE; CLAYS; SAMPLING;
PRESSURE CONTROL

Gas Permeability of Bentonite Samples of the FEBEX Dismantling Project (FEBEX-DP)

Villar, M^a. V.; Carbonell, B.; Martín, P. L.; Gutiérrez-Álvarez, C.; Barcala, M.
140 pp. 32 refs. 182 figs. 23 tablas

Abstract:

The FEBEX in situ test simulated the engineered barrier of a nuclear waste repository and was in operation for 18 years under natural conditions. The barrier was composed of blocks of compacted FEBEX bentonite and a heater simulated the waste container. The gas permeability of bentonite samples taken at different positions around the heater during the final dismantling of the experiment was measured. These samples had initial dry density between 1.51 and 1.64 g/cm³ and water contents between 19.5 and 29.0%. Some of these samples were drilled between two blocks, therefore they had an interface along. The aim of the tests was to check: 1) the influence on gas permeability of the physical state of the samples (water content, dry density), 2) the effect of injection and confining pressures on gas permeability, 3) the change of gas transport properties with respect to the untreated, reference FEBEX bentonite and 4) the role of interfaces on gas transport.

The gas permeability of the samples depended on water content and dry density, decreasing with the increase of both. These two variables changed across the barrier as a function of the distance to the heat and water sources, i.e. the heater and the granite. Thus, the gas permeability of the samples was also related to their position in the barrier, tending to be lower towards the granite, where the degree of saturation was higher. The gas permeability decreased with the accessible void ratio according to a power law, in the same way as expected for the FEBEX reference bentonite. Therefore, it seems that no changes on the gas transport properties of the bentonite took place during operation.

Samples with an interface drilled in the internal ring of the barrier had higher permeability than samples of similar accessible void ratio with no interface, and it was necessary to apply higher confining pressures to reduce or suppress gas flow in them. In contrast, wetter samples drilled along interfaces of the intermediate and external rings of the barrier (which had very low accessible void ratio, due to saturation), had permeabilities closer to that corresponding to the same accessible void ratio in the reference bentonite.

Permeabilidad al Gas de Muestras Procedentes del Desmantelamiento del Proyecto FEBEX (FEBEX-DP)

Villar, M^a. V.; Carbonell, B.; Martín, P. L.; Gutiérrez-Álvarez, C.; Barcala, M.
140 pp. 32 refs. 182 figs. 23 tablas

Resumen:

El ensayo in situ FEBEX estuvo en operación durante 18 años simulando a escala real la barrera de ingeniería en un almacenamiento de residuos radiactivos de alta actividad. La barrera estaba constituida por bloques de bentonita FEBEX compactada y un calentador simulaba el contenedor. Se ha medido la permeabilidad al gas de muestras de bentonita tomadas en diferentes puntos de la barrera durante el desmantelamiento final del ensayo. Las muestras tenían humedades entre 19,5 y 29,0%, densidades secas entre 1,51 y 1,64 g/cm³. Algunas muestras se obtuvieron perforando entre dos bloques adyacentes, por los que estaban atravesadas por una interfase. El objetivo de los ensayos ha sido comprobar: 1) la influencia del estado físico de la bentonita (densidad, humedad) en la permeabilidad al gas, 2) el efecto de las presiones de inyección y confinante en la permeabilidad al gas, 3) el posible cambio en las propiedades de transporte de gas con respecto a la bentonita FEBEX no tratada, y 4) el papel de las interfaces en el transporte de gas.

La permeabilidad al gas depende de la humedad y densidad seca de las muestras, disminuyendo con el aumento de ambas. Como estas dos variables mostraban cambios espaciales significativos en la barrera, la permeabilidad al gas mostró una clara dependencia de la posición de la barrera en la que la muestra se tomó, tendiendo a ser menor hacia la parte externa de la barrera, en la proximidad al granito, donde el grado de saturación era mayor. La permeabilidad al gas mostró una disminución con el índice de poros accesible de acuerdo a una ley potencial de la misma manera esperable para la bentonita FEBEX no tratada. Por tanto, parece que las condiciones de operación en la barrera mantenidas durante 18 años no afectaron la capacidad de transporte de gas de la bentonita.

Las muestras con interfase obtenidas cerca del calentador, donde la bentonita estaba más seca, mostraron permeabilidades más altas que muestras con el mismo índice de poros accesible pero sin interfase. Para reducir o suprimir el flujo de gas en muestras con interfase fue necesario aplicar mayores presiones confinantes. Por el contrario, las muestras con interfase tomadas en zonas más húmedas de la barrera mostraron el mismo comportamiento que muestras sin interfase equivalentes.



Technical report CIEMAT/DMA/2G218/3/18

GAS PERMEABILITY OF BENTONITE SAMPLES OF THE FEBEX DISMANTLING PROJECT (FEBEX-DP)

AUTHORS: María Victoria Villar, Beatriz Carbonell, Pedro Luis Martín, Carlos Gutiérrez-Álvarez, José Miguel Barcala

May 2018

GAS PERMEABILITY OF FEBEX-DP BENTONITE SAMPLES

1	INTRODUCTION	3
2	MATERIAL: THE FEBEX BENTONITE	8
3	METHODOLOGY.....	9
3.1	Sample preparation	10
3.2	Low-pressure equipment (LP).....	13
3.3	High-pressure equipment (HP)	14
3.3.1	High-pressure, unsteady-state (HP-US).....	14
3.3.2	High-pressure, steady-state (HP-S).....	16
3.4	Postmortem analyses.....	18
4	RESULTS.....	19
4.1	Gas permeability tests	21
4.1.1	Sample BC-36-1	22
4.1.2	Sample BC-44-1	23
4.1.3	Sample BC-44-2	25
4.1.4	Sample BC-44-3	27
4.1.5	Sample BC-44-4	29
4.1.6	Sample BC-44-5	30
4.1.7	Sample BC-44-6	31
4.1.8	Sample BC-44-7	33
4.1.9	Sample BC-47-1	35
4.1.10	Sample BC-47-2	36
4.1.11	Sample BC-47-3	38
4.1.12	Sample BC-47-4	39
4.1.13	Sample BC-47-6	42
4.1.14	Sample BB-53-4-2.....	44
4.1.15	Sample BB-53-5-1.....	44
4.1.16	Sample BB-53-5-2.....	45
4.1.17	Sample BC-53-1	46
4.1.18	Sample BC-53-2	47
4.1.19	Sample BC-53-3	50
4.1.20	Sample BC-53-4	52
4.1.21	Sample BC-53-5	54
4.1.22	Sample BC-53-6	56

4.2	Pore size distribution	58
5	DISCUSSION	62
5.1	Summary of gas permeability results.....	62
5.1.1	Low pressure setup.....	66
5.1.2	Effect of injection pressure.....	68
5.1.3	Effect of confining pressure on gas permeability	71
5.1.4	Effect of unloading on gas permeability	73
5.1.5	Effect of accessible void ratio and degree of saturation	75
5.1.6	Changes of gas permeability across the barrier	77
5.2	Changes in pore size distribution.....	78
5.3	Analysis of the Klinkenberg effect on gas permeability.....	80
5.4	Comparison with the reference bentonite	84
6	SUMMARY AND CONCLUSIONS.....	86
7	REFERENCES	88

ANNEX I: DETAILED CHARACTERISTICS OF THE TESTS

GAS PERMEABILITY OF FEBEX-DP BENTONITE SAMPLES

1 INTRODUCTION

The aim of FEBEX (Full-scale Engineered Barriers Experiment) was to study the behaviour of components in the near-field for a high-level radioactive waste (HLW) repository in crystalline rock. The project was based on the Spanish reference concept for disposal of radioactive waste in crystalline rock (AGP Granito): the waste canisters are placed horizontally in drifts and surrounded by a clay barrier constructed from highly-compacted bentonite blocks (ENRESA 1995). As part of this project, an “in situ” test, under natural conditions and at full scale, was performed at the Grimsel Test Site (GTS, Switzerland), an underground laboratory managed by NAGRA (ENRESA 2000, 2006). The thermal effect of the wastes was simulated by means of heaters, whereas hydration was natural.

The basic components of the test were: the gallery, measuring 70 m in length and 2.3 m in diameter, excavated through the Aare granite; the heating system, made up of two heaters placed inside a liner installed concentrically with the gallery and separated one from the other by a distance of 1.0 m, with dimensions and weights analogous to those of the real canisters; the clay barrier, formed by blocks of compacted bentonite; the instrumentation and the monitoring and control system for data acquisition and supervision and control of the test both autonomously and remotely from Madrid. Up to 632 sensors of very diverse types were initially installed to monitor the different thermo-hydro-mechanical processes that occurred in both the clay barrier and the surrounding rock throughout the entire life of the test. The gallery was closed by a concrete plug.

The clay barrier was made of FEBEX bentonite, which was extracted from the Cortijo de Archidona deposit (Almería, Spain). To build the clay barrier, blocks were manufactured from the bentonite in the shape of 12-cm thick circular crown sectors. The blocks were arranged in vertical slices consisting of concentric rings. The thickness of the bentonite barrier in the heater areas was 65 cm (distance from liner to granite). The blocks were obtained by uniaxial compaction of the FEBEX clay with its hygroscopic water content at pressures of between 40 and 45 MPa, what caused dry densities of 1.69-1.70 g/cm³. The initial dry density of the blocks was selected by taking into account the probable volume of the construction gaps and the need to have a barrier with an average dry density of 1.60 g/cm³ (ENRESA, 2000).

The heating stage of the in situ test began on February 27th 1997. The power of the heaters was adjusted so that to keep the temperatures at the liner surface at 100°C. After five years of uninterrupted heating at constant temperature, the heater closer to the gallery entrance (Heater #1) was switched off (February 2002). In the following months this heater and all the bentonite and instruments preceding and surrounding it were extracted (Bárcena et al., 2003). A large number of bentonite samples were also taken for analysis in different laboratories (Villar et al. 2006). The remaining part of the experiment was sealed with a new sprayed shotcrete plug. New sensors were installed in the buffer through the shotcrete plug, and a second operational phase started with the test configuration shown in Fig. 1. It shows how the buffer and all components were removed up to a distance of 2 metres from Heater #2 to minimize disturbance of the non-dismantled area. A dummy steel cylinder with a length of 1 m was inserted in the void left by Heater #1 in the centre of the buffer.

The test continued running until April 2015, when Heater #2 was switched off and the dismantling operations started. Many sensors were in operation until the end of the experiment, which allowed to follow the evolution of some thermo-hydro-mechanical variables during the second operational phase (Martínez et al. 2016). The dismantling operations, carried out in the context of the FEBEX Dismantling Project (FEBEX-DP), included the demolition of the shotcrete plug and the removal of all the bentonite in front of, surrounding the heater and at the back of it.

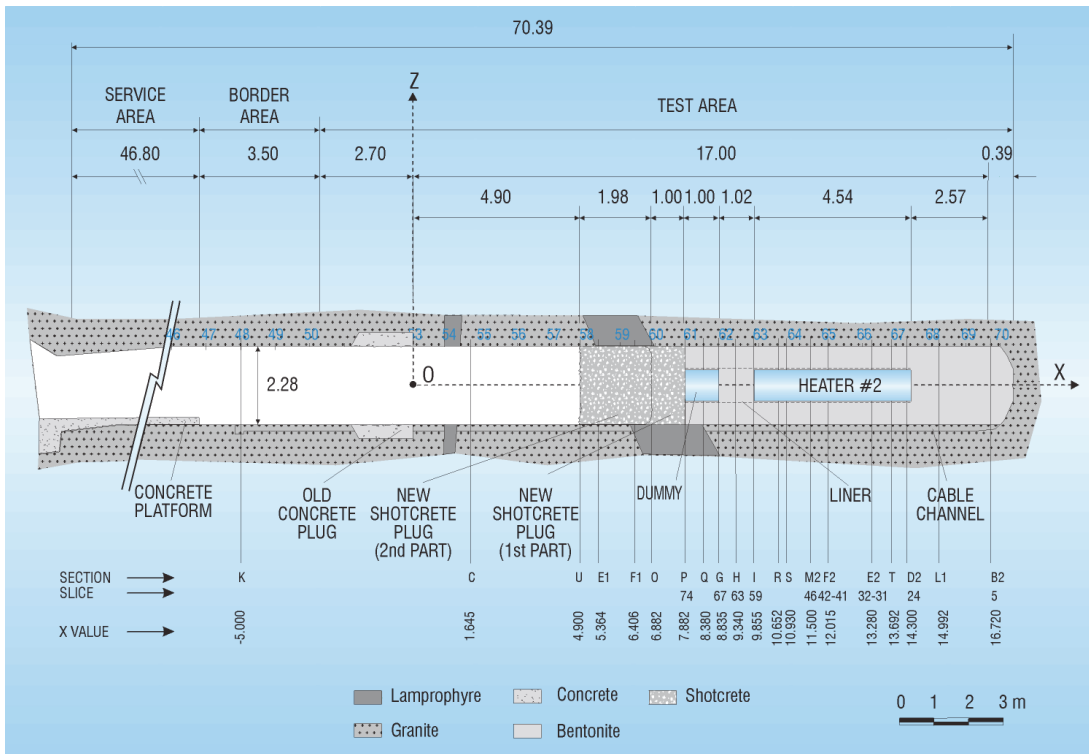


Fig. 1: General layout of the in situ test during Phase II, including instrumented sections (ENRESA 2006)

Upon exposure, the bentonite sections presented a consistent appearance; although the joints between blocks were in most cases visible, all the construction gaps were sealed, even the big apertures hewn in the bentonite for the passing of the cable bunches (Fig. 2). Differences in coloration of the bentonite related to the variations of its water content were observed, the outer rings of the barrier showing darker colours.



Fig. 2: Appearance of the bentonite barrier around Heater #2 during installation in 1997 and during dismantling in 2015

A large number of samples from all types of materials were taken during dismantling. In particular, clay samples were taken to characterise the solid and liquid phases, in order to confirm predictions and validate existing models of thermo-hydro-mechanical and geochemical (THM and THG) processes. The location of the bentonite sampling points was fixed to allow a good representation of physico-chemical

alterations and hydration distribution. The sampling took place in vertical sections normal to the axis of the tunnel, and in each section several samples were taken along different radii. In particular, the bentonite samples sent to CIEMAT were taken from the vertical sections detailed in Fig. 3. The samples were preserved in plastic film, two layers of aluminised PET-sheets and vacuum-sealed plastic bags immediately after their extraction. The PET-sheets were vacuum-sealed. Protection against mechanical actions was used to ensure the integrity of the material. The samples were referred to according to the key given in the Sampling Book (Bárcena & García-Siñeriz 2015).

Samples were also taken to determine on site the water content and dry density of the bentonite. The on-site determinations performed during dismantling showed that the physical conditions of the bentonite along the barrier had changed during operation, as a result of hydration and of the different temperatures to which the bentonite had been subjected. Water content and dry density gradients, both across the vertical sections and along the gallery, had been generated (Villar et al. 2016). Fig. 4 to Fig. 6 show the final distribution of dry density, water content and degree of saturation along the barrier obtained from the on-site determinations. It is clear that the initial conditions of the samples received by the different laboratories depended on the exact location along the barrier of the sampling section from which they were taken, as well as on the position of a particular sample with respect to the axis of the gallery. The main differences occurred between sections located around the heater (sections 42 to 53) or in cool areas.

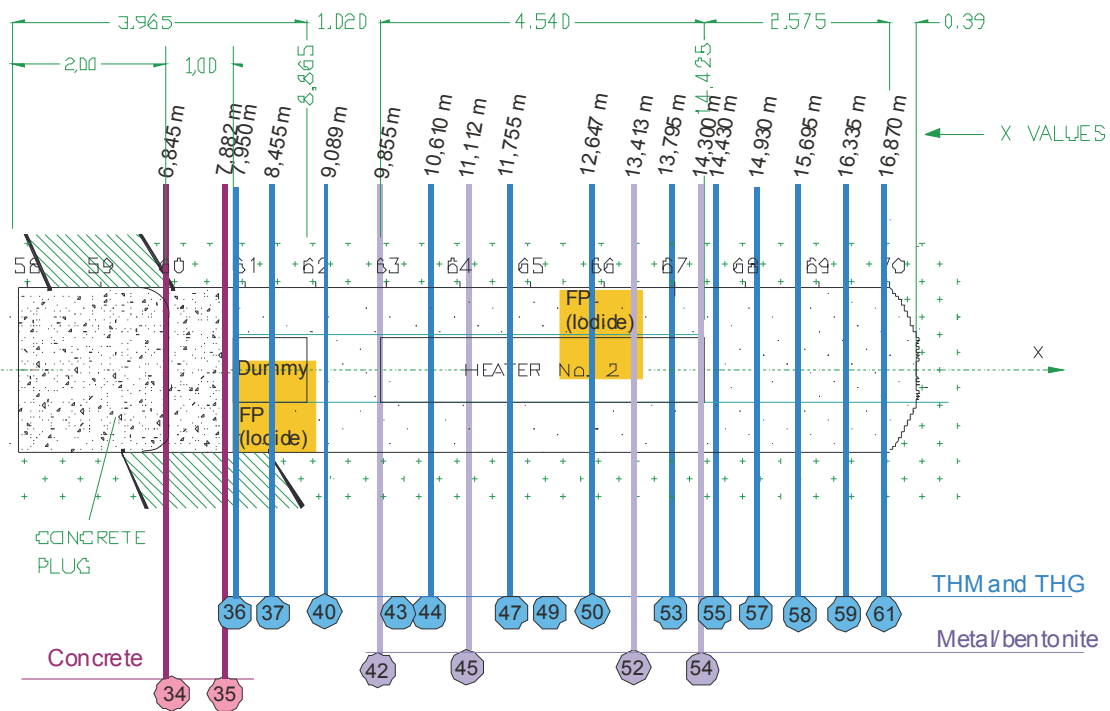


Fig. 3: Distribution of sampling sections for THM-THG and interfaces studies of CIEMAT (modified from AITEMIN 2015)

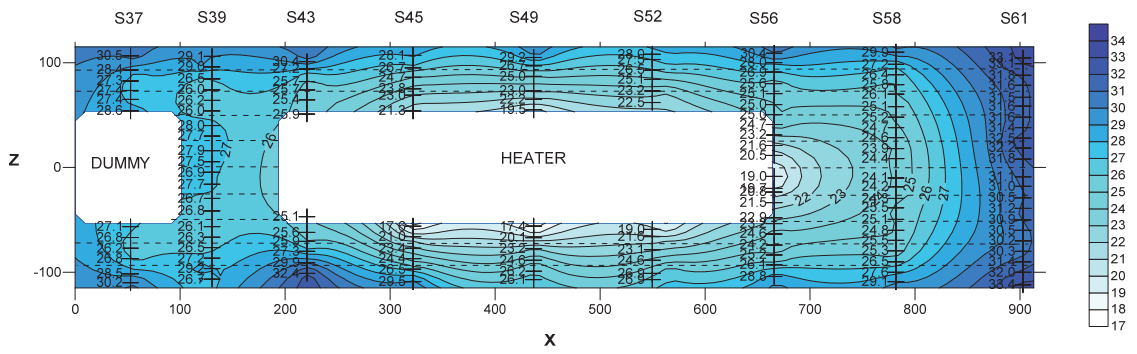


Fig. 4: Water content distribution in a vertical longitudinal section (Villar et al. 2016)

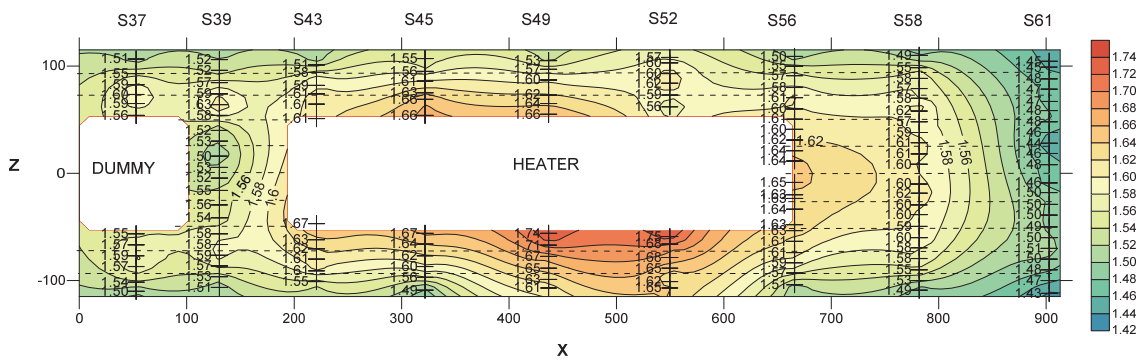


Fig. 5: Dry density distribution in a vertical longitudinal section (Villar et al. 2016)

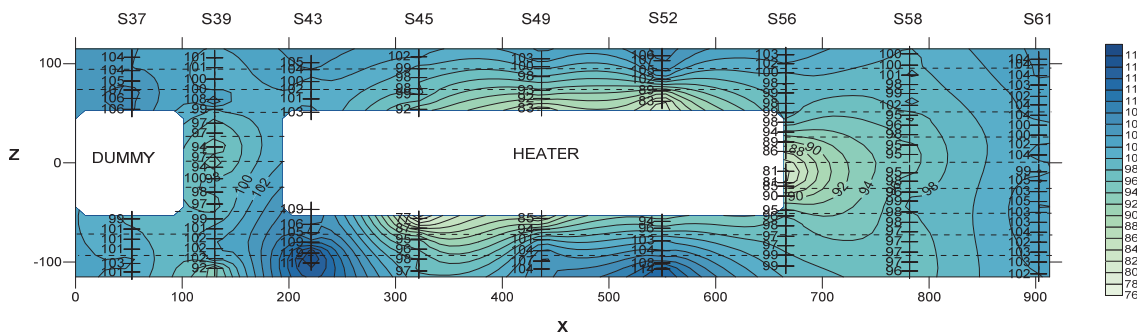


Fig. 6: Degree of saturation distribution in a vertical longitudinal section (Villar et al. 2016) (inexact values because of solid specific weight and water density uncertainties)

The present report details the experimental laboratory investigation on the gas transport properties of bentonite samples taken during dismantling, which was summarised in Villar et al. (2018), where the whole THM characterisation of the samples is reported. The mineralogical and geochemical characterisation of the same samples is given in (Fernández et al. 2018). Many of these results were also summarised and included in the synthesis report collecting results of the bentonite characterisation obtained by all the FEBEX-DP project partners (Villar 2018). The aim of the investigation described in this report was to assess the potential changes of the gas transport properties of the FEBEX bentonite as a consequence of the 18-year testing under barrier conditions.

Tab. 1 shows the sampling section and the radius (according to Fig. 7) from which the core samples sent to CIEMAT for the gas permeability tests were approximately taken. The radii have been named according to the same key used for the on-site determinations (Villar et al. 2016a). The date of the core retrieval at Grimsel (Retrieval GTS), of its arrival at CIEMAT (Arrival CIEMAT) and of its sampling at CIEMAT's laboratories (Sampling CIEMAT) are indicated, along with the time elapsed from the day they were taken until they were sampled in the laboratory. The time elapsed between retrieval and testing in the laboratory was very long, because the experimental setup for the gas permeability tests had to be

fine-tuned. Most of the samples were received on August 7th and 21st. The Table also shows if the samples were still vacuum sealed when they were sampled at CIEMAT or not. Note that not all of them have been tested.

Tab. 1: Summary of cores sent to CIEMAT for gas permeability determinations

Section	Radius	Sample reference	Retrieval GTS	Arrival CIEMAT	Sampling CIEMAT	Time elapsed (days)	Vacuum
S36	E-F	BC-36-1	8/5/15	27/5/15	28/5/15	20	yes
S36	E-F	BC-36-2	8/5/15	27/5/15			
S36	E-F	BC-36-3	8/5/15	27/5/15			
S44	A-B	BC-44-1	16/6/15	7/8/15	20/9/16	462	yes
S44	D-E	BC-44-2	18/6/15	7/8/15	17/8/16	426	yes
S44	E-F	BC-44-3	17/6/15	7/8/15	6/3/17	627	yes
S44	E-F	BC-44-4	17/6/15	7/8/15	3/10/16	473	yes
S44	F	BC-44-5	16/6/15	7/8/15	4/10/16	475	yes
S44	F	BC-44-6	16/6/15	7/8/15	8/11/16	510	yes
S44	E	BC-44-7	18/6/15	7/8/15	18/8/16	427	yes
S47	A	BC-47-1	26/6/15	7/8/15	18/7/16	388	yes
S47	A	BC-47-2	26/6/15	7/8/15	10/12/15	167	yes
S47	A	BC-47-3	26/6/15	7/8/15	14/6/16	354	yes
S47	A	BC-47-4	26/6/15	7/8/15	18/11/15	145	yes
S47	F-A	BC-47-5	26/6/15	7/8/15	7/6/16	347	yes
S47	F	BC-47-6	26/6/15	7/8/15	20/7/16	390	yes
S50	B	BC-50-1	7/7/15	21/8/15			
S50	B	BC-50-2	8/7/15	21/8/15			
S50	C-D	BC-50-3	8/7/15	21/8/15			
S50	C-D	BC-50-4	8/7/15	21/8/15			
S50	E-F	BC-50-5	8/7/15	21/8/15			
S50	F	BC-50-6	7/7/15	21/8/15			
S53	A-B	BC-53-1	14/7/15	21/8/15	20/6/17	706	Yes
S53	B	BC-53-2	15/7/15	21/8/15	16/10/17	854	yes
S53	CD	BC-53-3	15/7/15	21/8/15	16/3/17	609	yes
S53	CD	BC-53-4	15/7/15	21/8/15	19/4/17	643	yes
S53	E-F	BC-53-5	15/7/15	21/8/15	8/5/17	692	yes
S53	F	BC-53-6	14/7/15	21/8/15	30/5/17	714	yes
S57	B	BC-57-1	22/7/15	21/8/15			
S57	B	BC-57-2	22/7/15	21/8/15			
S57	C-D	BC-57-3	22/7/15	21/8/15			
S57	C-D	BC-57-4	22/7/15	21/8/15			
S57	E-F	BC-57-5	22/7/15	21/8/15			
S57	E-F	BC-57-6	22/7/15	21/8/15			
S59	B	BC-59-1	28/7/15	21/8/15			
S59	B	BC-59-2	28/7/15	21/8/15			
S59	C-D	BC-59-3	28/7/15	21/8/15			
S59	C-D	BC-59-4	28/7/15	21/8/15			
S59	E-F	BC-59-5	28/7/15	21/8/15			
S59	E-F	BC-59-6	28/7/15	21/8/15			

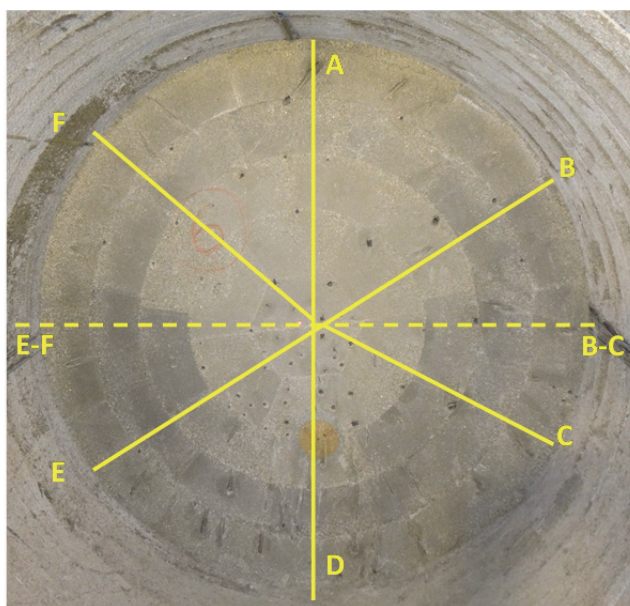


Fig. 7: References for the radii along which the bentonite cores were taken

2 MATERIAL: THE FEBEX BENTONITE

The material used to construct the clay buffer of the FEBEX in situ test was the FEBEX bentonite, extracted from the Cortijo de Archidona deposit (Almería, Spain). At the factory, the clay was disaggregated and gently dried to a water content of around 14%, all the material of particle size greater than 5 mm being rejected. The processed material was used for fabrication of the blocks for the large-scale test and for the laboratory tests performed for the characterization of the clay. The physico-chemical properties of the FEBEX bentonite, as well as its most relevant thermo-hydro-mechanical and geochemical characteristics obtained during the projects FEBEX I and II were summarised in the final reports of the project (ENRESA 2000, 2006) and later documents (Villar & Gómez-Espina 2009).

The montmorillonite content of the FEBEX bentonite is above 90 wt.%. The smectitic phases are actually made up of a smectite-illite mixed layer, with 10-15 wt.% of illite layers. Besides, the bentonite contains variable quantities of quartz, plagioclase, K-felspar, calcite, and cristobalite-trydimite. The cation exchange capacity of the smectite is 102 ± 4 meq/100g, the main exchangeable cations being calcium (35 ± 2 meq/100g), magnesium (31 ± 3 meq/100g) and sodium (27 ± 1 meq/100g). The predominant soluble ions are chloride, sulphate, bicarbonate and sodium.

The liquid limit of the bentonite is 102 ± 4 %, the plastic limit 53 ± 3 %, the density of the solid particles 2.70 ± 0.04 g/cm³, and 67 ± 3 % of particles are smaller than 2 µm. The hygroscopic water content in equilibrium with the laboratory atmosphere (relative humidity 50 ± 10 %, temperature 21 ± 3 °C) is 13.7 ± 1.3 %. The external specific surface area is 32 ± 3 m²/g and the total specific surface area is about 725 ± 47 m²/g.

The saturated hydraulic conductivity of compacted samples of the FEBEX reference bentonite is exponentially related to their dry density. The empirical relationship between intrinsic permeability (k_{iw} , m/s) and dry density (ρ_d , g/cm³) shown in Eq. 1 was obtained for samples compacted to dry densities above 1.47 g/cm³ and permeated with deionised water at room temperature. According to this relationship, for a dry density of 1.6 g/cm³ the intrinsic permeability of the bentonite is about $5 \cdot 10^{-21}$ m².

$$\log k_{iw} = -2.96 \rho_d - 15.57 \quad [1]$$

The swelling pressure (P_s , MPa) of compacted samples is also exponentially related to the bentonite dry density (ρ_d , g/cm³), according to the empirical expression in Eq. 2, which indicates that when the

bentonite at dry density of 1.6 g/cm^3 is saturated under constant volume with deionised water at room temperature, the swelling pressure has a value of about 6 MPa:

$$\ln P_s = 6.77 \rho_d - 9.07 \quad [2]$$

3 METHODOLOGY

The gas permeability of samples from sections S36, S44, S47 and S53 (Fig. 3) in their “as received” state was measured in the laboratory. These samples had a range of degrees of saturation from 79 to 100%, hence some of them were close to saturation (Tab. 5).

Two different experimental setups were used, a low-pressure and a high-pressure one. The aim of the tests performed in the low-pressure equipment was to determine the influence of water content and degree of saturation on gas permeability, whereas the aim of the tests performed in the high-pressure permeameter was to analyse the effect of boundary conditions, such as gas pressure and confining pressure, on gas permeability. Since most of the samples were close to saturation, it was expected that the permeabilities would be very low or even zero. In those cases, the aim of the tests was to determine the gas breakthrough pressures, which indeed could only be done with the high-pressure equipment.

When there are two fluids present in a porous material (gas and water in this case), the permeability of each fluid depends upon the saturation of the material in each fluid: these are called apparent (or effective) permeabilities. Hence, the value obtained in the determinations (apart from the gas permeability, k_g) is the intrinsic permeability measured with gas flow, k_{ig} , multiplied by the relative permeability to gas, k_{rg} . In turn, the relative permeability to gas is the ratio of the apparent (effective) permeability of gas at a particular saturation to the absolute permeability of gas at total gas saturation, *i.e.* in completely dry material, where the k_{rg} value would be 1.

Most samples were initially tested in the low-pressure equipment (described in 3.2) and afterwards in the high-pressure equipment (described in 3.3). The first one worked as an unsteady-state (falling-head) permeameter in which only pressure was measured (LP). The second one was used under two different configurations: as an unsteady-state (constant-head) permeameter, in which only pressures were measured (HP-US), and as a steady-state permeameter (HP-S) in which pressure and gas flow were measured. The second configuration consisted of two lines, a low confining pressure one (LCP) and a high confining pressure one (HCP). Tab. 2 shows the experimental setups used and their characteristics, which are described in more detail below.

Tab. 2: Characteristics of the experimental setups used for the gas permeability tests

Equipment	Working principle	Variables measured	Range confining P (MPa)	Range injection P (MPa - a)	
LP	Unsteady-state permeameter	Pressure	0.6-1.0	<0.2	
HP-US	Unsteady-state permeameter	Pressure	1.0-14.0	0.2-13.0	
HP-S	LCP	Steady-state permeameter	Pressure, gas flow	0.6-9.0	0.1-1.4
	HCP	Steady-state permeameter	Pressure, gas flow	0.6-2.0	0.1-0.6

The permeability coefficient thus measured represents the sum of the permeability coefficient of the material and any additional contribution (cracks or incomplete sealing between sample and body cell). So the measured value could be higher than the permeability coefficient of the material and, therefore, the best value of the permeability coefficient of the material would be the lowest value obtained in a series of tests.

3.1 Sample preparation

Two kinds of samples were used: core samples drilled on site and core samples drilled from blocks in the laboratory. Most of the samples tested were drilled on site in the same sections where the blocks for THM and THG characterisation were taken (Fig. 3). Half of them were drilled in the middle of blocks and the other half at the contact between two blocks, so that to have an interface along the core (Fig. 8, left). The other group of samples, only three of them, was drilled in the laboratory from blocks received for the THM and THG determinations (Fig. 8, right). Tab. 3 shows the location and characteristics of the samples tested.



Fig. 8: Sample drilled on site at the contact between blocks (left) and in the laboratory (right)

Tab. 3: Location of core samples tested for gas permeability

Section	Sample reference	Drilling	Location
S36	BC-36-1	On-site	Internal ring
S44	BC-44-1	On-site	External ring
	BC-44-2	On-site	Internal ring with interface
	BC-44-3	On-site	Internal ring with interface
	BC-44-7	On-site	Internal ring
S47	BC-47-1	On-site	External ring
	BC-47-2	On-site	External ring
	BC-47-3	On-site	Intermediate ring with interface
	BC-47-4	On-site	Intermediate ring
	BC-47-5	On-site	Internal ring
	BC-47-6	On-site	Internal ring with interface
S53	BB-53-4-2	Laboratory	External ring
	BB-53-5-1	Laboratory	Intermediate ring
	BB-53-5-2	Laboratory	Intermediate ring
	BC-53-1	On-site	Internal ring
	BC-53-2	On-site	Internal ring
	BC-53-3	On-site	External ring
	BC-53-4	On-site	External ring with interface
	BC-53-5	On-site	Intermediate ring with interface
BC-53-6	On-site	Intermediate ring	

To prepare the samples the core diameter was fit to that of the testing cells (36 or 50 mm) by using a cutting ring and a knife (Fig. 9) and sand paper in some cases. The cylindrical surface of the samples was smoothed and the parallelism of the cylinder's ends was ensured. The resulting specimens were between 2.4 and 5 cm in height and 10-20 cm² in surface area. In some cases the interface along the core became evident only after preparing the specimen (Fig. 10). In order to determine the initial water content and dry density of the samples (and in some cases the pore size distribution), a spare fragment resulting from the sample preparation was used.



Fig. 9: Sample preparation: adjusting the diameter



Fig. 10: Appearance of a specimen prepared for gas test with interface between blocks

Filter paper and porous stones were placed on top and bottom of the samples. Perforated PVC discs were used in some cases to adapt the specimen height to the cell dimensions. The assemblage thus prepared was laterally wrapped in different ways (Fig. 11). Some samples were laterally wrapped in double latex membranes or in EPDM (ethylene propylene diene monomer) rubber over a latex membrane. Other samples were wrapped in duct tape and finally in an EPDM rubber membrane. Vacuum grease was applied between membranes in order to prevent the loss of gas.



Fig. 11: Specimen placed between porous stones and perforated PVC discs (left), wrapped in double latex (middle) and latex + EPDM (right)

The assemblages shown in Fig. 11 were placed in triaxial cells. Two kinds of cells were used: with methacrylate or stainless steel walls, able of withstanding pressures of up to 3 or 21 MPa, respectively (Fig. 12). The cells had three inlets: for the sample drainage/backpressure, for the sample injection pressure, and for the confining pressure.



Fig. 12: Methacrylate triaxial cell (left) and stainless steel high pressure cell (right)

At the end of the tests, the bentonite specimens were measured and weighed and the water content and dry density at three different levels (two, if they were too short) along the cylindrical specimens were determined. To determine the dry mass of the samples they were oven-dried at 110°C for 48 h, and to compute the dry density, the volume of the same specimens was determined by immersing them in mercury prior to drying.

3.2 Low-pressure equipment (LP)

Once the triaxial cell was filled with water, a pressure high enough to ensure perfect adherence of the membranes to the surface of the sample was applied to the chamber of the triaxial cell. The inlet at the lower part of the sample was connected to an airtight tank of known volume, in which nitrogen gas was injected at a pressure slightly higher than atmospheric. The tank was instrumented with a pressure sensor connected to a data acquisition system which recorded the pressure of the fluid contained inside. The inlet at the upper part of the sample was left open to the atmosphere. The test consisted in allowing the air in the tank to go out to the atmosphere through the specimen, while the decrease in pressure in the tank was measured as a function of time. The tests were performed at constant, room temperature. Prior to every new permeability test, the airtightness of the system was checked. The cartoon of the assembly for the low-pressure determination is shown in Fig. 13.

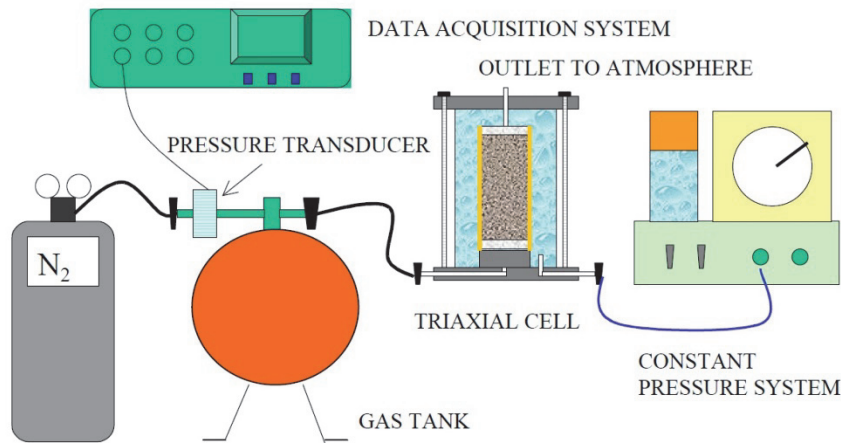


Fig. 13: Schematic representation of the low-pressure gas permeability system

The permeability to gas was calculated in accordance with the following equation (Yoshimi & Osterberg 1963):

$$k_{ig} \cdot k_{rg} = 2.3 \times \frac{V \times L \times \mu_g}{A \times \left(P_{atm} + \frac{P_0}{4} \right)} \times \frac{-\text{Log}_{10} \left(\frac{P(t)}{P_0} \right)}{t - t_0} \quad [3]$$

where $k_g \cdot k_{rg}$ is the effective permeability to gas (m²), V the volume of the tank (m³), L the length of the sample (m), A the surface area of the sample (m²), μ_g the dynamic viscosity of nitrogen (1.78 · 10⁻⁵ Pa·s), P_{atm} is atmospheric pressure (Pa), P_0 is the excess pressure over atmospheric pressure in time t_0 (s) and $P(t)$ is the excess over atmospheric pressure in the tank at time t (Pa). This equation was developed in a way analogous to that used for the expression of permeability to water using a falling head permeameter, with the air continuity equation being applied through consideration of compressibility (Lloret 1982). In developing the equation, it was assumed that the initial P_0 pressures are relatively small compared to atmospheric pressure. Also it must be assumed that while the pressure is decreasing in the tank, the distribution of pressure in the soil sample is the same as would exist if this instantaneous pressure had been maintained in the tank for a long period of time. The volume of the spherical tank used was 2.21 · 10⁻² m³ and the gas used for the tests was nitrogen, for which a density of 1.12 kg/m³ was taken. The pressure of the tank on test initiation was fixed to values close to 103 kPa (relative pressure).

Taking into account the cited values for the density and the viscosity of nitrogen, the following relation between permeability to gas (k_g , m/s) and the product of intrinsic permeability measured with nitrogen gas (k_{ig} , m²) times the relative permeability to gas (k_{rg}) is obtained:

$$k_g = \frac{\rho_g \times g}{\mu_g} \times k_{ig} \cdot k_{rg} = 6.2 \cdot 10^5 \times k_{ig} \cdot k_{rg} \quad [4]$$

The triaxial cell was initially pressurised to 0.6 MPa and gas was injected at a pressure close to 0.2 MPa (absolute pressure) through the bottom of the sample. If flow took place, the confining pressure was increased to 1 MPa, and the test was repeated. Afterwards, the cell with the sample was moved to the high-pressure equipment.

3.3 High-pressure equipment (HP)

Two different configurations of the high-pressure gas permeability setup were used for these tests, which were performed in the same samples previously tested in the low pressure equipment described above (LP). The first tests were performed in a setup in which a small gas cylinder was connected to the upper end of the sample, the pressure in it was initially fixed and allowed to decrease as flow took place through the sample, following the working principle of an unsteady-state permeameter (HP-US). Afterwards the setup was modified in order to improve the results of the tests, and flowmeters were installed to measure gas outflow. Under this configuration the tests were performed by keeping constant confining and injection pressures and atmospheric backpressure, i.e. following the working principle of a steady-state permeameter (HP-S). Most of the tests were performed under this configuration, which consisted of two lines that allowed performing two tests simultaneously. In one of the lines the confining pressure could reach values of up to 16 MPa (low confining pressure setup, LCP) and in the other line the confining pressure could be increased to as high as 33 MPa (high confining pressure, HCP).

For all the configurations, a data acquisition system under LabView running on a PC recorded the data and monitored the tests in progress.

3.3.1 High-pressure, unsteady-state (HP-US)

The general setup consisted of two stainless steel small cylinders connected to the valves of the cell and equipped with pressure sensors: an inlet transducer GE UNIK 5000 (350 bar-a, 0.04% FS BSL) and an outlet transmitter DRUCK PTX 1400 (100 bar-sg, 0.25% BSL max). Vacuum was applied to the downstream cylinder (the one connected to the bottom of the sample) and the other one was pressurised with nitrogen gas to 200 kPa. If no changes in pressure were recorded for 24 h, the injection pressure was increased by 200 kPa. The process was repeated until gas started to flow through the sample, causing a decrease of pressure in the upstream cylinder and an increase in the downstream one.

Two different gas injection lines were used: one with a high-pressure (HP) inlet cylinder (24.1 MPa, 150 cm³ nominal) and another one with a medium pressure (MP) inlet cylinder (12.8 MPa, 300 cm³ nominal). To apply the confining pressure to the water in the triaxial cell each line used a different method:

- A. a pressure bladder accumulator, which took the gas from a high-pressure nitrogen source. Confining pressures of up to 33 MPa could be reached with this system (Fig. 14, point A);
- B. a GDS pressure/volume piston controller with a working capacity of up to 16 MPa (Fig. 14, point B).

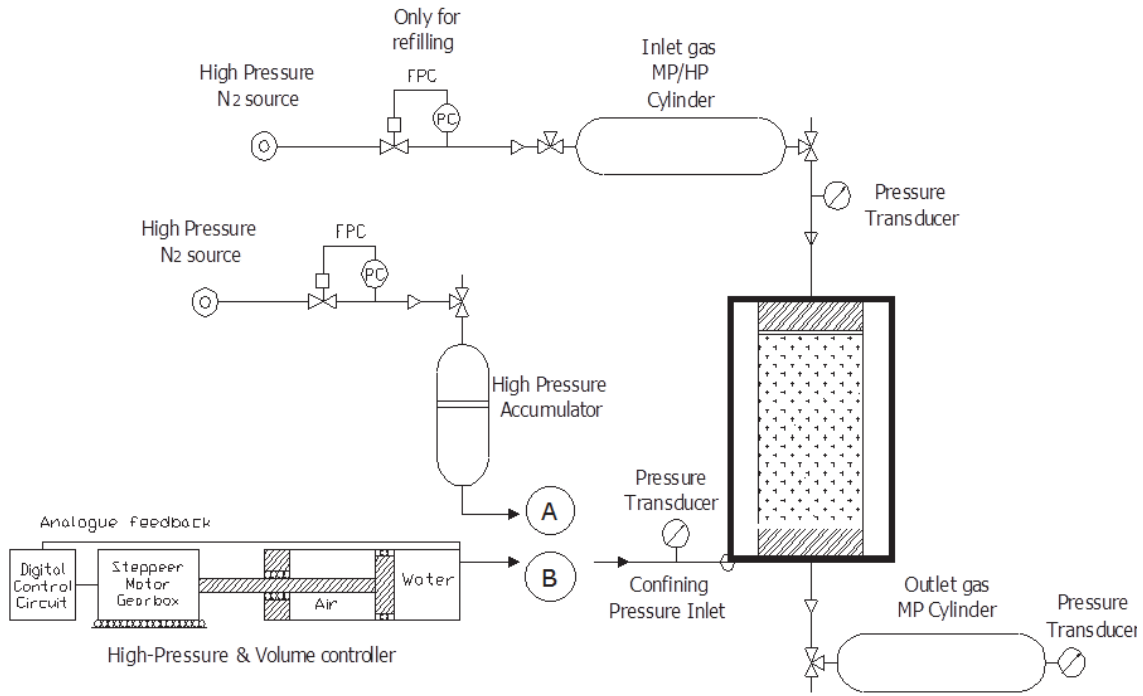


Fig. 14: Schematic diagram of the setup for the high-pressure unsteady equipment (HP-US) with the two options for applying confining pressure: A) HP accumulator; B) GDS controller

Although these tests were not intended to measure permeability, after breakthrough, instantaneous gas flow rates under the imposed pressure gradient, entering in or coming out from the sample, could be calculated (Loosveldt et al. 2002) from the volume of the upstream/downstream cylinders and the instantaneous rate of pressure change, avoiding the need for a flow-rate measuring device.

The mean volume flow rate Q_m , where the subscript 'm' refers to reference conditions of T and P under which the mass flow was measured, was calculated as:

$$Q_m = V_v \times \left(\frac{\Delta \rho}{\rho} \right) \times \frac{1}{\Delta t} \quad [5]$$

where V_v is the volume of the cylinder (HP inlet 150 cm³, MP inlet 300 cm³ and HP-MP outlet 150 cm³, all nominal values), $\Delta \rho / \rho$ is the relative change in gas density, and Δt is the time interval in which the change in gas density took place.

From the equation of state for real gases:

$$\rho = \frac{MP}{ZRT} \quad [6]$$

where P , T and V ($V=M/\rho$) are the actual conditions of pressure, temperature and volume, respectively, and $Z(T, P)$ is the compressibility factor that expresses the deviation between compressibility (density) of the real gas and the ideal gas at identical conditions of temperature and pressure.

However, when the actual densities deduced from the equation of state for real gases are introduced in Eq. 6, the compressibility factor Z disappears from the equation if the pressure change was small or the gas behaved as an ideal gas.

If the test is considered isothermal, then:

$$Q_m = V_v \times \left(\frac{\Delta P}{P_{av}} \right) \times \frac{1}{\Delta t} \quad [7]$$

where V_v is the volume of the cylinder, ΔP is the pressure change and P_{av} is the average pressure (upstream or downstream) in the cylinder (inlet or outlet) during the time interval considered.

To compute permeability the gas inflow or outflow can be used, applying the following equation for incompressible media with compressible pore fluids (Scheidegger 1974):

$$k_{ig} \cdot k_{rg} = \frac{Q_m \times \mu_g \times L \times 2 P_m}{A \times (P_{up}^2 - P_{dw}^2)} \quad [8]$$

where Q_m is the mean volume flow obtained applying Eq. 7, A is the sample cross-sectional area, μ_g is the fluid dynamic viscosity, L is the sample length and P_{up} and P_{dw} are the upstream and downstream pressures applied at the top (inlet) and the bottom (outlet), respectively, of the sample. In this kind of tests the measurement pressure P_m and the average pressure of the interval P_{av} are the same.

The accuracy of this analysis depends on the assumptions that the pressure change was slight or the gas behaved as an ideal gas and that a pseudo-steady state mass-flow was established, *i.e.* that the quantity of gas exiting the high pressure cylinder was approximately equal to that entering the low pressure cylinder.

If the values from tests running under different ambient conditions need to be compared, the volumetric flow-rate at standard conditions, Q_{STP} , must be obtained from Q_m by applying the corresponding relations between pressure, temperature and compressibility factors (ordered from the highest to the lowest effect).

3.3.2 High-pressure, steady-state (HP-S)

After performing three initial gas permeability tests with the unsteady-state configuration, the setup was modified and divided into two separate measurement lines. In the new version of the setup, the injection pressure could be independently varied and maintained constant during the period of time necessary to get steady flow, while the backpressure remained atmospheric and the outflow was measured. The gas outflow was measured by means of different range HITECH gas flowmeters (0.04-2, 0.2-10, and 2-100 STP cm³/min).

The same gas injection lines as in the HP-US configuration were used: one with a high pressure (HP) inlet cylinder (24.1 MPa, 150 cm³ nominal) and another one with a medium pressure (MP) inlet cylinder (12.8 MPa, 300 cm³ nominal). Similarly, two different pressure lines were used to apply the confining pressure: a low-confining pressure line (LCP) (Fig. 15), with a working capacity of up to 16 MPa, and a high-confining pressure line (HCP) to apply confining pressures of up to 33 MPa (Fig. 16). Injection pressures of up to 18 MPa could be applied.

The outlet of the cell connected to the bottom of the sample was open to atmosphere, with a series of different range gas mass flowmeters measuring the gas outflow, the value used to compute permeability being the one measured by the flowmeter working in the proper range. Tab. 4 shows the range of each flowmeter and its turndown values, which are the flow values below which accuracy is not guaranteed. Outflow gas rates, upstream and downstream pressure, confining pressure and temperature were monitored online.

Tab. 4: Range and turndown values of flowmeters in both lines

Flowmeter (HCP)	Flowmeter (LCP)	Range (mL /min)	Turndown (mL/min)
FT 1	FT 6	2	0.04
FT 2	FT 5	10	0.2
FT 3	FT 4	100	2

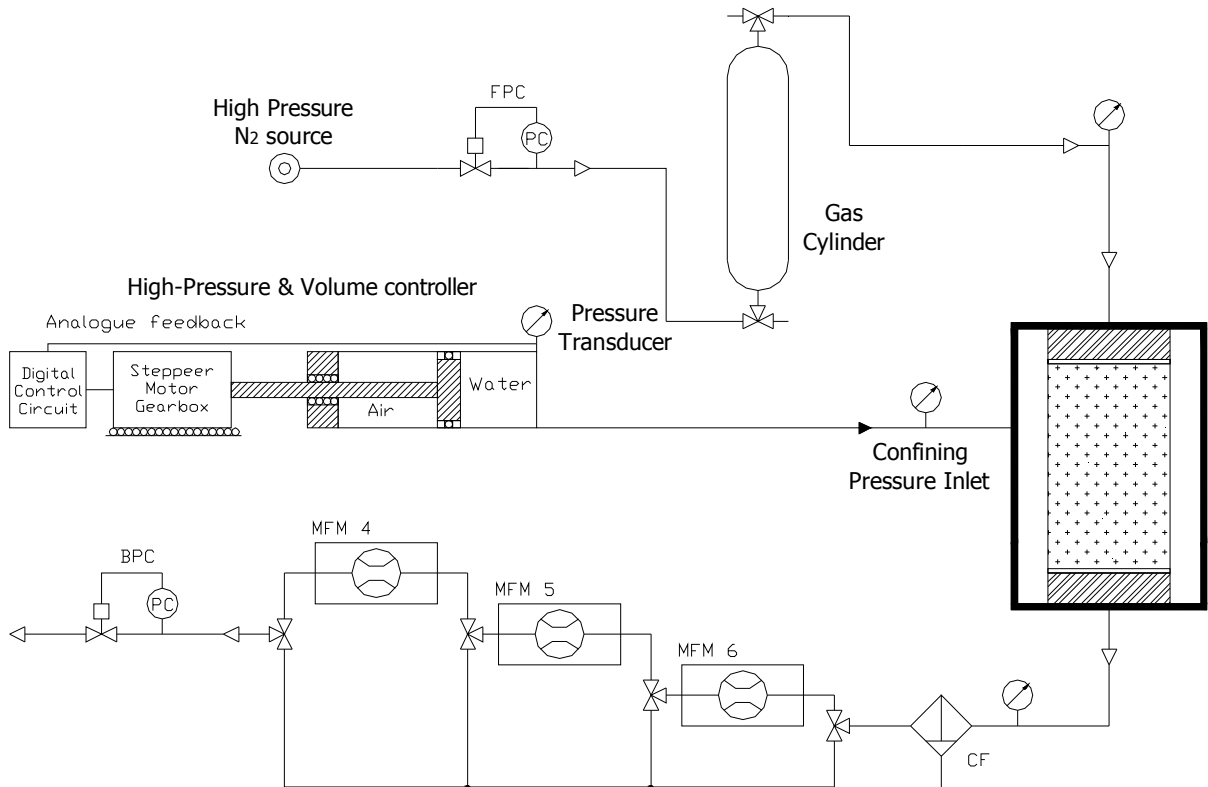


Fig. 15: Experimental setup of the low confining pressure line (LCP) (CF: coalescing filter, PC: forward-pressure controller, BPC: back-pressure controller, MFM: mass flow meter)

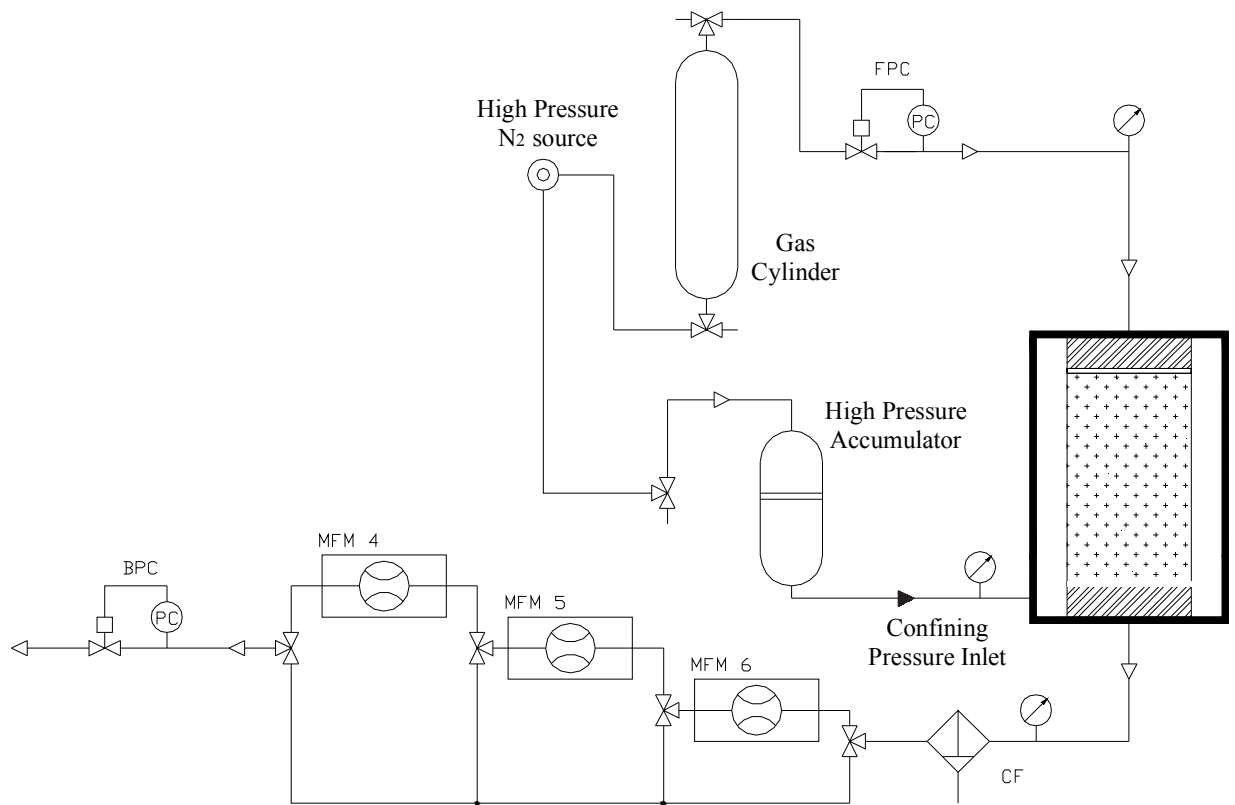


Fig. 16: Experimental setup of the high confining pressure line (HCP) (CF: coalescing filter, FPC: forward-pressure controller, BPC: back-pressure controller, MFM: mass flow meter)

To compute the apparent (or effective) permeability, the gas inflow or outflow can be used, applying Eq. 8. In this kind of test, Q_m is the mean volume flow rate measured by the appropriate flowmeter, P_m is the standard atmospheric pressure (101.325 kPa) due to the STP conditions of the gas mass flowmeters and $(P_{up}^2 - P_{dw}^2)$ is the difference between the gas injection pressure and the backpressure (actual atmospheric pressure in this setup).

To analyse the effect of injection and confining pressures on permeability, the tests consisted of several steps. Usually the tests started under confining pressure of 0.6 or 1 MPa (depending on the last confining pressure applied in the low-pressure equipment) and atmospheric backpressure. In most tests the injection pressure was initially set to 0.2 MPa (absolute pressure) and increased by 0.1 MPa every step until flow took place or was sufficiently high as to be accurately measured. When the difference between confining and injection pressure was below a certain value (0.2 MPa in most cases), the confining pressure was progressively increased until no gas flow occurred. The particular pressure paths of each test are given in Annex I.

3.4 Postmortem analyses

The water content and dry density of the samples were determined in spare fragments resulting from the trimming of the specimens, which represent the initial conditions, and then at the end of the gas testing.

The gravimetric water content (w) is defined as the ratio between the mass of water and the mass of dry solid expressed as a percentage. Consequently, all the values given in this report are weight percentages. The mass of water was determined as the difference between the mass of the sample and its mass after oven drying at 110°C for 48 h (mass of dry solid). Dry density (ρ_d) is defined as the ratio between the mass of the dry sample and the volume occupied by it prior to drying. The volume of the spare fragments used to determine the initial conditions of the samples was determined by immersing them in a recipient containing mercury and by weighing the mercury displaced, taking for the density of mercury a value of 13.6 g/cm³. The absolute error of this measurement is in the order of 10⁻² g/cm³. The same sample whose volume had been determined was used for the water content determination. The balance used was an AND GF2000, with a capacity up to 2100 g and a precision of 0.01 g. The dry density of the cylindrical specimens after gas testing was computed from their volume (as measured with a ±0.01 mm caliper) and water content determined by oven drying.

The degrees of saturation (S_r) have been computed from the dry density and water content determined in the laboratory, taking a value for the water density of 1 g/cm³ and a value for the specific weight of solid particles (dried for 48 h at 110°C) of 2.70 g/cm³. This is the average value of numerous determinations carried out on FEBEX bentonite following a fine-tuned technique (Villar 2002).

In order to determine the pore size distribution, two pieces of each sample were used: a spare fragment resulting from the sample preparation and a fragment from the sample at the end of the gas permeability test. The aim of these tests was to analyse the effect of gas flow on the pore size distribution of each sample. It was determined by mercury intrusion porosimetry (MIP). This technique allows the determination of the pore size distribution by injecting mercury into the sample at different pressures while controlling the volume intruded. The pressure applied may be related to the minimum pore diameter intruded, taking into account the characteristics of the fluid. The ratio of the volume of mercury intruded (pore volume) to the applied pressure (which conditions the minimum pore diameter) allows distribution curves to be obtained establishing the percentage of pores of a size included within a given range.

In order to alter as less as possible the clay microstructure during drying, the samples were put in the ice condenser of a Telstar LioQuest equipment at -50°C for 3 h. Afterwards they were lyophilised for 19 h at a temperature of -50°C under a vacuum of 0.2 mbar, so that to eliminate the water in the pores by sublimation. Before the MIP tests the samples were heated to 35°C for 2 h. The porosimeter used was a Micromeritics AutoPore Series IV 9500, which allowed the exploration of pore diameters between 0.006 and 600 µm. Prior to mercury injection the sample was outgassed by applying a vacuum of 50 µm-Hg. Afterwards the mercury injection pressure was increased from 2.7 kPa to 220 MPa in 109 steps. To determine the extrusion branch of the curve, the pressure was released in 56 steps down to a pressure

of 68.6 kPa. A contact angle of mercury of 139° both on advancing and of receding on the clay surface was considered.

The mercury intrusion method allows access to be gained only to part of the macroporosity (pores between 600 µm and 50 nm) and to part of the mesopores (those of sizes between 50 and 6 nm), since mercury does not intrude the microporosity (pores of a size of less than 2 nm, according to the classification of Sing et al. 1985). In the high-density clay materials retrieved from the FEBEX-DP, pores larger than those that can be quantified by MIP are not expected. However, the pores connected to the external surface by narrow openings will not be intruded until sufficient pressure is applied to intrude the entryways. All of the volume of such pores will be allocated to the threshold radius class of the most restricted part of the entryway (bottleneck effect). Nevertheless, considering that most of the non-intruded porosity corresponds to the pores of a size smaller than the limit of the apparatus, an estimation of the percentage of pores actually intruded can be made by comparing the actual void ratio of the samples (e , computed from their dry density and density of solid particles) and the apparent void ratio calculated from mercury intrusion (e_{nw} , mercury being a non-wetting (nw) fluid). Thus, the pore size distribution curves obtained by MIP were corrected to take into account the percentage of pores not intruded.

4 RESULTS

Twenty two gas permeability tests were performed in triaxial cells with bentonite core samples obtained by drilling on-site or by drilling from blocks in the laboratory. In every section at least six cores were drilled, two in each barrier ring: external, intermediate and internal. Of every couple of samples drilled in the same bentonite ring, one of them was drilled in the middle of a block, and the other one at the contact between that block and the neighbouring one, such that the core had along it an interface between two bentonite blocks. The aim of this sampling procedure was to analyse the effect of sealed joints –which are usually acknowledged to have no effect on water permeability– on gas permeability. Fig. 17 shows the location of the cores drilled in the sampling sections.

Gas permeability was measured in samples with initial dry density values between 1.51 and 1.64 g/cm³, and with water contents between 20 and 29%, corresponding to initial degrees of saturation between 79 and 100%. Tab. 5 summarises the characteristics of the specimens tested. The initial characteristics of these samples were different in terms of water content and dry density, since during the 18-year operation significant gradients in these properties were generated across the barrier (see for example the changes in water content in Fig. 4). This allowed to analyse the effect on the gas transport properties of the changes in the bentonite physical state occurred during operation.

For the computation of permeability the equations shown in the previous section were selected depending on the particular setup used. The use of these Darcy-based equations has limitations for expansive materials, because they are compressible to a certain degree and flow does probably not take place along cylindrical capillary bundles. Nevertheless, it is considered that, for lack of an alternate straightforward approach, this permeability computation is useful to assess changes between samples.

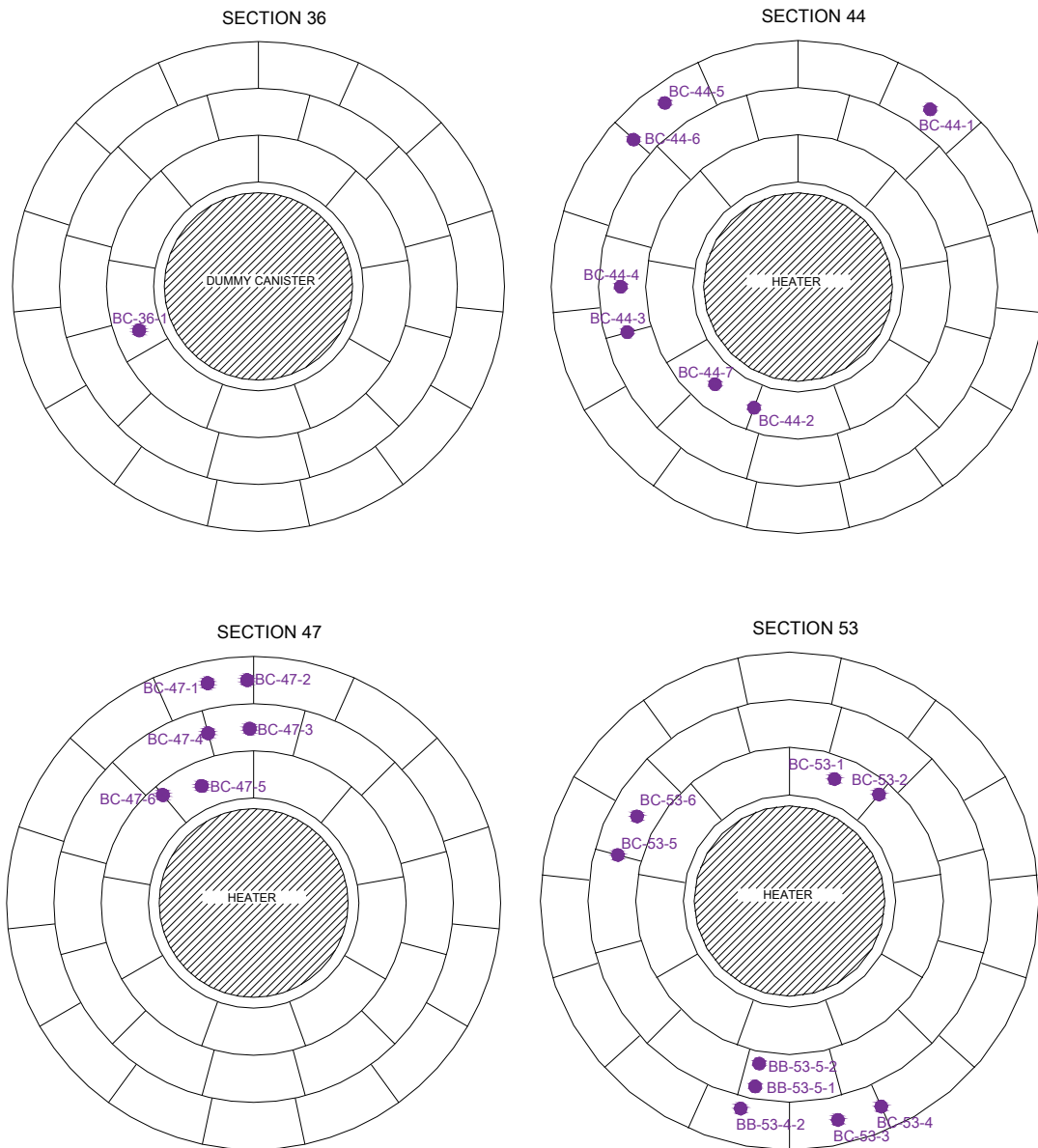


Fig. 17: Location of the samples tested for gas permeability (the actual position of the cores differs in some cases from the one in the Sampling Book. Samples from section S53 were drilled in the laboratory)

Tab. 5: Characteristics of the bentonite samples used for gas permeability tests (see location in Fig. 17)

Reference	Distance to axis (cm)	Initial ρ_d (g/cm ³)	Initial w (%)	Initial S_r (%)	Height (cm)	Diameter (cm)	Suction ^a (MPa)	Comments	Setup ^b
BC-36-1	59	1.52	26.7	93	3.11	3.80	5.5		HP-US
BC-44-1	103	1.57	26.2	98	3.73	3.98	5.5		LP/LCP
BC-44-2	62	1.56	23.2	86	2.41	4.15	46.6	Interface between blocks	LP/LCP
BC-44-3	82	1.59	25.2	97	4.49	3.98	20.0	Interface between blocks	LP/HCP

Reference	Distance to axis (cm)	Initial ρ_d (g/cm ³)	Initial w (%)	Initial S_r (%)	Height (cm)	Diameter (cm)	Suction ^a (MPa)	Comments	Setup ^b
BC-44-4	61	1.61	24.5	97	4.11	4.19	20.0		LP/LCP
BC-44-5	103	1.52	28.4	100	4.10	4.18	3.7		LP/LCP
BC-44-6	102	1.51	28.4	97	3.90	4.18	3.7	Interface between blocks	LP/LCP
BC-44-7	61	1.62	19.5	79	3.59	4.17	46.6		LP/HCP to LCP
BC-47-1	103	1.55	26.4	96	3.86	4.12	5.0		LP/LCP
BC-47-2	104	1.54	26.4	94	3.98	3.80	5.0		HP-US
BC-47-3 ^c	82	1.61	23.7	95	3.79	4.15	19.8		LCP
BC-47-4 ^c	81	1.59	24.8	97	3.70	3.60	19.8	Interface between blocks	HP-US
BC-47-6	66	1.64	19.6	82	3.92	4.12	29.0	Interface between blocks	LP/HCP
BB-53-4-2	87	1.59	25.1	96	5.21	4.96	0.4		LP
BB-53-5-1	76	1.63	23.3	96	4.85	4.95	22.9		LP/LCP
BB-53-5-2	99	1.63	22.9	94	4.99	5.00	28.1		LP/HCP
BC-53-1	64	1.59	23.7	91	4.08	4.00	24.0		LP/HCP
BC-53-2	64	1.63	22.5	93	4.10	3.99	24.0	Interface between blocks	LP/LCP
BC-53-3 ^c	104	1.54	29	104	3.30	3.99	1.4		LP/HCP
BC-53-4 ^c	104	1.53	27.1	96	3.68	4.00	1.4	Interface between blocks	LP/HCP
BC-53-5	80	1.58	24.8	95	3.90	4.00	17.8	Interface between blocks	LP/HCP
BC-53-6	80	1.55	25.0	91	3.45	3.98	17.8		LP/HCP

^a measured with psychrometers or capacitive sensors in adjacent samples (Villar et al. 2018)

^b LP: low pressure equipment, HP-US: high-pressure, unsteady-state, HCP: high-pressure, steady-state, high confining pressure, LCP: high-pressure, steady-state, low confining pressure

^c the position of these blocks is interchanged with respect to the Sampling Book (Bárcena & García-Siñeriz 2015)

4.1 Gas permeability tests

As it can be checked in Tab. 5, most of the samples were initially tested in the low pressure equipment. The aim of the tests performed in this setup was to determine the gas permeability under low confining and injection pressure conditions. The tests followed two stages:

- Stage 1: constant confining pressure of 0.6 MPa and initial gas injection pressure of 0.2 MPa (absolute pressure).
- Stage 2: constant confining pressure of 1.0 MPa and initial gas injection pressure of 0.2 MPa (absolute pressure).

The samples in which no flow had occurred or it had been very low when tested in the low-pressure equipment were also tested in the high-pressure (HP) equipment. The HP equipment allowed to analyse the influence of boundary conditions (injection and confining pressures) on the value of permeability. To

accomplish this, the tests consisted of several steps which followed a pressure path that was adjusted to each sample characteristics. The tests started under constant confining pressure of 0.6 or 1 MPa and injection pressure of 0.2 MPa, which were the pressures previously reached in the low-pressure setup. Afterwards the injection pressure was increased by 0.1 MPa every step. Once a noticeable flow was reached, the confining pressure was progressively increased until gas could not flow through the sample. Tab. 6 summarises the samples measured and the range of pressures applied in the high-pressure equipment. In the following subchapters the main results of every test are summarised, and for each sample the results obtained in the LP setup are also included. Annex I shows the detailed description and results of every test.

Tab. 6: Kind of tests performed in each sample and range of pressures applied with the high-pressure equipment (values are given in absolute pressures)

Sample	Setup	Confining P (MPa)	Injection P (MPa)
BC-36-1	HP-US	1.0-14.0	0.2-13.0
BC-44-1	LP/LCP	1.0-2.5	0.2-0.6
BC-44-2 ^a	LP/LCP	1.0-9.0	0.15-0.5
BC-44-3 ^a	LP/HCP	1.0-3.0	0.2
BC-44-4	LP/LCP	0.6-3.5	0.2-0.5
BC-44-5	LP/LCP	0.6-1.5	0.2-1.4
BC-44-6 ^a	LP/LCP	1.0-3.0	0.2-0.6
BC-44-7	LP/HCP to LCP	1.0-9.5	0.2-0.5
BC-47-1	LP/LCP	0.6-2.5	0.2-0.7
BC-47-2	HP-US	1.5-12.0	0.2-1.6
BC-47-3	LCP	0.6-1.0	0.1-1.0
BC-47-4	HP-US	1.8-9.0	0.2-2.5
BC-47-6 ^a	LP/HCP	0.6-3.0	0.1
BB-53-5-1	LP/LCP	0.6-1.7	0.2-1.2
BB-53-5-2	LP/HCP	0.6-1.7	0.2-0.6
BC-53-1	LP/HCP	0.6-2.2	0.2-0.6
BC-53-2	LP/LCP	1.0-4.0	0.2-0.4
BC-53-3	LP/HCP	1.0-2.0	0.2-0.8
BC-53-4 ^a	LP/HCP	1.0-6.0	0.2
BC-53-5 ^a	LP/HCP	1.0-3.0	0.2-0.3
BC-53-6	LP/HCP	1.0-5.0	0.2-0.3

^a samples with interface

4.1.1 Sample BC-36-1

Sample BC-36-1 was taken from the ring in contact with the dummy canister in section S36 (Fig. 17). Consequently it was subjected to drying for 5 years and afterwards to wetting at temperatures around 20°C in contact with the shotcrete plug for 13 additional years. Hence, the sample was almost saturated ($S_r=98\%$) and had a dry density of 1.52 g/cm³.

The sample was tested in the high-pressure equipment with the unsteady-state method (HP-US). During the test the confining pressure was increased from 1 MPa to 14 MPa. The injection pressure was gradually increased from 0.2 MPa to 13 MPa, keeping a constant difference between confining and injection pressures of 0.1 MPa (Fig. 18).

The permeability values computed from the decrease of pressure in the upwards vessel for each step (Eq. 8) are shown in Fig. 19. As expected, the permeability of the sample decreased with the increase in confining pressure from 1 to 14 MPa. The increase in confining pressure from 1 to 4 MPa caused a permeability decrease of four orders of magnitude. The decrease in permeability for higher confining pressures was less significant. The test lasted almost 5 months, and the water content decreased during testing from 28.1% to 26.7%, particularly in the upper part of the specimen, through which gas was injected. Because of the high confining pressures applied, the final dry density of the sample increased to 1.57 g/cm³.

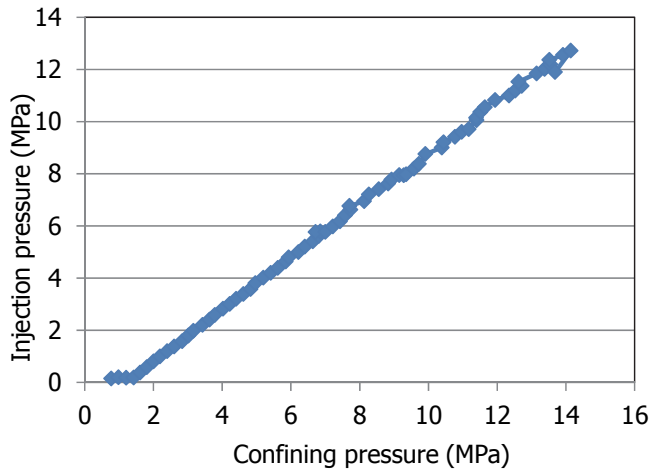


Fig. 18: Pressure path followed in the HP-US setup for sample BC-36-1

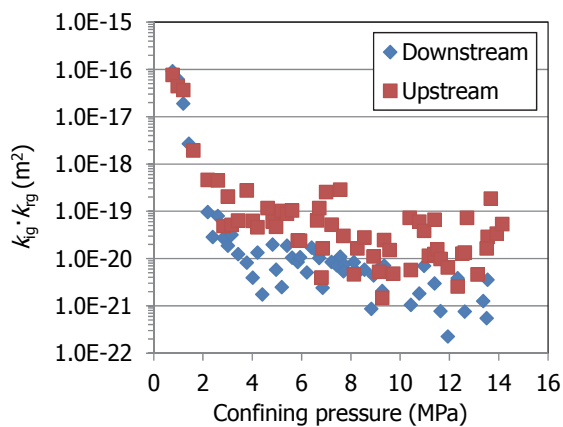


Fig. 19: Evolution of gas permeability ($k_{ig} \cdot k_{rg}$) for sample BC-36-1 as confining pressure increased (HP-US equipment)

4.1.2 Sample BC-44-1

Sample BC-44-1 was a core sample drilled in the external ring of a barrier section around the heater (Fig. 17) and had a dry density of 1.57 g/cm³ and a degree of saturation close to 100%.

The sample was tested in the low-pressure equipment (LP), with confining pressures of 0.6 and 1 MPa. The decrease in relative injection pressure during the tests and the permeability values computed from them are shown in Fig. 20. The initial increase in relative injection pressure was related to the increase in temperature in the laboratory.

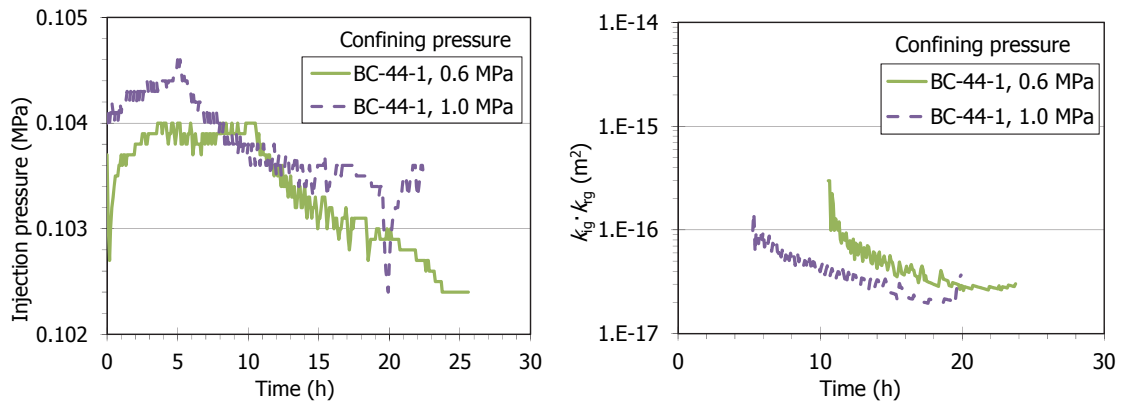


Fig. 20: Evolution of injection pressure (relative values) and gas effective permeability ($k_{ig} \cdot k_{rg}$) measured in the low pressure equipment (LP) for sample BC-44-1

Afterwards, the sample was tested in the high-pressure, steady-state permeameter (low confining pressure line, LCP). In this equipment the test followed the phases shown in Fig. 21:

- Phase 1: the injection pressure was increased, keeping constant confining pressure. Then, the confining pressure was gradually increased from 1 to 2.5 MPa. The injection pressure was increased until reaching a value of 0.6 MPa. Backpressure was kept atmospheric.
- Phase 2: the confining pressure was reduced, keeping the same injection pressure value and atmospheric backpressure.

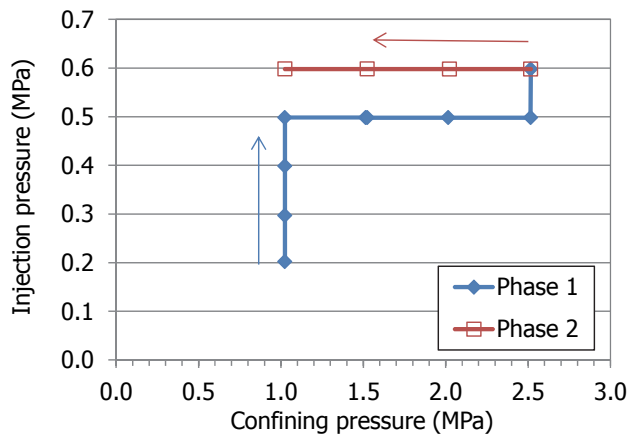


Fig. 21: Pressure path followed in the LCP setup for sample BC-44-1 (injection gas pressure given in absolute values)

Fig. 22 (left) shows the permeability values obtained during the increase of injection pressure while confining pressure was kept at 1 MPa. The repercussion on gas permeability of the increase in injection pressure was insignificant. However, the increase of confining pressure at constant injection pressure caused a reduction of gas permeability, and conversely, when the confining pressure decreased in Phase 2, the gas permeability increased (Fig. 22, right). During this unloading, the gas permeability was lower than that previously measured for the same confining pressures during loading. This would indicate that the sample consolidated irreversibly during the initial increase in confining pressure.

The permeability values obtained in the low-pressure equipment (LP) are also shown in the Figure. They were higher than those measured in the LCP equipment.

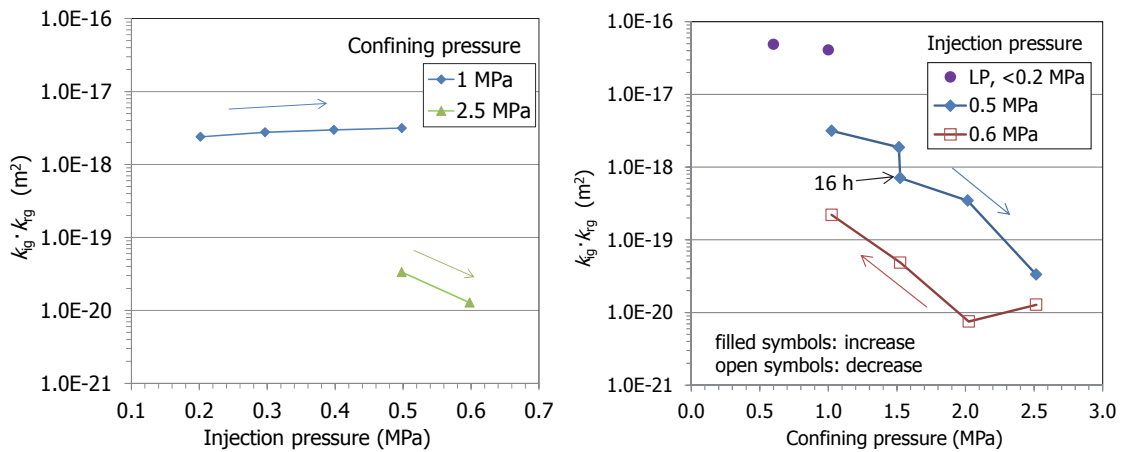


Fig. 22: Evolution of gas permeability at constant confining pressure (left) and constant injection pressure (right) for sample BC-44-1

4.1.3 Sample BC-44-2

This core sample was drilled on site in the sense parallel to the contact surface between two blocks of the same section, consequently it had a longitudinal interface (Fig. 23). The dry density of the sample was 1.56 g/cm^3 and the water content 23.2%, corresponding to a degree of saturation of 86%, since it was taken from the inner ring of the barrier, close to sample BC-44-7 (Fig. 17).

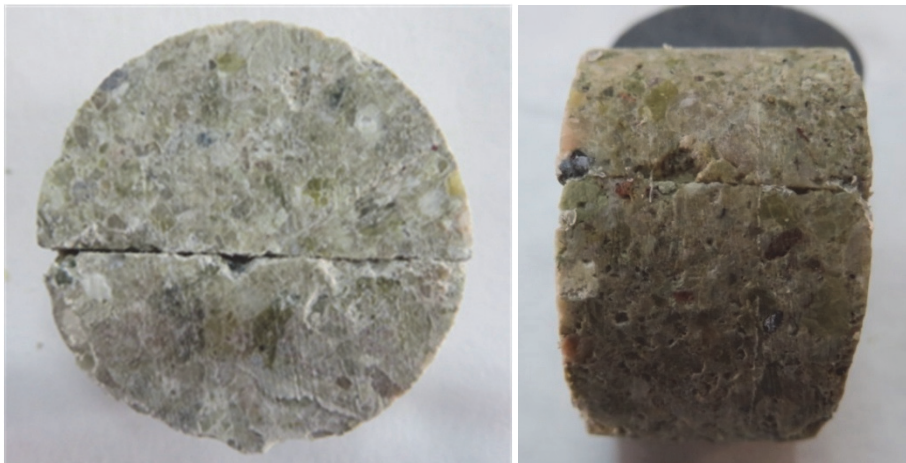


Fig. 23: Initial appearance of sample BC-44-2

The sample was first measured in the low-pressure equipment (LP) under confining pressures of 0.6 and 1 MPa. Afterwards the sample was tested in the high-pressure, steady-state equipment in the low confining pressure line (LCP), following these phases (Fig. 24):

- Phase 1: the injection pressure was increased until reaching a value of 0.2 MPa. Then, the confining pressure increased with constant injection pressure of 0.2 MPa.
- Phase 2: the injection pressure was gradually increased under constant confining pressure, the confining pressure was subsequently increased and the injection pressure was again reduced. The process was repeated reaching a lower injection pressure.
- Phase 3: just before this Phase the confining pressure was decreased to 7 MPa and then, the confining pressure and the injection pressure were increased to 9 and 0.5 MPa, respectively.

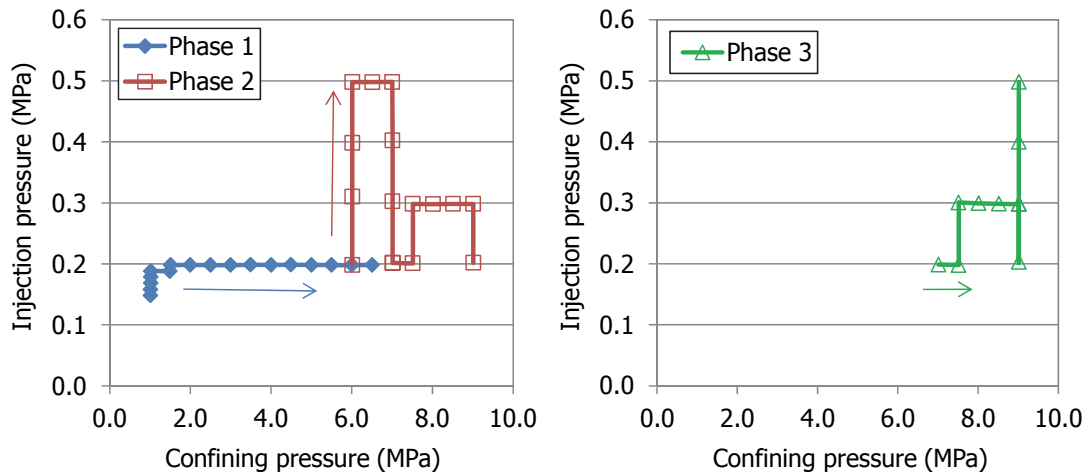


Fig. 24: Pressure path followed in the LCP permeameter for sample BC-44-2 (injection gas pressure given in absolute values)

The permeability values obtained during the phases of confining pressure increase for different injection pressures are plotted in Fig. 25. The reduction of gas permeability with confining pressure was not significant for confining pressures lower than 6 MPa, which is a value above the swelling pressure corresponding to the dry density of the sample (4.4 MPa according to Eq. 2). The test showed a large reduction in gas permeability when the confining pressure increased from 6 to 6.5 MPa, which was related to a longer period of time between these steps (21 h), during which the sample was subjected to a confining pressure of 6 MPa). This seems to have led to a significant consolidation of the sample and especially to the sealing of the joint between blocks, with the resulting decrease in gas permeability.

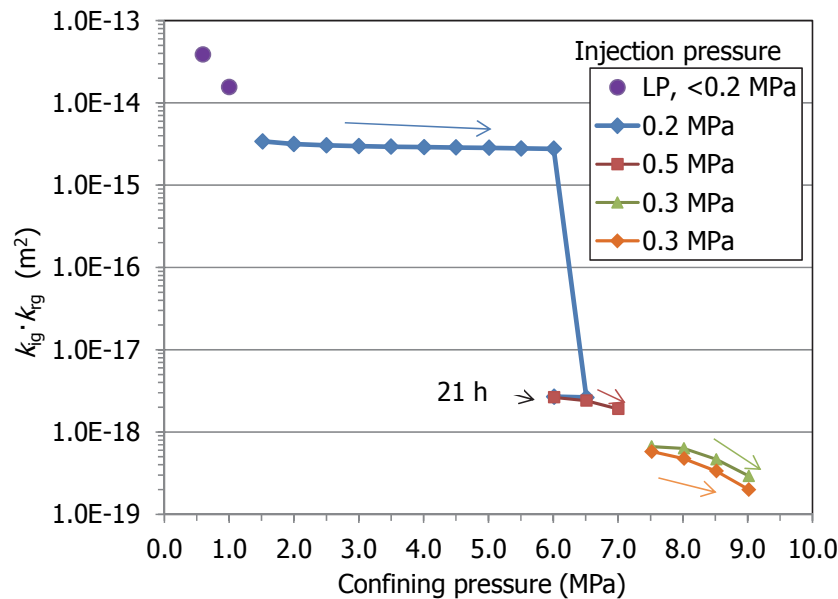


Fig. 25: Evolution of gas effective permeability ($k_{ig} \cdot k_{rg}$) for sample BC-44-2, as confining pressure increased

Fig. 26 shows the change of permeability with changes of injection pressure for different constant confining pressures. For a given confining pressure, there was not a noticeable influence of the injection pressure on gas permeability, except for the lowest confining pressure (1 MPa). However, the effect of confining pressure on gas permeability is clear and seems to be the main factor affecting permeability. In fact, the joint in the sample was apparently sealed after dismantling (Fig. 27).

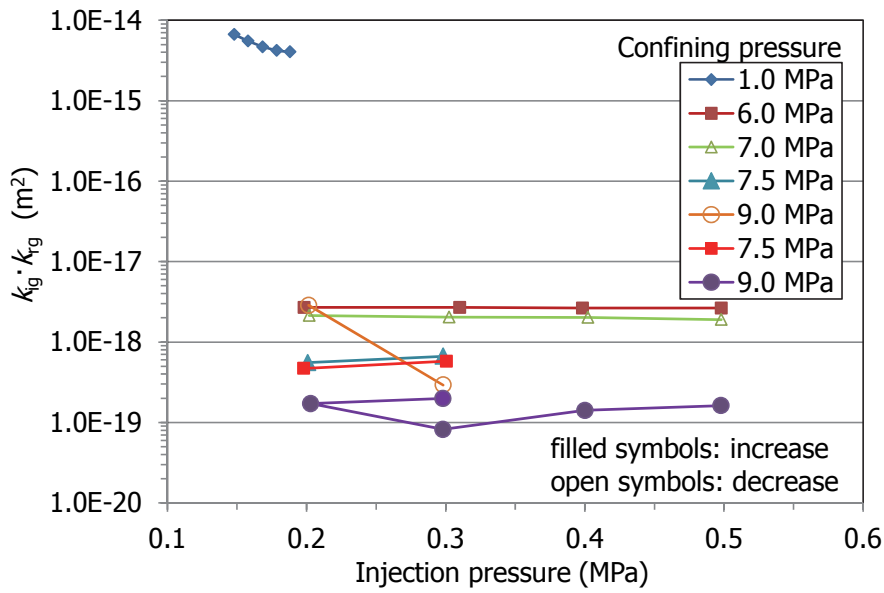


Fig. 26: Evolution of gas permeability at constant confining pressure for sample BC-44-2



Fig. 27: Final appearance of sample BC-44-2 (the interface can be seen in the upper left)

4.1.4 Sample BC-44-3

This core sample was drilled on site between two blocks, in the intermediate ring of section S44, close to sample BC-44-4. As a consequence, there was a longitudinal interface along the core, although it was barely visible (Fig. 28, left). However, at the end of the gas test the specimen split along the interface (Fig. 28, right). The initial dry density and water content were 1.59 g/cm^3 and 25.2%, respectively.



Fig. 28: Initial and final appearance of sample BC-44-3

Sample BC-44-3 was first tested in the low-pressure equipment (LP), with confining pressures of 0.6 and 1 MPa. The decrease in injection pressure during both tests and the permeability values calculated from it are shown in Fig. 29. The increase in confining pressure caused a reduction of gas permeability. The gas pressure in the upstream tank was affected during both tests by the laboratory temperature changes (differences between day and night).

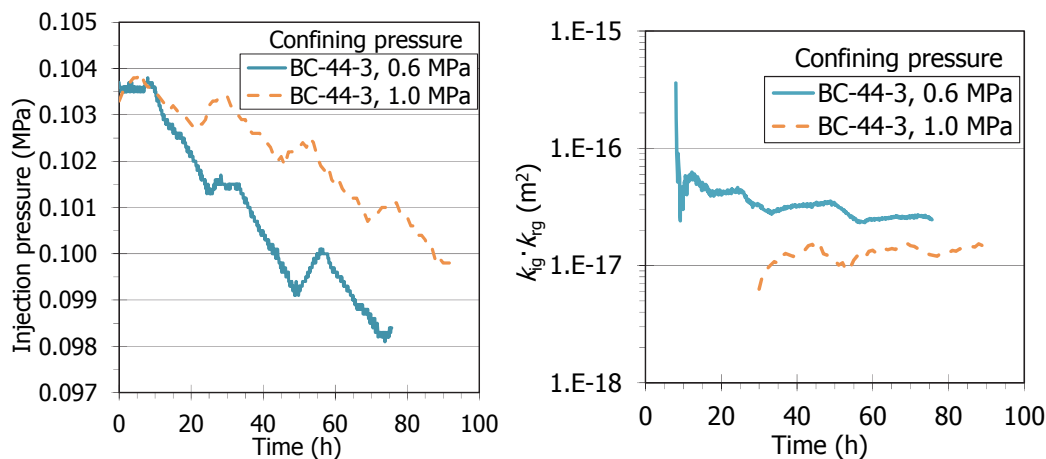


Fig. 29: Evolution of injection pressure and gas effective permeability ($k_{ig} \cdot k_{rg}$) in the low pressure equipment (LP) for sample BC-44-3 (injection gas pressure given in relative values)

Afterwards, the sample was tested in the high-pressure equipment (low confining line, LCP), following these two phases: an increase of confining pressure from 1 to 3 MPa (Phase 1), until flow stopped, and then a reduction in confining pressure until reaching the initial value (Phase 2). The injection pressure was maintained at 0.2 MPa.

The permeability values obtained during the changes of confining pressure are plotted in Fig. 30. The increase of confining pressure at a constant injection pressure caused a reduction of gas permeability, but when the confining pressure decreased (Phase 2) the gas permeability barely changed, and consequently the values did not reach the initial values for the same confining pressures. This effect would indicate that the sample consolidated irreversibly during Phase 1 or that the interface closed by the effect of confining pressure. In fact the dry density increased slightly (from 1.59 to 1.60 g/cm³) while the water content decreased (from 25.2 to 24.2%) during the test, which would indicate that some water displacement took place during gas injection. The duration of each step was 24 h, except for the application of 3 MPa of confining pressure, which was applied for almost 4 days. The larger duration of this step did not influence the gas permeability. Fig. 30 also shows gas permeability values obtained in

the low-pressure equipment, which are consistent with the values obtained in the high-pressure equipment.

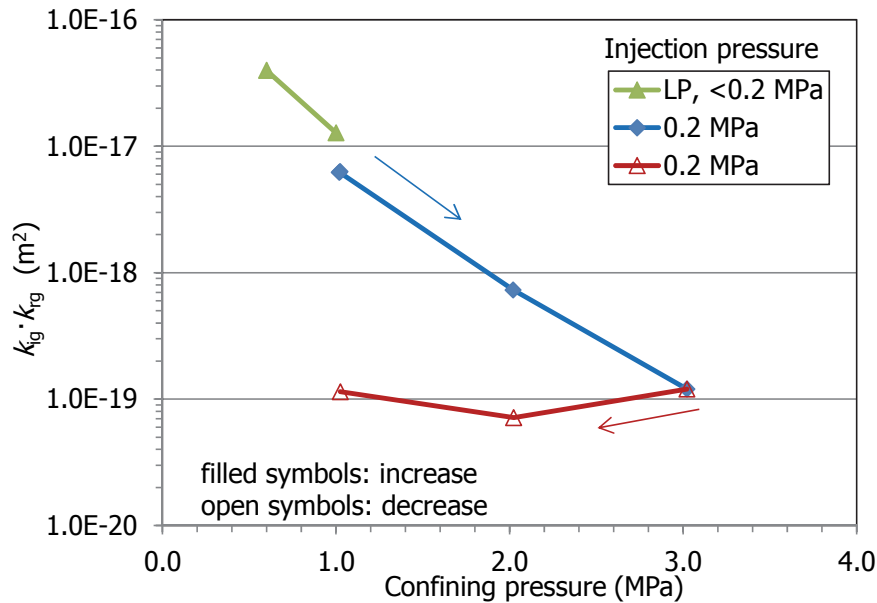


Fig. 30: Evolution of gas permeability at constant injection pressure (absolute values) for sample BC-44-3

4.1.5 Sample BC-44-4

This core sample was drilled on site in the centre of a block of the intermediate ring of the barrier (Fig. 17). The dry density of the sample was 1.61 g/cm^3 and the water content 24.5%, corresponding to a degree of saturation of 97%.

Sample BC-44-4 was tested in the high-pressure steady-state setup, in the low confining pressure line (LCP) following the pressure path showed in Fig. 31, consisting of two phases:

- Phase 1: with an injection pressure of 0.2 MPa the confining pressure was increased from 0.6 to 1.0 MPa, and then the injection pressure was increased up to 0.5 MPa.
- Phase 2: keeping the injection pressure constant at 0.5 MPa, the confining pressure was increased up to 3.5 MPa and then decreased.

The change in injection pressure did not modify permeability, but it clearly decreased when the confining pressure increased and then the permeability increased again as the confining pressure was released (Fig. 32). Nevertheless, the permeability values measured during unloading were an order of magnitude lower than those measured for the same confining pressure during loading. The duration of the steps was between 1 and 2 hours, although between some of the steps (during night and weekends) the valves of the cell were closed and the sample remained for longer under the last pressure situation. This allowed checking that the time the sample remained under a given confining pressure also had an influence on the permeability value, which was slightly lower if the sample had remained for longer under the same confining pressure (Fig. 32, right).

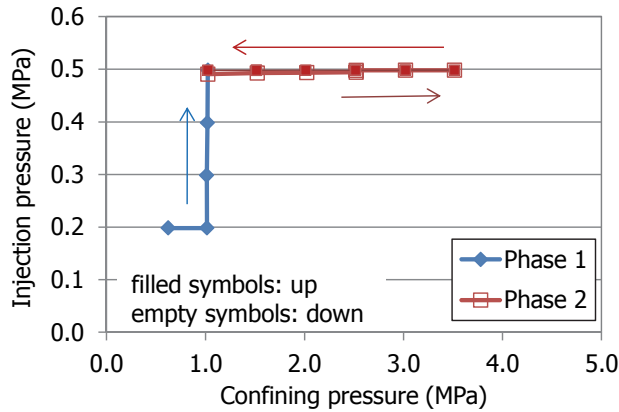


Fig. 31: Pressure path followed in the LCP setup for sample BC-44-4 (injection gas pressure given in absolute values)

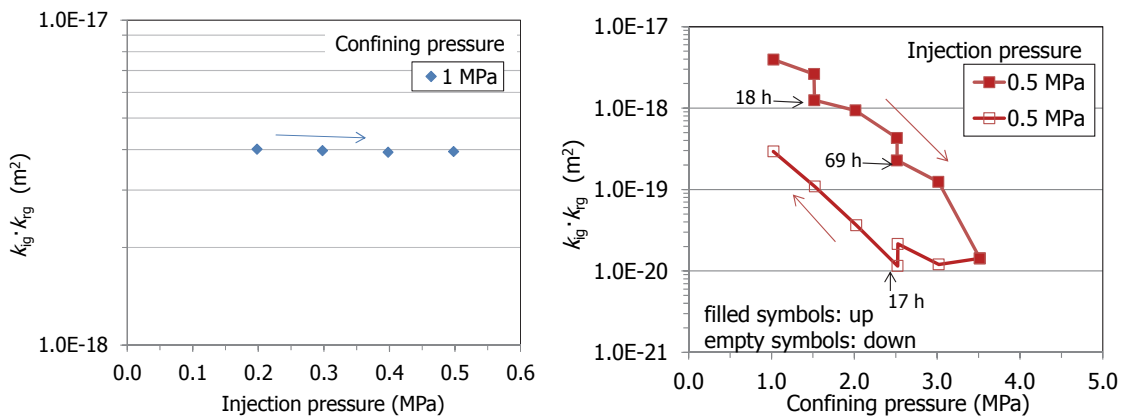


Fig. 32: Evolution of gas effective permeability at constant confining pressure (left) and constant injection pressure (right) for sample BC-44-4 (the duration of longer steps is indicated in hours)

4.1.6 Sample BC-44-5

This core sample was drilled on site in the centre of a block of the external ring of the barrier (Fig. 17). The dry density of the sample was 1.52 g/cm^3 and the water content 28.5 %, corresponding to a degree of saturation of 100%.

Sample BC-44-5 was first tested in the low-pressure equipment (LP), with confining pressure of 0.6 MPa, but after 214 h of testing no flow occurred. The sample was then tested in the high-pressure steady-state setup, in the low confining pressure line (LCP) following the pressure path showed in Fig. 33, consisting of three phases:

- Phase 1: with an injection pressure of 0.2 MPa the confining pressure was increased from 0.6 to 1.0 MPa, and then the injection pressure was increased up to 0.5 MPa.
- Phase 2: the confining pressure was increased up to 1.5 MPa and then the injection pressure was increased up to 1.4 MPa
- Phase 3: under the same confining pressure (1.5 MPa) the injection pressure was decreased to 0.9 MPa and finally the confining pressure was decreased to 1.0 MPa.

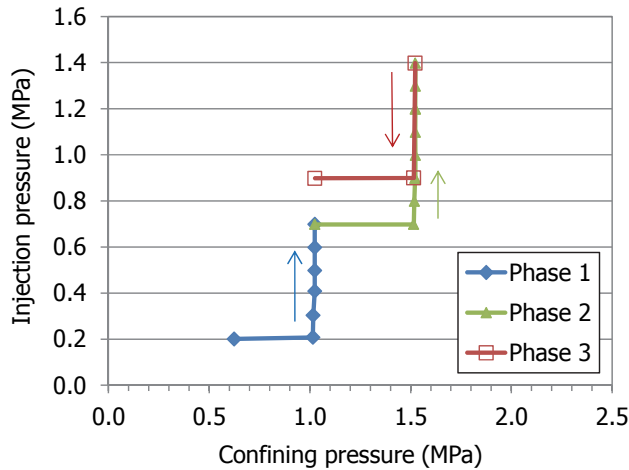


Fig. 33: Pressure path followed in the LCP setup for sample BC-44-5 (injection gas pressure given in absolute values)

Because of the high degree of saturation of the sample, flow did not take place for all the steps. Under a confining pressure of 1 MPa the injection pressure had to be increased up to 0.6 MPa to get a measurable flow. Under a confining pressure of 1.5 MPa, flow did not occur for injection pressures lower than 0.8 MPa. Fig. 34 shows the values of effective permeability computed in those steps in which flow occurred. The gas permeability was lower as the confining pressure was higher, but the effect of injection pressure was minor. The time in which the sample remained under a given stress situation had an effect on permeability. Hence, the lowest permeability was measured for a step in which the same confining pressure was kept for 119 h.

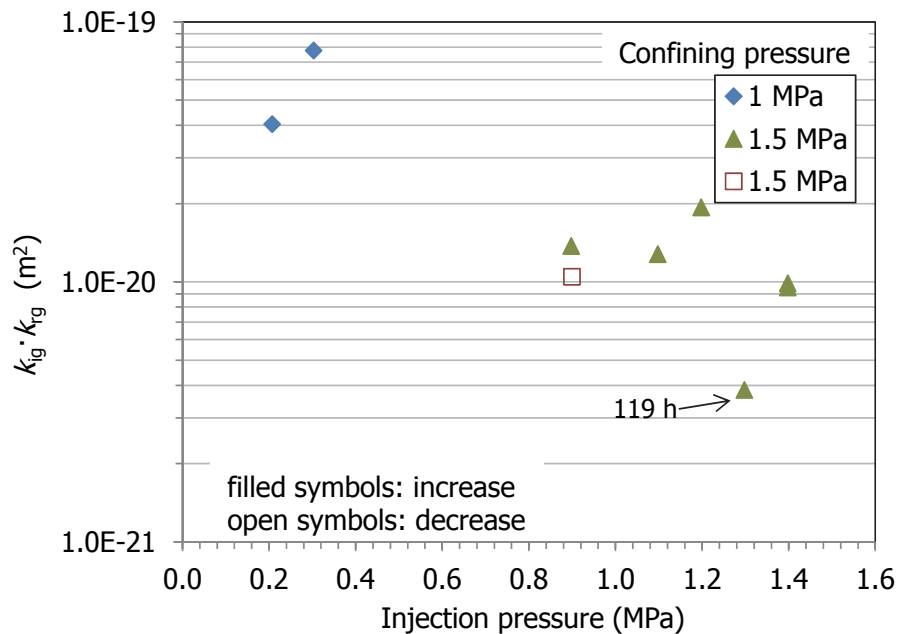


Fig. 34: Evolution of gas effective permeability at constant confining pressure for sample BC-44-5 (the duration of the longest step is indicated in hours)

4.1.7 Sample BC-44-6

This core sample was drilled on site between two blocks of the external ring of the barrier, one of which was the block from which sample BC-44-5 was drilled (Fig. 17). Hence, the difference between the two

samples was that BC-44-6 had an interface along. The dry density of the sample prepared for testing was 1.51 g/cm^3 and the water content 28.4%, corresponding to a degree of saturation of 97%.

The sample was first tested in the low-pressure equipment (LP), with confining pressures of 0.6 and 1 MPa. The decrease in injection pressure during the successive tests and the permeability values computed from them are shown in Fig. 35. The oscillations recorded replicate the daily temperature changes. The increase in confining pressure reduced the gas permeability.

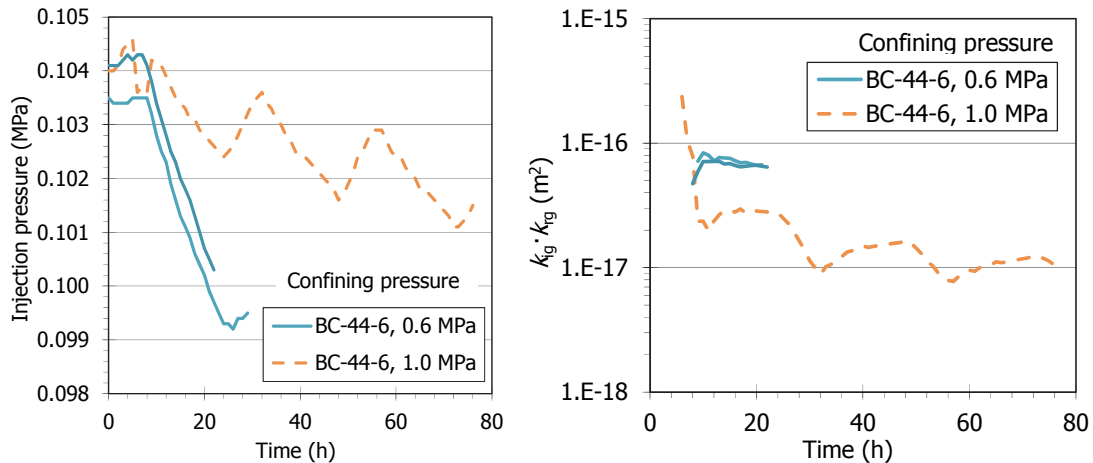


Fig. 35: Evolution of injection pressure and gas effective permeability ($k_{ig} \cdot k_{rg}$) in the low pressure equipment (LP) for sample BC-44-6 (injection gas pressure given in relative values)

Afterwards, the sample was tested in the high-pressure steady-state setup, in the low confining pressure line (LCP) following the pressure path showed in Fig. 36, consisting of two phases:

- Phase 1: starting from a confining pressure of 1 MPa and an injection pressure of 0.2 MPa, the two pressures were increased successively until reaching a confining pressure of 2.5 MPa and an injection pressure of 0.6 MPa.
- Phase 2: keeping a constant injection pressure of 0.6 MPa the confining pressure was increased up to 3 MPa and then it was decreased to 1 MPa.

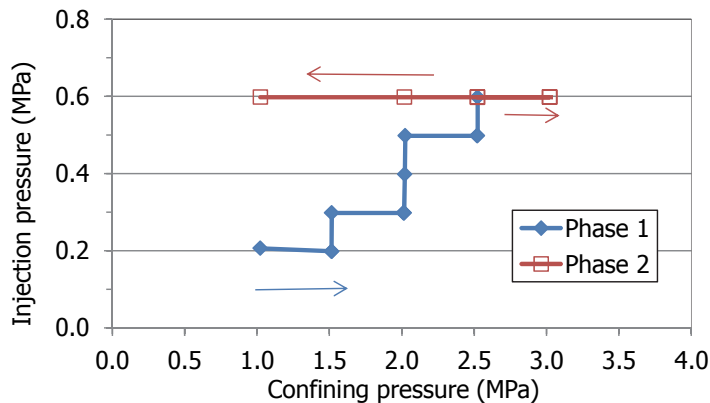


Fig. 36: Pressure path followed in the LCP setup for sample BC-44-6 (injection gas pressure given in absolute values)

Fig. 37 shows the effective permeabilities computed from the flow for different injection and confining pressures. The gas permeability decreased clearly with the increase in confining pressure and did not recover to the initial values when the sample was unloaded. The effect of injection pressure was not very significant, whereas when the sample was left to consolidate for some time under a given pressure situation, its permeability decreased.

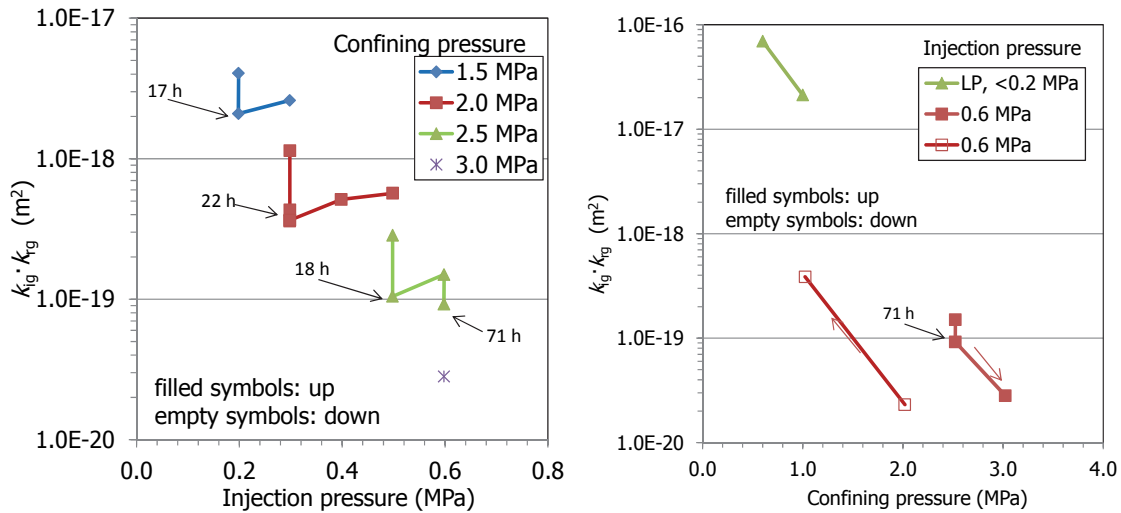


Fig. 37: Evolution of gas effective permeability during Phase 1 (left) and Phase 2 (right) for sample BC-44-6. The results obtained in the LP setup are also included. The duration of longer steps is indicated in hours

4.1.8 Sample BC-44-7

This core sample was drilled on site in the centre of a block of the inner ring of the barrier, close to sample BC-44-2 (Fig. 17). The dry density of the sample was 1.62 g/cm^3 and the water content 19.5%, corresponding to a degree of saturation of 79%.

Sample BC-44-7 was tested in the low-pressure equipment (LP) at confining pressures of 0.6 and 1 MPa. Fig. 38 shows the decrease in injection pressure during the tests (left) and the corresponding gas permeability values.

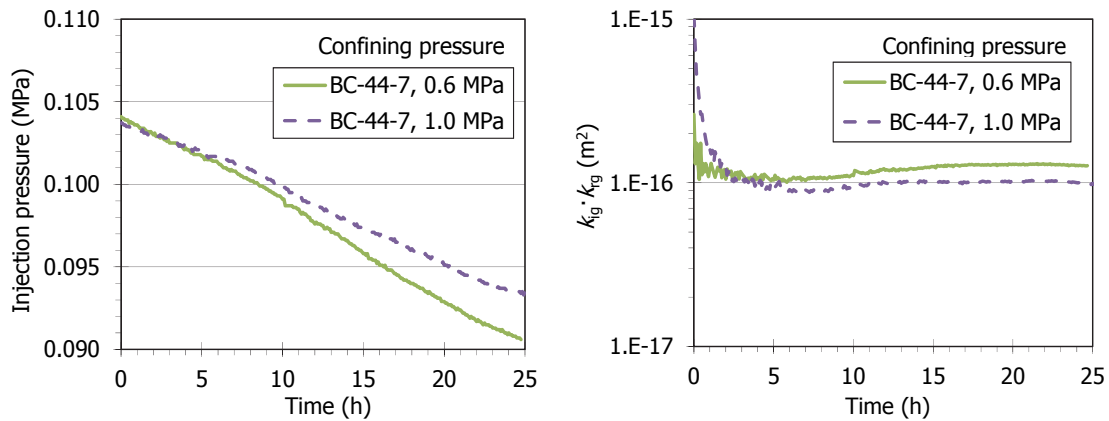


Fig. 38: Evolution of injection pressure and gas effective permeability ($k_{ig} \cdot k_{rg}$) in the low pressure equipment (LP) for sample BC-44-7 (injection gas pressure given in relative values)

Afterwards, the cell with the sample inside was moved to the high-pressure, steady state equipment, where it was initially tested in the high confining pressure line (HCP). After a failure caused by the tearing of the membrane, the cell had to be dismantled and the sample re-trimmed, because part of it was damaged (Fig. 39). The modified sample was further tested in the low confining pressure line (LCP). The detailed pressure path is shown in Fig. 40:

- Phase 1: In the HCP line the confining pressure was increased until reaching 6 MPa. At that point, the membrane was torn. The cell was dismantled and a modified sample of lower height was prepared to remove the damaged part of the sample.

- Phase 2: The test continued in the LCP line. The injection pressure was maintained at 0.2 MPa and the confining pressure was gradually increased until 9.5 MPa and finally decreased.



Fig. 39: Tearing of membrane during testing in the HCP line

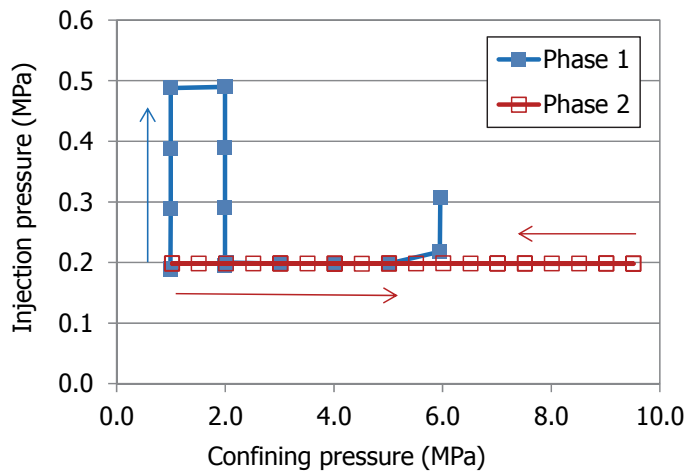


Fig. 40: Pressure path followed in the HP-S setup for sample BC-44-7. Phase 1: original sample tested in HCP line, Phase 2: modified sample tested in LCP line (injection gas pressure given in absolute values)

Gas permeability barely changed with the change of injection pressure under constant confining pressure (Fig. 41, left). However, the increase of confining pressure at constant injection pressure caused a clear gas permeability decrease. The permeability values obtained in the LP equipment were consistent with those obtained later in the HP-S equipment. It is also remarkable that the behaviour of the sample in the HP-S equipment before and after the failure was comparable. The confining pressure was increased after reaching a value of 9.5 MPa. The gas permeability increased with confining pressure reduction, but it was almost an order of magnitude lower for the same confining pressure than during loading (Fig. 41, right). This would indicate that the consolidation reached was irreversible. In fact, the dry density increased during the test from 1.62 to 1.65 g/cm³.

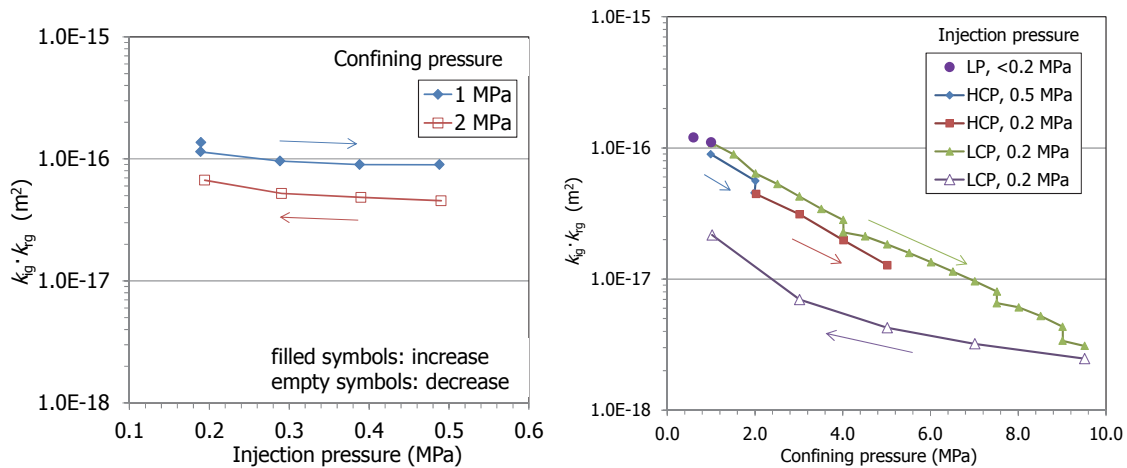


Fig. 41: Evolution of gas effective permeability at constant confining pressure (left, in the LCP equipment) and constant injection pressure (right) for sample BC-44-7

4.1.9 Sample BC-47-1

Sample BC-47-1 was drilled on site from the central part of a block in the external bentonite ring of section S47 (Fig. 17). The initial dry density and water content of the trimmed specimen were 1.55 g/cm^3 and 26.4%, respectively. The specimen was initially tested in the low-pressure equipment using a confining pressure of 0.6 MPa. Because of the low permeability of the sample, the decrease in injection pressure in the upstream tank during the test was very low and affected by the laboratory temperature (Fig. 42).

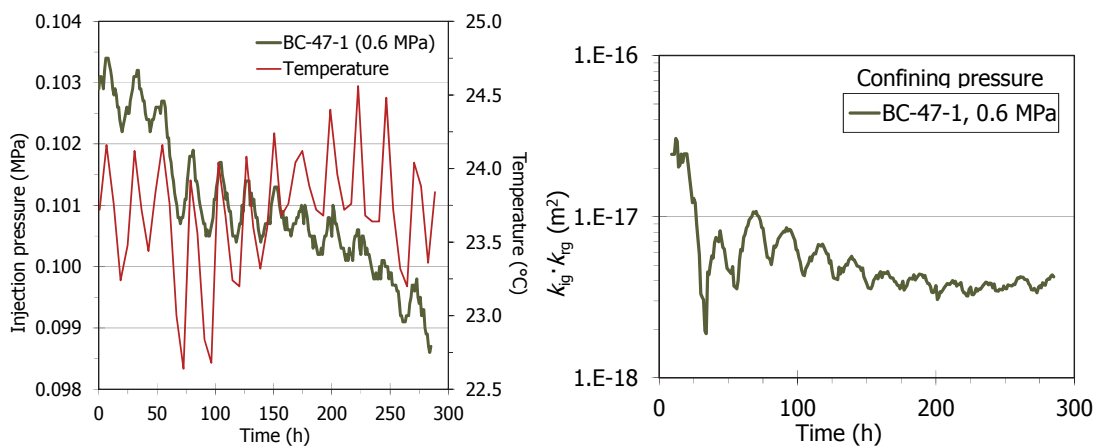


Fig. 42: Evolution of injection pressure and gas effective permeability ($k_{ig} \cdot k_{rg}$) in the low pressure equipment for sample BC-47-1 (injection gas pressure given in relative values)

Afterwards the sample was tested in the high-pressure, steady state (HP-S) equipment following two phases (Fig. 43) in the low confining pressure line (LCP):

- Phase 1: while confining pressure was maintained at 0.6 MPa, injection pressure was gradually increased from 0.2 to 0.5 MPa. Afterwards, confining pressure was increased until reaching 2.5 MPa, keeping an injection pressure of 0.5 MPa.
- Phase 2: the confining pressure was reduced while injection pressure remained at 0.5 MPa. Eventually the injection pressure was decreased.

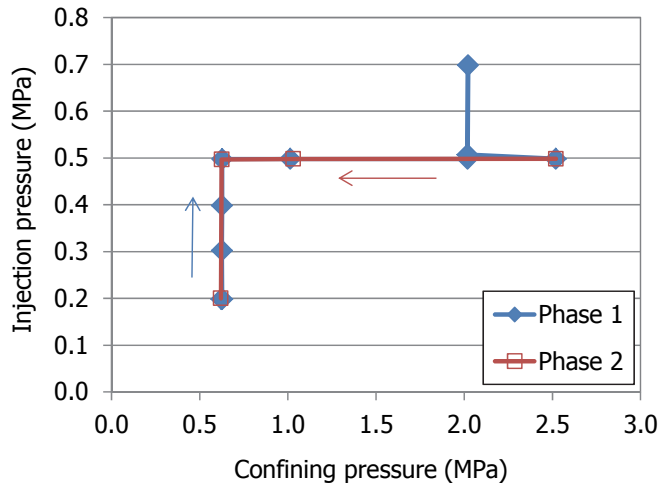


Fig. 43: Pressure path followed in the HP-S setup (LCP line) for sample BC-47-1 (injection gas pressure given in absolute values)

The effect of injection pressure on permeability was not clear, but in any case seemed minor (Fig. 44, left). However, the increase of confining pressure caused a clear decrease in permeability which was not recovered upon the release in confining pressure (Fig. 44, right). The fact that the sample remained two days under the maximum confining pressures (2-2.5 MPa) could be the explanation to this behaviour. It seems that the duration of the steps had an effect on permeability: thus, for a confining pressure of 2 MPa the permeability decreased noticeably while the sample was tested with different injection pressures. However, despite the fact that the duration of the unloading steps was very long, the initial permeability values were not recovered.

The permeability value obtained in the LP equipment was consistent with those obtained in the LCP.

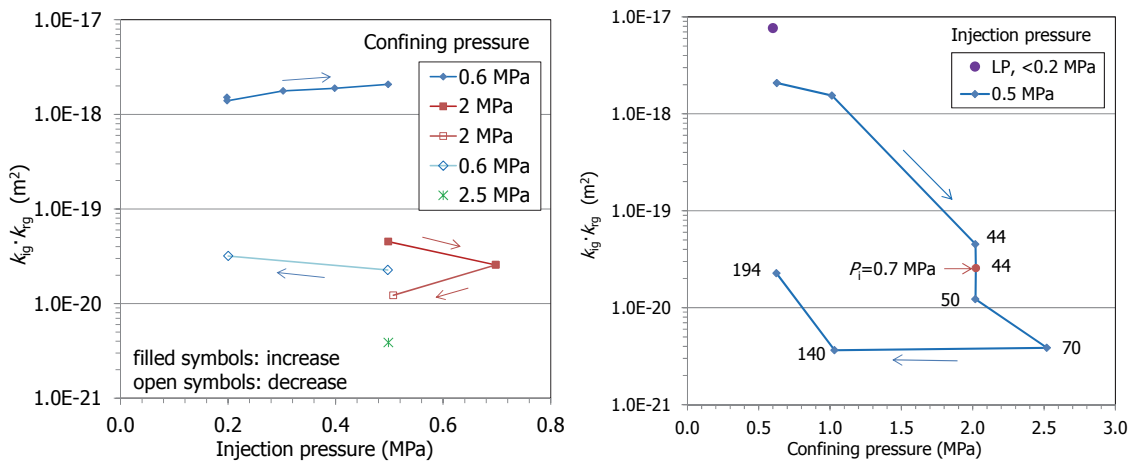


Fig. 44: Evolution of effective gas permeability at constant confining pressure (left) and constant injection pressure (right) in LCP equipment for sample BC-47-1. The duration of some steps is indicated in days

4.1.10 Sample BC-47-2

This sample was drilled on site from the lateral border of a block in the external bentonite ring of section S47 (Fig. 17), although according to the Sampling Book (Bárcena & García-Siñeriz 2015) it should have been drilled between two blocks and include the interface between them. The specimen resulting after trimming had a dry density of 1.54 g/cm³ and a water content of 26.4%. The sample was only measured in the high-pressure, unsteady-state equipment (HP-US), following two phases (Fig. 45):

- Phase 1: the confining pressure and the injection pressure were gradually increased to 3 and 0.5 MPa, respectively.
- Phase 2: the injection pressure was increased up to 1.6 MPa keeping a constant confining pressure of 3 MPa.
- Phase 3: the confining pressure was increased up to 12 MPa and then decreased while injection pressure was maintained at 1.6 MPa.

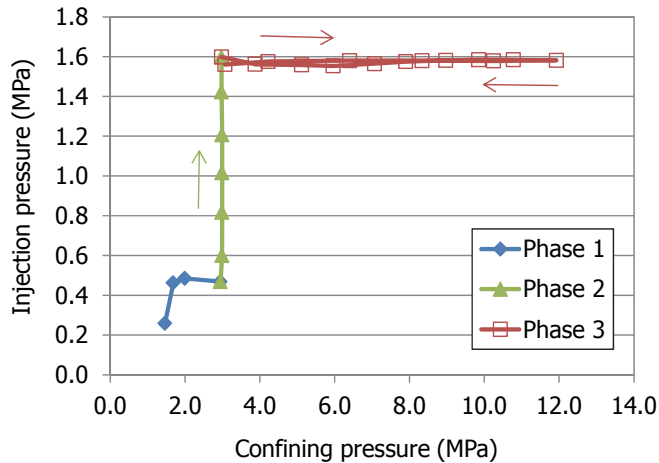


Fig. 45: Pressure path followed in the HP-US permeameter for sample BC-47-2 (injection gas pressure given in absolute values)

The permeability values –obtained using the pressure decrease in the downstream cylinder to compute flow with Eq. 7– are shown in Fig. 46. The initial increase in confining pressure up to 3 MPa (Phase 1) resulted in a steep decrease in permeability of more than two orders of magnitude. A possible explanation is that the sample remained for long (569 h) under this pressure condition. In contrast, the increase of confining pressure from 3 to 12 MPa (Phase 3) did not change permeability, which neither changed when the confining pressure was gradually released. The change in injection pressure for a constant confining pressure (Phase 2) did not affect significantly the permeability value.

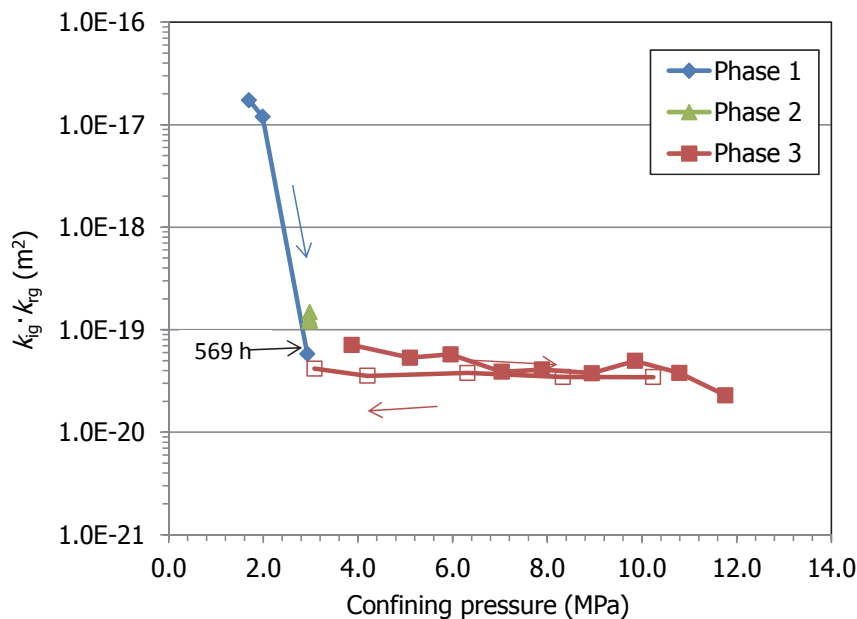


Fig. 46: Evolution of gas effective permeability ($k_g \cdot k_{rg}$) for sample BC-47-2, as confining pressure increased

4.1.11 Sample BC-47-3

Sample BC-47-3 was drilled on site from the central part of a block in the intermediate bentonite ring of section S47 (Fig. 17), although according to the Sampling Book (Bárcena & García-Siñeriz 2015) it should have been drilled between two blocks. Its initial dry density and water content were 1.61 g/cm^3 and 23.7%. The sample was tested in the high-pressure, steady-state equipment in the low confining pressure line (LCP). The sample was accidentally wetted during dismantling, which is why the final water content is higher than the initial. The phases followed during the test were (Fig. 47):

- Phase 1: the injection pressure was increased from 0.1 to 0.5 MPa, while confining pressure was maintained at 0.6 MPa.
- Phase 2: the confining pressure was increased to 0.8 MPa, and afterwards the injection pressure was reduced from 0.5 to 0.1 MPa.
- Phase 3: the confining pressure was increased until 1 MPa and then the injection pressure was increased from 0.1 to 0.9 MPa.
- Phase 4: the injection pressure was reduced to 0.1 MPa while the confining pressure was kept at 1 MPa.
- Phase 5: the confining pressure was decreased to 0.6 MPa, increased and decreased again, with the injection pressure kept at values close to 0.1 MPa

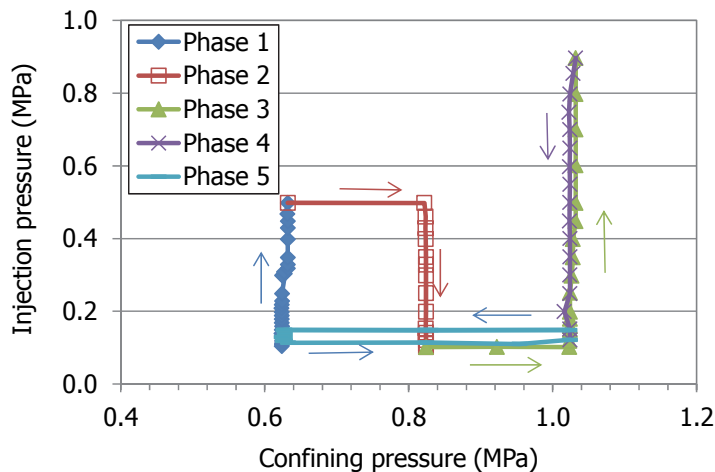


Fig. 47: Pressure path followed in the LCP setup for sample BC-47-3 (injection gas pressure given in absolute values)

The duration of most of the steps was less than 1 hour, because the flow was high and became quickly steady. The permeability values obtained during the phases in which the injection pressure was changed while the confining pressure was constant are shown in Fig. 48 (left), and the values obtained in the phases of constant injection pressure and changing confining pressure are shown on the right of the same Figure. The maximum confining pressure applied, 1 MPa, was much lower than the expected swelling pressure. For all the confining pressures tested the change in injection pressure did not affect the permeability value, except for injection pressures below 0.15 MPa. Below this value the permeability decreased with the decrease in injection pressure. Fig. 48 (right) shows that in the range of confining pressures between 0.6 and 1.0 MPa, the permeability tended to decrease very slightly with the increase in confining pressure, and for a given confining pressure the permeability was lower the lower the injection pressure (maybe because higher injection pressures would make the confining pressure less effective). When the confining pressure was released keeping a constant injection pressure of 0.15 MPa, the permeability for a given confining pressure was lower than previously, which would point to the occurrence of irreversible changes in the bentonite microstructure, despite the fact that the pressures applied were low.

A few of the steps lasted more than 1 hour because the gas injection was stopped while the confining pressure kept acting on the sample. This caused in some cases a decrease in permeability that was

usually recovered in the following step. A couple of these “longer-than-average” steps are indicated with arrows in Fig. 48 (left).

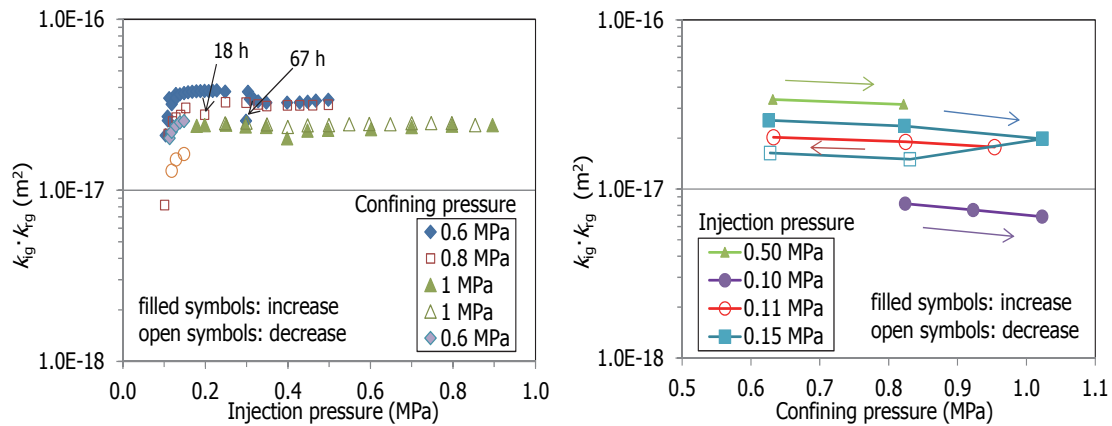


Fig. 48: Evolution of gas effective permeability at constant confining pressure (left) and constant injection pressure (right) for sample BC-47-3

4.1.12 Sample BC-47-4

Sample BC-47-4 was drilled on site between two blocks of the middle ring of the bentonite barrier (Fig. 17), hence the core had a longitudinal interface (although according to the Sampling Book (Bárcena & García-Siñeriz 2015) it should have been drilled in the central part of a block). Although the interface was not initially visible, upon trimming of the sample the two parts of it detached (Fig. 49). The initial dry density and water content of the specimen once trimmed were 1.59 g/cm³ and 24.8%, respectively.



Fig. 49: Appearance of longitudinal interface of sample BC-47-4

This sample was only tested in the high-pressure, unsteady-state (HP-US) equipment, following these phases (Fig. 50):

- Phase 1: the injection pressure was set to values between 0.1 and 0.3 MPa and the confining pressure was increased from 2 to 7 MPa; afterwards, keeping constant this confining pressure, the injection pressure was increased up to 2.5 MPa.
- Phase 2: the confining pressure was increased from 7 to 9 MPa.
- Phase 3: the confining pressure was decreased from 9 to 3 MPa and then the injection pressure was decreased to 1.5 MPa.

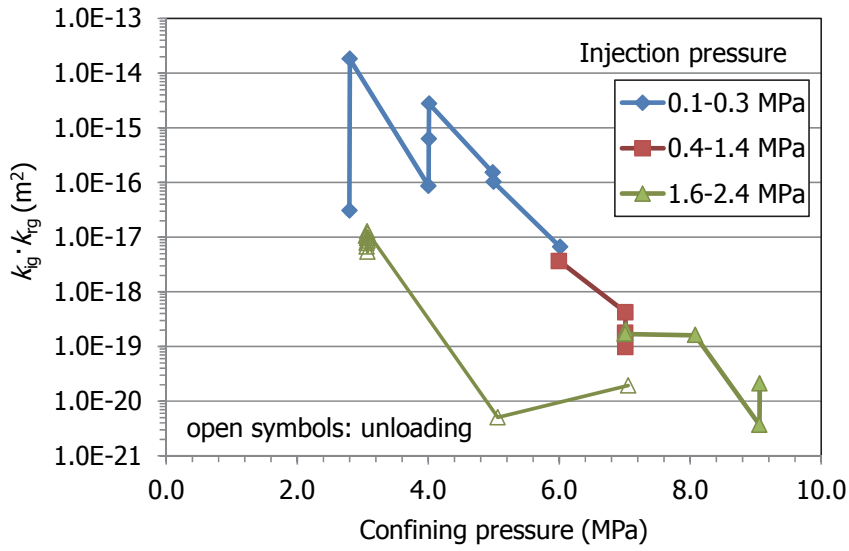


Fig. 52: Evolution of gas effective permeability ($k_{ig} \cdot k_{rg}$) for sample BC-47-4 as a function of confining pressure

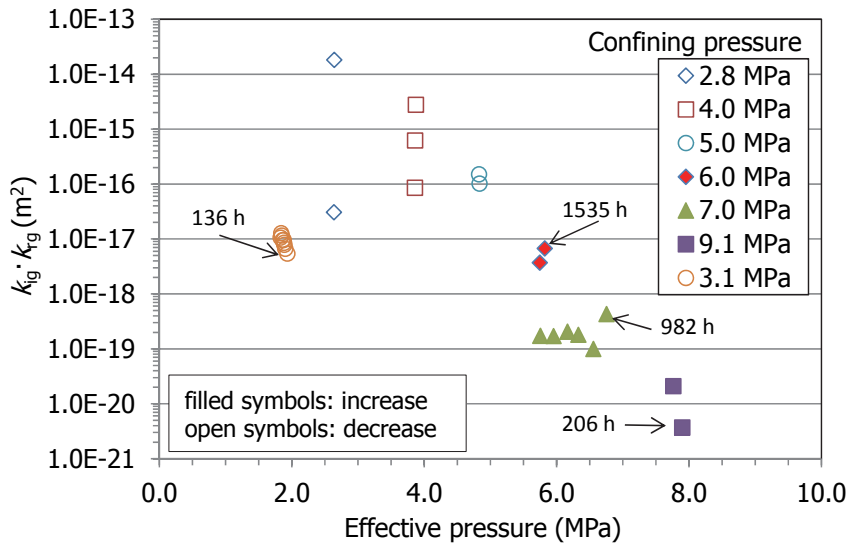


Fig. 53: Evolution of gas permeability at constant confining pressure for sample BC-47-4 (the duration of longer steps is indicated in hours)



Fig. 54: Initial and final appearance of sample BC-47-4 (the arrows indicate the same position before and after testing)

4.1.13 Sample BC-47-6

Sample BC-47-6 was drilled on site between two blocks in the internal ring of the bentonite barrier, i.e. close to the heater (Fig. 17). Accordingly, it had a longitudinal interface along the core (Fig. 55) and an initial dry density and water content of 1.64 g/cm^3 and 19.6%. This sample was tested in the low-pressure equipment (LP), and then in the high confining pressure line (HCP) of the high-pressure, steady state permeameter.

Fig. 56 shows the evolution in injection pressure (left) during the tests performed in the LP equipment, and the gas permeability computed from this decrease (right) at different confining pressures. The increase in confining pressure stabilized and reduced permeability.



Fig. 55: Initial appearance of sample BC-47-6

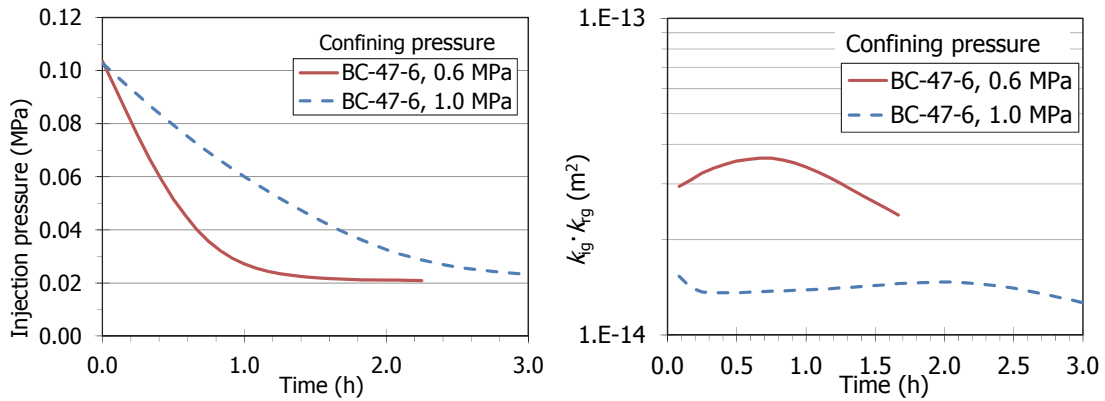


Fig. 56: Evolution of injection pressure and gas effective permeability ($k_{ig} \cdot k_{rg}$) in the low pressure equipment for sample BC-47-6 (injection gas pressure given in relative values)

The sample was afterwards tested in the high-pressure, steady state equipment in the high confining pressure line (HCP). The injection pressure was maintained at 0.1 MPa and the backpressure was kept atmospheric while the confining pressure was increased from 0.6 to 2 MPa.

The gas permeability obtained in both setups is shown in Fig. 57. The gas permeability decreased with the confining pressure increase, but the values obtained in the high-pressure equipment were higher for the same confining pressures, which could be because the confining stress could be more effective in the low pressure setup, since the injection pressure decreased continuously in this setup (Fig. 56 left). The decrease in permeability between the two consecutive steps at 1.5 MPa of confining pressure was caused by the time between steps (2.5 h vs. a few minutes in the previous steps). The decrease in gas permeability observed after the sample was compressed at this pressure could have been caused by the closing of the interface, which would have been the main gas pathway at the beginning of the test. At that point, the membrane was pierced and the cell had to be dismantled. The sample was wetted at the ends (Fig. 58, right).

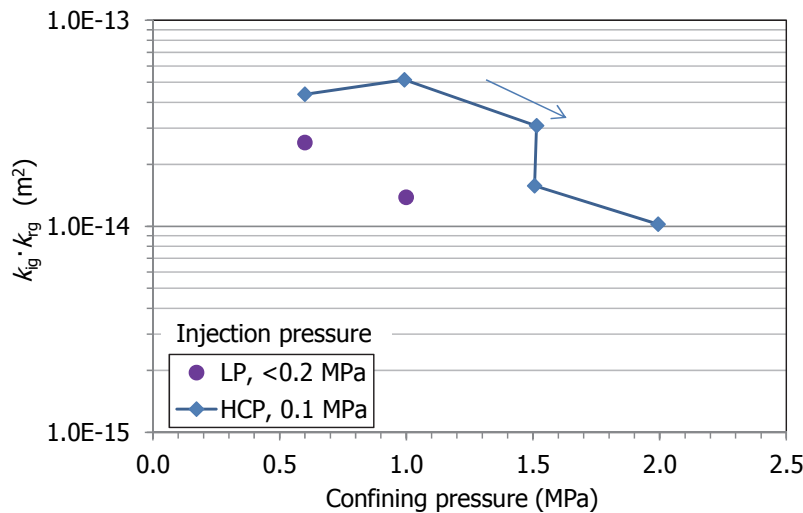


Fig. 57: Evolution of gas effective permeability ($k_{ig} \cdot k_{rg}$) for sample BC-47-6 as confining pressure increased



Fig. 58: Piercing of membranes (left) and appearance of the sample after failure (right)

4.1.14 Sample BB-53-4-2

Sample BB-53-4-2 was drilled in the laboratory from a block from the external ring of the barrier in section S53 (Fig. 17). The initial dry density and water content of the specimen once trimmed were 1.59 g/cm^3 and 25.1%, corresponding to a degree of saturation of 96%. The sample was only tested in the low-pressure equipment (LP) at a constant confining pressure of 0.6 MPa, but although the pressure was applied for more than 300 h no flow took place.

4.1.15 Sample BB-53-5-1

Sample BB-53-5-1 was drilled in the laboratory in a block from the middle ring of the barrier in section S53 (Fig. 17). Its initial dry density and water content were 1.63 g/cm^3 and 23.3%, corresponding to a degree of saturation of 97%. The specimen was first tested for almost 500 h in the low-pressure equipment under a confining pressure of 0.6 MPa, but no flow took place.

Afterwards the sample was tested in the low confining pressure line (LCP) of the high-pressure, steady-state equipment, in which the confining pressure and the injection pressure were increased gradually up to 1.7 and 1.2 MPa, respectively (Fig. 59).

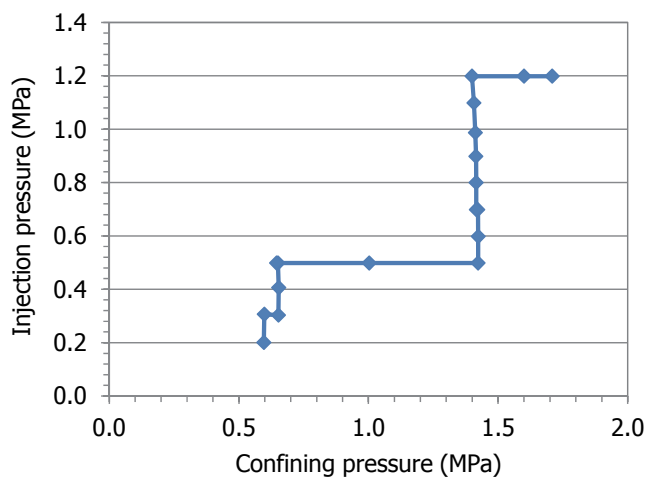


Fig. 59: Pressure path followed in the LCP setup for sample BB-53-5-1 (injection gas pressure given in absolute values)

The gas permeability values obtained are plotted in Fig. 60 as a function of the injection pressure applied (left) and of the confining pressure (right). For a given confining pressure, the increase in injection pressure caused an increase of permeability. On the other hand, the increase in confining pressure from 0.6 to 1.7 MPa caused a significant decrease in permeability.

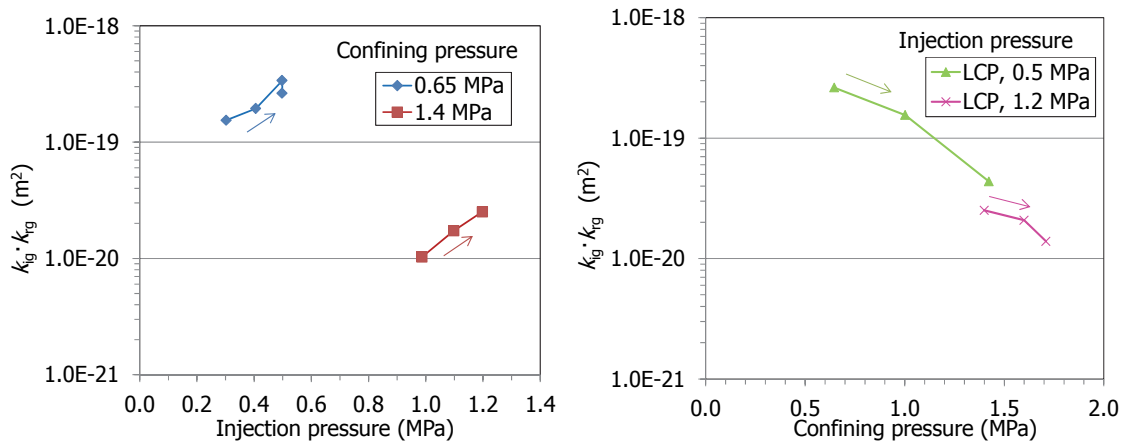


Fig. 60: Evolution of gas effective permeability at constant confining pressure (left) and constant injection pressure (right) for sample BB-53-5-1

4.1.16 Sample BB-53-5-2

Sample BB-53-5-2 was drilled in the laboratory in a block from the middle ring of the barrier in section S53 (Fig. 17). Its initial dry density and water content were 1.63 g/cm^3 and 22.9%, corresponding to a degree of saturation of 94%. Their characteristics were similar to those of specimen BB-53-5-1 because they were both drilled from the same block.

The sample was initially tested for 300 h in the low pressure equipment (LP) but no flow took place. Afterwards the sample was tested in the high confining pressure line (HCP) of the high-pressure, steady-state equipment following two phases:

- Phase 1: the injection pressure and the confining pressure were increased to 0.6 and 1.4 MPa, respectively.
- Phase 2: the injection pressure decreased while confining pressure remained constant and finally increased.

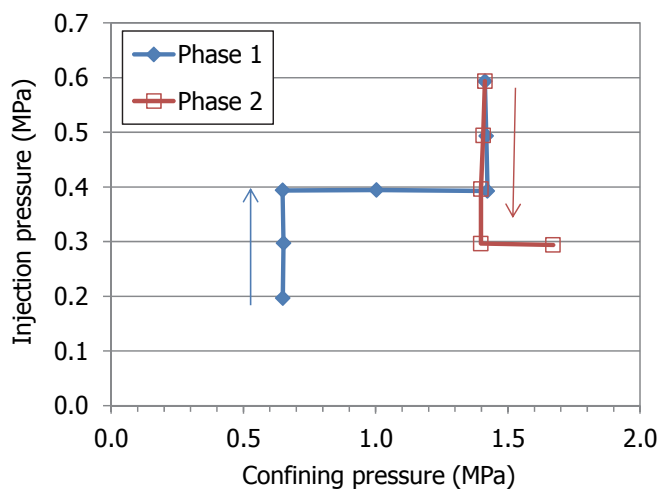


Fig. 61: Pressure path followed in the HCP setup for sample BB-53-5-2 (injection gas pressure given in absolute values)

The gas permeability values obtained are plotted in Fig. 62 as a function of the injection pressure applied (left) and of the confining pressure (right). For a given confining pressure, the permeability tended to increase as the injection pressure increased. On the other hand, the increase in confining pressure from 0.6 to 1.7 MPa caused a significant decrease in permeability.

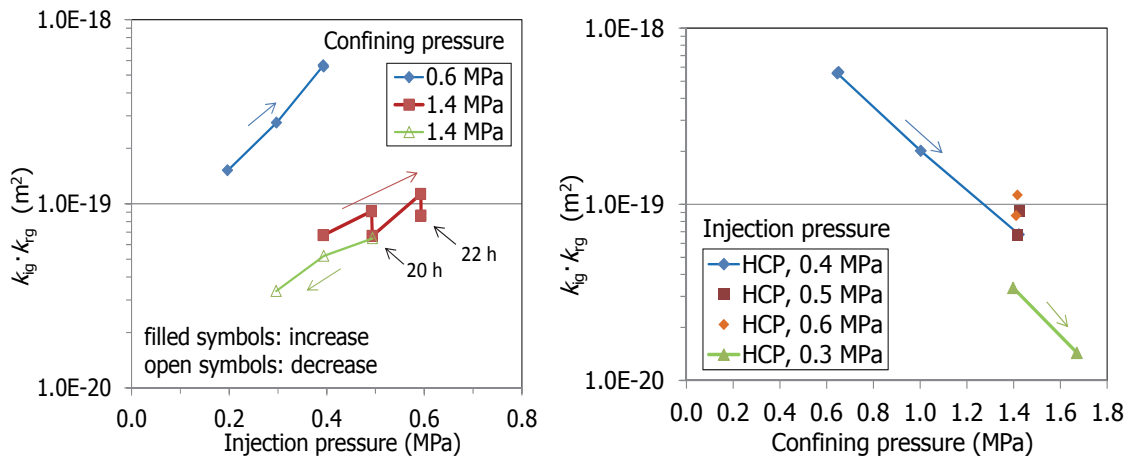


Fig. 62: Evolution of gas permeability at constant confining pressure (left) and constant injection pressure (right) for sample BB-53-5-2

4.1.17 Sample BC-53-1

This core sample was drilled on site in the internal ring of section S53, close to sample BC-53-2. Its initial dry density and water content were 1.59 g/cm³ and 23.7 %.

The specimen was initially tested in the low-pressure setup at a confining pressure of 0.6 MPa (Fig. 63).

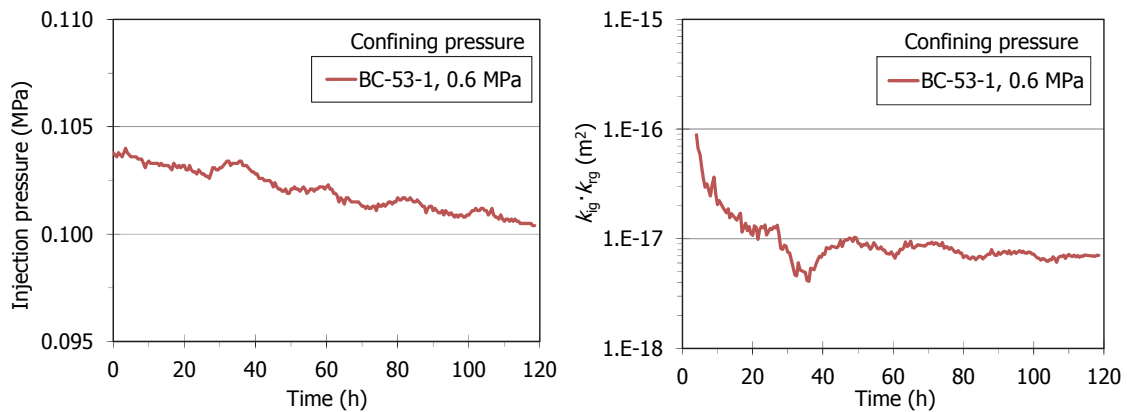


Fig. 63: Evolution of injection pressure and gas effective permeability ($k_{ig} \cdot k_{rg}$) in the low pressure equipment (LP) for sample BC-53-1 (injection gas pressure given in relative values)

Afterwards, the sample was tested in the high-pressure steady-state equipment (LCP) starting with a confining pressure of 0.6 MPa, in order to maintain the same conditions as in the low-pressure equipment. The stress path followed in this test was the following:

- Phase 1: the test started at 0.6 MPa of confining pressure and 0.2 MPa of injection pressure. Then, the confining pressure was increased up to 1.0 MPa.
- Phase 2: the injection pressure was increased from 0.2 to 0.6 MPa, keeping a confining pressure of 1.0 MPa.
- Phase 3: the confining pressure was increased from 1.0 to 2.2 MPa, which was the maximum confining pressure that could be applied in the triaxial cell.

- Phase 4: unloading of the sample down to 1.0 MPa.

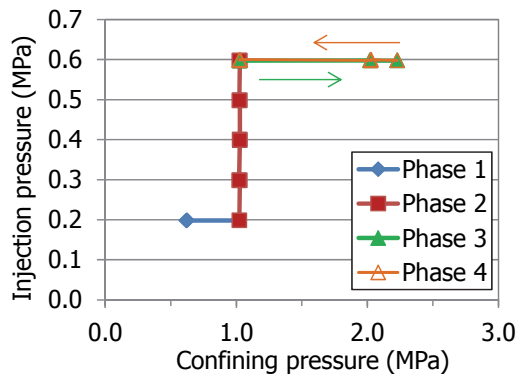


Fig. 64: Pressure path followed in the LCP setup for sample BC-53-1 (injection gas pressure given in absolute values)

The results of the gas permeability test are plotted in Fig. 65. The injection pressure did not affect the permeability values obtained under 1 MPa of confining pressure (Fig. 65, left). However, the decrease of gas permeability with the increase of confining pressure is clear (Fig. 65, right). The effect of the duration of the step can be seen in the values obtained for two consecutive steps under confining pressure 2 MPa, the second of which lasted 21 h, resulting in a decrease of permeability. The value obtained in the LP equipment is consistent with those obtained in the steady-state permeameter. Because of a failure in the equipment the confining pressure could not be increased beyond 2.2 MPa. For this reason, in this test the maximum confining pressure reached did not correspond to the pressure necessary to suppress gas flow through it. After this event, the sample was unloaded. During unloading, the sample did not recover the original values obtained during loading for the same confining pressures, probably because of the irreversible consolidation experienced by the sample during loading. In fact, the dry density of the sample increased from 1.59 to 1.61 g/cm³ during the test.

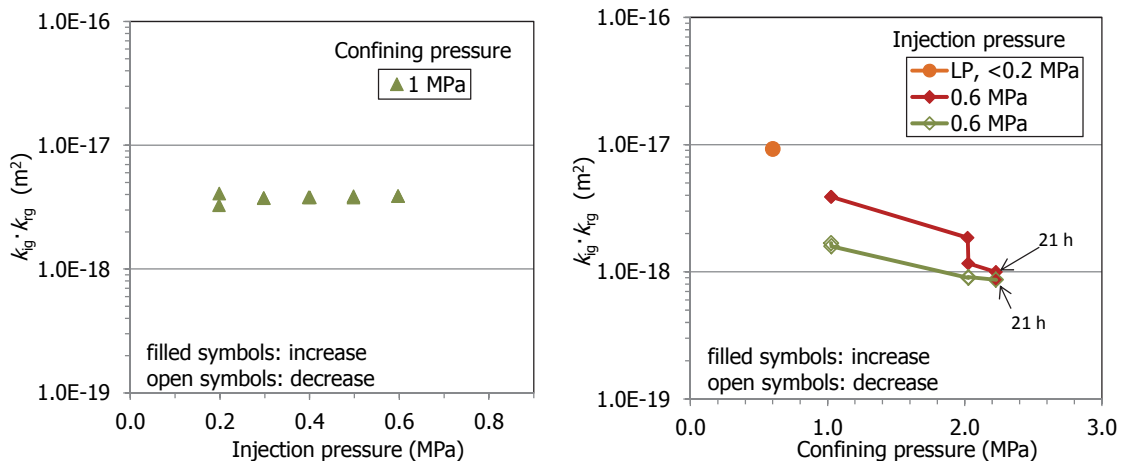


Fig. 65: Evolution of gas effective permeability at constant confining pressure (left) and constant injection pressure (right) for sample BC-53-1

4.1.18 Sample BC-53-2

This core sample was drilled on site between two blocks in the inner ring of the barrier, close to sample BC-53-1 (Fig. 17). As a consequence, it had a longitudinal interface along the core. Although the interface was not initially visible, after drying at the end of the test to determine the final water content of the sample, the two parts of the core split. The dry density of the sample was 1.63 g/cm³ and the water content 22.5%, corresponding to a degree of saturation of 93%.



Fig. 66: Initial (left) and final (middle) appearance of sample BC-53-2. The interface was visible only after drying in the oven (right)

Sample BC-53-2 was first tested in the low-pressure equipment (LP), under confining pressures of 0.6 and 1.0 MPa. The pressure decrease in the upwards vessel during both tests and the permeability values computed from it are shown in Fig. 67. For a confining pressure of 0.6 MPa the gas permeability tended to increase towards the end of the test, which could indicate that certain drying took place because of the gas flow.

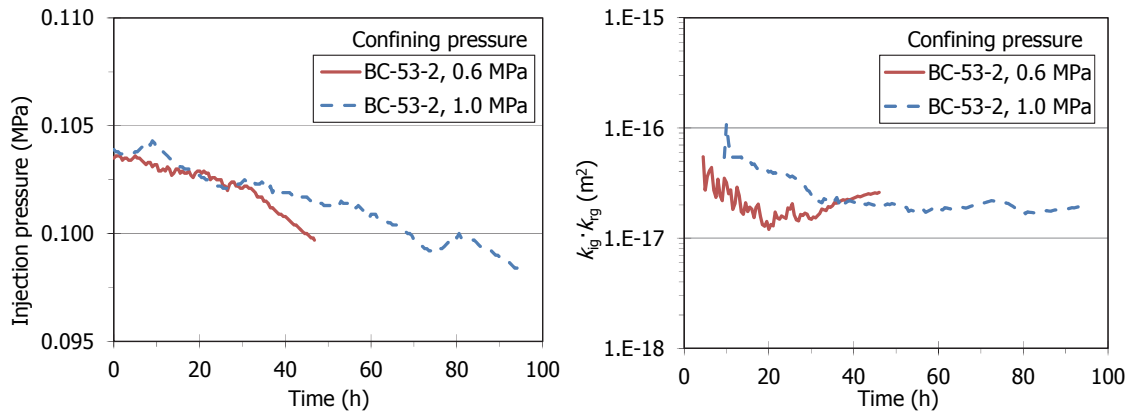


Fig. 67: Evolution of injection pressure and gas effective permeability ($k_{ig} \cdot k_{rg}$) in the low pressure equipment (LP) for sample BC-53-2 (injection gas pressure given in relative values)

Afterwards, the sample was tested in the high-pressure steady-state equipment (low confining pressure line, LCP) starting with the last confining pressure applied in the LP equipment, 1.0 MPa. The stress path followed in this test is shown in Fig. 68:

- Phase 1: the test started at a confining pressure of 1.0 MPa and 0.2 MPa of injection pressure. The injection pressure was increased from 0.2 to 0.4 MPa, keeping constant confining pressure.
- Phase 2: the confining pressure was increased from 1.0 to 5.0 MPa, keeping an injection pressure of 0.4 MPa.
- Phase 3: unloading of the sample to a pressure as low as the initial value.

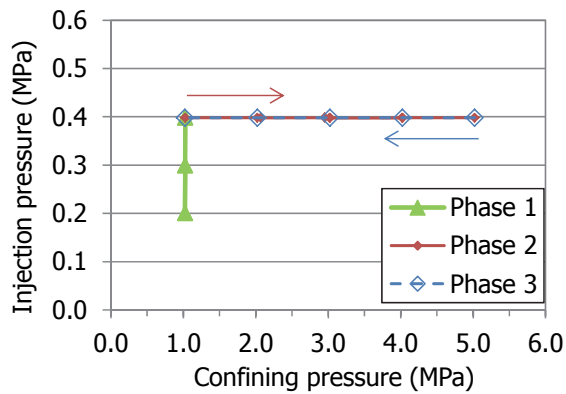


Fig. 68: Pressure path followed in the LCP setup for sample BC-53-2 (injection gas pressure given in absolute values)

During the increase of injection pressure from 0.2 to 0.4 MPa in Phase 1, the gas permeability remained constant (Fig. 69, left). However, the increase of confining pressure caused a clear decrease of gas permeability. Fig. 69 (right) shows the effect of confining pressure on gas permeability in both setups. The increase of confining pressure from 1 to 5 MPa caused a progressive decrease of flow until no flow took place for a confining pressure of 5 MPa. Then, the sample was unloaded. During this phase, there was no measurable flow until the confining pressure was decreased to 2 MPa, when the gas permeability computed was an order of magnitude lower than that for the same confining pressures during loading. This would indicate that the consolidation was irreversible. In fact, the dry density increased during the test from 1.63 to 1.64 g/cm³. During dismantling of the sample, the interface revealed and the sample was easily separated into two pieces (Fig. 70).

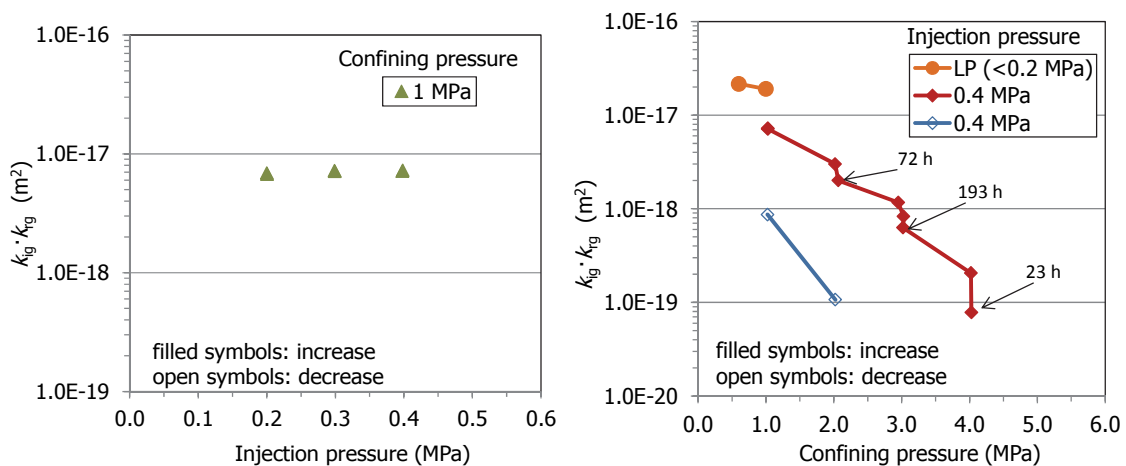


Fig. 69: Evolution of gas effective permeability at constant confining pressure (Phase 1, left) and constant injection pressure (Phase 2 and 3, right) for sample BC-53-2



Fig. 70: Appearance of sample BC-53-2 at the end of gas testing (left, the arrow indicates the interface) and after drying in the oven (right)

4.1.19 Sample BC-53-3

Sample BC-53-3 was drilled from the central part of a block in the external ring, in section S53, close to sample BC-53-4. The initial dry density and water content once trimmed were 1.54 g/cm^3 and 29%, corresponding to a degree of saturation of 104%.

The sample was first tested in the low-pressure equipment (LP) at confining pressure of 0.6 MPa. Then the confining pressure was increased to 1.0 MPa. Under this pressure the flow was very low and the changes recorded were related to temperature oscillations, which is why no permeability values could be computed (Fig. 71).

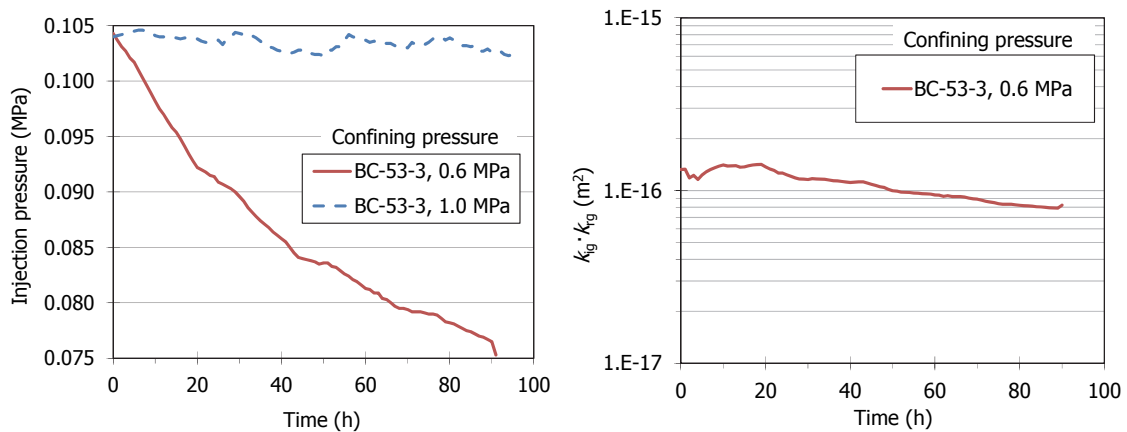


Fig. 71: Evolution of injection pressure and gas effective permeability ($k_{ig} \cdot k_{rg}$) in the low pressure equipment (LP) for sample BC-53-3 (injection gas pressure given in relative values)

The sample was then tested in the high-pressure steady-state setup (low confining pressure line, LCP), where the injection pressure was increased under a constant confining pressure of 1 MPa, in order to allow flow as the confining stress became less effective. Fig. 72 shows the three phases followed during the test:

- Phase 1: with a confining pressure of 1 MPa, the injection pressure was increased from 0.2 to 0.8 MPa.

- Phase 2: keeping an injection pressure of 0.8 MPa, the confining pressure was increased up to 2 MPa.
- Phase 3: unloading of the sample, decreasing the confining pressure up to the initial value (1 MPa).

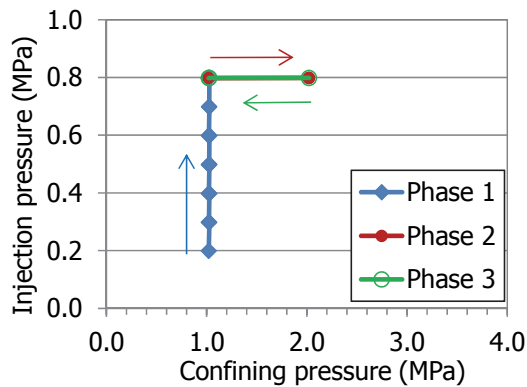


Fig. 72: Pressure path followed in the LCP setup for sample BC-53-3 (injection gas pressure given in absolute values)

Fig. 73 (left) shows the effective gas permeability at a constant confining pressure, computed for different injection pressures. Keeping a constant confining pressure of 1 MPa, the increase of the injection pressure had an effect on the permeability values, causing them to increase. The increase in injection pressure (0.1 MPa each step) caused a permeability increase of half an order of magnitude each step. The duration of each step was 24 h, except for the application of 0.5 MPa of injection pressure, which lasted almost 4 days. The larger duration of this step did not seem to affect the gas permeability value. Then, the confining pressure was increased up to 2 MPa (Phase 2), causing a permeability decrease of two orders of magnitude (Fig. 73, right). In fact the flow was very low, below the turndown value. It is remarkable that during the first 22 hours of application of this confining pressure, there was a reduction of one order of magnitude in the gas permeability. However, after 69 more hours of applying the same confining pressure, the modification of permeability was minor. This would indicate that the sample consolidation occurred during the first day of application of the confining pressure. During this time the valves of the cell were closed, and hence no gas flow took place through the specimen. The permeability was computed from the flow measured after the valves were opened again, and they remained open for just one hour, which was enough time to get a steady flow. This procedure was established in order to avoid excessive drying of the bentonite because of the dry gas flow. Upon unloading (Phase 3), the sample recovered the gas permeability previously measured for the same confining pressure during loading. The sample did consolidate during the test (the dry density increased from 1.54 to 1.56 g/cm³) and hence the fact that the permeability came back to the initial value upon unloading could have been caused by the drying that took place, with the water content decreasing from 29.0 to 25.7%.

The gas permeability value obtained in the low-pressure equipment (LP) was consistent with those measured in the LCP equipment.

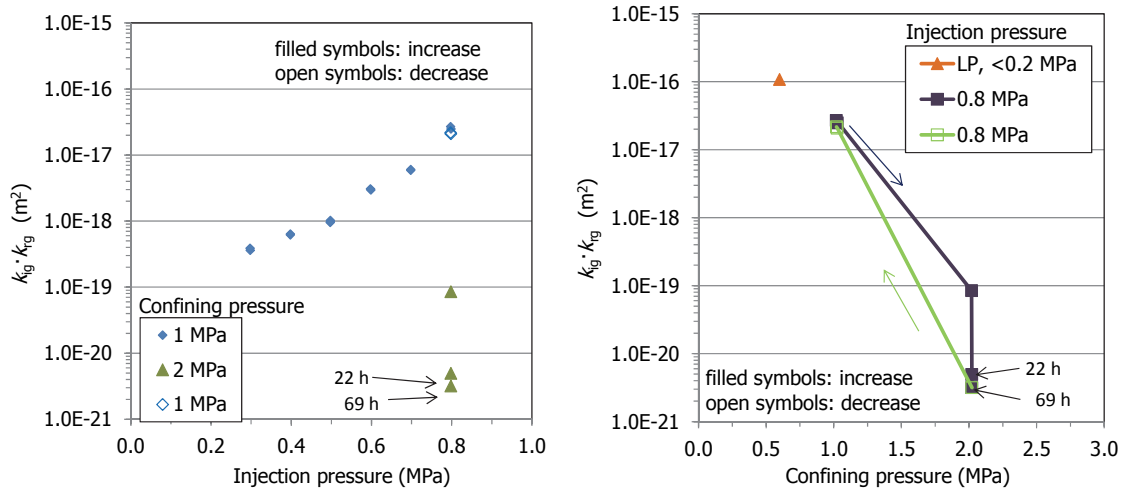


Fig. 73: Evolution of gas effective permeability at constant confining pressure (left) and constant injection pressure (right) for sample BC-53-3

4.1.20 Sample BC-53-4

This core sample was drilled on-site between two blocks, in the external ring of section S53, close to sample BC-53-3. Although the degree of saturation of this sample was high (96%), the longitudinal interface along the core was very clear and open. The initial dry density and water content of the sample were 1.53 g/cm^3 and 27.1%, respectively.



Fig. 74: Initial appearance of sample BC-53-4

This sample was tested in the low-pressure equipment under two confining pressures, 0.6 and 1.0 MPa. As it is shown in Fig. 75, all the gas in the tank went through the sample in less than 30 min for both confining pressures.

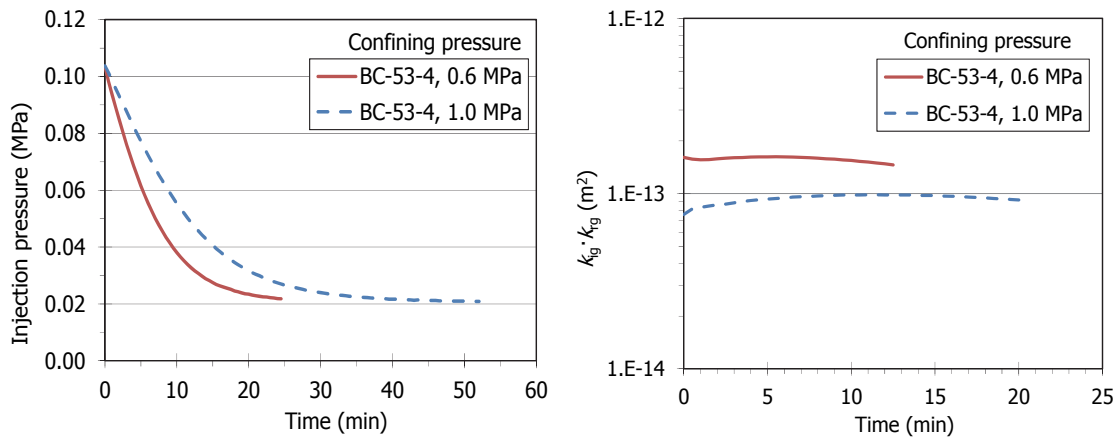


Fig. 75: Evolution of injection pressure and gas effective permeability ($k_{ig} \cdot k_{rg}$) in the low pressure equipment (LP) for sample BC-53-4 (injection gas pressure given in relative values)

Afterwards, the sample was measured in the high-pressure, steady-state equipment, in the low confining pressure line. Because of the large flow, the test followed only two phases:

- Phase 1: the confining pressure was increased from 1 to 6 MPa, keeping constant the injection pressure.
- Phase 2: the confining pressure was decreased up to the initial value of 1 MPa.

In the first step, for a confining pressure of 1 MPa, the flow was too high to be measured, because the equipment cannot measure gas flows over 100 mL/min. For this reason the confining pressure was quickly increased, in order to reduce the gas flow. The increase of confining pressure at constant injection pressure caused a reduction of gas permeability, higher the higher the time elapsed between steps (Fig. 76). It has to be reminded that most of the time the valves of the cell were closed, and they were open only for short periods of time to allow the gas flow through the samples and compute permeability. But during those periods in which the valves were closed, the confining pressure was acting on the sample, and that is the reason why when the valves were opened again the flow was lower, even if the pressure state was the same. The flow decreased drastically when the confining pressure of 5 MPa was kept for four days. The increase of confining pressure to 6 MPa caused a reduction of flow to values below the turndown of the flowmeter, and consequently the permeability value computed was only tentative and the confining pressure was not further increased, because it can be considered that the interface closed. No measurable flow took either place when the confining pressure was released to 5 MPa. Conversely, the gas permeability increased when confining pressure decreased below 4 MPa, but the increase was not significant until the confining pressure went down to 2 MPa. Above this confining pressure flow was very low, below the turndown value of the flowmeters. The permeability values during the uploading were lower than values measured during loading for the same confining pressures. This would indicate that the consolidation reached and the closing of the interface was irreversible. In fact, the dry density increased during the test from 1.53 to 1.60 g/cm³ (the water content decreased from 27.1 to 25.1%, but the degree of saturation increased during the test). During dismantling of the sample, the interface revealed and the sample easily split into two pieces, although the two parts were tighter and the gap between them was much thinner than before the test (Fig. 77).

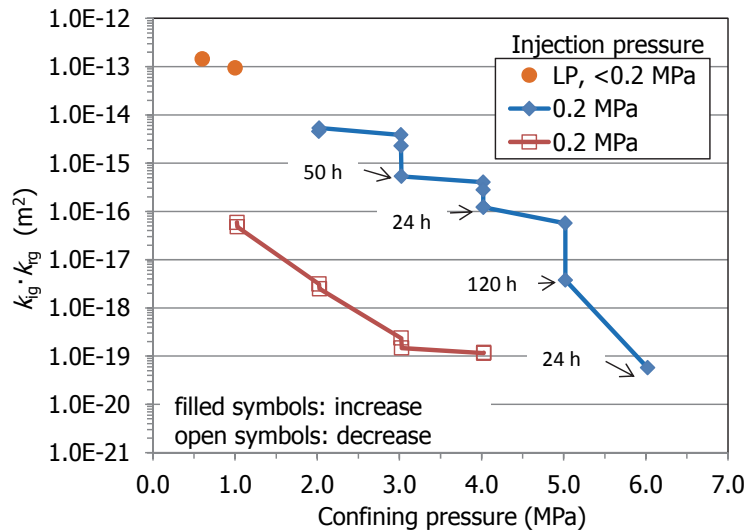


Fig. 76: Evolution of gas effective permeability at constant injection pressure for sample BC-53-4



Fig. 77: Final appearance of sample BC-53-4. The arrows indicate the interface after testing

4.1.21 Sample BC-53-5

This core sample was drilled on site between two blocks in the intermediate ring of section S53, close to sample BC-53-6. Accordingly, it had a longitudinal interface along the core (Fig. 78). The initial dry density and water content were 1.58 g/cm^3 and 24.8%, respectively. This sample was tested in the low-pressure equipment (LP), and then in the low confining pressure line (LCP) of the high-pressure, steady-state permeameter.

Fig. 79 shows the evolution of the injection pressure (left) and the gas permeability computed for 0.6 and 1.0 MPa of confining pressure (right) in the low pressure equipment. The flow was very slow in both cases.

Then the sample was tested in the high-pressure steady-state setup (LCP), following the phases showed in Fig. 80:

- Phase 1: the confining pressure was increased to 2 MPa, and since there was no flow, the injection pressure was increased up to 0.3 MPa, in order to get a measurable flow. Then, the confining pressure was increased up to 3 MPa, keeping the previous injection pressure value.
- Phase 2: unloading of the sample from 3 MPa to 1 MPa, with constant injection pressure of 0.3 MPa.

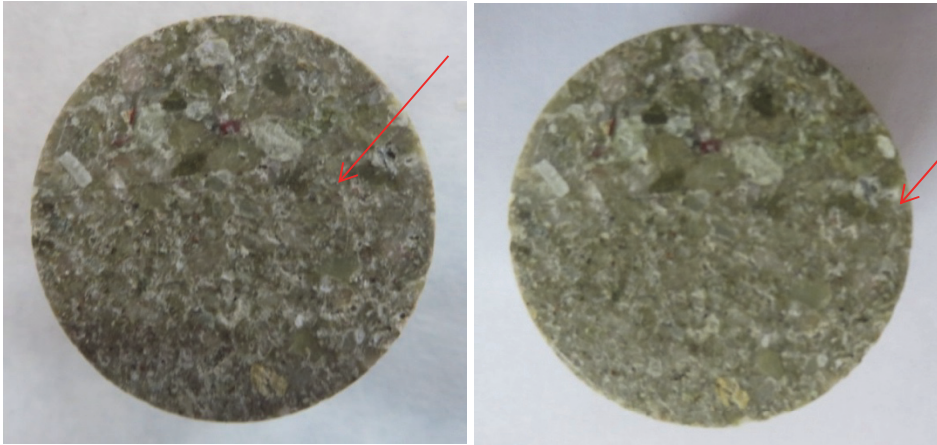


Fig. 78: Initial and final appearance of sample BC-53-5 (the arrows indicate the same position before and after testing)

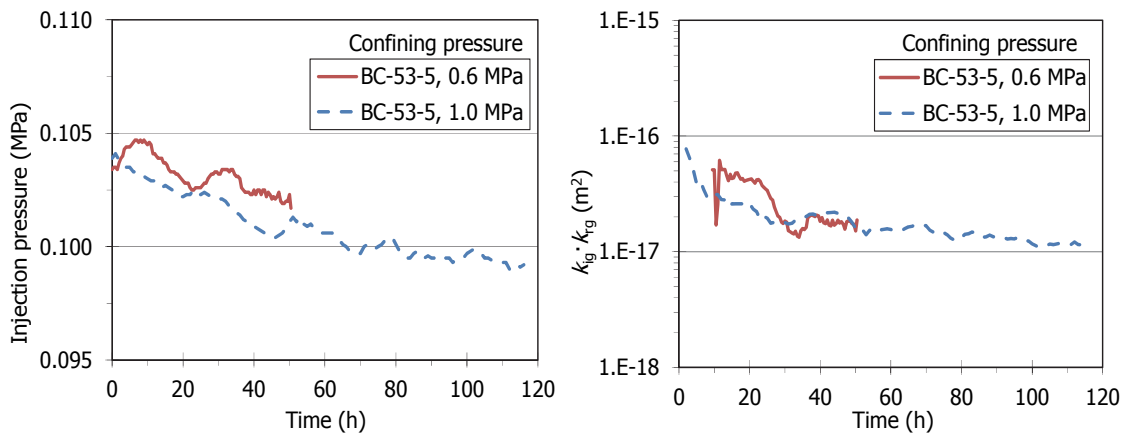


Fig. 79: Evolution of injection pressure and gas effective permeability ($k_{ig} \cdot k_{rg}$) in the low pressure equipment (LP) for sample BC-53-5 (injection gas pressure given in relative values)

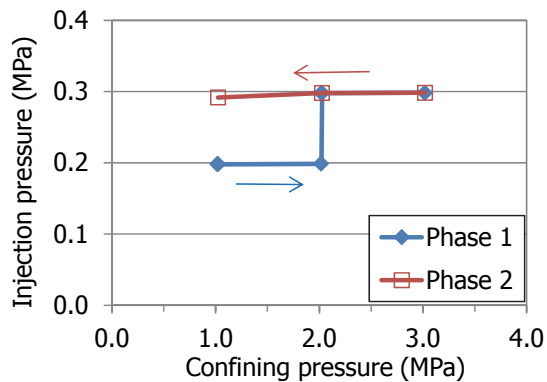


Fig. 80. Pressure path followed in the LCP setup for sample BC-53-5 (injection gas pressure given in absolute values)

Fig. 81 shows the gas permeability values obtained in both setups. The increase of confining pressure from 1 to 2 MPa caused the flow to decrease below the turndown value of the flowmeters. For this reason the injection pressure was increased from 0.2 to 0.3 MPa and the gas permeability increased almost an order of magnitude, but when the confining pressure was further increased to 3 MPa, no flow took place until the confining pressure was reduced again to 1 MPa, i.e. the initial confining pressure of the test. Nevertheless the permeability value measured was lower than the one initially measured. The

degree of saturation of the sample did not change during testing, although slight changes in dry density and water content did take place. Thus, the decrease in permeability could have been caused exclusively by the closing of the interface, which would have taken place for confining pressures higher than 2 MPa.

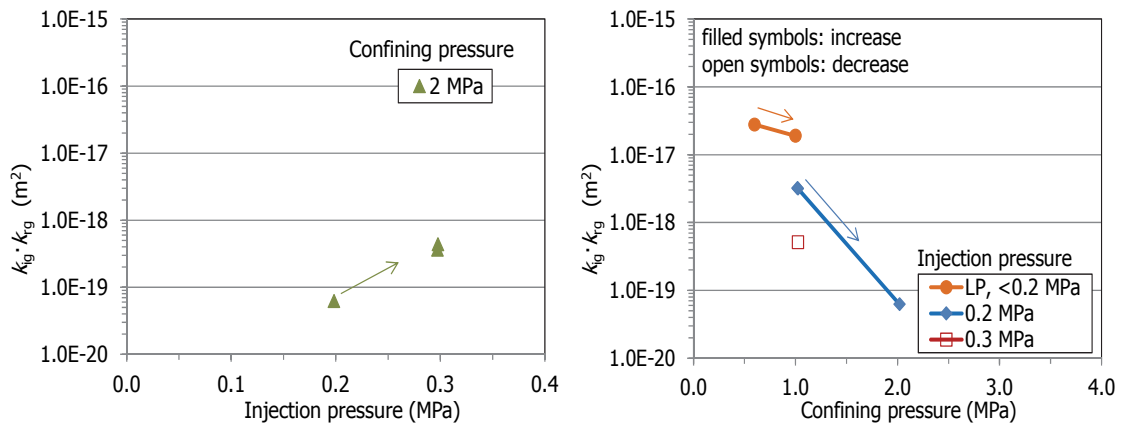


Fig. 81: Evolution of gas effective permeability at constant confining pressure (left) and constant injection pressure (right) for sample BC-53-5

4.1.22 Sample BC-53-6

Sample BC-53-6 was drilled on site in the middle of a block in the intermediate ring of section S53, close to sample BC-53-5. The dry density of the sample was 1.55 g/cm^3 and the water content 25.0%, corresponding to a degree of saturation of 91%. The core sample consisted of two pieces. The sample tested was taken from the longest piece, which once trimmed had a height of 3.45 cm (Fig. 82, left).



Fig. 82. Appearance of the core sample BC-53-6 before trimming (left) and after trimming (right)

This sample was initially tested in the low-pressure equipment (LP), using confining pressures of 0.6 and 1.0 MPa. The decrease in injection pressure in the upstream tank during both tests and the permeability values computed from it are shown in Fig. 83. The increase in confining pressure caused a decrease in gas permeability.

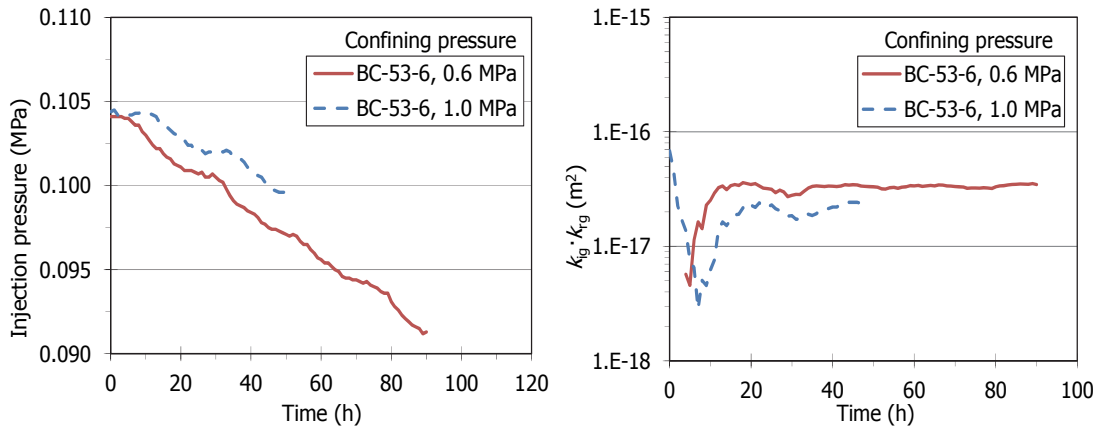


Fig. 83: Evolution of injection pressure and gas effective permeability ($k_{ig} \cdot k_{rg}$) in the low pressure equipment (LP) for sample BC-53-6 (injection gas pressure given in relative values)

Afterwards, the sample was tested in the high-pressure steady-state permeameter, in which these phases were followed (Fig. 84):

- Phase 1: initial step at a confining pressure of 1 MPa and 0.2 MPa of injection pressure. The injection pressure was increased to 0.3 MPa, in order to guarantee flow during the next steps.
- Phase 2: The confining pressure was increased until reaching 5 MPa, when no flow took place.
- Phase 3: unloading of the sample to as low as the initial confining pressure.

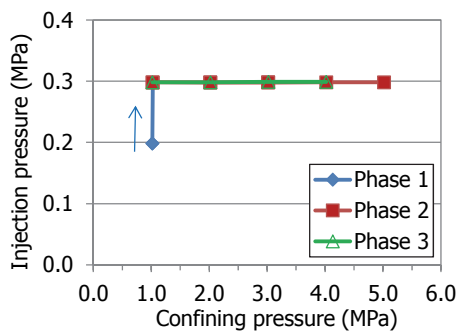


Fig. 84: Pressure path followed in the LCP setup for sample BC-53-6 (injection gas pressure given in absolute values)

The permeability values obtained are plotted in Fig. 85. The permeability computed at 1 MPa of confining pressure and 0.2 MPa of injection pressure, was almost the same in both setups (LP and HP). When the injection pressure increased from 0.2 to 0.3 MPa in Phase 1, the gas permeability remained constant. However, the decrease of gas permeability with confining pressure was clear. For a confining pressure of 5 MPa no flow took place. During unloading, there was no flow until the confining pressure decreased to 1 MPa, when the gas permeability computed was an order of magnitude lower than that for the same confining pressure during loading. This would indicate that the consolidation was irreversible (the dry density increased from 1.55 to 1.57 g/cm³ during the test), despite the fact that the sample also dried slightly, causing a decrease in the degree of saturation from 91 to 88%.

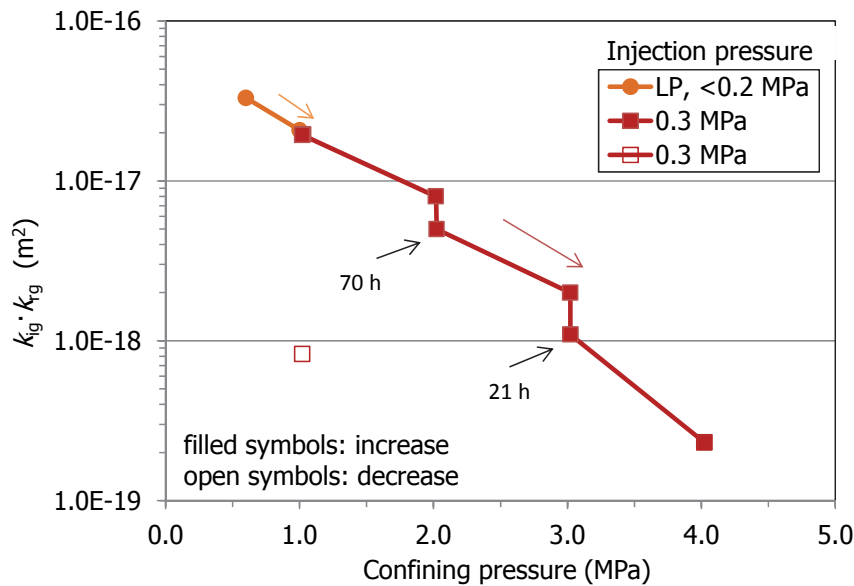


Fig. 85: Effect of confining pressure on gas effective permeability for sample BC-53-6

4.2 Pore size distribution

The pore size distribution of some of the samples was determined before and after gas testing. A spare fragment resulting from the sample preparation and a fragment from the sample at the end of the test were used. The aim of these tests was to analyse the effect of gas flow on the pore size distribution of the bentonite. The pore size distribution of the sample was analysed by mercury intrusion porosimetry as described in subchapter 3.4.

Due to the limitations of the method, only part of the macropores (pores of sizes between $5.4 \cdot 10^5$ and 50 nm) and part of the mesopores (pores between 50 and 6 nm) were explored. It is not expected to find pores larger than $6 \cdot 10^5$ nm in compacted clay materials, but the number of pores smaller than 6 nm can be very relevant. To overcome this undervaluation of porosity, an estimation of the percentage of pores not intruded by mercury can be made by comparing the actual void ratio of the samples (computed from their dry density and density of solid particles) and the apparent void ratio calculated from mercury intrusion. Thus, the pore size distribution obtained by MIP was corrected to take into account the percentage of pores not intruded.

The pore size distributions before and after gas testing of the samples analysed are shown in Fig. 86 to Fig. 92. The figures on the left show the cumulative intruded void ratio. These void ratios have been corrected by taking into account the actual pore volume of the samples as explained in the previous paragraph and subchapter 3.4. The total void ratio of the samples is indicated in the figures by dotted horizontal lines, which show that the void ratio intruded was in all samples of only about 50%. This would mean that the percentage of pores smaller than 6 nm or not interconnected is very relevant. All the samples experienced certain decrease in void ratio (increase in dry density) after gas testing, which is attributed to the compression exerted by the confining pressure applied. This aspect is discussed below in subchapter 5.1.3.

The figures on the right show the incremental mercury intrusion (mL/g) over the range of pore sizes explored in the tests. Two pore families appeared systematically in all the samples, one in the size range of macropores and another one in the size range of mesopores. Overall the curves before and after gas testing were similar for each sample, and only the samples from the external ring, with very high degrees of saturation (BC53-3, BC53-4), showed a clear increase in the size mode of the macropores after gas testing.

The corrected results are detailed in Tab. 7, where the maximum confining pressure reached at the end of the gas permeability tests is also shown (P_{max}). As mentioned above no major changes occurred during gas testing, although in most cases a decrease in the percentage of macropores was observed,

probably related to the compression exerted by the confining pressure. These results are further discussed in Chapter 5.2.

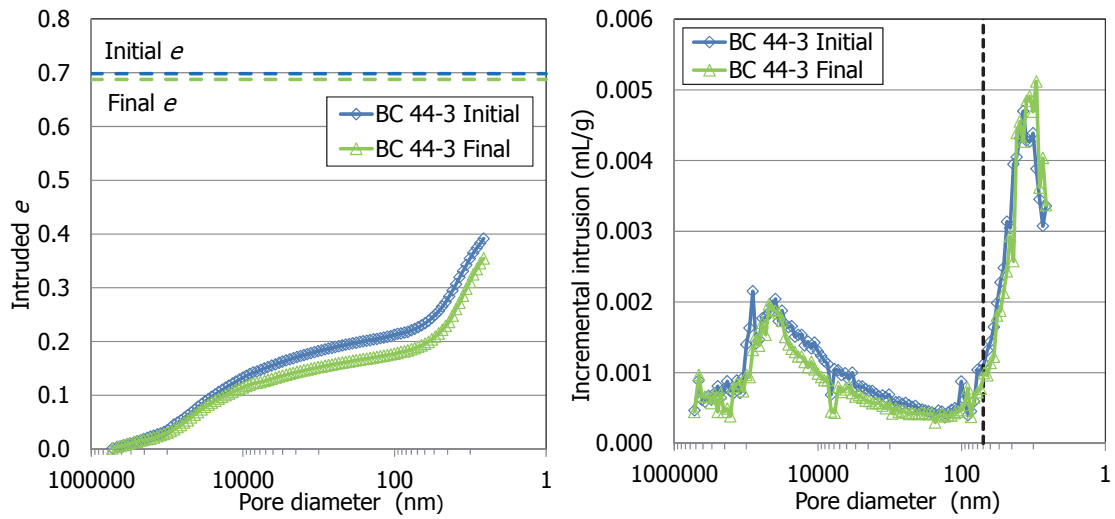


Fig. 86: Pore size distribution of sample BC-44-3 ($S_r=97\%$, distance to gallery axis 82 cm, with interface) before and after gas testing (the dotted vertical line indicates de separation between macro and mesopores)

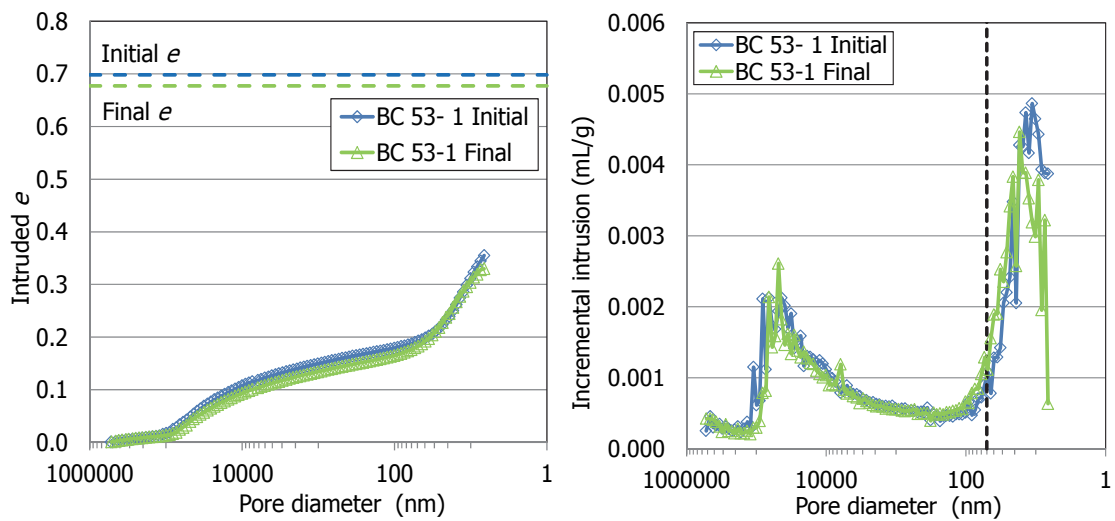


Fig. 87: Pore size distribution of sample BC-53-1 ($S_r=91\%$, distance to gallery axis 64 cm) before and after gas testing (the dotted vertical line indicates de separation between macro and mesopores)

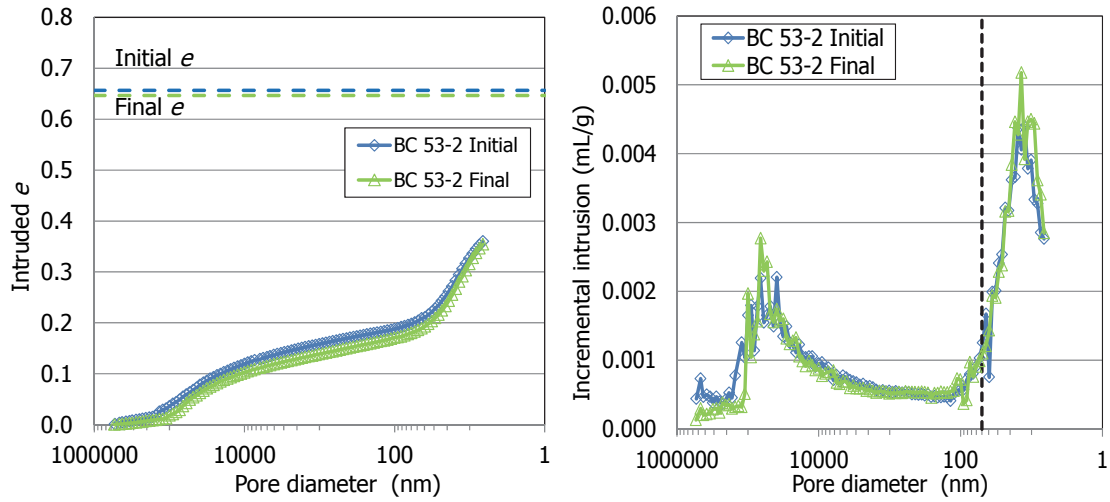


Fig. 88: Pore size distribution of sample BC-53-2 ($S_r=93\%$, distance to gallery axis 64 cm) before and after gas testing (the dotted vertical line indicates de separation between macro and mesopores)

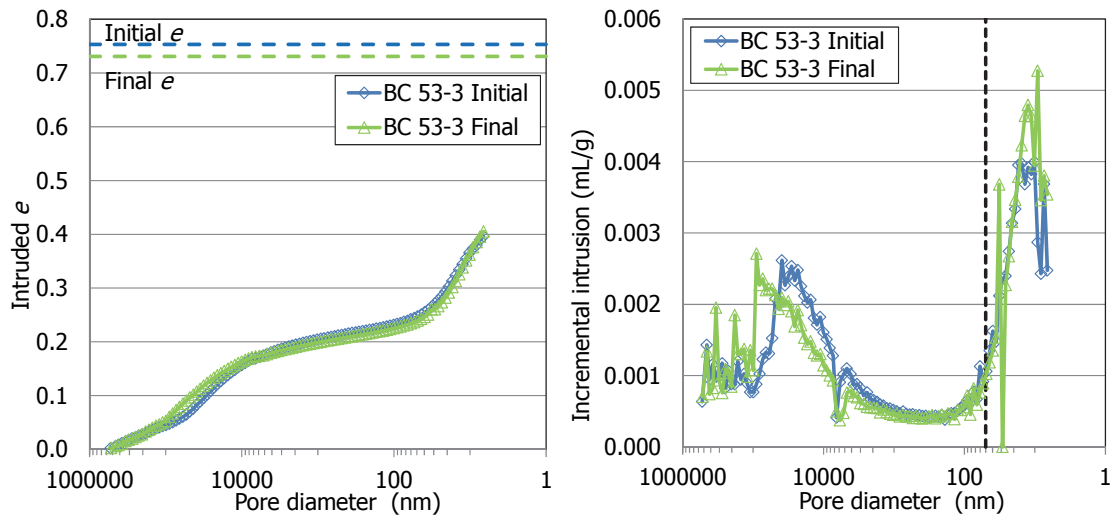


Fig. 89: Pore size distribution of sample BC-53-3 ($S_r=104\%$, distance to gallery axis 104 cm) before and after gas testing (the dotted vertical line indicates de separation between macro and mesopores)

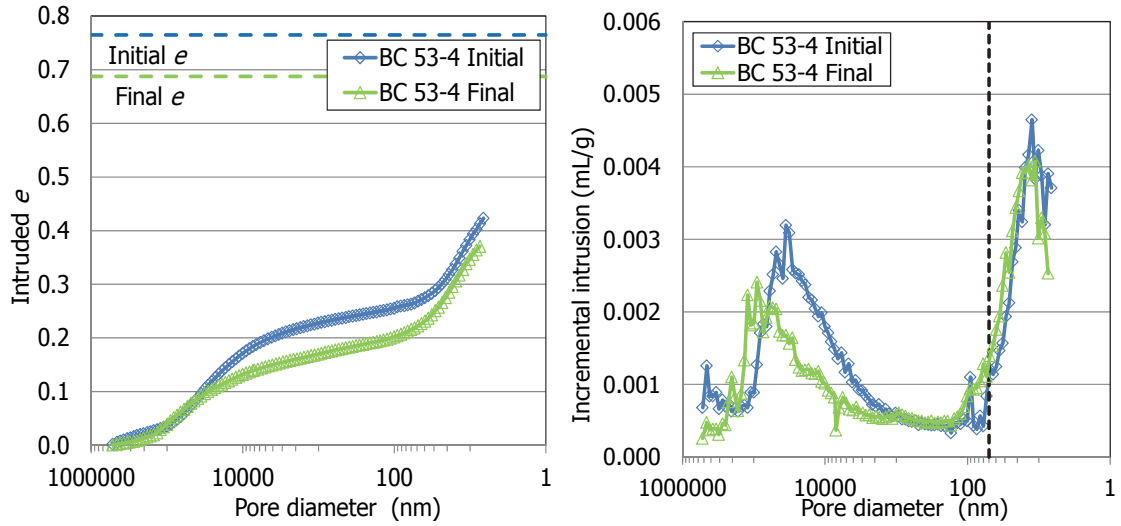


Fig. 90: Pore size distribution of sample BC-53-4 ($S_r=96\%$, distance to gallery axis 104 cm, with interface) before and after gas testing (the dotted vertical line indicates de separation between macro and mesopores)

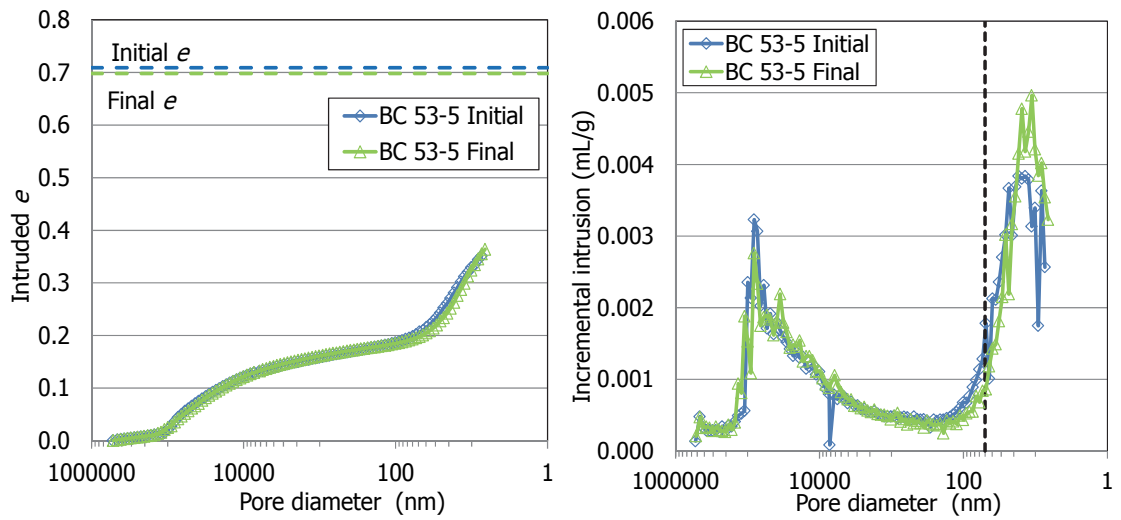


Fig. 91: Pore size distribution of sample BC-53-5 ($S_r=95\%$, distance to gallery axis 80 cm, with interface) before and after gas testing (the dotted vertical line indicates de separation between macro and mesopores)

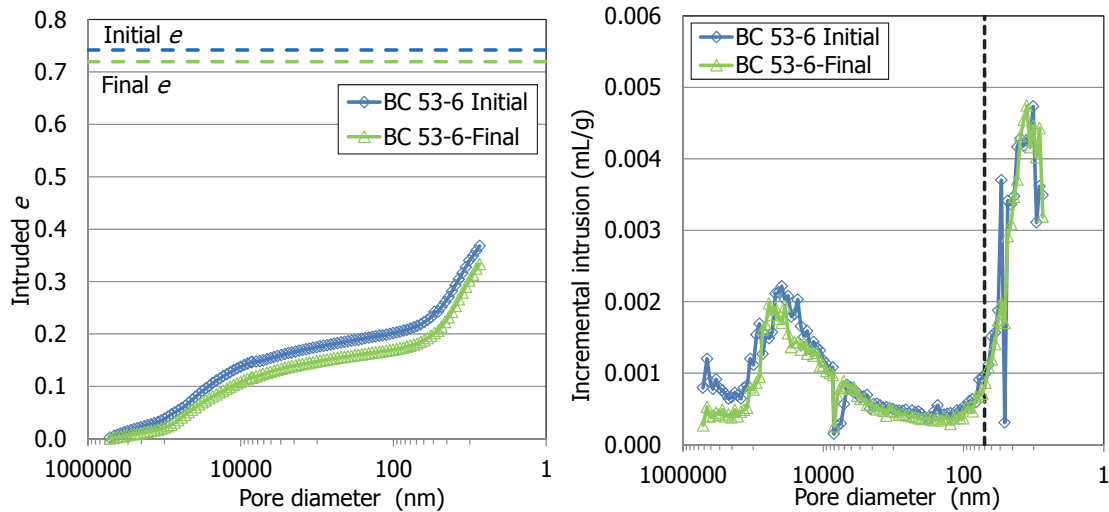


Fig. 92: Pore size distribution of sample BC-53-6 ($S_r=91\%$, distance to gallery axis 80 cm) before and after gas testing (the dotted vertical line indicates de separation between macro and mesopores)

Tab. 7: Pore size distribution obtained by MIP of samples from sections S44 and S53 and maximum confining pressures applied for each sample (e : void ratio)

Reference ^a	Distance to axis (cm)	P max (MPa)	Intruded e (% of total)	Macro (% vol)	Mode macro (nm)	Meso+micro (% vol)	Mode meso (nm)
BC 44-3 I	82		56	32	80995	68	13.9
BC 44-3 F ^b	82	3.0	44	23	48131	77	9.1
BC 53-1 I	64		51	27	65915	73	11.2
BC 53-1 F	64	2.2	49	27	48128	73	17.1
BC 53- 2 I	64		55	31	39127	69	12.5
BC 53-2 F ^b	64	4.0	55	28	66101	72	13.8
BC 53-3 I	104		53	32	39045	68	10.1
BC 53-3 F	104	2.0	55	32	89561	68	9.1
BC 53-4 I	104		55	35	35170	65	12.5
BC 53-4 F ^b	104	6.0	54	31	89553	69	11.2
BC 53-5 I	80		50	28	80976	72	17.1
BC 53-5 F ^b	80	2.0	52	28	80865	72	11.2
BC 53-6 I	80		50	28	39061	72	10.1
BC 53-6-F	80	4.0	46	25	59279	75	12.5

^a I: before gas testing (initial), F: after gas testing (final); ^b: with interface

5 DISCUSSION

5.1 Summary of gas permeability results

Twenty two gas permeability tests were performed in triaxial cells with bentonite samples obtained by drilling on site (19 samples) or core samples drilled from blocks in the laboratory (3 samples). The average dry density of the samples was $1.58 \pm 0.04 \text{ g/cm}^3$ and water content of $24.6 \pm 2.6\%$ ($S_r = 94 \pm 6\%$). The samples were not artificially saturated prior to gas testing. All the tests started with a confining pressure of 0.6 or 1.0 MPa. The injection pressure was slowly increased until a notable flow was reached and then the confining pressure was increased, normally to a value as high as to stop gas flow. Finally,

the confining pressure was reduced to the initial values in most of the tests. The precise pressure path followed depended on the characteristics of the samples and consequently they were quite heterogeneous. Although a summary of the results for each test was given in subchapter 4.1, the characteristics of each sample tested, the pressure path followed and the detailed results obtained are given in Annex I.

A summary of the initial and final characteristics of the samples and of the results obtained both in the low-pressure (LP) permeameter and in the high-pressure (HP) one (including the testing time in each setup) is shown in Tab. 8 to Tab. 10 for the different sampling sections indicated in Fig. 3 and Fig. 17. The effective permeability values given in the Tables are the average of all the values obtained for consecutive steps under the same confining pressure, irrespective of the injection pressure applied. As it has been seen above (see chapter 4.1) and will be explained below (subchapter 5.1.2), the effect of injection pressure on permeability in the range of pressures tested was for most samples negligible. The Tables include also the minimum injection pressure necessary to get flow (Min injection P) and the confining pressure applied for that injection pressure (Conf P min injec P).

When flow occurred under a given pressure situation, the duration of the steps was generally short (1-2 hours). In many cases it was observed that, if the same pressure situation was kept for longer, flow decreased and the permeabilities computed were lower. This aspect has not been analysed in detail but could have some effect on the results obtained.

Final checking of water content at different levels along the samples showed that the differences in water content inside the samples were smaller than 0.5%, which indicates that there was no significant water displacement inside the samples during gas testing. The void ratio accessible for gas flow, which expresses the ratio between gas accessible volume and particle volume and is computed as $e(1-S_r)$, is also shown in the Tables. Because of the high water saturation of most of the barrier after the long operation period, the accessible void ratio was below 0.15 in all the samples tested.

The following subchapters discuss the effect of boundary conditions and intrinsic properties of the samples on the gas permeability values obtained, as well as the changes in gas permeability occurred across the bentonite barrier. The effect of interfaces is discussed crosswise almost in all the following subchapters.

Tab. 8: Results of the gas permeability tests in core samples from section S44

	BC-44-1	BC-44-2	BC-44-3	BC-44-4	BC-44-5	BC-44-6	BC-44-7
Comments		Interface	Interface			Interface	
Initial ρ_d (g/cm ³)	1.57	1.56	1.59	1.61	1.52	1.51	1.62
Initial w (%)	26.2	23.2	25.2	24.5	28.5	28.4	19.5
Initial S_r (%)	98	86	97	97	100	97	79
Final ρ_d (g/cm ³)	1.58	1.62	1.60	1.61	1.53	1.53	1.65
Final w (%)	25.7	22.3	24.2	24.4	27.5	26.7	19.9
Final S_r (%)	98	91	96	97	98	94	84
$e(1-S_r)$	0.01	0.10	0.02	0.02	0.003	0.02	0.14
Confining P (MPa)	$k_{ig} \cdot k_{rg}$ (m ²) – LP setup						
0.6	$4.9 \cdot 10^{-17}$	$3.9 \cdot 10^{-14}$	$4.0 \cdot 10^{-17}$		No flow	$6.9 \cdot 10^{-17}$	$1.2 \cdot 10^{-16}$
1.0	$4.1 \cdot 10^{-17}$	$1.6 \cdot 10^{-14}$	$1.3 \cdot 10^{-17}$			$2.1 \cdot 10^{-17}$	$1.1 \cdot 10^{-16}$
Duration test LP (days)	6	1	7	Not tested	16	4	2
Confining P (MPa)	$k_{ig} \cdot k_{rg}$ (m ²) – HP setup						
0.6				$6.4 \cdot 10^{-18}$	No flow		
1.0	$2.8 \cdot 10^{-18}$	$5.0 \cdot 10^{-15}$	$6.3 \cdot 10^{-18}$	$4.0 \cdot 10^{-18}$	$5.9 \cdot 10^{-20}$	$1.0 \cdot 10^{-17}$	$1.1 \cdot 10^{-16}$
1.5	$1.3 \cdot 10^{-18}$	$3.5 \cdot 10^{-15}$		$1.9 \cdot 10^{-18}$	$8.4 \cdot 10^{-21}$	$2.9 \cdot 10^{-18}$	
2.0	$3.5 \cdot 10^{-19}$	$3.2 \cdot 10^{-15}$	$7.3 \cdot 10^{-19}$	$9.4 \cdot 10^{-19}$		$5.6 \cdot 10^{-19}$	$5.2 \cdot 10^{-17}$

	BC-44-1	BC-44-2	BC-44-3	BC-44-4	BC-44-5	BC-44-6	BC-44-7
2.5	$2.3 \cdot 10^{-20}$	$3.1 \cdot 10^{-15}$		$3.3 \cdot 10^{-19}$		$1.6 \cdot 10^{-19}$	
3.0		$3.0 \cdot 10^{-15}$	$1.2 \cdot 10^{-19}$	$1.2 \cdot 10^{-19}$		$2.8 \cdot 10^{-20}$	$3.1 \cdot 10^{-17}$
3.5		$2.9 \cdot 10^{-15}$		$1.4 \cdot 10^{-20}$			
4.0		$2.9 \cdot 10^{-15}$					$2.0 \cdot 10^{-17}$
4.5		$2.9 \cdot 10^{-15}$					
5.0		$2.8 \cdot 10^{-15}$					$1.3 \cdot 10^{-17}$
5.5		$2.8 \cdot 10^{-15}$					
6.0		$2.8 \cdot 10^{-15}$					No flow
6.5		$2.6 \cdot 10^{-18}$					
7.0		$1.7 \cdot 10^{-18}$					
7.5		$6.1 \cdot 10^{-19}$					
8.0		$6.3 \cdot 10^{-19}$					
8.5		$4.7 \cdot 10^{-19}$					
9.0		$1.6 \cdot 10^{-18}$					
Duration test HP (days)	2	6	8	5	7	8	14
Min injection P (MPa)	0.20	0.15	0.20	0.20	0.60	0.20	0.20
Conf P min injec P (MPa)	1.00	1.00	1.00	0.60	1.00	1.00	1.00

Tab. 9: Results of the gas permeability tests in core samples from section S47

	BC-47-1	BC-47-2	BC-47-3	BC-47-4	BC-47-6
Comments				Interface	Interface
Initial ρ_d (g/cm ³)	1.55	1.54	1.61	1.59	1.64
Initial w (%)	26.4	26.4	23.7	24.8	19.6
Initial S_r (%)	96	94	95	97	82
Final ρ_d (g/cm ³)	1.55	1.55	1.57	1.61	1.64
Final w (%)	26.3	25.9	23.9	23.1	19.6
Final S_r (%)	95	91	90	91	82
e (1- S_r)	0.03	0.05	0.03	0.02	0.12
Confining P (MPa)	$k_{ig} \cdot k_{rg}$ (m ²) – LP setup				
0.6	$7.7 \cdot 10^{-18}$				$2.5 \cdot 10^{-14}$
1.0					$1.4 \cdot 10^{-14}$
Duration test LP (days)	12	Not tested	Not tested	Not tested	1
Confining P (MPa)	$k_{ig} \cdot k_{rg}$ (m ²) – HP setup				
0.6	$1.7 \cdot 10^{-18}$		$3.5 \cdot 10^{-17}$		$4.4 \cdot 10^{-14}$
0.8			$2.8 \cdot 10^{-17}$		
1.0	$1.5 \cdot 10^{-18}$		$2.3 \cdot 10^{-17}$		$5.1 \cdot 10^{-14}$
1.5					$2.3 \cdot 10^{-14}$
2.0	$2.8 \cdot 10^{-20}$	$1.2 \cdot 10^{-17}$			$1.0 \cdot 10^{-14}$
2.5	$3.9 \cdot 10^{-21}$				
3.0		$1.2 \cdot 10^{-19}$		$9.1 \cdot 10^{-15}$	
4.0		$7.1 \cdot 10^{-20}$		$1.7 \cdot 10^{-15}$	

	BC-47-1	BC-47-2	BC-47-3	BC-47-4	BC-47-6
5.0		$5.3 \cdot 10^{-20}$		$5.4 \cdot 10^{-17}$	
6.0		$5.7 \cdot 10^{-20}$			
7.0		$3.9 \cdot 10^{-20}$		$2.1 \cdot 10^{-19}$	
8.0		$4.1 \cdot 10^{-20}$		$1.6 \cdot 10^{-19}$	
9.0		$3.8 \cdot 10^{-20}$		$3.7 \cdot 10^{-21}$	
10.0		$5.0 \cdot 10^{-20}$			
11.0		$3.8 \cdot 10^{-20}$			
12.0		$2.3 \cdot 10^{-20}$			
Duration test HP (days)	9	167	13	172	0.2
Min injection P (MPa)	0.20	0.40	0.10	0.20	0.10
Conf P min inyec P (MPa)	0.60	2.00	0.60	2.00	0.60

Tab. 10: Results of the gas permeability tests in core samples from section S36 and drilled samples in the laboratory from section 53.

	BC-36-1	BB53-4-2	BB53-5-1	BB53-5-2
Comments		Lab	Lab	Lab
Initial ρ_d (g/cm ³)	1.52	1.59	1.63	1.63
Initial w (%)	28.1	25.1	23.3	22.9
Initial S_r (%)	98	96	97	94
Final ρ_d (g/cm ³)	1.57	1.59	1.60	1.59
Final w (%)	26.7	24.8	24.6	24.3
Final S_r (%)	96	96	92	94
e (1- S_r)	0.01	0.02	0.02	0.04
Confining P (MPa)		$k_{ig} \cdot k_{rg}$ (m ²) – LP setup		
0.6		No flow	No flow	No flow
Duration test LP (days)	Not tested	13	20	12
Confining P (MPa)		$k_{ig} \cdot k_{rg}$ (m ²) – HP setup		
0.6			$2.4 \cdot 10^{-19}$	$3.3 \cdot 10^{-19}$
1.0	$8.3 \cdot 10^{-16}$		$1.6 \cdot 10^{-19}$	$5.5 \cdot 10^{-19}$
1.4			$1.8 \cdot 10^{-20}$	$1.2 \cdot 10^{-19}$
1.6			$1.4 \cdot 10^{-20}$	$6.5 \cdot 10^{-20}$
2.0	$4.0 \cdot 10^{-17}$			
3.0	$5.4 \cdot 10^{-18}$			
4.0	$6.7 \cdot 10^{-18}$			
5.0	$1.3 \cdot 10^{-18}$			
6.0	$1.5 \cdot 10^{-18}$			
7.0	$1.6 \cdot 10^{-18}$			
8.0	$5.6 \cdot 10^{-19}$			
9.0	$4.3 \cdot 10^{-19}$			
10.0	$6.4 \cdot 10^{-18}$			
11.0	$7.5 \cdot 10^{-19}$			
12.0	$4.7 \cdot 10^{-19}$			
13.0	$1.3 \cdot 10^{-18}$			

	BC-36-1	BB53-4-2	BB53-5-1	BB53-5-2
14.0	$4.4 \cdot 10^{-19}$			
Duration test HP (days)	168	Not tested	23	15
Min injection P (MPa)	0.20		0.30	0.20
Conf P min injec P (MPa)	1.00		0.60	0.60

Tab. 11: Results of the gas permeability tests in core samples from section S53

	BC-53-1	BC-53-2	BC-53-3	BC-53-4	BC-53-5	BC-53-6
Comments		Interface		Interface	Interface	
Initial ρ_d (g/cm ³)	1.59	1.63	1.54	1.53	1.58	1.55
Initial w (%)	23.7	22.5	29	27.1	24.8	25.0
Initial S_r (%)	91	93	104	96	95	91
Final ρ_d (g/cm ³)	1.61	1.64	1.56	1.60	1.59	1.57
Final w (%)	22.3	23.3	25.7	25.1	24.4	23.4
Final S_r (%)	90	97	95	98	95	88
e (1- S_r)	0.06	0.04	0.00	0.03	0.04	0.07
Confining P (MPa)		$k_{ig} \cdot k_{rg}$ (m ²) – LP setup				
0.6	$1.3 \cdot 10^{-17}$	$2.2 \cdot 10^{-17}$	$1.1 \cdot 10^{-16}$	$1.4 \cdot 10^{-13}$	$2.8 \cdot 10^{-17}$	$3.3 \cdot 10^{-17}$
1.0	Not tested	$1.9 \cdot 10^{-17}$	No flow	$8.8 \cdot 10^{-14}$	$1.9 \cdot 10^{-17}$	$2.1 \cdot 10^{-17}$
Duration test LP (days)	5	6	8	<1	7	6
Confining P (MPa)		$k_{ig} \cdot k_{rg}$ (m ²) – HP setup				
0.6	$6.2 \cdot 10^{-18}$					
1.0	$3.8 \cdot 10^{-18}$	$7.0 \cdot 10^{-18}$	$5.7 \cdot 10^{-18}$	No flow	$3.2 \cdot 10^{-18}$	$2.0 \cdot 10^{-17}$
2.0	$1.5 \cdot 10^{-18}$	$2.5 \cdot 10^{-18}$	$3.1 \cdot 10^{-20}$	$4.9 \cdot 10^{-15}$	$2.9 \cdot 10^{-19}$	$6.5 \cdot 10^{-18}$
2.5	$9.3 \cdot 10^{-19}$					
3.0		$7.3 \cdot 10^{-19}$		$2.2 \cdot 10^{-15}$	No flow	$1.5 \cdot 10^{-18}$
4.0		$1.4 \cdot 10^{-19}$		$2.3 \cdot 10^{-16}$		$2.3 \cdot 10^{-19}$
5.0		No flow		$3.0 \cdot 10^{-17}$		No flow
6.0				$5.7 \cdot 10^{-20}$		
Duration test HP (days)	14	24	15	17	8	14
Min injection P (MPa)	0.20	0.20	0.30	0.20	0.20	0.20
Conf P min injec P (MPa)	0.60	1.00	1.00	2.00	1.00	1.00

5.1.1 Low pressure setup

Most of the samples were initially tested in the low pressure equipment. The aim of these tests was to determine the gas permeability under low confining and injection pressure conditions. The tests followed two stages:

- Stage 1: constant confining pressure of 0.6 MPa and initial gas injection pressure of 0.1 MPa.
- Stage 2: constant confining pressure of 1.0 MPa and initial gas injection pressure of 0.1 MPa.

The effect of confining pressure was noticeable in most cases. Accordingly, the pressure decrease rate during the tests was lower in the samples tested under higher confining pressure. Also, when an interface was present the pressure decrease rate was higher. An example of both aspects is given in Fig. 93.

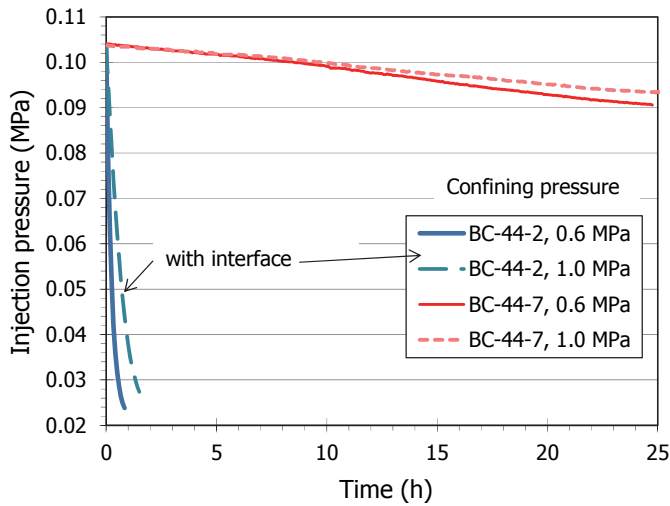


Fig. 93: Pressure decrease in the gas tank during testing of two samples of section S44 taken at ~61 cm from the gallery axis (sample BC-44-2 with interface) under two different confining pressures (injection gas pressure given in relative values)

Obviously, higher pressure decrease rates resulted in higher effective permeabilities (Eq. 3). Tab. 8 to Tab. 11 summarise the results obtained for the measurements performed in each sample, expressed in terms of effective gas permeability ($k_{ig} \cdot k_{rg}$). These results have been plotted as a function of the distance to the gallery axis in Fig. 94 and Fig. 95 (left). The relation between permeability and degree of saturation is shown in Fig. 94 and Fig. 95 (right). The highest permeabilities were measured in some samples with interface. However, for the samples with higher degree of saturation there was not a clear difference in permeability between samples with or without interface. In these more saturated samples the two parts of the core were tightly joined. Fig. 96 shows an interface between the two parts of a core sample from the external ring, barely discernible, and the open interface between the two parts of a drier core from the inner ring. An exception was a highly saturated sample with interface located in the external ring of section S53 (BC-53-4), which should have the interface tightly joined, but it was clearly visible during the preparation of the sample (Fig. 74). The results corresponding to this sample are indicated with an arrow in Fig. 94 and Fig. 95. The role of interfaces is further discussed in the following subchapters.

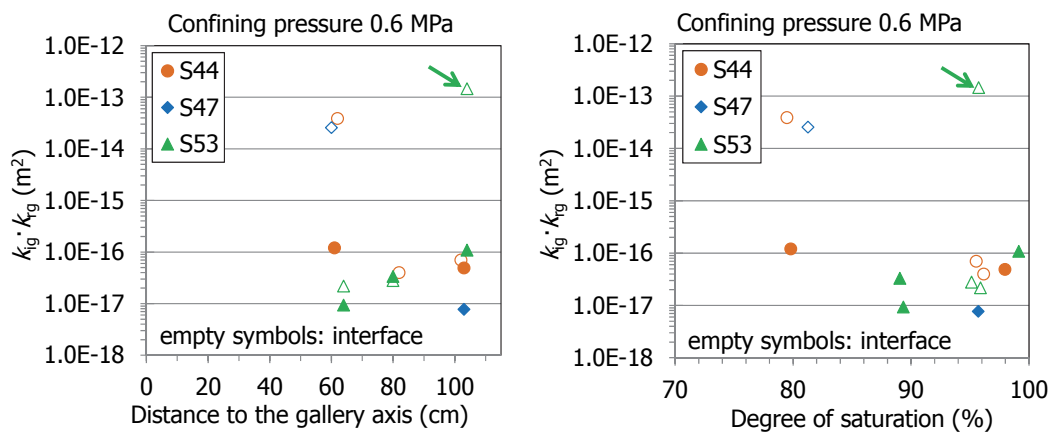


Fig. 94: Effective permeability values obtained in the low-pressure equipment as a function of the position in the barrier (left) and the initial degree of saturation (right) at constant confining pressure of 0.6 MPa (the arrow indicates sample BC-53-4)

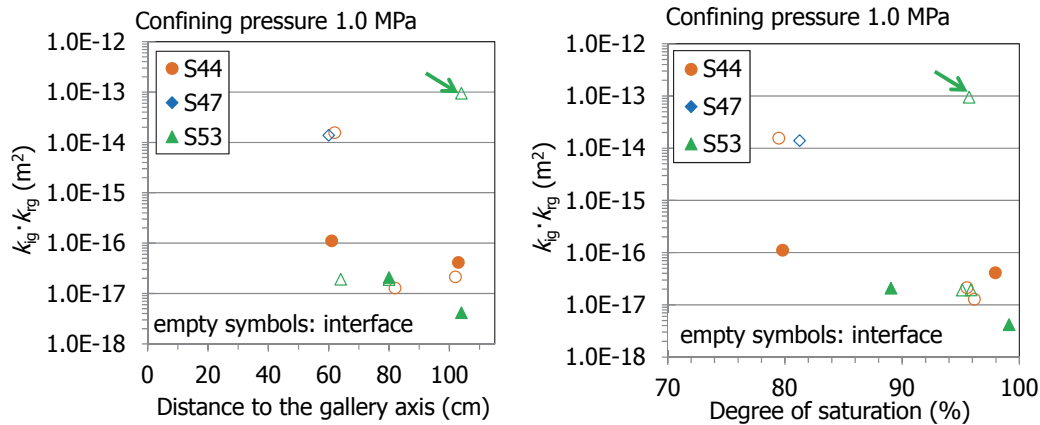


Fig. 95: Effective permeability values obtained in the low-pressure equipment as a function of the position in the barrier (left) and the initial degree of saturation (right) at a constant confining pressure of 1.0 MPa (the arrow indicates the sample BC-53-4)



Fig. 96: Interface in a sample from the external ring (indicated by an arrow, BC-44-6) and from the inner ring (BC-44-2)

5.1.2 Effect of injection pressure

After testing in the LP setup most samples were also tested in the high-pressure setup, the samples being kept in the same triaxial cell in which they were initially tested. The tests started by increasing the injection pressure under constant confining pressure. In the range of pressures tested no clear effect of the injection pressure on the permeability value was observed for most of the samples. Hence, for most samples the gas permeability under a constant confining pressure was essentially constant despite the injection pressure changes. This can be seen in Fig. 97 and Fig. 98, in which the results obtained for different samples tested under confining pressures of 0.6 and 1 MPa have been plotted. Only in a few cases the gas permeability increased slightly with the increase in injection pressure.

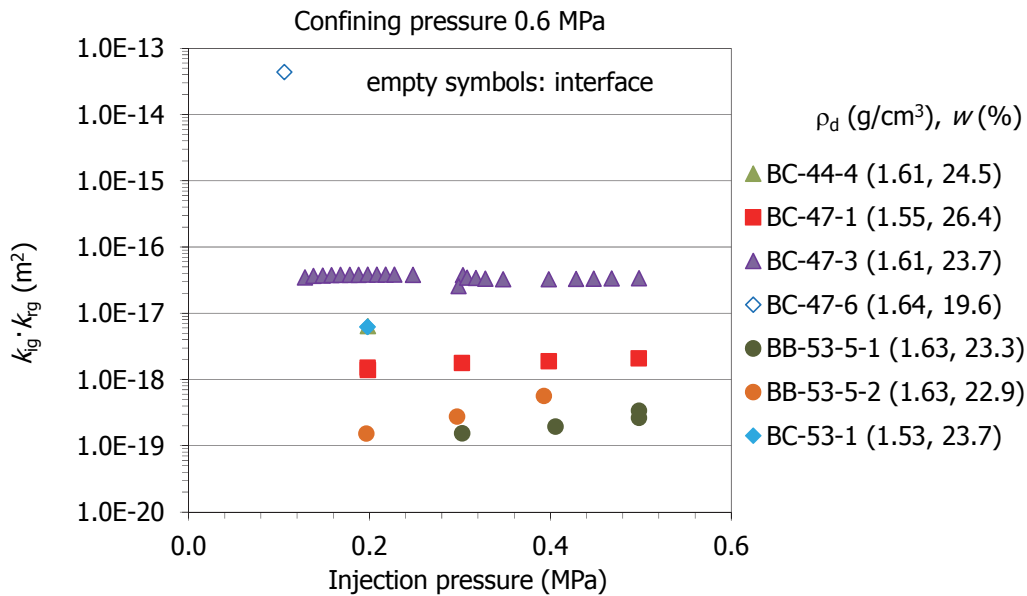


Fig. 97: Effective gas permeability measured at constant confining pressure of 0.6 MPa in the HP setup

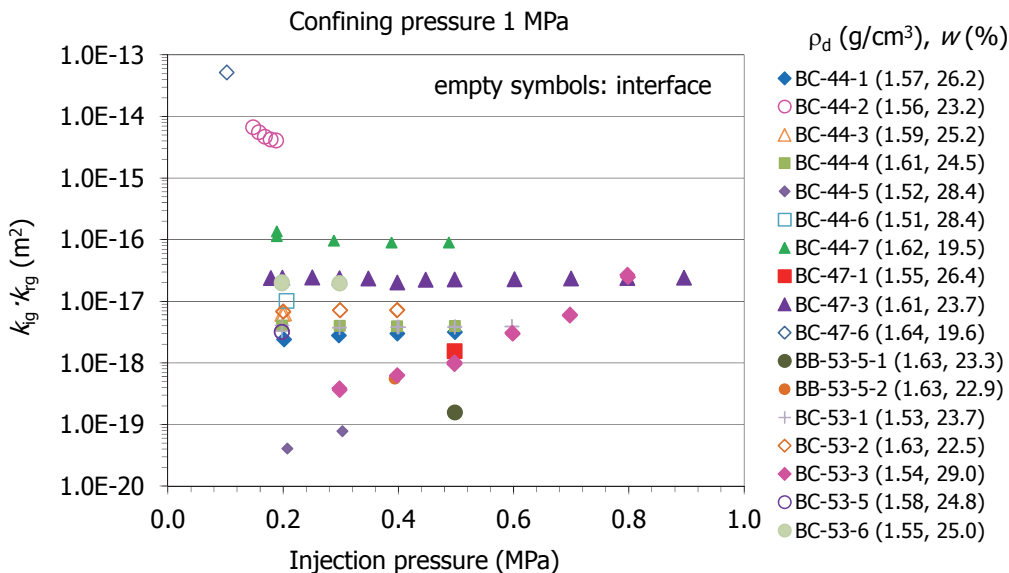


Fig. 98: Effective gas permeability measured at constant confining pressure of 1 MPa in the HP setup

Previous works performed with samples of the reference FEBEX bentonite compacted to different dry densities with various water contents showed empirically that the gas permeability was not affected by the injection or confining pressures for pressures below 1.2 MPa (Villar et al. 2013, Gutiérrez-Rodrigo et al. 2014). In the results presented here, only in the case of samples with the highest water content and lowest suctions (Tab. 5), the increase in injection pressure caused a clear increase in gas permeability. This was the case of samples BC-44-5 and BC-53-3, BB-53-5-1 and BB-53-5-2, all of them taken from the external ring of the barrier or with a degree of saturation higher than 94%. It was checked that for these samples flow was not linearly related to the difference of squared pressures along the sample (injection, P_{up} , and backpressures, P_{dw}), which indicates that flow was not stationary and Darcy's law cannot strictly be applied to compute permeability. Fig. 99 and Fig. 100 show some examples of the relation between flow and the difference of the squared pressures. For the samples mentioned above (Fig. 99) this relationship was not linear, and hence, the permeability values computed with Eq. 8 are not reliable. Although these particular samples had in all cases high degrees of saturation, not all the samples with high degree of saturation showed unsteady flow. In fact for most samples this relation was linear (Fig.

100), which indicates that single-phase flow of the compressible gas took place and that the permeability values computed are right.

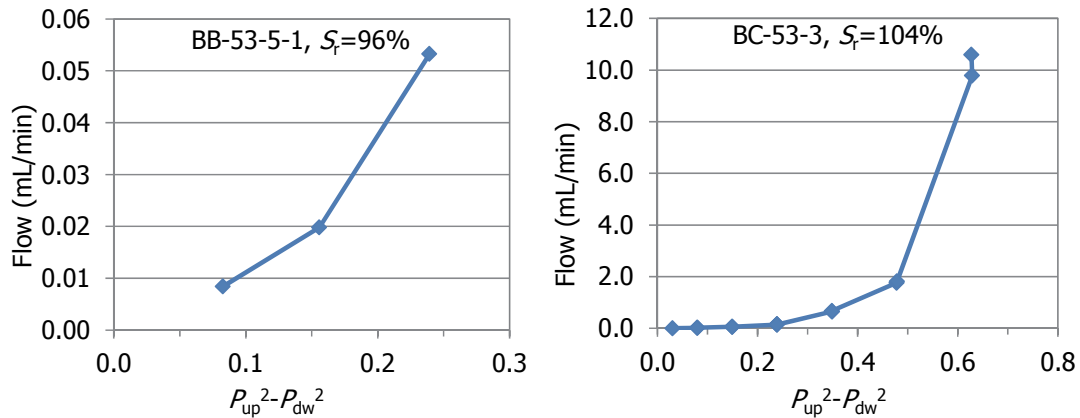


Fig. 99: Examples of samples in which flow was not stationary

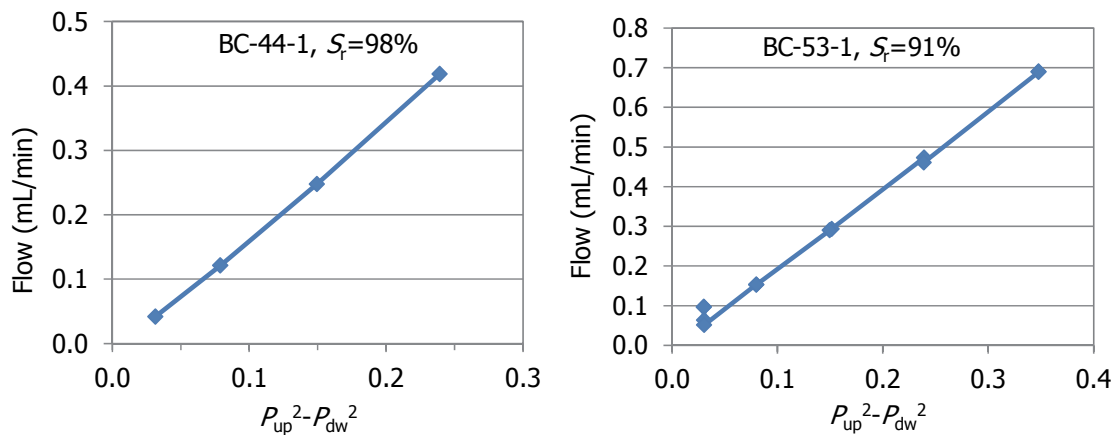


Fig. 100: Examples of samples in which flow was stationary

Even before reaching the maximum confining pressure, in some of the steps there was no flow and the injection pressure had to be increased in order to get a measurable flow. The injection pressure values necessary to get flow for some of the confining pressures applied are shown in Fig. 101 as a function of the degree of saturation and the accessible void ratio. These values were also shown in Tab. 8 to Tab. 11. Although the relation is not straightforward, there seems to be a trend for the minimum injection pressure to be higher as the degree of saturation was higher (and the accessible void ratio lower). This minimum injection pressure was lower for the samples with interface.

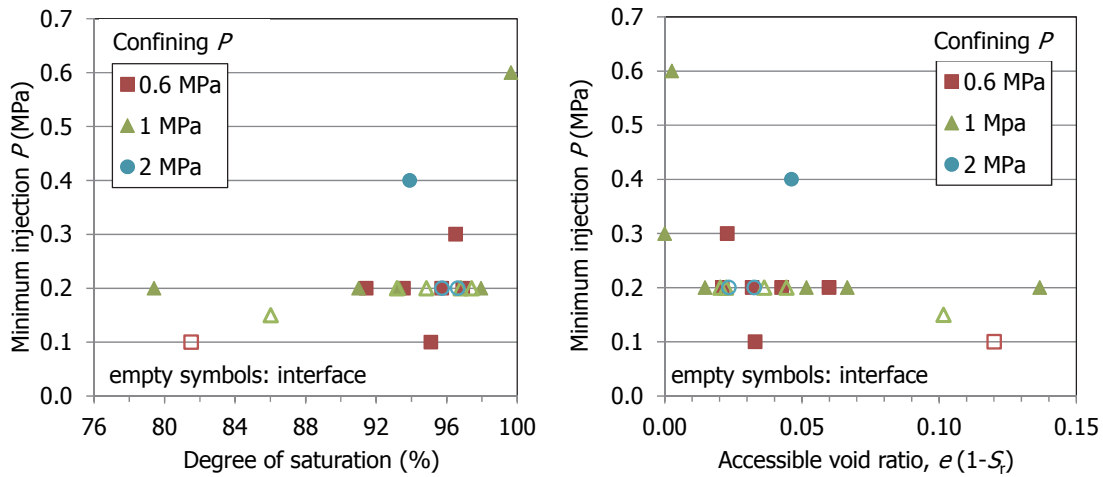


Fig. 101: Minimum injection pressure necessary to get measurable flow for different confining pressures as a function of the degree of saturation of the samples (left) and of their accessible void ratio (right)

5.1.3 Effect of confining pressure on gas permeability

Fig. 102 to Fig. 104 show the gas permeability values measured for each confining pressure in samples of the different sampling sections. These values are the averages obtained for steps of different injection pressure under constant confining pressure, since it was checked that in most samples permeability under a given confining pressure was independent of injection pressure. Only for a few samples gas permeability changed with injection pressure which, as discussed in subchapter 5.1.2, probably indicates that the flow was transient. These samples have been excluded from the Figures. The distance from the sample to the gallery axis and the initial degree of saturation are also indicated in the Figures (Tab. 5).

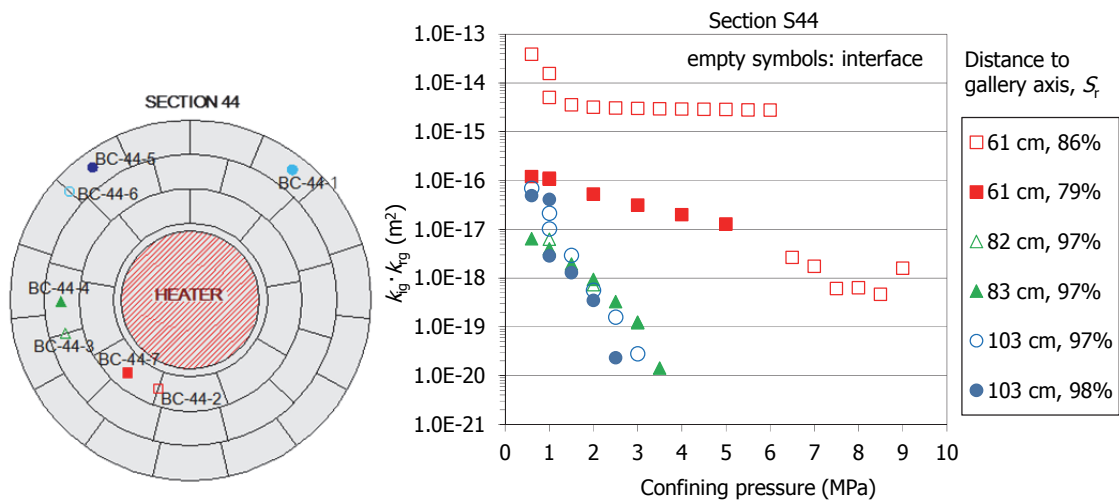


Fig. 102: Change of effective gas permeability with increasing confining pressure in samples from section S44 (the values are the average of all the steps in which confining pressure was the same, irrespective of the injection pressure)

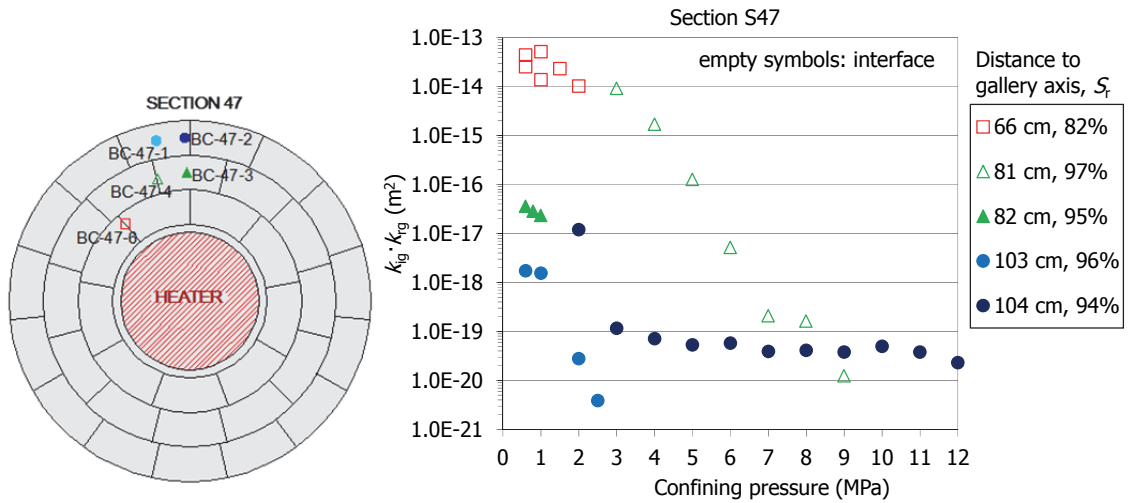


Fig. 103: Change of effective gas permeability with increasing confining pressure in samples from section S47 (the values are the average of all the steps in which confining pressure was the same, irrespective of the injection pressure)

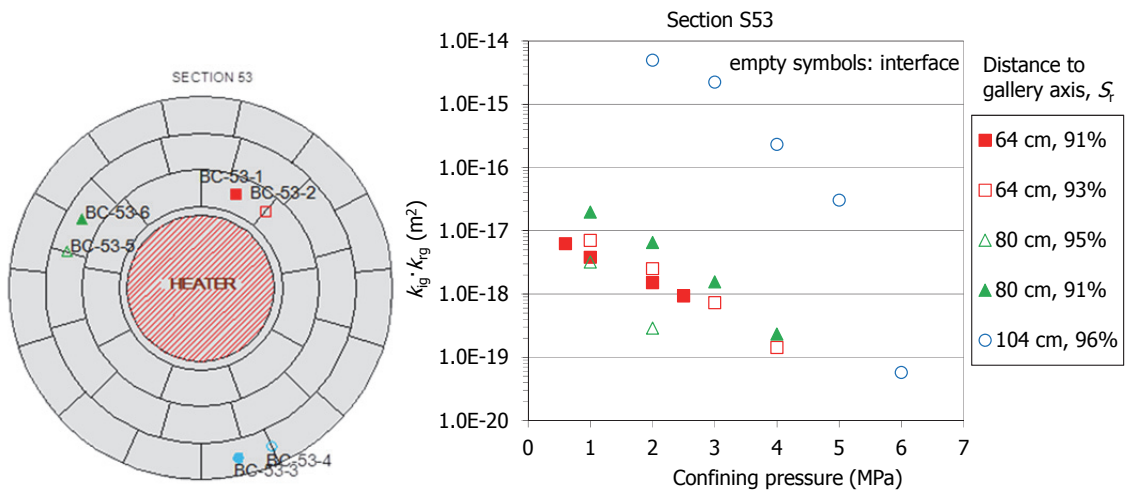


Fig. 104: Change of effective gas permeability with increasing confining pressure in samples from section S53 (the values are the average of all the steps in which confining pressure was the same, irrespective of the injection pressure)

Overall, the samples closest to the heater (around 60 cm from the gallery axis), which were drier and had lower degrees of saturation (Villar et al. 2016), showed higher gas permeability (subchapter 5.1.6). The decrease of gas permeability with confining pressure was significant. For confining pressures below 4 MPa most samples experienced a significant decrease in permeability as the confining pressure increased. For higher confining pressures the decrease was less significant, except when the sample had an interface. The samples from the external and middle rings, those more saturated, had the lowest permeability, and no flow took place through them for confining pressures higher than 3-4 MPa. In contrast, for the sample of the internal ring from section S44 (BC-44-7), the confining pressure had to be increased up to 9.5 MPa to stop flow. The confining stress reduced the size of the gas pathways, also increasing their tortuosity. In the case of the highly-saturated samples there was no need of applying a high confining pressure to completely block the air passages, whereas in the less saturated samples the gas found ways out until the confining pressure was enough to sufficiently reduce the air-filled pore space. This also would explain the fact that the effect of injection pressure increase was only noticeable in the samples with the highest water content, in which small changes in the size of the gas pathways would trigger significant changes in very low permeability.

The samples with interface had higher permeability than neighbouring samples drilled in the middle of a block, and this permeability decreased suddenly for confining pressures higher than the 4 MPa previously mentioned. The permeability of sample BC-44-2, drilled between two blocks of the internal ring of section S44 (Fig. 102), decreased three orders of magnitude when the confining pressure was increased to 6 MPa. The permeability of sample BC-47-4 (Fig. 103), decreased four orders of magnitude when the confining pressure increased from 4 to 7 MPa, and sample BC-53-4, which had a similar degree of saturation in section S53 (Fig. 104), showed a similar behaviour.

Previous laboratory studies showed that, in the FEBEX compacted bentonite and under isochoric conditions, two-phase flow seemed to take place for degrees of saturation lower than about 97%, whereas for higher degrees of saturation pathway dilation could be the predominant mechanism (Villar et al. 2013, Gutiérrez-Rodrigo et al. 2014, 2015). The threshold pressure for gas entry into the bentonite was higher than the swelling pressure and seemed to be lower than the gas pressure required for fracturing (macroscopically) the material. In contrast, in the research reported here, two-phase flow seems to have taken place in most cases, even for samples with degree of saturation higher than 97%. The fact that these samples were tested under constant confining stress instead of under no volume change conditions (isochoric), would have made easier the transport of gas, with opening of trajectories for gas flow. As the confining stress increased, the tortuosity of these gas pathways would increase, which would have caused the decrease in gas permeability, and eventually the closing of pathways.

5.1.4 Effect of unloading on gas permeability

After reaching the maximum confining pressure, corresponding to a value above which no flow took place, the samples were progressively unloaded. Only in the test with sample BC-53-1, drilled from the internal ring of the barrier, the maximum confining pressure applied (2.2 MPa) was determined by a technical failure and not by flow cessation. Fig. 105 to Fig. 107 show the changes in gas effective permeability during loading-unloading for samples of the different sections (the values for the loading path are the same plotted in Fig. 102 to Fig. 104). The permeability values plotted are the average of all the consecutive steps in which confining pressure was the same.

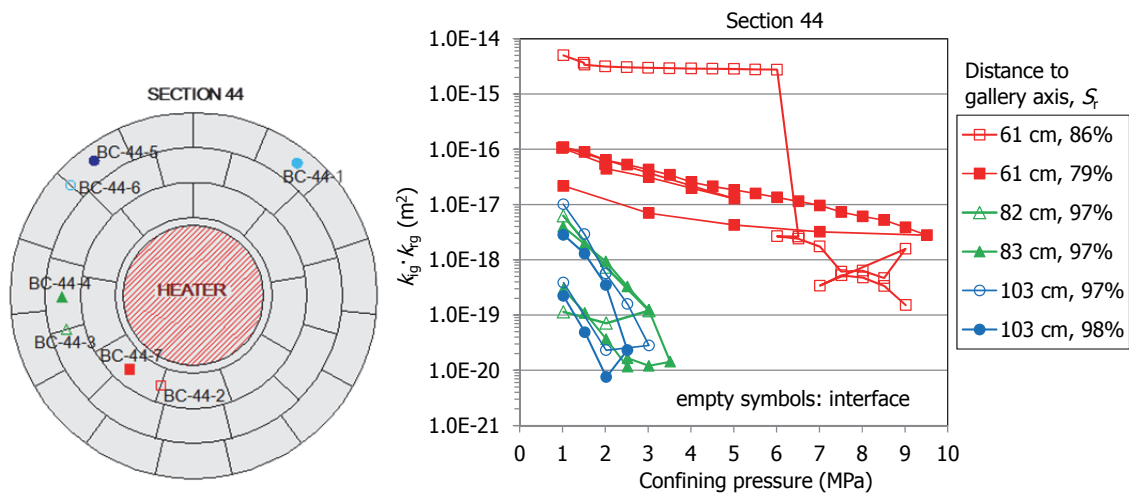


Fig. 105: Change of effective gas permeability with increase/decrease of confining pressure for samples from section S44

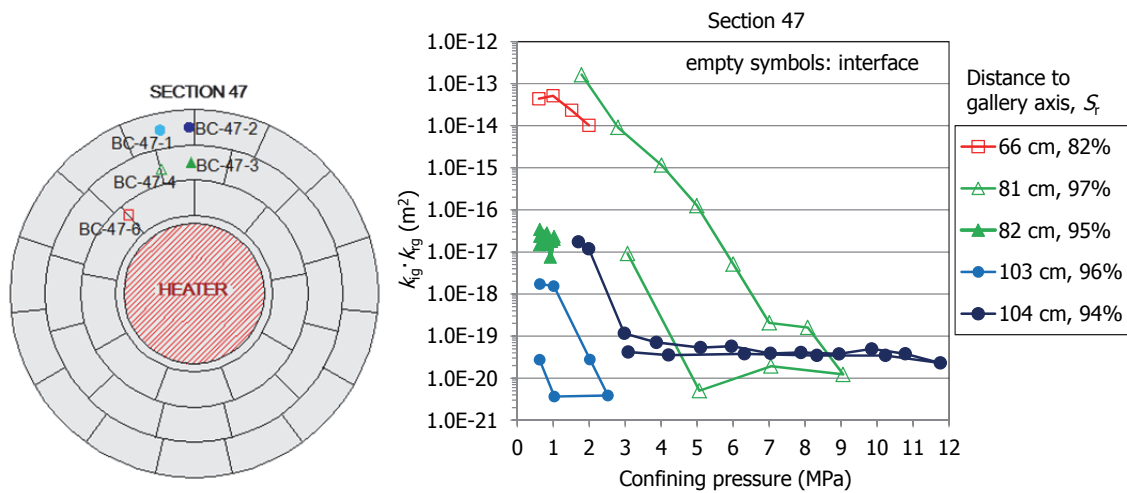


Fig. 106: Change of effective gas permeability with increase/decrease of confining pressure for samples from section S47

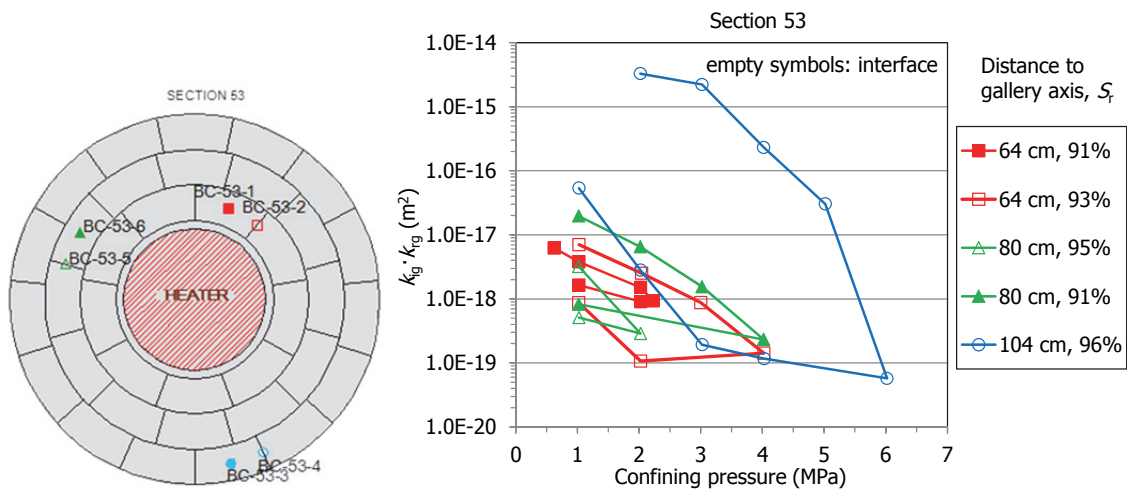


Fig. 107: Change of effective gas permeability with increase/decrease of confining pressure for samples from section S53

During unloading, as the confining pressure decreased the effective permeability increased, but the original values were never recovered. The irreversibility of this change was more noticeable in the samples with interface. Overall, the samples that had higher initial permeability –either because their degree of saturation was low or because they had an interface– had to be submitted to higher confining pressures to stop flow.

At the end of the tests it was checked that, during most of the gas permeability tests, the dry density of the samples increased (initial and final values are given in Tab. 8 to Tab. 10), which is consistent with the decrease in effective gas permeability occurred during the tests. The dry density of the samples increased after testing in all those tests in which the maximum confining pressure applied was higher than 2.5 MPa (except samples BC-47-1, BC-44-4 and BC-53-3). In fact, there is a positive linear correlation between the change in dry density and the maximum pressure applied ($R^2=0.6$), but the increase was more notable for maximum confining pressures below 5 MPa (Fig. 108).

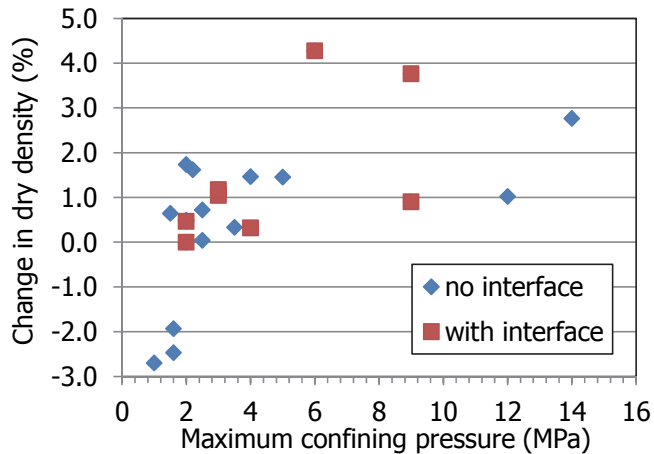


Fig. 108: Change in dry density occurred during gas testing (positive values indicate increase)

Most of the samples experienced during operation in the barrier an increase in void ratio, because the dry density of the blocks was higher than the average dry density of the barrier. Consequently the apparent preconsolidation stress decreased (Villar et al. 2017). The fact that they consolidated easily during gas testing would indicate that they were in the post-yield plastic region, and that the confining pressures applied were below the apparent preconsolidation stress. In fact, the apparent preconsolidation stress determined in the laboratory for the samples retrieved was in all cases higher than 11 MPa (Villar 2017). This also would explain the irreversibility of the gas permeability reduction, which did not increase to the original values upon unloading.

Final checking of water content along the samples showed that the gravimetric water content was usually lower in the upper part where gas was injected (although the differences inside a given sample were lower than 0.5%), which indicates that certain drying of the upper part of the samples took place as a consequence of gas flow, the water being pushed by the gas towards the bottom of the samples. In some cases water must have been expelled out of the sample, because the final water content was found to be lower than the initial one (Tab. 8 to Tab. 11).

5.1.5 Effect of accessible void ratio and degree of saturation

As demonstrated in previous researches (Villar 2002, Villar et al. 2013) gas permeability was best correlated with accessible void ratio, which expresses the ratio between gas accessible volume (not blocked by water) and particle volume and is computed as $e(1-S_r)$. This factor shows in fact a higher correlation with the permeability values than the dry density or the water content do. In order to analyse the effective gas permeability as a function of the accessible void ratio of each sample, the gas permeability measurements for six confining pressures have been plotted in Fig. 109. The accessible void ratio values of the samples tested were below 0.15, and the permeability was clearly higher the higher the accessible void ratio. The scatter in the data was high because the range of dry densities and water contents involved was large and there were also samples with and without interface.

Fig. 110 and Fig. 111 show the effect of different confining pressures on gas effective permeability (samples with and without interface) as a function of the degree of saturation and the accessible void ratio. The accessible void ratios were very low because the degrees of saturation of the FEBEX-DP samples are very high (79-100%). The effective gas permeability tended to be lower for higher degrees of saturation. In the range of confining pressures tested, the permeability decreased with the increase in confining pressure, as discussed above. Overall, for similar values of accessible void ratio, the samples with interface had higher permeability for all the range of confining pressures analysed. In fact, it has been checked that the presence of an interface had higher relevance than dry density on the gas permeability, probably because the gas transport mechanisms in both kinds of samples were not the same: flow took place through the accessible porous structure, but in the samples with interface it preferentially occurred along the interface according to a cubic law.

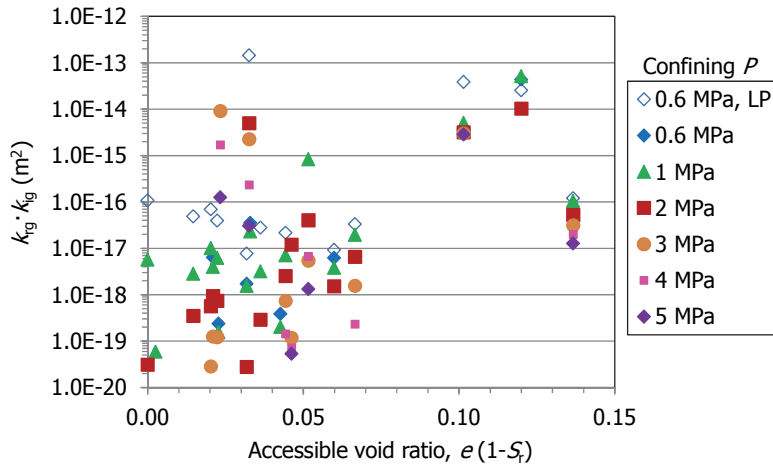


Fig. 109: Effective gas permeability measured in FEBEX-DP samples under different confining pressures, both in the low-pressure permeameter (LP) and in the high-pressure one

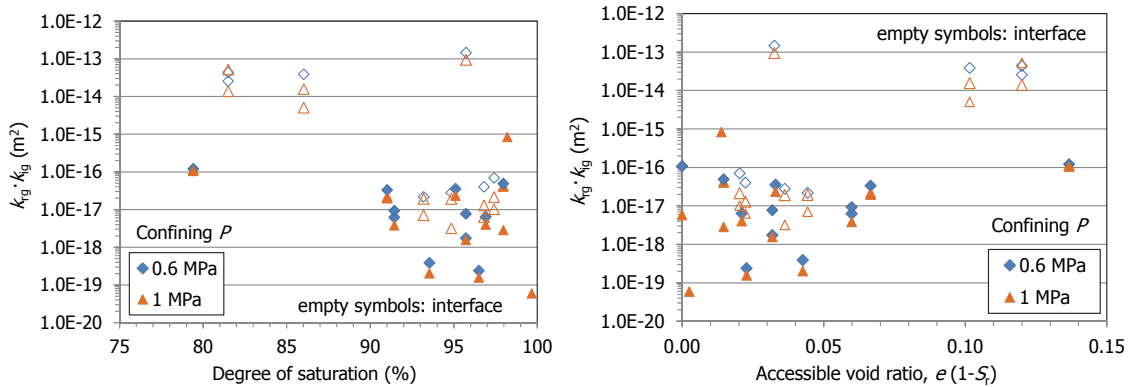


Fig. 110: Effect of confining pressure of 0.6 and 1 MPa on gas effective permeability for samples with and without interface, as a function of the degree of saturation (left) and the accessible void ratio (right)

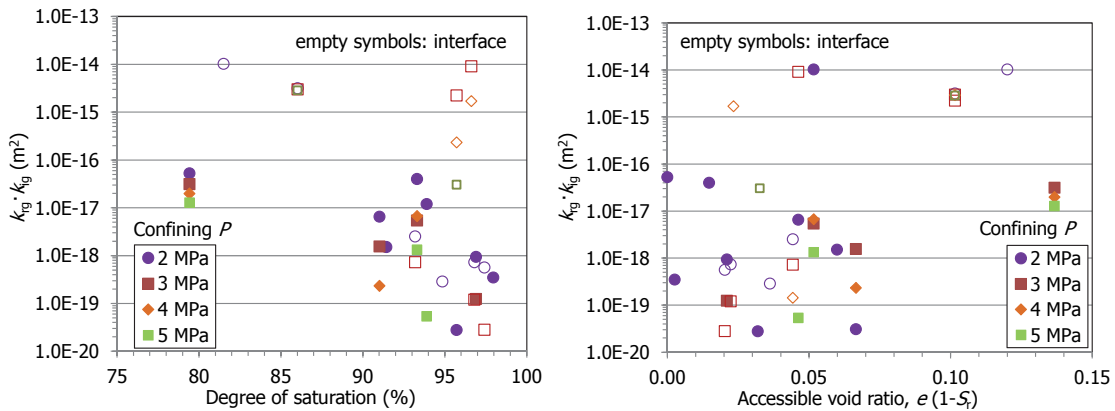


Fig. 111: Effect of confining pressure from 2 to 5 MPa on gas effective permeability for samples with and without interface, as a function of the degree of saturation (left) and the accessible void ratio (right)

5.1.6 Changes of gas permeability across the barrier

In line with the results from the LP setup presented in Fig. 94 and Fig. 95, the results obtained for the different sampling sections in the high-pressure equipment at constant confining pressure are plotted in Fig. 112 to Fig. 114. The distance of the samples tested to the gallery axis and the initial degree of saturation were shown in Tab. 5. Distances about 100 cm indicate that the sample was taken from the external ring of the barrier (the radius of the gallery was 114 cm), values around 80 cm correspond to samples taken from the middle ring and values around 60 cm correspond to samples taken from the inner ring, the one closest to the heater. For all the confining pressures applied the effective gas permeability decreased from the inner part of the barrier towards the granite in all sections. Indeed, the samples taken from the external ring of the barrier had the highest water contents and lowest dry densities. As it was observed in the LP setup, the samples with interface from the inner ring were the ones with the highest gas permeability, whereas in the samples from the external and middle ring of the barrier there was no difference between samples with or without interface, except for the sample BC-53-4 already commented above.

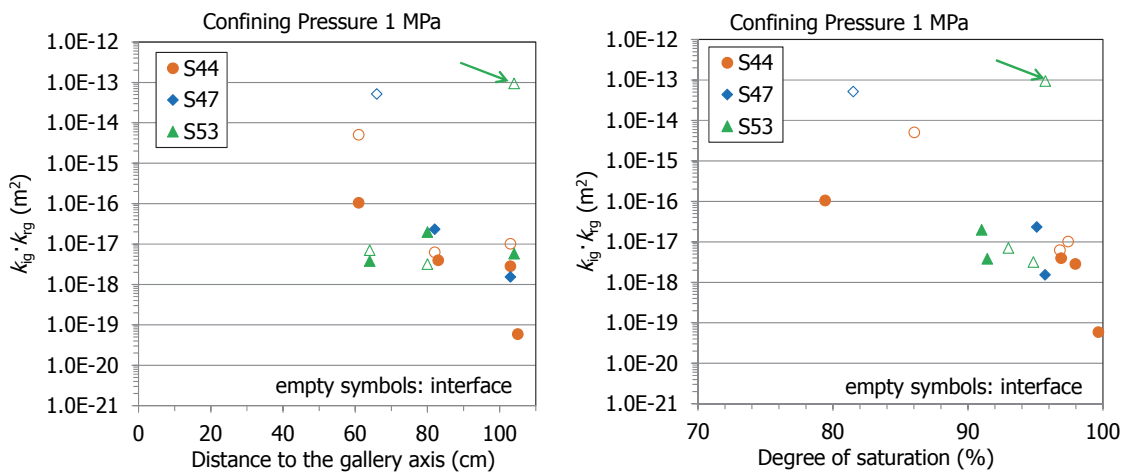


Fig. 112: Effective permeability values obtained in the high-pressure equipment as a function of the position in the barrier (left) and the initial degree of saturation (right) at a constant confining pressure of 1.0 MPa (the arrow indicates sample BC-53-4)

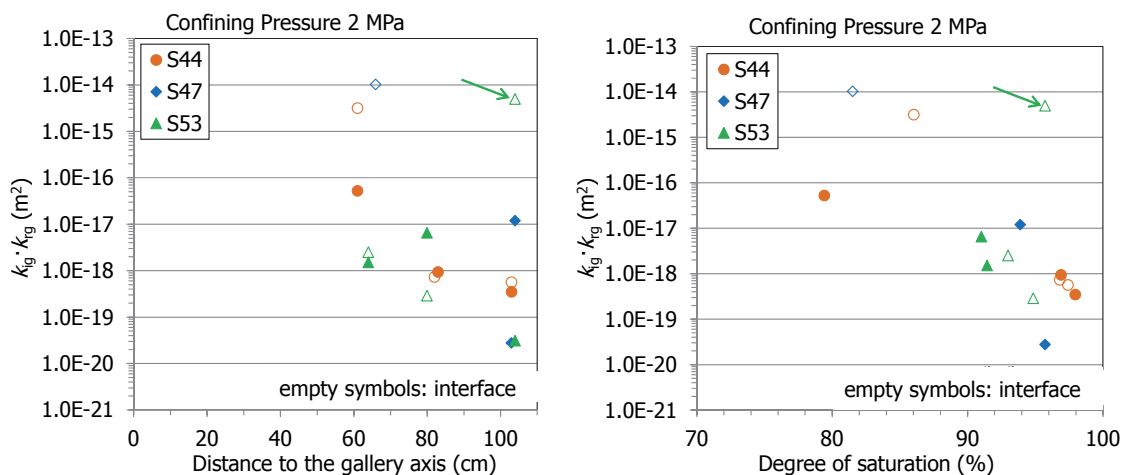


Fig. 113: Effective permeability values obtained in the high-pressure equipment as a function of the position in the barrier (left) and the initial degree of saturation (right) at a constant confining pressure of 2.0 MPa (the arrow indicates sample BC-53-4)

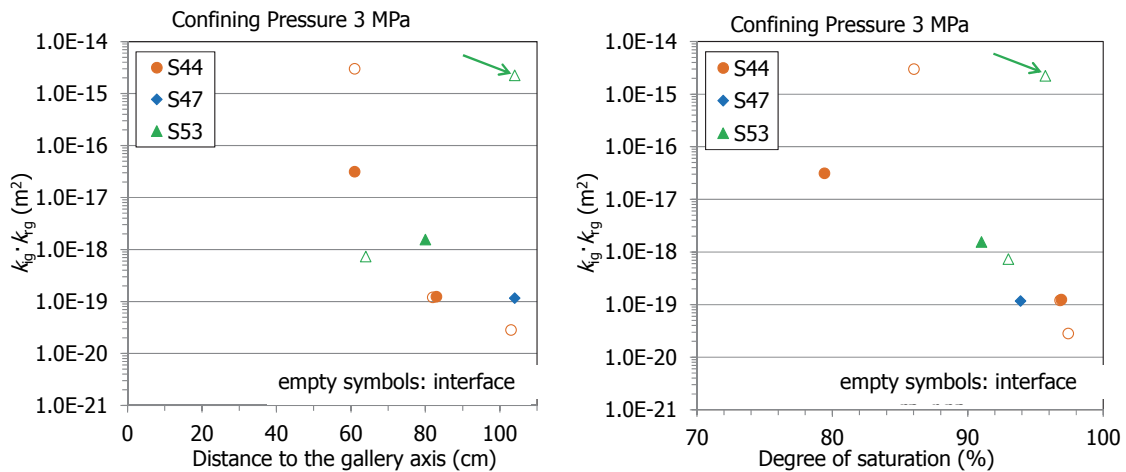


Fig. 114: Effective permeability values obtained in the high-pressure equipment as a function of the position in the barrier (left) and the initial degree of saturation (right) at a constant confining pressure of 3.0 MPa (the arrow indicates sample BC-53-4)

5.2 Changes in pore size distribution

The pore size distribution of some of the samples was determined before and after the gas permeability test by mercury intrusion porosimetry (MIP). A summary of the results obtained was given in subchapter 4.2. The curves in Fig. 86 to Fig. 92 did not show major changes in the pore size distribution occurred as a consequence of gas flow, apart from the overall decrease in void ratio of most samples already discussed in subchapter 5.1.3. The initial condition for each sample was obtained from a non-tested fragment adjacent to the tested core. If the pore size distribution is analysed in detail, it can be observed that there was an overall decrease in the macropore void ratio (pores >50 nm) after gas testing, whereas the void ratio corresponding to pores <50 nm did not clearly change (Fig. 115, left). However, in terms of the proportion of total void ratio corresponding to each of these pore sizes, the percentage of macropores decreased after gas testing while the percentage of pores <50 nm increased (Fig. 115, right). Hence, the increase in dry density observed in most samples after gas testing (Fig. 108) would have been achieved by the decrease in macropore volume. The interfaces did not seem to affect these pore size distribution changes. Fig. 116 shows the mode of the macropore and the mesopore sizes before and after gas testing. In the samples from the external ring the size of the macropores increased after gas testing, which could be connected with the opening of pathways, because the accessible void ratio in these samples was very low. The size of the mesopores did not change in a clear consistent way during gas testing, although it mostly tended to increase, except in the samples with interface.

The percentage of void ratio change occurred during gas testing for pores larger and smaller than 50 nm is shown in Fig. 117 as a function of the maximum confining pressure reached during gas testing. The higher the confining pressure applied the higher the decrease in macropore void ratio, whereas smaller pores did not seem to change coherently with confining pressure. These results agree well with the change of dry density as a consequence of the confining pressure applied during gas testing observed in Fig. 108, which was significant for confining pressures higher than 2 MPa. Since all the samples for which the PSD was analysed had been subjected to confining pressures higher than this value, the total void ratio, and particularly the void ratio corresponding to macropores, decreased in all of them.

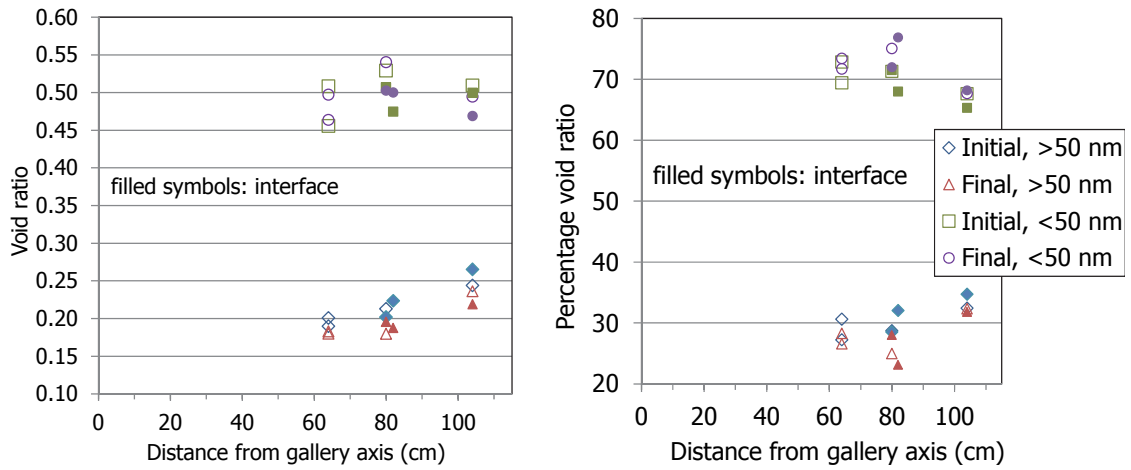


Fig. 115: Void ratio corresponding to pores larger and smaller than 50 nm of the bentonite samples before and after gas testing (same legend for the two figures)

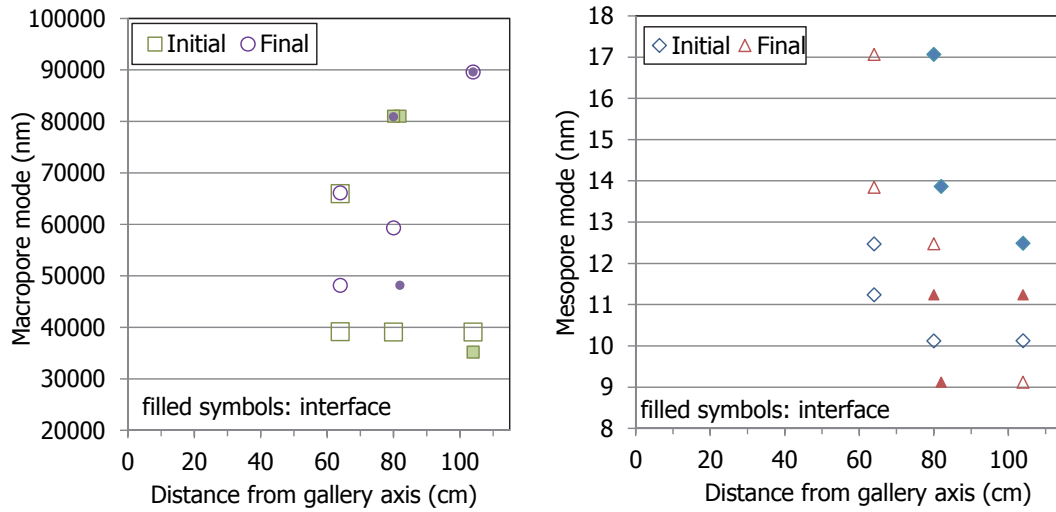


Fig. 116: Macropore and mesopore mode of the bentonite samples before and after gas testing

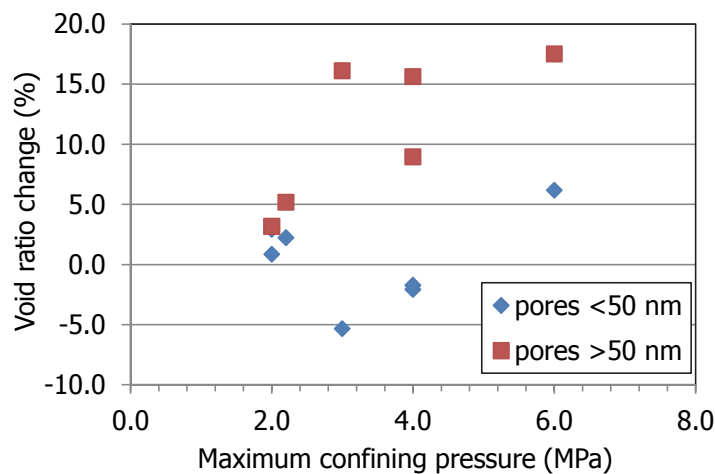


Fig. 117: Change in the void ratio corresponding to pores larger and smaller than 50 nm after gas testing (positive values indicate decrease)

5.3 Analysis of the Klinkenberg effect on gas permeability

In porous materials there can be a difference between the permeability values measured using gas or liquids as permeating fluid. Gas flows easily because it finds less obstacles on the grain surfaces than liquids. This effect is known as the Klinkenberg effect. Klinkenberg discovered that the permeability of a sample measured with gas flow is always higher than the permeability obtained using a liquid as fluid. Klinkenberg postulated (Klinkenberg 1941), thanks to his laboratory experiments, that the velocity of a liquid at the contact surface with the solid is zero whereas gases present certain mobility at this contact surface. In other words, gases slide on the solid surface. This slide generates a high flow rate for a specific differential pressure. Klinkenberg stated that the gas permeability depends on the mean free path of the gas molecules, therefore, it depends on the factors that affect such free path (temperature, pressure, type of gas). High gas pressure reduces the mean free path of the molecules and minimizes Klinkenberg effect. Therefore, gas permeability measured under high gas pressure will decrease, approaching liquid permeability.

If the permeability measured is plotted against the inverse of the medium pressure ($1/P_{\text{medium}}$) and a straight line intersects the y -axis at $1/P_{\text{medium}}=0$ (in other words, where P_{medium} is infinite) the permeability would be equal to the permeability obtained with a liquid as fluid (Fig. 118). This value effectively represents the permeability at which the gas is compressed by infinite pressure and becomes a near perfect liquid and is known as Klinkenberg apparent permeability.

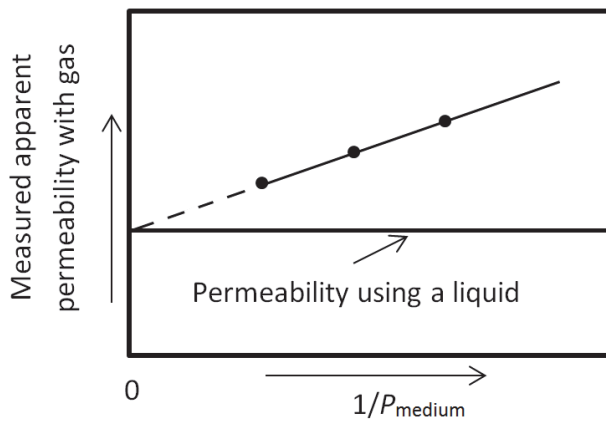


Fig. 118: Klinkenberg correction

$$k_{app} = \frac{k_g}{\left(1 + \frac{b}{P_{\text{medium}}}\right)} \quad [9]$$

where k_g is the measured gas permeability at a specific medium pressure (P_{medium}), k_{app} is the Klinkenberg apparent gas permeability corresponding to a k_g value, b is a constant value which depends on the porous size and P_{medium} is the medium pressure, $(P_{\text{up}} + P_{\text{dw}}) / 2$.

The Klinkenberg effect was analysed for the tests performed in FEBEX-DP samples in the high-pressure, steady-state setup, in which the backpressure was atmospheric. The analysis was performed for those steps in which the injection pressure was changed while confining pressure (P_c) was constant, which resulted in changes in the medium pressure. Since different confining pressures were applied, several ranges of $P_c - P_{\text{medium}}$ were analysed. Only those samples in which a noticeable range of medium pressure was applied were considered. The results of the analysis are shown in Fig. 119 to Fig. 123. The slopes of the fittings were in general very small, because the influence of the medium pressure on the permeability value was not significant.

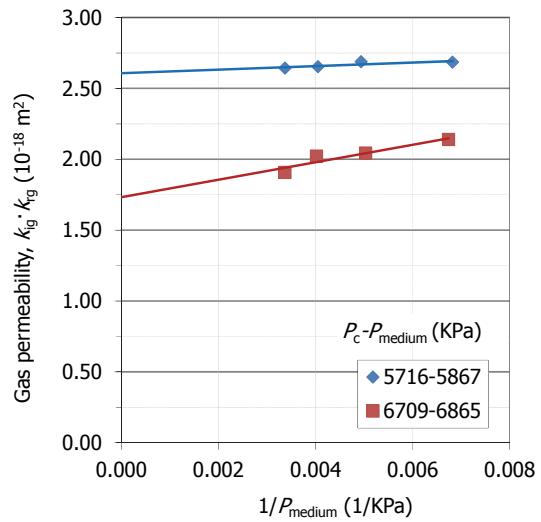
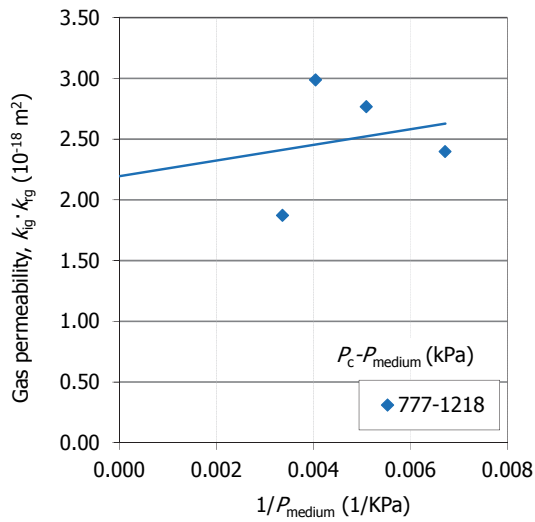


Fig. 119: Measured permeability versus inverse of medium pressure (P_{medium}) for tests BC-44-1 (left) and BC-44-2 (right)

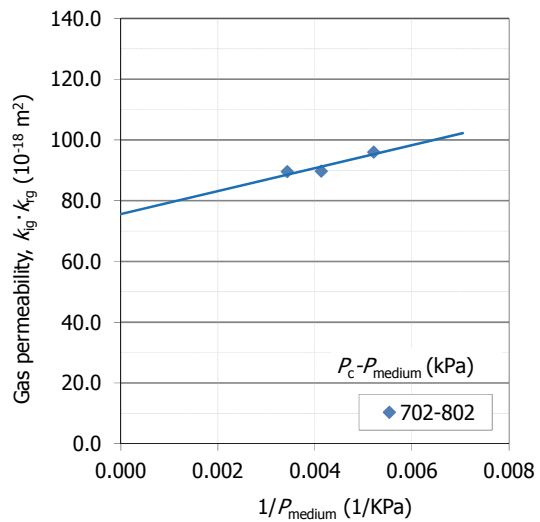
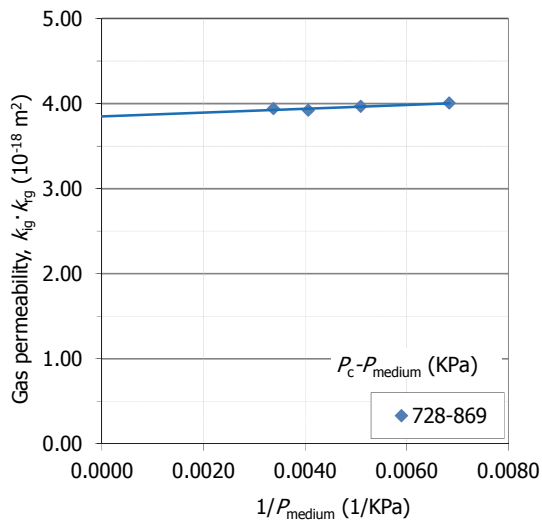


Fig. 120: Measured permeability versus inverse of medium pressure (P_{medium}) for tests BC-44-4 (left) and BC-44-7 (right)

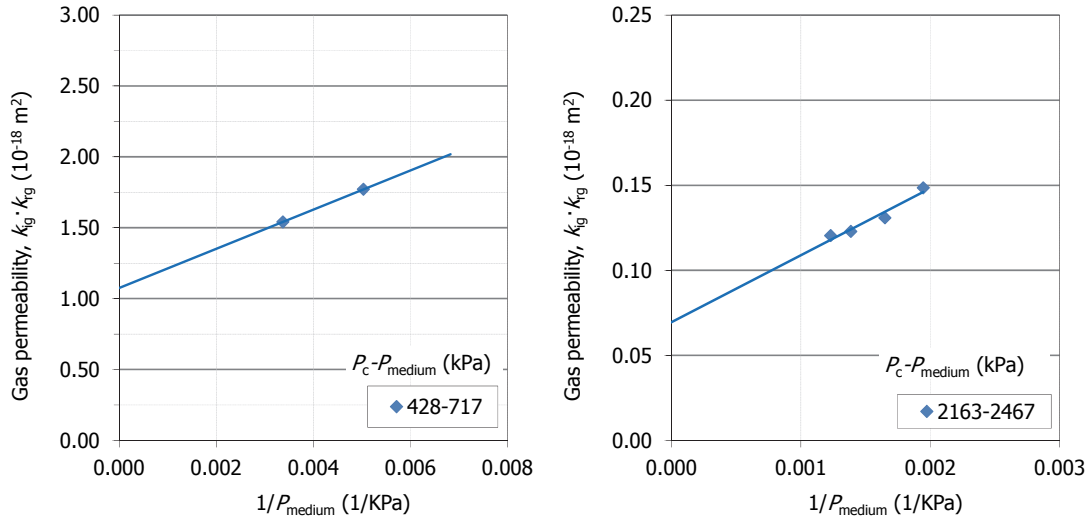


Fig. 121: Measured permeability versus inverse of medium pressure (P_{medium}) for tests BC-47-1 (left) and BC-47-2 (right)

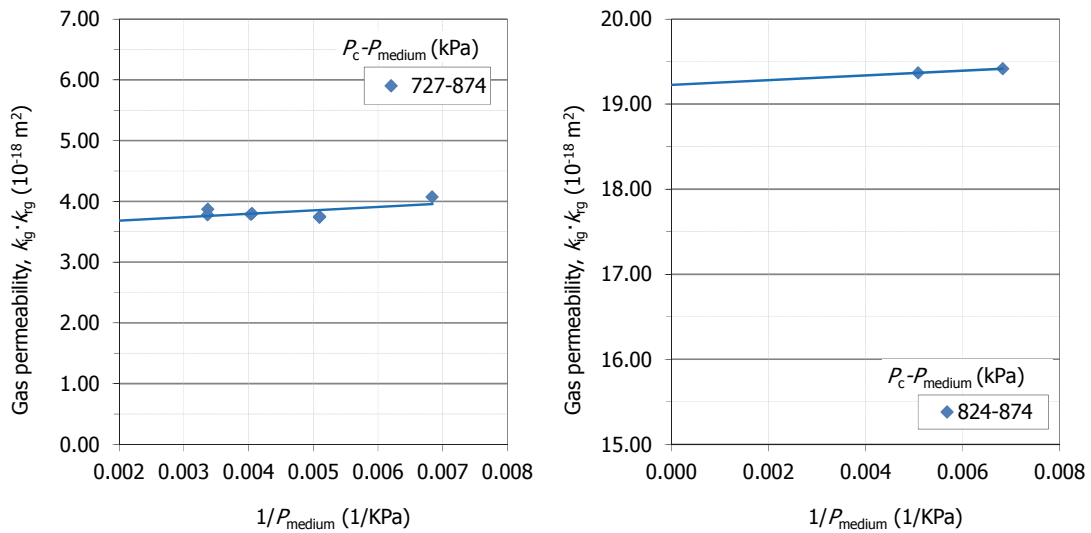


Fig. 122: Measured permeability versus inverse of medium pressure (P_{medium}) for tests BC-53-1 (left) and BC-53-6 (right)

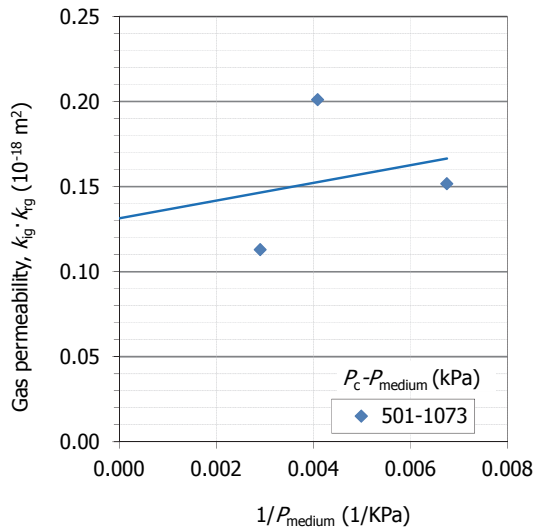


Fig. 123: Measured permeability versus inverse of medium pressure (P_{medium}) for tests BB-53-5-2

The apparent gas permeability values (k_{app}) obtained applying the Klinkenberg correction are summarised for each range of $P_c - P_{medium}$ in Tab. 12. The permeability values obtained applying the Klinkenberg correction are similar to the average of all the permeability values measured in each sample for a given confining pressure. This would mean that the injection pressures applied did not have a large influence on permeability. The effective gas permeability values for each test are shown in Fig. 124 against their gas permeability correcting the gas slippage (apparent gas permeability). There are no noticeable differences between both values. For this reason, it is considered that the Klinkenberg effect was not relevant in the range of pressures applied, since they probably were high enough and there was no slippage contribution to gas flow.

Tab. 12: Analysis of the Klinkenberg effect

Reference	Final ρ_d (g/cm ³)	Final w (%)	Initial S_r (%)	Range $P_c - P_{medium}$ (kPa)	$P_c - P_{medium}$ (kPa)	Average ^a $k_{ig} \cdot k_{rg}$ (m ²)	k_{app} ^b (m ²)
BC-44-1	1.58	25.7	98	777-1218	924	$2.5 \cdot 10^{-18}$	$2.2 \cdot 10^{-18}$
BC-44-2	1.62	22.3	86	5716-5867	5790	$2.7 \cdot 10^{-18}$	$2.6 \cdot 10^{-18}$
				6709-6865	6788	$2.0 \cdot 10^{-18}$	$1.7 \cdot 10^{-18}$
BC-44-4	1.61	24.4	97	728-869	797	$4.0 \cdot 10^{-18}$	$3.8 \cdot 10^{-18}$
BC-44-7	1.65	19.9	79	702-802	2276	$9.2 \cdot 10^{-17}$	$7.6 \cdot 10^{-17}$
BC-47-1	1.55	26.3	96	428-717	420	$1.7 \cdot 10^{-18}$	$1.1 \cdot 10^{-18}$
BC-47-2	1.55	25.9	94	2163-2467	2316	$1.3 \cdot 10^{-19}$	$6.9 \cdot 10^{-20}$
BC-53-1	1.93	23.4	91	727-874	779	$3.8 \cdot 10^{-18}$	$3.6 \cdot 10^{-18}$
BC-53-6	1.57	23.4	91	824-874	851	$1.9 \cdot 10^{-17}$	$1.9 \cdot 10^{-17}$
BB-53-5-2	1.59	24.3	94	501-1073	781	$1.6 \cdot 10^{-19}$	$1.3 \cdot 10^{-19}$

^a average of all the values obtained using different injection pressures under a given $P_c - P_{medium}$ range

^b apparent gas permeability correcting the Klinkenberg effect

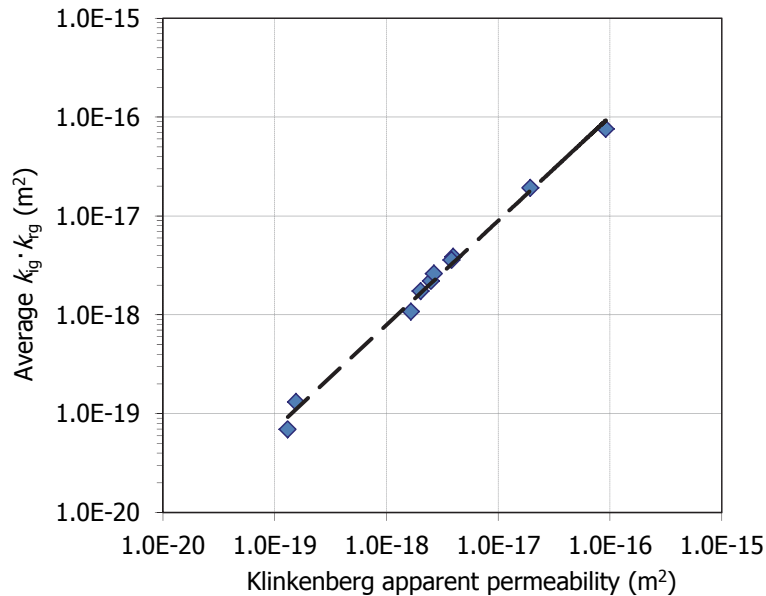


Fig. 124: Effective gas permeability (average of all the measurements obtained for different ranges of P_c - P_{medium}) versus apparent gas permeability applying Klinkenberg correction. The measurements were performed in samples of different water contents and dry densities (Tab. 12)

5.4 Comparison with the reference bentonite

The gas permeability of the reference FEBEX bentonite samples, compacted to different dry densities with various water contents, was measured during the FEBEX project in the same LP setup used in the current research (Villar 2002) and during the FORGE project in the same HP-S setup used in this work (Villar et al. 2013). In the first case (falling-head or unsteady-state permeameter) the confining pressure applied was 0.6 MPa and the injection pressure decreased during the tests from an initial value of 0.1 MPa. In the second case (constant pressure or steady-state permeameter), confining pressures of 0.6 and 1 MPa were applied. For gas pressures below 1.2 MPa no effect of the injection or confining pressures on the value of permeability was empirically detected in those tests. The samples tested in those researches had degrees of saturation lower than 0.97. The results obtained in FEBEX and in FORGE are plotted in Fig. 125, along with the correlation curve between gas effective permeability, $k_{ig} \cdot k_{rg}$, and accessible void ratio, $e(1-S_r)$, which has the following expression, with $a = 1.25 \cdot 10^{-12} \pm 1.34 \cdot 10^{-12}$ and $b = 3.22 \pm 1.26$ (Villar et al. 2013):

$$k_{ig} \cdot k_{rg} = a (e(1-S_r))^b \quad [10]$$

The new values measured for the samples retrieved during the FEBEX-DP have also been plotted in Fig. 125 and are more clearly seen in the enlargement presented in Fig. 126. In order to make the results strictly comparable, only those values obtained under confining pressures of 0.6 and 1 MPa have been represented. These values were obtained in the two same setups as the values obtained for the reference sample. The accessible void ratio of the FEBEX-DP samples is in the low range of the FEBEX samples, because their degree of saturation was very high. Nevertheless, the new values obtained after 18 years under barrier conditions are consistent with those of the reference bentonite, except for the samples with interface, some of which had gas permeabilities clearly higher than those obtained with Eq. 10. However, the samples with interface that had a very low accessible void ratio (such as BC-44-6, which was drilled in the external ring of the barrier) had permeabilities closer to that of the reference bentonite. An exception is sample BC-53-4, which was drilled in the external ring of the barrier, and showed higher permeability than expected. A reason could be that the interface was quite open before testing (see comments in subchapter 5.1.1 and Fig. 74).

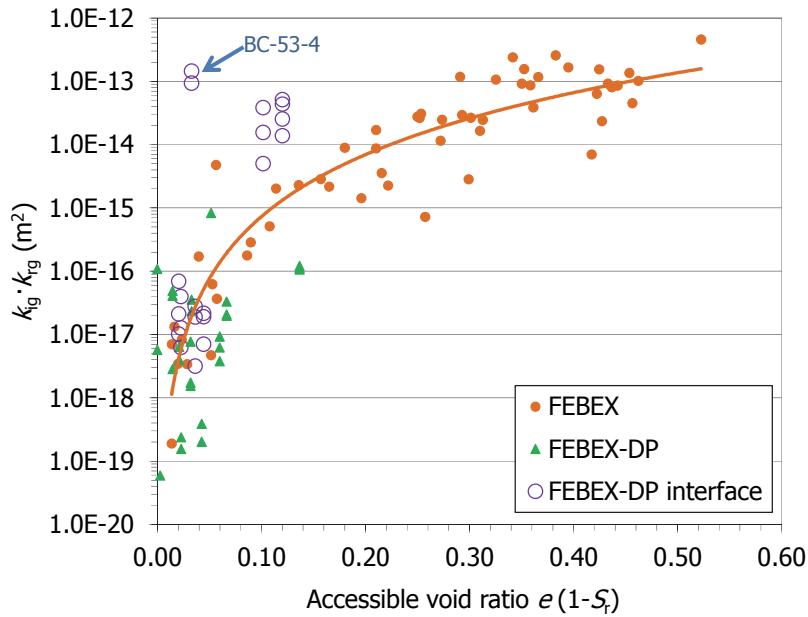


Fig. 125: Gas permeability as a function of the accessible porosity for FEBEX samples tested during the FEBEX and FORGE projects (Eq. 10) and for FEBEX-DP samples with and without interface

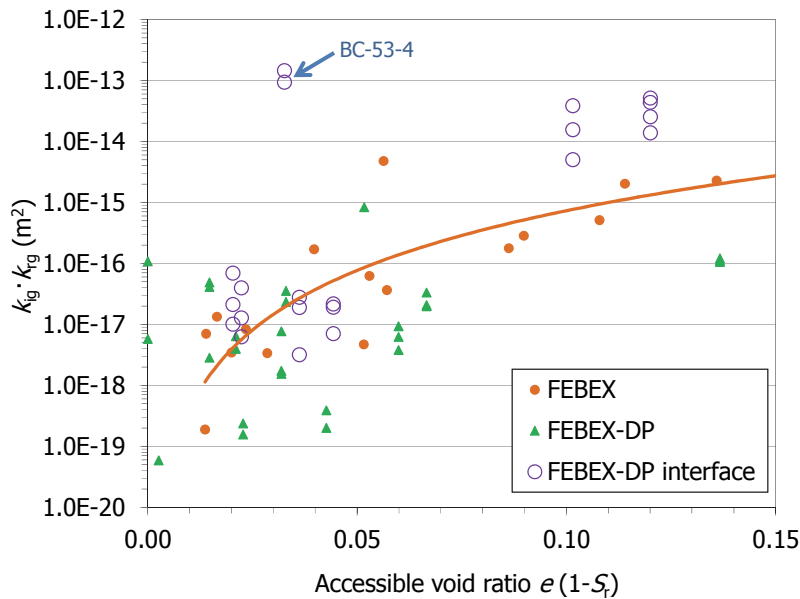


Fig. 126: Gas permeability as a function of the accessible porosity for FEBEX samples tested during the FEBEX and FORGE projects and for FEBEX-DP samples with and without interface (enlargement of Fig. 125)

If the correlation between accessible void ratio and gas permeability shown in Eq. 10 is extrapolated towards a value close to null accessible void ratio (say 0.002), which would almost correspond to completely saturated samples, the intrinsic permeability would be in the order of 10^{-21} m^2 , which is the same order of magnitude as the intrinsic permeability measured in saturated samples of dry density 1.6 g/cm^3 with water flow (Eq. 1).

6 SUMMARY AND CONCLUSIONS

The FEBEX in situ test was a full-scale experiment performed under natural conditions to reproduce the Engineered Barrier System (EBS) of an underground repository for nuclear waste. The barrier around the heater that simulated the waste container was composed of FEBEX bentonite blocks and had an average dry density of 1.6 g/cm^3 . After 18 years of operation under repository conditions, namely natural hydration from the granitic host rock and heating from the canister, the heater was switched off and after some cooling the experiment was dismantled. During dismantling many bentonite samples were taken, preserved and sent to different laboratories, among which CIEMAT's.

The gas permeability of core samples from the FEBEX-DP project, taken at different positions around the heater by drilling the bentonite blocks on site (22 samples) or in the laboratory (3 samples), were measured for different confining and injection pressures. These samples had initial dry density values between 1.51 and 1.64 g/cm^3 and water contents between 19.5 and 29.0%, corresponding to initial degrees of saturation between 79 and 104%. Some of these samples were drilled between two blocks, therefore they had an interface along the core.

The aim of the tests was to check, for bentonite samples submitted to EBS conditions for 18 years, the following:

- the influence on gas permeability of the physical state of the samples in terms of water content and dry density and consequently of degree of saturation,
- the effect of the boundary conditions on gas permeability, namely gas injection pressure and confining pressure,
- the change of gas transport properties with respect to the untreated, reference FEBEX bentonite and
- the role of interfaces on gas transport.

To accomplish this the core samples were tested in two custom-built setups, one of them working as an unsteady-state permeameter under low injection and confining pressures (below 1 MPa), and the other one working as a steady-state permeameter in which injection pressures and confining pressures as high as 1.4 and 9 MPa, respectively, were applied. The samples were not artificially saturated prior to or during gas testing.

The gas permeability of the samples depended on water content and dry density, decreasing with the increase of both. These two variables changed across the barrier as a function of the distance to the heat and water sources, i.e. the heater and the granite. The samples closest to the heater had lower water content and higher dry density, whereas the samples closest to the granite had the highest water content and lowest dry density. Thus, the gas permeability of the samples was also related to their position in the barrier, tending to be lower towards the granite, where the degree of saturation was higher.

During the tests, the gas flow observed was steady in most cases, except for some of the more saturated samples. Except for these few samples, no effect of the injection pressure on the permeability values was detected. Moreover, it was checked that the Klinkenberg effect was not significant in the range of pressures applied in the tests. However, the gas permeability was clearly affected by the stress state. It decreased noticeably with the increase in confining pressure up to 4 MPa, particularly for the wetter samples, those taken closer to the granite. Beyond a confining stress of 9 MPa no gas flow took place through any of the wetter samples, hence the breakthrough pressure for them would be higher than this value. In contrast, flow took place through the drier samples, which had initial suctions well below the air entry value for the FEBEX compacted bentonite, even for confining pressures as high as 9 MPa. This would indicate that there was insufficient moisture to reduce or block the air-filled pore network of the specimens and minimise gas flow. The decrease in permeability occurred during loading was not reversible, and the gas permeability of the samples after unloading was lower than the initial one. The fact that the samples consolidated easily during gas testing would indicate that they were in the post-yield plastic region, and that the confining pressures applied were below the apparent preconsolidation stress. In fact, the apparent preconsolidation stress determined in the laboratory for the samples retrieved was in all cases higher than 11 MPa (Villar 2017). This also would explain the irreversibility of the gas permeability reduction, which did not increase to the original values upon unloading. In fact, the

dry density of the samples at the end of the tests in which confining pressures higher than 2 MPa were applied was higher than the initial one.

The pore size distribution analyses carried out by mercury intrusion porosimetry (MIP) showed a decrease in the macropore void ratio in all the samples tested (all of them applying maximum confining pressures higher than 2 MPa). This decrease was more significant as the confining pressure applied during gas testing was higher. This would mean that the compression exerted by the confining pressure was mostly absorbed by the macropores, whereas the pores smaller than 50 nm were not affected by gas flow. In some of the wetter samples an increase of the size of the macropores was observed after gas testing, which could correspond to the opening of pathways allowing gas flow, given the very low accessible void ratio of these nearly saturated samples.

The gas permeability of the samples was mainly related to their void ratio accessible for gas flow, $e(1-S_r)$, which depends on water content and dry density. Because of the high water saturation of most of the barrier after the long operation period, the accessible void ratio was below 0.15 in all the samples tested, and decreased towards the external part of the barrier, where the degree of saturation was higher. The gas permeability decreased with the accessible void ratio according to a power law, in the same way as expected for the FEBEX reference bentonite. Therefore, it seems that no changes on the gas transport properties of the bentonite took place during operation.

Previous laboratory studies showed that, in the FEBEX compacted bentonite and under isochoric condition, two-phase flow seemed to take place for degrees of saturation lower than about 97%, whereas for higher degrees of saturation pathway dilation could be the predominant mechanism. The threshold pressure for gas entry into the bentonite was higher than the swelling pressure and seemed to be lower than the gas pressure required for fracturing (macroscopically) the material. In contrast, in the research reported here, two-phase flow seems to have taken place in most cases, even for samples with degree of saturation higher than 97%. The fact that these samples were tested under constant confining stress instead of under no volume change conditions (isochoric), would have made easier the transport of gas, with opening of trajectories for gas flow. As the confining stress increased, the tortuosity of these gas pathways would increase, which would have caused the decrease in gas permeability, and eventually the closing of pathways.

Samples with an interface drilled in the internal ring of the barrier had higher permeability than samples of similar accessible void ratio with no interface, and it was necessary to apply higher confining pressures to reduce or suppress gas flow in them. The gas transport in these samples took probably place preferably along the interface, following "models" of flow in deformable rock fractures, in which liquid flow takes place according to a local cubic law or its variations. In contrast, wetter samples drilled along interfaces of the intermediate and external rings of the barrier (which had very low accessible void ratio, due to saturation), had permeabilities closer to that corresponding to the same accessible void ratio in the reference bentonite. In fact, in the latter samples the interfaces were barely visible and looked like sealed already before gas testing.

The effective permeability values given in this report are probably conservative, since they were obtained for stress situations maintained for relatively short periods of time (a few hours), whereas in some cases it has been checked that gas permeability was lower if the samples were compressed for longer periods of time. Besides, the effect of temperatures in the range of those expected around the canisters of a real repository has not been checked, since all the measurements were performed at laboratory temperature.

The results obtained suggest that the gas generated in the proximity to the waste containers would be able to move by advection as long as the bentonite around it remains unsaturated, more easily along interfaces. However, it is likely that in a real repository even the drier interfaces in the internal part of the bentonite barrier would not be preferential gas pathways once the external part of the barrier is saturated, because the high stresses in the system would close them. Total pressures above 2 MPa were measured in the intermediate bentonite ring of the FEBEX in situ test at the end of operation (Martínez et al. 2016). In any case, the external, fully saturated part of the barrier would block gas movement away from the barrier, and gas would only be able to escape slowly by diffusion in the pore water or suddenly by breakthrough if gas pressure builds up above a value that would be higher than the swelling pressure of the bentonite if conditions are isochoric, or around 3-4 MPa under constant stress conditions.

ACKNOWLEDGEMENTS

This work has been financed by the FEBEX-DP consortium (NAGRA, SKB, POSIVA, CIEMAT, KAERI) and through the Annex XLII of the ENRESA-CIEMAT framework agreement. Part of the laboratory work was performed by J. Aroz, R.J. Iglesias, and F.J. Romero. The mercury intrusion porosimetry tests were performed at the Petrophysical laboratory of CIEMAT by N. Brea, supervised by Dr. R. Campos. Beatriz Carbonell was hired in the framework of the Spanish National System of Youth Guarantee in R+D 2014, with financing of the European Social Fund and the Youth Employment Initiative.

7 REFERENCES

- Bárcena, I., Fuentes-Cantillana, J.L., García-Siñeriz, J.L., 2003. Dismantling of the heater 1 at the FEBEX "in situ" test. Description of operations. Publicación Técnica ENRESA 09/2003, Madrid, 134 pp.
- Bárcena, I, García-Siñeriz, J.L. 2015. FEBEX-DP (GTS) Full Dismantling Sampling Plan (in situ Experiment). Nagra Arbeitsbericht NAB 15-14. 103 pp.
- Bárcena, I., García-Siñeriz, J.L., Huertas, F. 2006. FEBEX Project Final Report. Addendum sensors data report. In situ experiment. Publicación Técnica ENRESA 05-5/2006. Madrid, 157 pp.
- Carbonell, B., Villar, M.V., Martín, P.L., Gutiérrez-Álvarez, C. (in press). Gas transport in compacted bentonite after 18 years under barrier conditions. *Geotechnics for Energy and the Environment*.
- ENRESA 1995. Almacenamiento geológico profundo de residuos radiactivos de alta actividad (AGP). Diseños conceptuales genéricos. Publicación Técnica ENRESA 11/95. 105 pp. Madrid.
- ENRESA 2000. FEBEX Project. Full-scale engineered barriers experiment for a deep geological repository for high level radioactive waste in crystalline host rock. Final Report. Publicación Técnica ENRESA 1/2000, Madrid, 354 pp.
- ENRESA 2006. FEBEX Full-scale Engineered Barriers Experiment, Updated Final Report 1994-2004. Publicación Técnica ENRESA 05-0/2006, Madrid, 590 pp.
- Fernández, A.M., Sánchez-Ledesma, D.M., Melón, A., Robredo, L. M., Rey, J.J., Labajo, M., Clavero, M.A., Carretero, S., González, A.E. 2018. Thermo-hydro-geochemical behaviour of a Spanish bentonite after of the FEBEX in situ test at the Grimsel Test Site. Technical report CIEMAT/DMA/2G216/03/16. NAB16-025. Madrid, 256 pp.
- Fuentes-Cantillana, J.L., García-Siñeriz, J.L. 1998. FEBEX. Final design and installation of the "in situ" test at Grimsel. Publicación Técnica ENRESA 12/98. Madrid, 184 pp.
- García-Siñeriz, J.L., Abós, H., Martínez, V., de la Rosa, C., Mäder, U., Kober, F. 2016. FEBEX-DP Dismantling of the heater 2 at the FEBEX "in situ" test. Description of operations. NAB 16-011. 92 pp.
- Gutiérrez-Rodrigo, V., Villar, M.V., Martín, P.L. & Romero, F.J. 2014: Gas transport properties of compacted bentonite. In: Khalili, N., Russell, A., Khoshghalb, A. (Eds.): *Unsaturated Soils: Research and Applications*, vol. 2: 1735-1740. Taylor & Francis Group, London. ISBN: 978-1-138-00150-3.
- Gutiérrez-Rodrigo, V., Villar, M.V., Martín, P.L., Romero, F.J., Barcala, J.M. 2015. Gas-breakthrough pressure of FEBEX bentonite. In: Shaw, R. P. (ed.) *Gas Generation and Migration in Deep Geological Radioactive Waste Repositories*. Geological Society, London, Special Publications, 415, 47-57. First published online November 14, 2014. <http://dx.doi.org/10.1144/SP415.4>.
- Iglesias, R.J., Carbonell, B., Villar, M.V. 2018. FEBEX-DP. Postmortem analyses of bentonite performed at CIEMAT. Laboratory sampling logs. Technical Report CIEMAT/DMA/2G218/2/18. Madrid, 114 pp.
- Klinkenberg, L.J. 1941. The permeability of porous media to liquids and gases. *Drilling and Production Practice*, American Petroleum Institute, New York, 200-2013.

- Lloret, A. 1982. Comportamiento deformacional del suelo no saturado bajo condiciones drenadas y no drenadas. Ph. D. Thesis. Universidad Politécnica de Cataluña.
- Lloret, A., Villar, M.V. 2007. Advances on the knowledge of the thermo-hydro-mechanical behaviour of heavily compacted FEBEX bentonite. *Physics and Chemistry of the Earth Parts A/B/C* 32 (8-14): 701-715.
- Loosveldt, H., Lafhaj, Z. & Skoczylas, F. 2002. Experimental study of gas and liquid permeability of a mortar. *Cement and Concrete Research* 32: 1357–1363
- Martínez, V., Abós, H., García-Siñeriz, J.L. 2016. FEBEX-e: Final Sensor Data Report (FEBEX In Situ Experiment). *Nagra Arbeitsbericht NAB 16-019*. Madrid, 244 pp.
- Scheidegger, A. E. 1974. *The Physics of Flow Through Porous Media*, 3rd ed. University of Toronto Press, Toronto.
- Shaw, R.P. 2015. The Fate of Repository Gases (FORGE) Project. In: Shaw, R. P. (ed.) *Gas Generation and Migration in Deep Geological Radioactive Waste Repositories*. Geological Society, London, Special Publications 415: 1-8.
- Sing, KSW, Everett, DH, Haul, RAW, Moscou, L, Pierotti, RA, Rouquérol, J & Siemieniewska, T (1985) Reporting physisorption data for gas/solid systems with special reference to the determination of surface area and porosity. *Pure & Appl. Chem.* 57(4): 603-619. IUPAC.
- Villar, M.V. 2002. Thermo-hydro-mechanical characterisation of a bentonite from Cabo de Gata. A study applied to the use of bentonite as sealing material in high level radioactive waste repositories. *Publicación Técnica ENRESA 01/2002*, Madrid, 258 pp.
- Villar, M.V. (Ed.) 2006. FEBEX Project Final report. Post-mortem bentonite analysis. *Publicación Técnica ENRESA 05-1/2006*, Madrid, 183 pp.
- Villar, M.V.(Ed). 2017. FEBEX-DP Postmortem THM/THC Analysis Report. NAB 16-017. 143 pp.
- Villar, M.V., Lloret, A. 2001. Variation of the intrinsic permeability of expansive clay upon saturation. In: ADACHI, K. & FUKUE, M.(eds.): *Clay Science for Engineering*. Balkema, Rotterdam. 259-266.
- Villar, M.V., Lloret, A. 2008. Influence of dry density and water content on the swelling of a compacted bentonite. *Applied Clay Science* 39: 38-49.
- Villar, M.V., Gómez-Espina, R. 2009. Report on thermo-hydro-mechanical laboratory tests performed by CIEMAT on febex bentonite 2004-2008. *Informes Técnicos CIEMAT 1178*. Madrid, 67 pp. Agosto 2009.
- Villar, M.V., Gutiérrez-Rodrigo, V., Martín, P.L., Romero, F.J., Barcala, J.M. 2013. Gas transport in bentonite. *Informes Técnicos CIEMAT 1301*. Madrid, 63 pp.
- Villar, M.V., Iglesias, R.J., Abós, H., Martínez, V., de la Rosa, C., Manchón, M.A. 2016a. FEBEX-DP onsite analyses report. NAB 16-012. 106 pp.
- Villar, M.V.; Iglesias, R.J.; Gutiérrez, C. & Campos, G. 2017. Use of psychrometers, capacitive sensors and vapour transfer technique to determine the water retention curve of compacted bentonite. In: Ferrari, A. & Laloui, L. (Eds.) *Advances in Laboratory Testing and Modelling of Soils and Shales (ATMSS)*. Springer Series in Geomechanics and Geoenvironment, pp 123-130. Springer, Cham, Switzerland. DOI 10.1007/978-3-319-52773-4_13.
- Villar, M.V., Iglesias, R.J., Gutiérrez-Álvarez, C., Carbonell, B., Campos, R., Campos, G., Martín, P.L., Castro, B. 2018b. FEBEX-DP: Thermo-hydro-mechanical postmortem analysis of bentonite performed at CIEMAT. Technical report CIEMAT/DMA/2G216/2/16. NAB16-024. Madrid, 134 pp.
- Yoshimi, Y., Osterberg, J.O. 1963. Compression of partially saturated cohesive soils. *J. Soil Mechanics and Foundations Division. ASCE* 89, SM 4, 1-24.



GAS PERMEABILITY OF BENTONITE SAMPLES OF THE FEBEX DISMANTLING PROJECT (FEBEX-DP)

ANNEX I “DETAILED CHARACTERISTICS OF THE TESTS”

GAS PERMEABILITY

SAMPLE	BC-36-1	
START DATE:	03/06/2015	
END DATE:	25/11/2015	
SETUP:	HP-US	

GAS CHARACTERISTICS

viscosity N₂ 1.78E-05 Pa·s (at 20°C)
 density N₂: 1.12 kg/m³
 g: 9.80665 m/s²

CYLINDER	INPUT	1.526E-04
VOLUME (m ³)	OUTPUT	1.482E-04
CELL	Steel triaxial	
SAMPLE	latex + neoprene	
WRAPPING		

SAMPLE CHARACTERISTICS

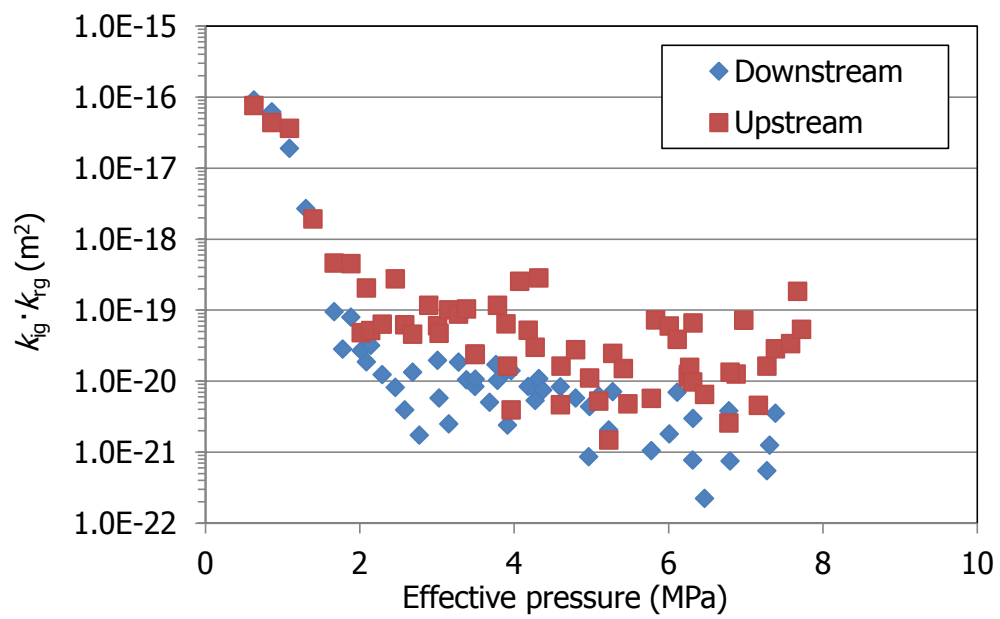
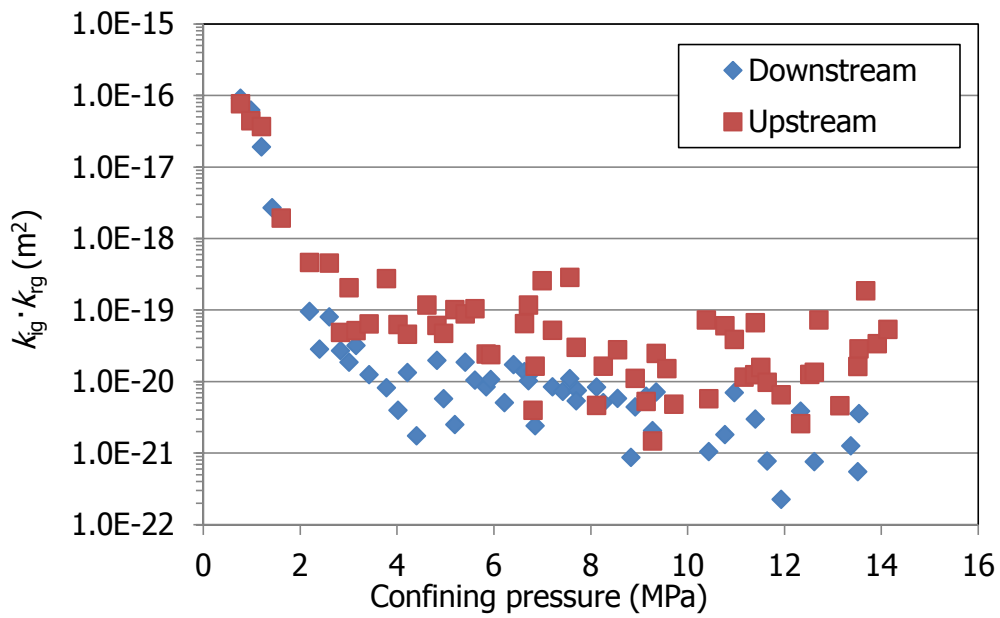
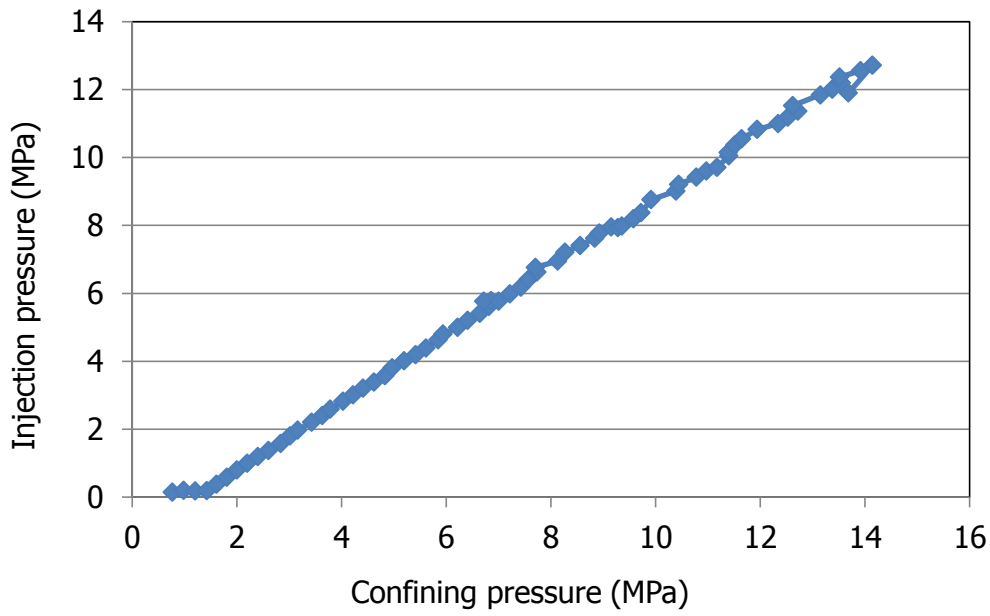
			Initial	Final
Specific weight (g/cm ³)	2.70	ρ _d (g/cm ³)	1.52	1.57
Initial weight (g)	68.07	h (cm)	3.11	3.16
Final weight (g)	67.09	φ (cm)	3.80	3.72
Dry weight (g)	53.73	Area (cm ²)	11.34	10.87
		w (%)	28.1	26.7
		S _r (%)	98	96

Stage	Time elapsed (h)	Confining P (MPa)	Injection P (MPa)	Back P (MPa)	k _{ig} · k _{rg} H (m ²)	k _{ig} · k _{rg} L (m ²)	k _g H (m/s)	k _g L (m/s)	T (°C)	P _{medium} (MPa)	P _c -P _{medium} (MPa)
1	216	0.77	0.14	0.13	7.6E-17	9.1E-17	9.1E-11	4.0E-11	24.9	0.14	0.63
2	284	0.98	0.20	0.04	4.4E-17	6.2E-17	5.7E-11	9.7E-12	23.5	0.12	0.86
3	312	1.21	0.18	0.05	3.6E-17	1.9E-17	4.3E-11	5.3E-12	23.4	0.12	1.09
4	336	1.42	0.19	0.05		2.7E-18		8.5E-13	23.4	0.12	1.30
5	360	1.61	0.38	0.05	1.9E-18		4.5E-12		23.5	0.21	1.40
6	384	1.81	0.59	0.05					23.5	0.32	1.49
7	456	2.00	0.80	0.05					23.6	0.43	1.57
8	480	2.19	0.99	0.05	4.6E-19	9.5E-20	2.8E-12	3.1E-14	23.6	0.52	1.67
9	500	2.40	1.19	0.05		2.8E-20		9.3E-15	23.7	0.62	1.78
10	528	2.60	1.38	0.05	4.5E-19	8.0E-20	3.8E-12	2.6E-14	23.6	0.71	1.89
11	552	2.84	1.58	0.05	4.8E-20	2.7E-20	4.7E-13	8.8E-15	23.5	0.82	2.02
12	624	3.02	1.80	0.05	2.0E-19	1.9E-20	2.3E-12	6.1E-15	23.5	0.93	2.09
13	648	3.16	1.97	0.05	5.1E-20	3.2E-20	6.3E-13	1.1E-14	23.9	1.01	2.14
14	672	3.43	2.21	0.05	6.4E-20	1.2E-20	8.7E-13	4.2E-15	23.8	1.13	2.29
15	720	3.63	2.41	0.06					24.1	1.23	2.40
16	788	3.78	2.59	0.06	2.7E-19	8.1E-21	4.4E-12	2.8E-15	23	1.32	2.46
17	812	4.03	2.82	0.06	6.2E-20	3.9E-21	1.1E-12	1.4E-15	22.9	1.44	2.59
18	840	4.22	3.01	0.06	4.6E-20	1.3E-20	8.5E-13	4.9E-15	22.9	1.53	2.68
19	864	4.41	3.20	0.06		1.7E-21		6.5E-16	22.8	1.63	2.78
20	884	4.62	3.39	0.06	1.2E-19		2.4E-12		22.6	1.73	2.89
21	960	4.83	3.58	0.06	6.1E-20	2.0E-20	1.3E-12	7.6E-15	22.6	1.82	3.01
22	984	4.97	3.81	0.07	4.7E-20	5.8E-21	1.1E-12	2.3E-15	22.7	1.94	3.03
23	1004	5.20	4.01	0.07	1.0E-19	2.5E-21	2.5E-12	1.0E-15	22.6	2.04	3.16
24	1032	5.41	4.19	0.07	8.8E-20	1.9E-20	2.3E-12	7.8E-15	22.6	2.13	3.28
25	1056	5.61	4.39	0.07	1.0E-19	1.0E-20	2.8E-12	4.5E-15	22.6	2.23	3.38
26	1132	5.85	4.63	0.07	2.4E-20	8.4E-21	6.9E-13	3.7E-15	23.1	2.35	3.49
27	1152	5.94	4.80	0.08	2.4E-20	1.1E-20	7.0E-13	4.8E-15	22.4	2.44	3.50
28	1176	6.22	5.00	0.08		5.0E-21		2.4E-15	22.6	2.54	3.68
29	1200	6.41	5.21	0.08		1.7E-20		8.3E-15	22.6	2.64	3.77
30	1224	6.64	5.41	0.08	6.4E-20	1.4E-20	2.1E-12	6.7E-15	22.6	2.74	3.90
31	1268	6.81	5.62	0.08	3.9E-21	1.4E-20	1.4E-13	7.0E-15	22.7	2.85	3.96
32	1292	6.86	5.79	0.08	1.6E-20	2.4E-21	5.8E-13	1.2E-15	22.5	2.94	3.92
33	1300	6.72	5.77	0.09	1.2E-19	1.0E-20	4.2E-12	5.4E-15	22.6	2.93	3.79
34	1324	7.00	5.77	0.09	2.5E-19		9.1E-12		22.4	2.93	4.07
35	1344	7.22	5.98	0.09	5.2E-20	8.4E-21	1.9E-12	4.5E-15	22.5	3.03	4.18
36	1372	7.43	6.18	0.09		7.2E-21		4.0E-15	22.7	3.14	4.29
37	1392	7.57	6.41	0.09	2.8E-19	1.1E-20	1.1E-11	6.1E-15	22.7	3.25	4.32
38	1460	7.73	6.63	0.09		7.4E-21		4.2E-15	22.6	3.36	4.37
39	1488	7.71	6.77	0.10	3.0E-20	5.3E-21	1.3E-12	3.2E-15	22.6	3.43	4.27
40	1512	8.13	6.95	0.10	4.6E-21	8.3E-21	2.0E-13	5.1E-15	22.6	3.53	4.60

GAS PERMEABILITY

BC-36-1

41	1540	8.27	7.21	0.10	1.6E-20	5.0E-21	7.3E-13	3.2E-15	22.6	3.66	4.61
42	1560	8.56	7.41	0.10	2.8E-20	5.8E-21	1.3E-12	3.7E-15	22.4	3.76	4.80
43	1632	8.84	7.63	0.11		8.6E-22		5.6E-16	22.7	3.87	4.97
44	2064	8.92	7.78	0.11	1.1E-20	4.4E-21	5.3E-13	3.0E-15	22.7	3.94	4.98
45	2304	9.15	7.95	0.15	5.2E-21	6.2E-21	2.6E-13	5.1E-15	22.7	4.05	5.10
46	2364	9.28	7.94	0.16	1.5E-21	2.1E-21	7.2E-14	2.0E-15	22.7	4.05	5.23
47	2496	9.36	7.98	0.17	2.5E-20	7.1E-21	1.2E-12	7.3E-15	22.6	4.08	5.28
47	2548	9.58	8.19	0.12	1.5E-20		7.6E-13		22.7	4.16	5.42
48	2712	9.72	8.37	0.12	4.8E-21		2.5E-13		22.8	4.25	5.48
49	2736	9.91	8.76	0.11					22.7	4.43	5.48
50	2808	10.39	9.01	0.10	7.2E-20		4.0E-12		22.5	4.56	5.83
51	2832	10.44	9.21	0.11	5.7E-21	1.0E-21	3.3E-13	6.9E-16	22.8	4.66	5.78
52	2856	10.78	9.42	0.11	6.0E-20	1.8E-21	3.5E-12	1.2E-15	22.8	4.77	6.01
53	3220	10.97	9.60	0.11	3.9E-20	7.0E-21	2.3E-12	4.8E-15	22.8	4.86	6.11
54	3240	11.17	9.71	0.11	1.1E-20		6.9E-13		22.6	4.91	6.26
55	3336	11.40	10.05	0.11	6.6E-20	3.0E-21	4.1E-12	2.1E-15	22.7	5.08	6.32
56	3412	11.39	10.15	0.11	1.2E-20		7.8E-13		22.5	5.13	6.26
57	3556	11.51	10.37	0.11	1.6E-20	5.2E-23	1.0E-12	3.5E-17	21.4	5.24	6.27
58	3652	11.64	10.55	0.11	9.7E-21	7.7E-22	6.4E-13	5.2E-16	21.4	5.33	6.31
59	3676	11.94	10.83	0.11	6.5E-21	2.2E-22	4.3E-13	1.5E-16	21.5	5.47	6.47
60	3700	12.34	11.00	0.11	2.6E-21	3.8E-21	1.7E-13	2.6E-15	21.6	5.56	6.79
61	3724	12.53	11.18	0.11	1.3E-20		8.7E-13		21.6	5.65	6.88
62	3844	12.72	11.37	0.11	7.2E-20		5.1E-12		21.5	5.74	6.98
63	3868	12.62	11.53	0.11	1.3E-20	7.5E-22	9.5E-13	5.2E-16	21.6	5.82	6.80
64	3892	13.15	11.84	0.11	4.6E-21		3.3E-13		21.6	5.98	7.17
65	3912	13.38	12.01	0.12		1.3E-21		8.9E-16	21.7	6.06	7.31
66	3988	13.55	12.20	0.12	2.9E-20	3.5E-21	2.2E-12	2.5E-15	21.5	6.16	7.39
67	4012	13.52	12.37	0.12	1.6E-20	5.5E-22	1.2E-12	3.9E-16	21.7	6.24	7.27
68	4036	13.92	12.56	0.12	3.4E-20		2.6E-12		21.6	6.34	7.58
69	4196	14.14	12.72	0.12	5.3E-20		4.2E-12		21.7	6.42	7.73
70		13.68	11.90	0.12	1.8E-19		1.4E-11		21.9	6.01	7.67



GAS PERMEABILITY

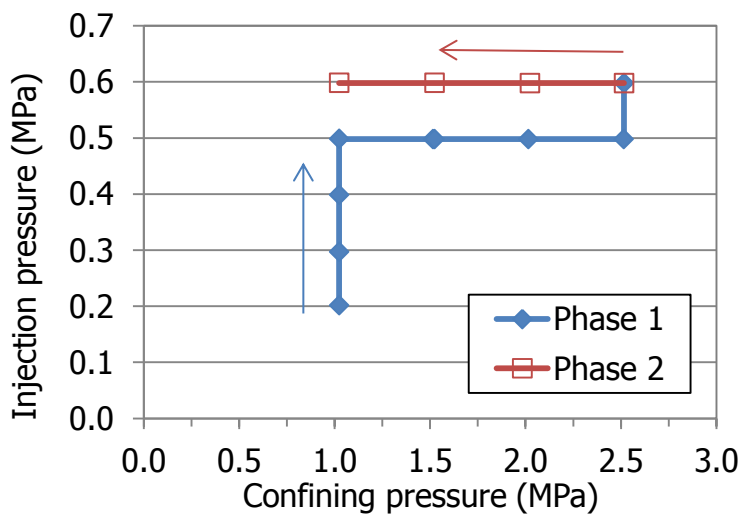
SAMPLE	BC-44-1	
START DATE:	28/09/2016	
END DATE:	30/09/2016	
SETUP:	Flow (LCP)	
CYLINDER VOLUME (m ³)	INPUT	1.526E-04
CELL	Steel triaxial	
SAMPLE WRAPPING	Duct tape + Double latex	
FLOWMETER	Range (mL/min)	Turndown (mL/min)
FT6	2	0.04

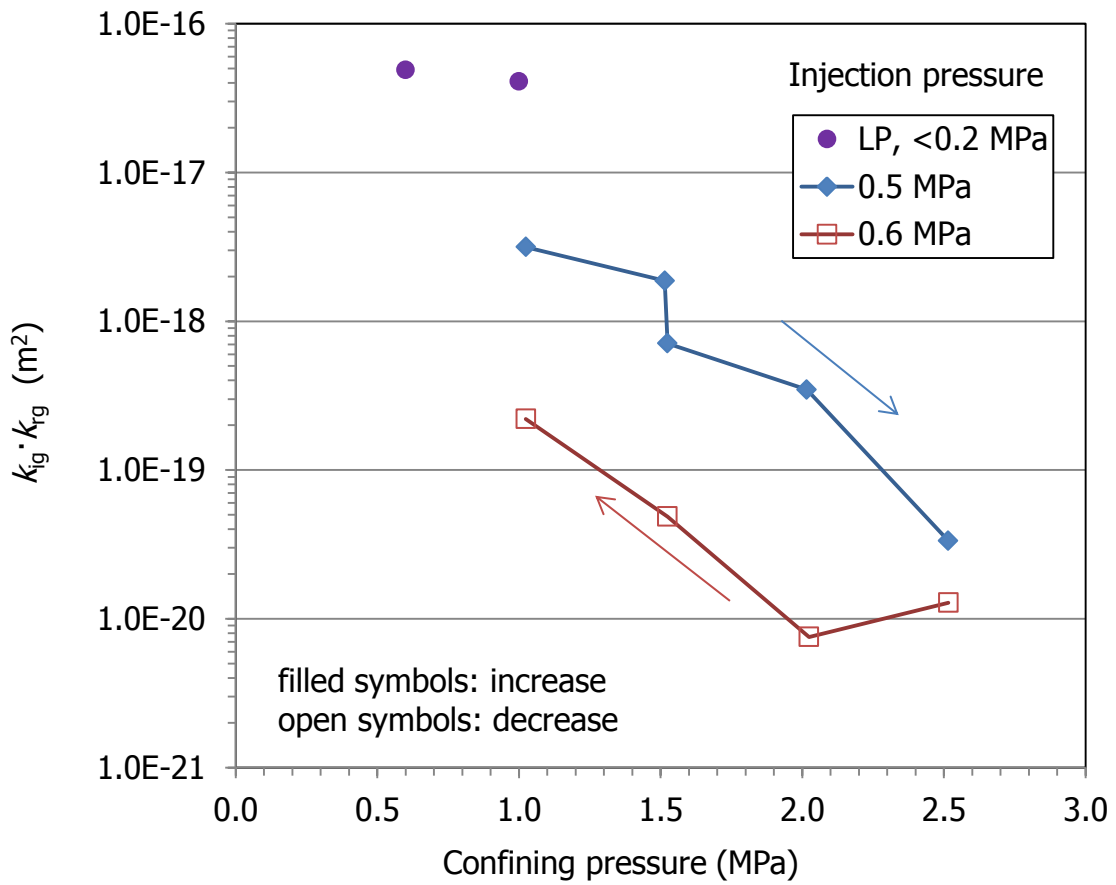
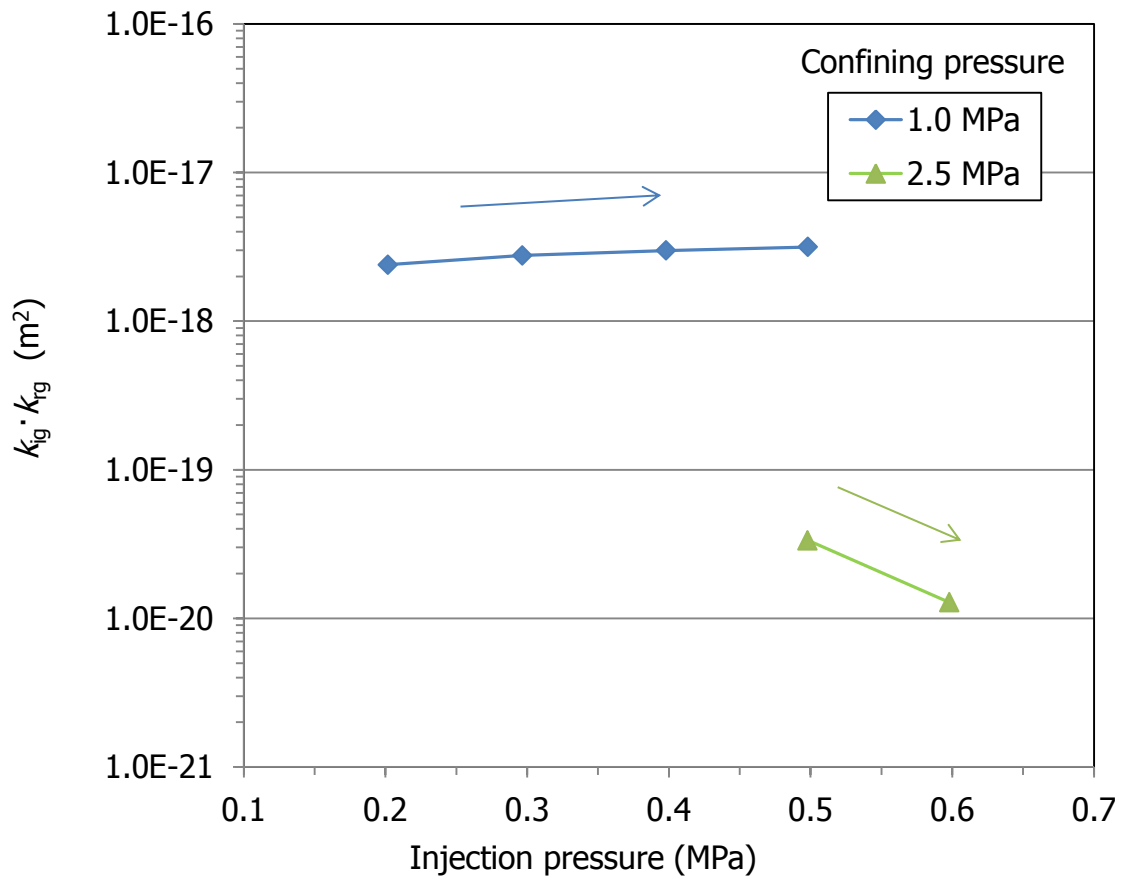
GAS CHARACTERISTICS
 viscosity N₂: 1.78E-05 Pa·s (at 20°C)
 density N₂: 1.12 kg/m³
 g: 9.80665 m/s²

SAMPLE CHARACTERISTICS				
			Initial	Final
Specific weight (g/cm ³)	2.70	ρ _d (g/cm ³)	1.57	1.58
Initial weight (g)	91.55	h (cm)	3.73	3.71
Final weight (g)	91.18	φ (cm)	3.98	3.97
Dry weight (g)	72.54	Area (cm ²)	12.42	12.40
		w (%)	26.2	25.7
		S _r (%)	98	98

Stage	Time elapsed (h)	Confining P (MPa)	Injection P (MPa)	Back P (MPa)	Flow (mL/min)	k _{ig} ·k _{rg} (m ²)	k _g (m/s)	T (°C)	P _{medium} (MPa)	P _c -P _{medium} (MPa)
1	0.5	1.02	0.20	0.10	0.042	2.4E-18	1.4E-12	23.1	0.15	0.87
2	2.5	1.02	0.30	0.10	0.121	2.8E-18	1.6E-12	23.4	0.20	0.83
3	3.0	1.02	0.40	0.10	0.248	3.0E-18	1.8E-12	23.7	0.25	0.78
4	3.6	1.02	0.50	0.10	0.418	3.2E-18	1.9E-12	23.8	0.30	0.73
5	4.6	1.51	0.50	0.10	0.248	1.9E-18	1.1E-12	23.9	0.30	1.22
6	20.8	1.52	0.50	0.10	0.094	7.1E-19	4.2E-13	24.0	0.30	1.23
7	24.8	2.02	0.50	0.10	0.046	3.5E-19	2.0E-13	24.0	0.30	1.72
8	26.3	2.52	0.50	0.10	0.004	3.3E-20	2.0E-14	24.2	0.30	2.22
9	44.0	2.52	0.60	0.10	0.002	1.3E-20	7.5E-15	24.1	0.35	2.17
10	45.8	2.02	0.60	0.09	0.001	7.5E-21	4.4E-15	24.1	0.35	1.68
11	47.6	1.52	0.60	0.09	0.009	4.9E-20	2.9E-14	24.1	0.35	1.18
12	49.1	1.02	0.60	0.09	0.043	2.2E-19	1.3E-13	24.3	0.35	0.68

LP equipment	
Confining P (MPa)	k _{ig} ·k _{rg} (m ²)
0.6	4.9E-17
1.0	4.1E-17





GAS PERMEABILITY

SAMPLE	BC-44-2	
START DATE:	08/09/2016	
END DATE:	14/09/2016	
SETUP:	Flow (LCP)	
CYLINDER	INPUT	1.526E-04
VOLUME (m ³)		
CELL	Steel triaxial	
SAMPLE WRAPPING	Duct tape + Double latex	
FLOWMETER	Range (mL/min)	Turndown (mL/min)
FT5 (a)	100	2
FT6 (b)	2	0.04

GAS CHARACTERISTICS

viscosity N₂: 1.78E-05 Pa·s (at 20°C)density N₂: 1.12 kg/m³g: 9.80665 m/s²

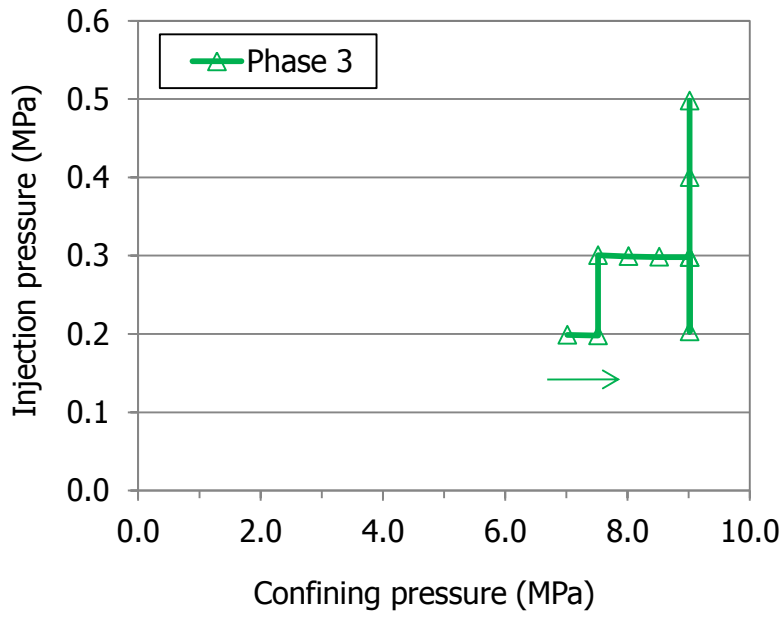
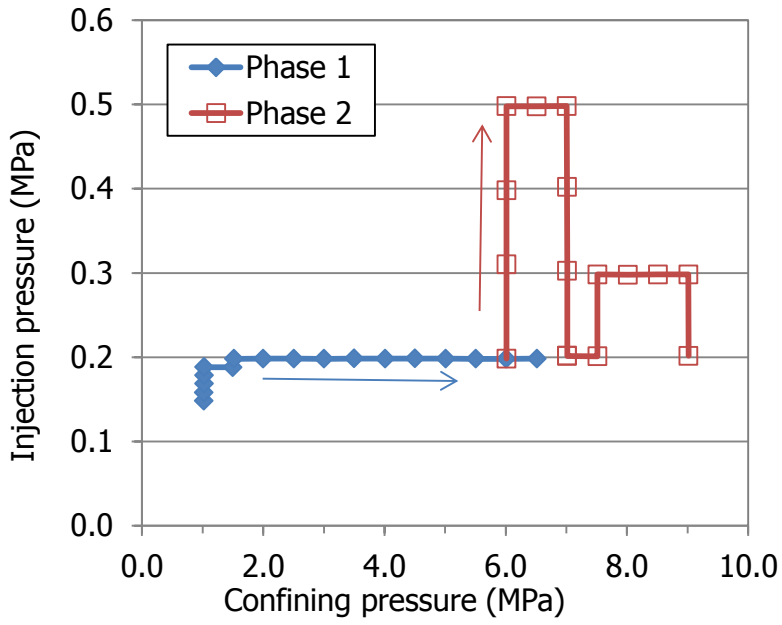
SAMPLE CHARACTERISTICS

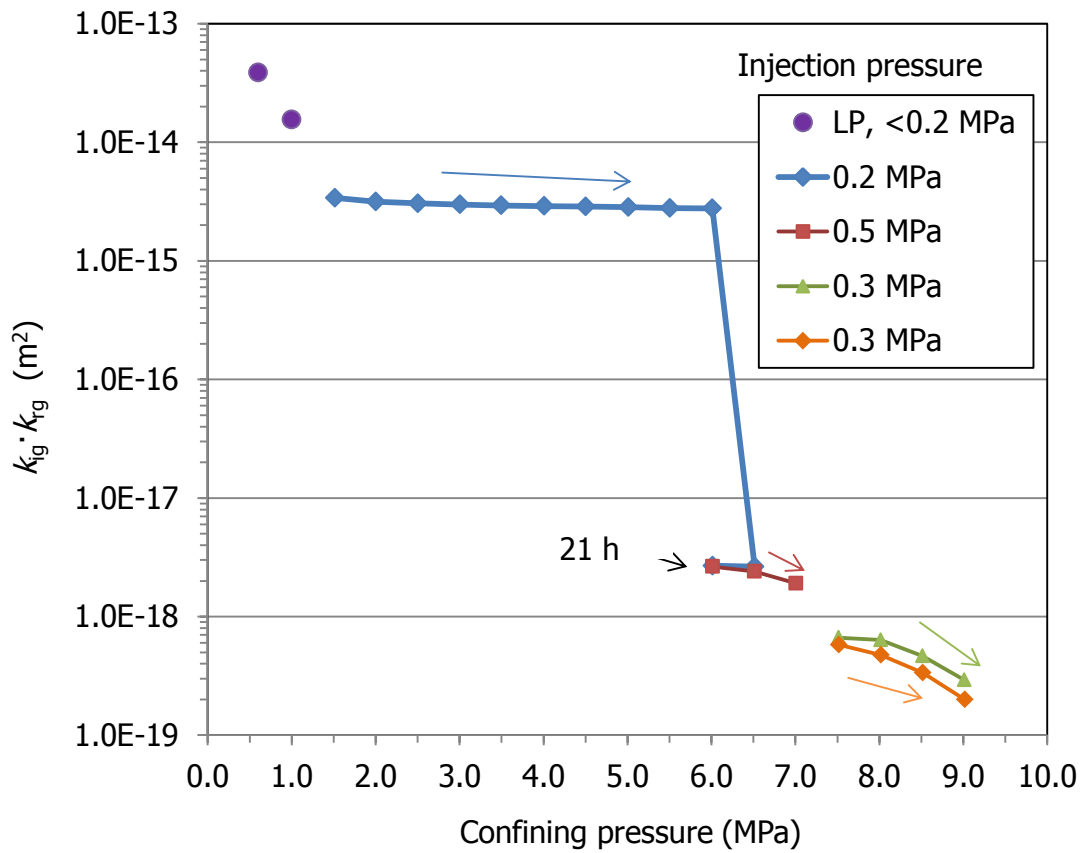
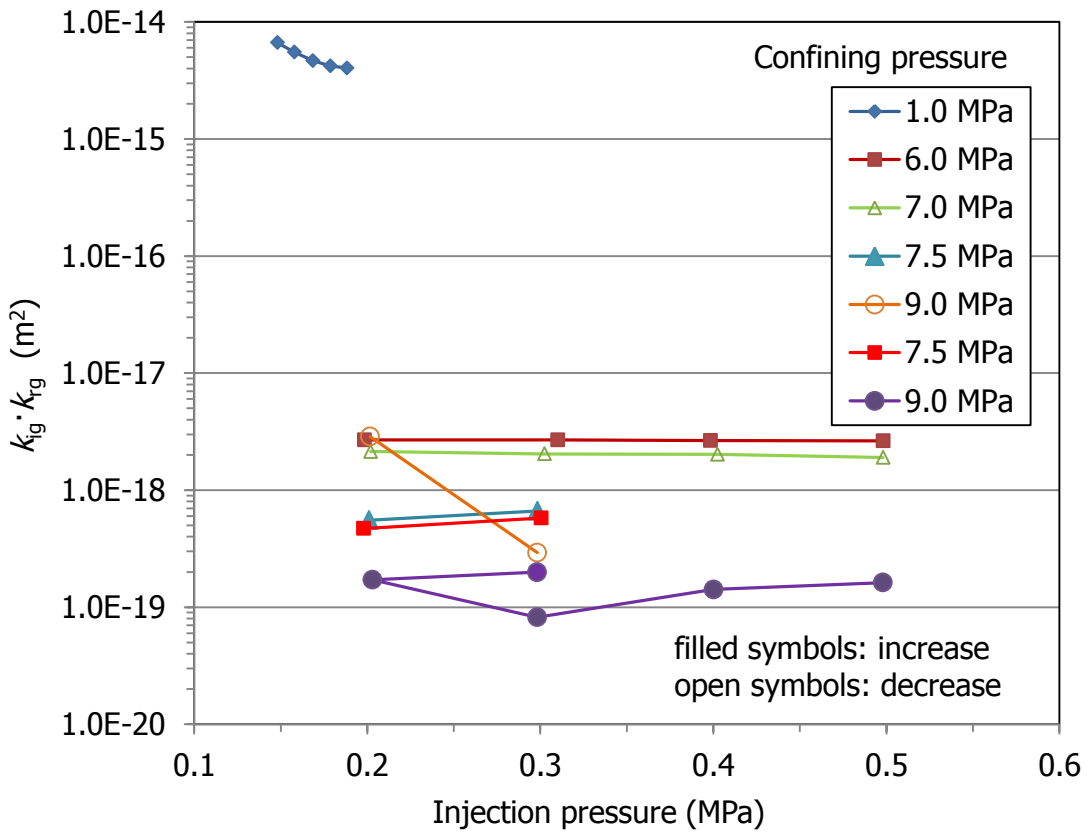
Interface between blocks			Initial	Final
Specific weight (g/cm ³)	2.70	ρ _d (g/cm ³)	1.56	1.62
Initial weight (g)	62.91	h (cm)	2.41	2.39
Final weight (g)	62.46	φ (cm)	4.15	4.09
Dry weight (g)	51.08	Area (cm ²)	13.53	13.15
		w (%)	23.2	22.3
		S _r (%)	86	91

a) steps 1-16, b) steps 17-43

Stage	Time elapsed (h)	Confining P (MPa)	Injection P (MPa)	Back P (MPa)	Flow (mL/min)	k _{ig} ·k _{rg} (m ²)	k _g (m/s)	T (°C)	P _{medium} (MPa)	P _c -P _{medium} (MPa)
1	0.2	1.02	0.15	0.10	77.501	6.7E-15	4.0E-09	24.5	0.12	0.90
2	0.2	1.02	0.16	0.10	79.723	5.5E-15	3.3E-09	24.5	0.13	0.89
3	0.3	1.02	0.17	0.10	82.409	4.7E-15	2.8E-09	24.5	0.13	0.89
4	0.4	1.02	0.18	0.10	87.794	4.2E-15	2.5E-09	24.5	0.14	0.89
5	0.6	1.02	0.19	0.10	97.320	4.0E-15	2.4E-09	24.5	0.14	0.88
6	0.7	1.50	0.19	0.10	88.877	3.7E-15	2.2E-09	24.6	0.14	1.35
7	0.8	1.52	0.20	0.10	93.863	3.4E-15	2.0E-09	24.6	0.15	1.37
8	0.8	2.00	0.20	0.10	87.687	3.2E-15	1.9E-09	24.6	0.15	1.85
9	0.9	2.50	0.20	0.10	84.673	3.1E-15	1.8E-09	24.6	0.15	2.36
10	1.1	3.00	0.20	0.10	82.768	3.0E-15	1.8E-09	24.7	0.15	2.86
11	1.1	3.50	0.20	0.10	81.755	2.9E-15	1.8E-09	24.7	0.15	3.35
12	1.3	4.01	0.20	0.10	80.650	2.9E-15	1.7E-09	24.7	0.15	3.86
13	1.4	4.50	0.20	0.10	79.966	2.9E-15	1.7E-09	24.8	0.15	4.35
14	1.6	5.01	0.20	0.10	79.037	2.8E-15	1.7E-09	24.8	0.15	4.86
15	1.6	5.51	0.20	0.10	77.537	2.8E-15	1.7E-09	24.8	0.15	5.36
16	1.9	6.01	0.20	0.10	76.863	2.8E-15	1.7E-09	24.9	0.15	5.86
17	23.1	6.51	0.20	0.09	0.075	2.6E-18	1.5E-12	24.1	0.15	6.37
18	24.2	6.01	0.20	0.09	0.076	2.7E-18	1.6E-12	24.1	0.15	5.87
19	24.4	6.01	0.31	0.09	0.219	2.7E-18	1.6E-12	24.1	0.20	5.81
20	24.6	6.01	0.40	0.10	0.370	2.7E-18	1.6E-12	24.2	0.25	5.77
21	24.8	6.01	0.50	0.10	0.589	2.6E-18	1.6E-12	24.2	0.30	5.72
22	25.7	6.51	0.50	0.10	0.535	2.4E-18	1.4E-12	24.2	0.30	6.22
23	26.2	7.01	0.50	0.10	0.425	1.9E-18	1.1E-12	24.4	0.30	6.71
24	26.4	7.01	0.40	0.09	0.289	2.0E-18	1.2E-12	24.5	0.25	6.76
25	26.5	7.01	0.30	0.09	0.157	2.0E-18	1.2E-12	24.5	0.20	6.81
26	26.7	7.01	0.20	0.09	0.064	2.1E-18	1.2E-12	24.6	0.15	6.86
28	94.0	7.01	0.20	0.09	0.017	5.7E-19	3.4E-13	24.0	0.15	6.87
29	95.0	7.51	0.20	0.09	0.016	5.5E-19	3.2E-13	24.0	0.15	7.37
30	95.3	7.51	0.30	0.09	0.050	6.7E-19	3.9E-13	24.0	0.20	7.32
31	96.9	8.01	0.30	0.09	0.047	6.3E-19	3.7E-13	24.0	0.20	7.82
32	97.9	8.51	0.30	0.09	0.035	4.7E-19	2.7E-13	23.9	0.20	8.32
33	98.7	9.01	0.30	0.09	0.022	2.9E-19	1.7E-13	23.9	0.20	8.82
34	99.9	9.01	0.20	0.09	0.085	2.9E-18	1.7E-12	24.0	0.15	8.87
35	118.3	7.02	0.20	0.09	0.010	3.4E-19	2.0E-13	24.1	0.15	6.87
36	118.4	7.52	0.20	0.09	0.013	4.7E-19	2.7E-13	24.1	0.15	7.37
37	118.9	7.52	0.30	0.09	0.044	5.8E-19	3.4E-13	24.1	0.20	7.32
38	119.7	8.02	0.30	0.09	0.036	4.8E-19	2.8E-13	24.1	0.20	7.82
39	120.4	8.52	0.30	0.09	0.025	3.4E-19	2.0E-13	24.1	0.20	8.32
40	121.8	9.02	0.30	0.09	0.015	2.0E-19	1.2E-13	24.1	0.20	8.82
41	141.5	9.02	0.20	0.09	0.005	1.7E-19	1.0E-13	24.0	0.15	8.87
42	142.6	9.02	0.30	0.09	0.006	8.2E-20	4.8E-14	23.9	0.20	8.82
43	143.6	9.02	0.40	0.09	0.020	1.4E-19	8.3E-14	23.9	0.25	8.77
44	144.9	9.02	0.50	0.09	0.036	1.6E-19	9.5E-14	23.9	0.30	8.72

LP equipment	
Confining P (MPa)	$k_{ig} \cdot k_{rg}$ (m^2)
0.6	3.9E-14
1.0	1.6E-14





GAS PERMEABILITY

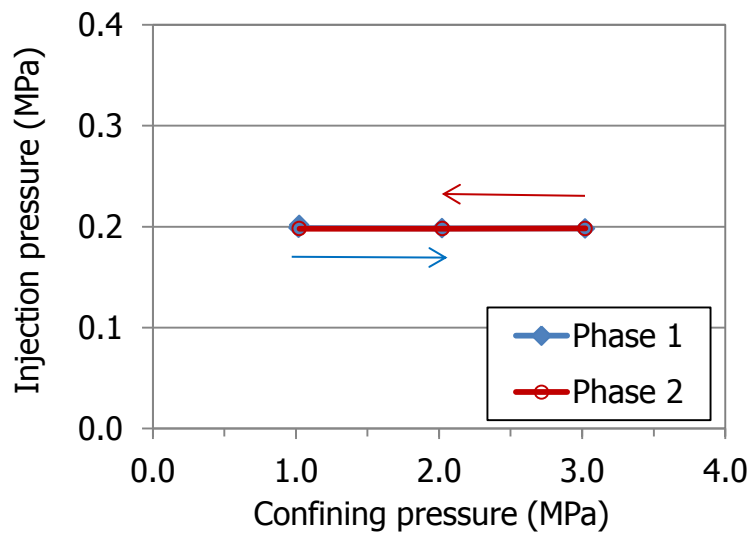
SAMPLE	BC-44-3	
START DATE:	15/03/2017	
END DATE:	23/03/2017	
SETUP:	LCP	
CYLINDER VOLUME (m ³)	INPUT	1.526E-04
CELL	Steel triaxial	
SAMPLE WRAPPING	Duct tape + Double latex	
FLOWMETER	Range (mL/min)	Turndown (mL/min)
FT6	2	0.04

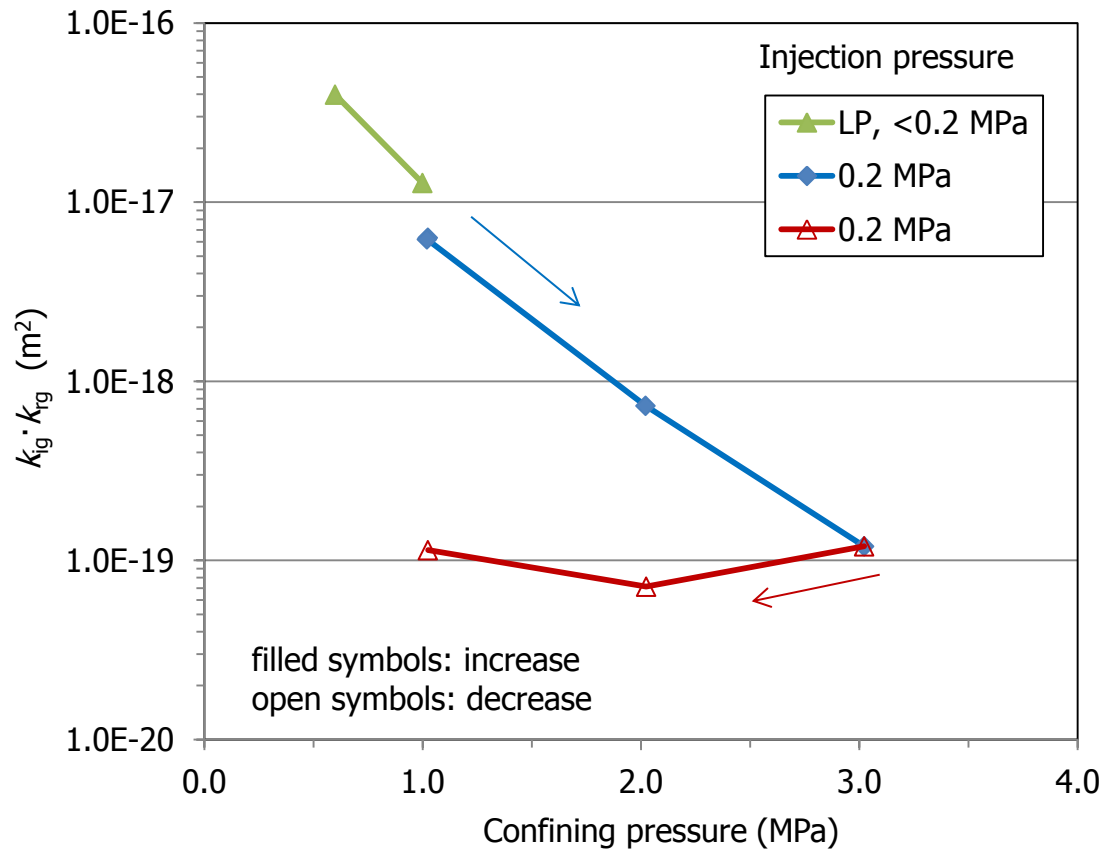
GAS CHARACTERISTICS		
viscosity N ₂ :	1.78E-05 Pa·s (at 20°C)	
density N ₂ :	1.12	kg/m ³
g:	9.80665	m/s ²

SAMPLE CHARACTERISTICS				
Interface between blocks			Initial	Final
Specific weight (g/cm ³)	2.70	ρ _d (g/cm ³)	1.59	1.60
Initial weight (g)	110.92	h (cm)	4.49	4.47
Final weight (g)	110.29	φ (cm)	3.98	3.97
Dry weight (g)	88.59	Area (cm ²)	12.45	12.36
		w (%)	25.2	24.2
		S _r (%)	97	96

Stage	Time elapsed (h)	Confining P (MPa)	Injection P (MPa)	Back P (MPa)	Flow (mL/min)	k _{ig} ·k _{rg} (m ²)	k _g (m/s)	T (°C)	P _{medium} (MPa)	P _c - P _{medium} (MPa)
1	7.5	1.02	0.20	0.10	0.092	6.3E-18	3.7E-12	23.33	0.15	0.88
2	24.4	1.02	0.20	0.10	0.087	6.2E-18	3.6E-12	23.74	0.15	0.87
3	48.3	2.02	0.20	0.10	0.010	7.3E-19	4.3E-13	23.87	0.15	1.87
4	144.2	3.02	0.20	0.09	0.002	1.2E-19	7.0E-14	23.38	0.15	2.88
5	168.4	2.02	0.20	0.09	0.001	7.1E-20	4.2E-14	24.02	0.15	1.88
6	192.4	1.02	0.20	0.09	0.002	1.1E-19	6.6E-14	23.68	0.15	0.88

LP equipment	
Confining P (MPa)	k _{ig} ·k _{rg} (m ²)
0.6	4.0E-17
1.0	1.3E-17





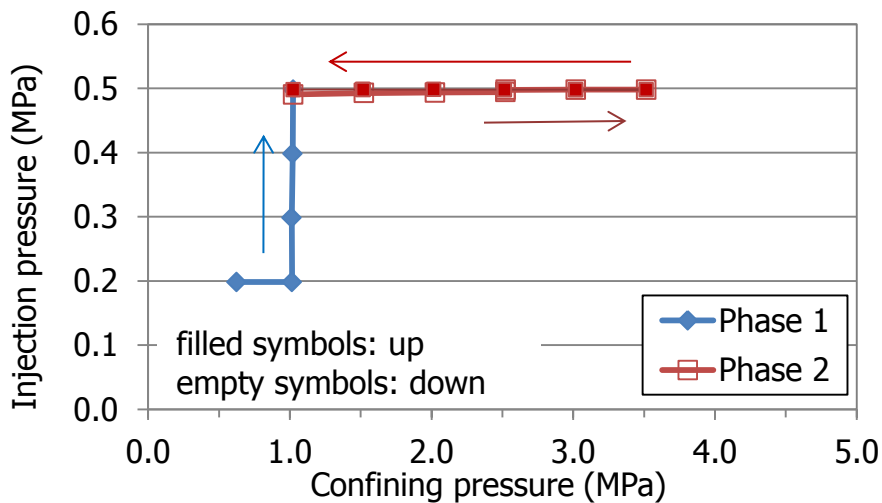
GAS PERMEABILITY

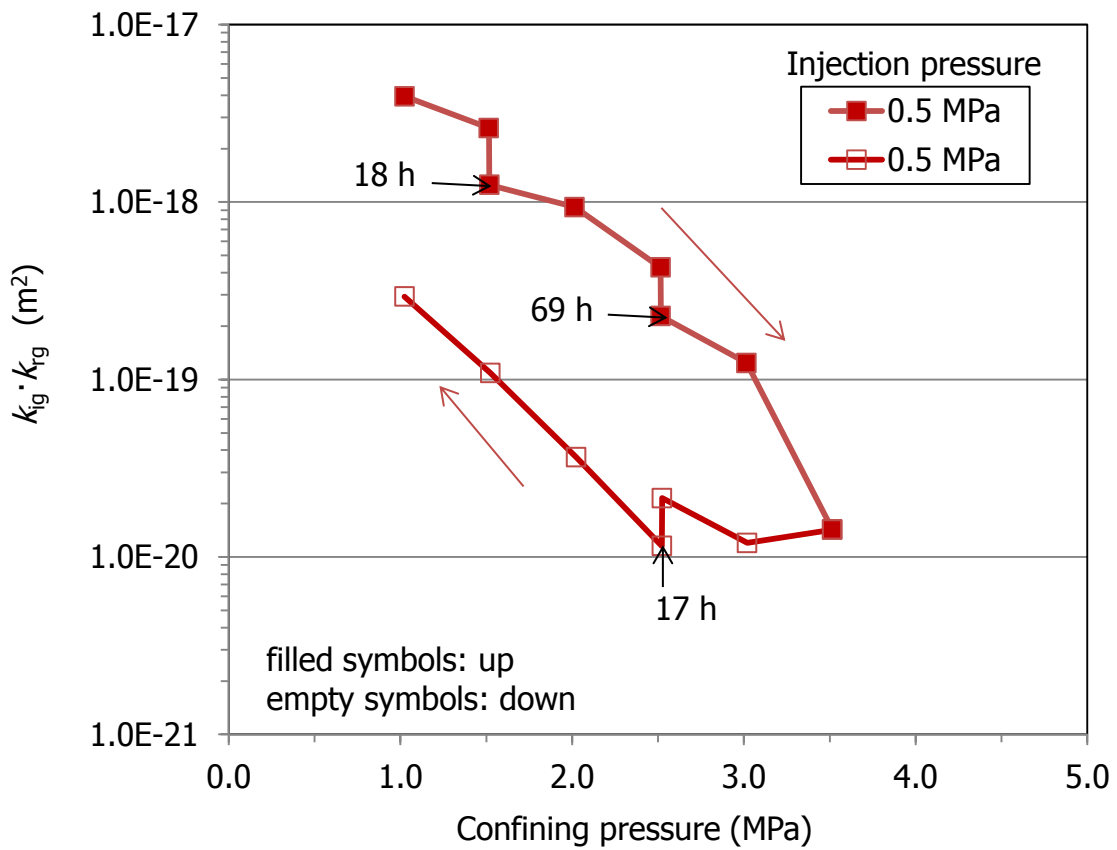
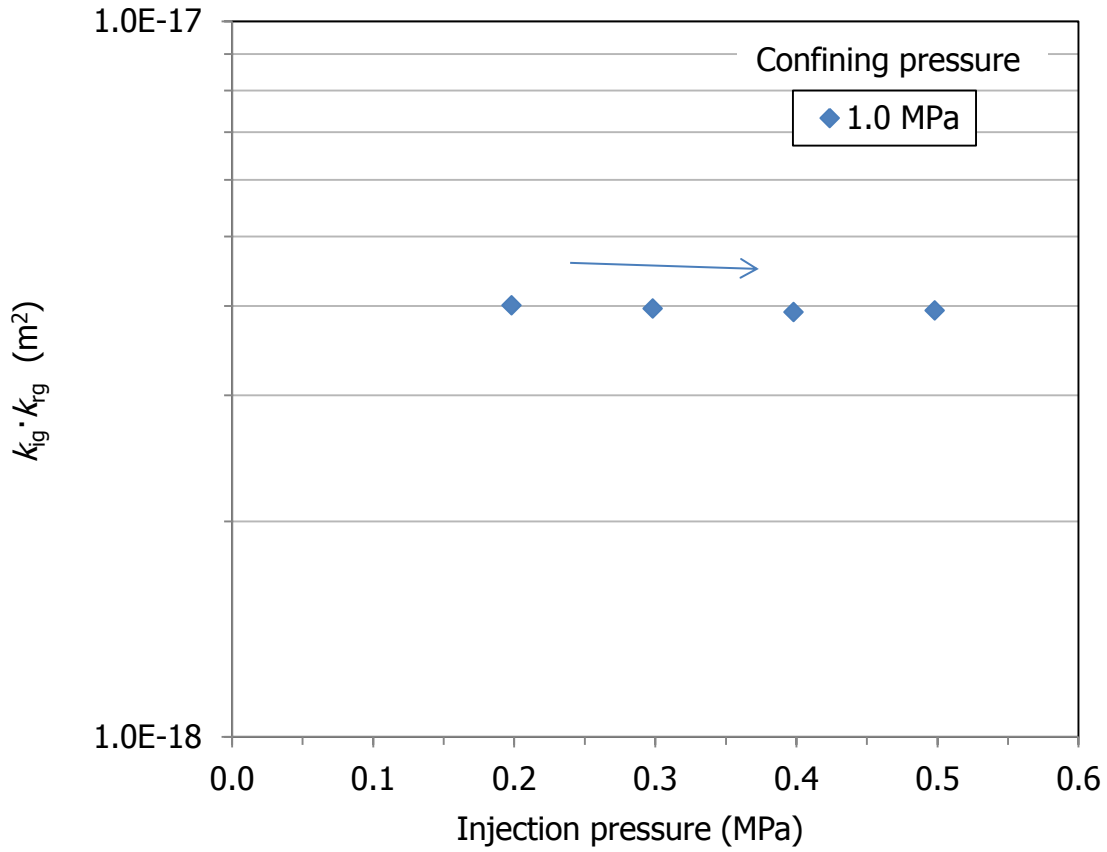
SAMPLE	BC-44-4	
START DATE:	06/10/2016	
END DATE:	11/10/2016	
SETUP:	LCP	
CYLINDER	INPUT	1.526E-04
VOLUME (m ³)		
CELL	Steel triaxial	
SAMPLE WRAPPING	Duct tape + Double latex	
FLOWMETER	Range (mL/min)	Turndown (mL/min)
FT6	2	0.04

GAS CHARACTERISTICS
 viscosity N₂: 1.78E-05 Pa·s (at 20°C)
 density N₂: 1.12 kg/m³
 g: 9.80665 m/s²

SAMPLE CHARACTERISTICS				
			Initial	Final
Specific weight (g/cm ³)	2.70	ρ _d (g/cm ³)	1.61	1.61
Initial weight (g)	113.21	h (cm)	4.11	4.10
Final weight (g)	112.87	φ (cm)	4.19	4.19
Dry weight (g)	90.96	Area (cm ²)	13.80	13.79
		w (%)	24.5	24.4
		S _r (%)	97	97

Stage	Time elapsed (h)	Confining P (MPa)	Injection P (MPa)	Back P (MPa)	Flow (mL/min)	k _{ig} ·k _{rg} (m ²)	k _g (m/s)	T (°C)	P _{medium} (MPa)	P _c / P _{medium} (MPa)
1	0.7	0.62	0.20	0.09	0.01	6.4E-18	3.7E-12	23.20	0.15	0.48
2	2.2	1.02	0.20	0.09	0.07	4.0E-18	2.3E-12	23.62	0.15	0.87
3	3.8	1.01	0.30	0.09	0.18	4.0E-18	2.3E-12	23.91	0.20	0.82
4	4.4	1.02	0.40	0.09	0.33	3.9E-18	2.3E-12	23.98	0.25	0.77
5	4.9	1.02	0.50	0.09	0.53	3.9E-18	2.3E-12	24.00	0.30	0.73
6	5.5	1.51	0.50	0.09	0.35	2.6E-18	1.5E-12	24.03	0.30	1.22
7	23.8	1.52	0.50	0.09	0.17	1.2E-18	7.3E-13	25.94	0.30	1.22
8	25.4	2.01	0.50	0.09	0.13	9.4E-19	5.5E-13	25.11	0.30	1.72
9	27.3	2.52	0.50	0.09	0.06	4.3E-19	2.5E-13	24.70	0.30	2.22
10	96.0	2.52	0.50	0.09	0.03	2.3E-19	1.3E-13	24.04	0.30	2.22
11	97.8	3.02	0.50	0.09	0.02	1.2E-19	7.2E-14	24.12	0.30	2.72
12	99.9	3.52	0.50	0.09	0.00	1.4E-20	8.3E-15	24.16	0.30	3.22
13	101.2	3.02	0.50	0.09	0.00	1.2E-20	7.0E-15	24.13	0.30	2.72
14	101.8	2.52	0.50	0.09	0.00	2.1E-20	1.3E-14	24.16	0.30	2.23
15	118.8	2.52	0.49	0.09	0.00	1.2E-20	6.7E-15	24.08	0.29	2.23
16	120.1	2.02	0.49	0.09	0.00	3.6E-20	2.1E-14	24.12	0.29	1.73
17	121.4	1.52	0.49	0.09	0.01	1.1E-19	6.3E-14	24.18	0.29	1.23
18	123.8	1.02	0.49	0.09	0.04	2.9E-19	1.7E-13	24.24	0.29	0.73





GAS PERMEABILITY

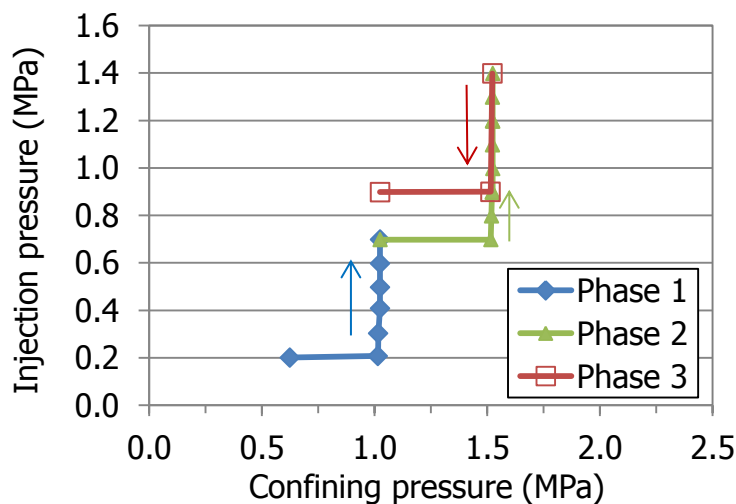
SAMPLE	BC-44-5	
START DATE:	27/10/2016	
END DATE:	03/11/2016	
SETUP:	LCP	
CYLINDER VOLUME (m ³)	INPUT	1.526E-04
CELL	Steel triaxial	
SAMPLE WRAPPING	Duct tape + Double latex	
FLOWMETER	Range (mL/min)	Turndown (mL/min)
FT6	2	0.04

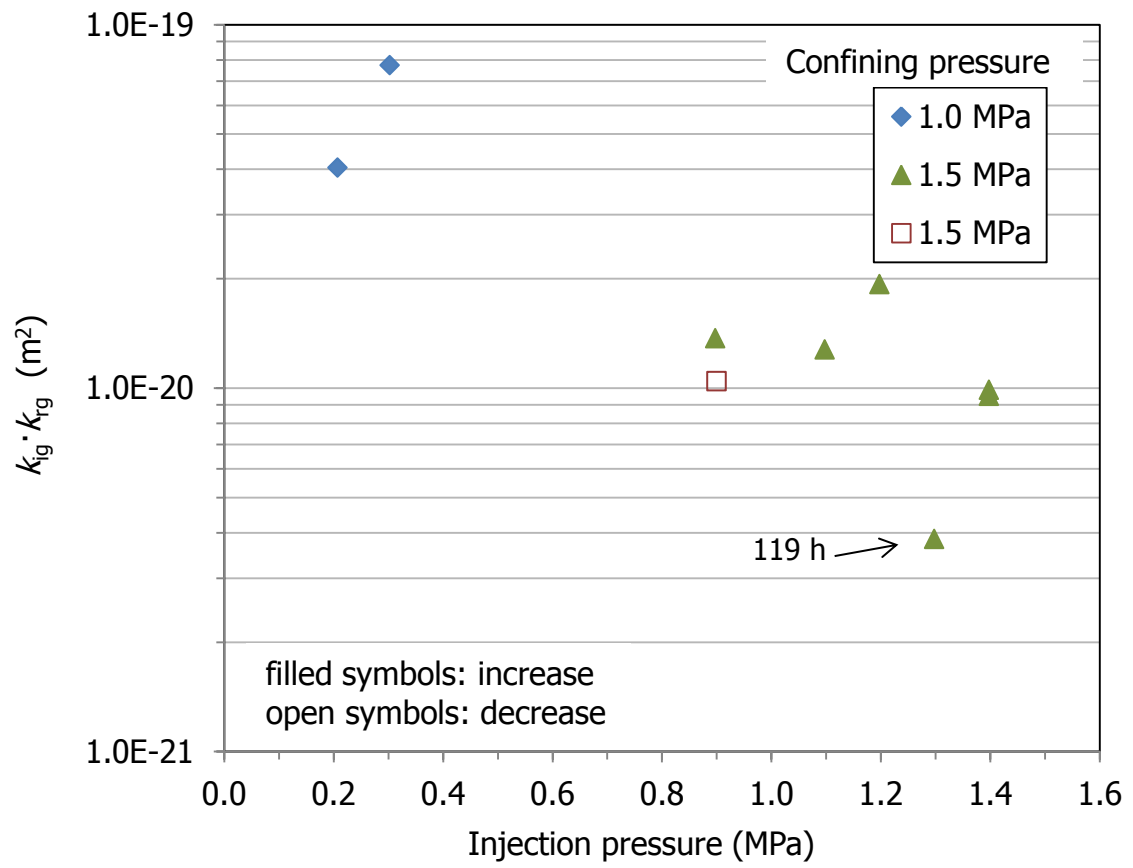
GAS CHARACTERISTICS		
viscosity N ₂ :	1.78E-05 Pa·s (at 20°C)	
density N ₂ :	1.12	kg/m ³
g:	9.80665	m/s ²

SAMPLE CHARACTERISTICS				
			Initial	Final
Specific weight (g/cm ³)	2.70	ρ _d (g/cm ³)	1.52	1.53
Initial weight (g)	109.96	h (cm)	4.10	4.09
Final weight (g)	109.52	φ (cm)	4.18	4.17
Dry weight (g)	85.61	Area (cm ²)	13.70	13.64
		w (%)	28.5	27.5
		S _r (%)	100	98

Stage	Time elapsed (h)	Confining P (MPa)	Injection P (MPa)	Back P (MPa)	Flow (mL/min)	k _{ig} ·k _{rg} (m ²)	k _g (m/s)	T (°C)	P _{medium} (MPa)	P _{c-medium} (MPa)
1	0.5	0.62	0.20	0.10				24.1	0.15	0.48
2	0.6	1.01	0.21	0.10				24.1	0.15	0.86
3	0.8	1.02	0.30	0.10				24.2	0.20	0.82
4	0.9	1.02	0.41	0.10				2.4	0.25	0.77
5	1.0	1.02	0.50	0.10				24.3	0.30	0.73
6	1.8	1.02	0.60	0.10	0.008	4.0E-20	2.4E-14	24.3	0.35	0.68
7	2.6	1.02	0.70	0.10	0.021	7.7E-20	4.6E-14	24.3	0.40	0.63
8	4.0	1.52	0.70	0.10				24.3	0.40	1.12
9	6.2	1.52	0.80	0.10				24.3	0.45	1.07
10	7.7	1.52	0.90	0.10	0.006	1.4E-20	8.1E-15	24.4	0.50	1.03
11	24.7	1.52	0.90	0.10				24.2	0.50	1.03
12	25.9	1.52	1.00	0.10				24.2	0.55	0.98
13	28.0	1.52	1.10	0.10	0.008	1.3E-20	7.6E-15	24.2	0.60	0.93
14	29.4	1.52	1.20	0.10	0.015	1.9E-20	1.1E-14	24.3	0.65	0.88
15	144.7	1.52	1.20	0.10				22.0	0.65	0.88
16	148.7	1.52	1.30	0.10	0.004	3.8E-21	2.3E-15	22.7	0.70	0.83
17	151.8	1.52	1.40	0.09	0.011	9.9E-21	5.8E-15	22.8	0.75	0.78
18	170.0	1.52	1.40	0.09	0.010	9.5E-21	5.6E-15	22.8	0.75	0.78
19	170.5	1.52	0.90	0.09	0.005	1.0E-20	6.1E-15	23.2	0.50	1.02
20	172.3	1.02	0.90	0.09				23.3	0.50	0.53

LP equipment	
Confining P (MPa)	k _{ig} ·k _{rg} (m ²)
0.6	no flow





GAS PERMEABILITY

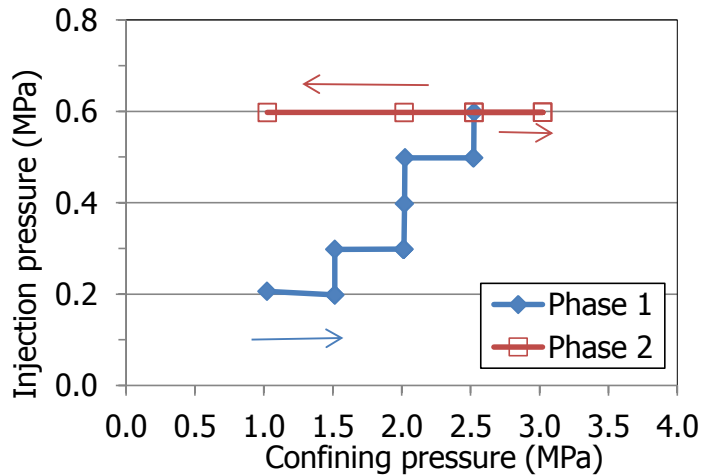
SAMPLE	BC-44-6	
START DATE:	22/11/2016	
END DATE:	30/11/2016	
SETUP:	LCP	
CYLINDER	INPUT	1.526E-04
VOLUME (m ³)		
CELL	Steel triaxial	
SAMPLE WRAPPING	Duct tape + Double latex	
FLOWMETER	Range (mL/min)	Turndown (mL/min)
FT6	2	0.04

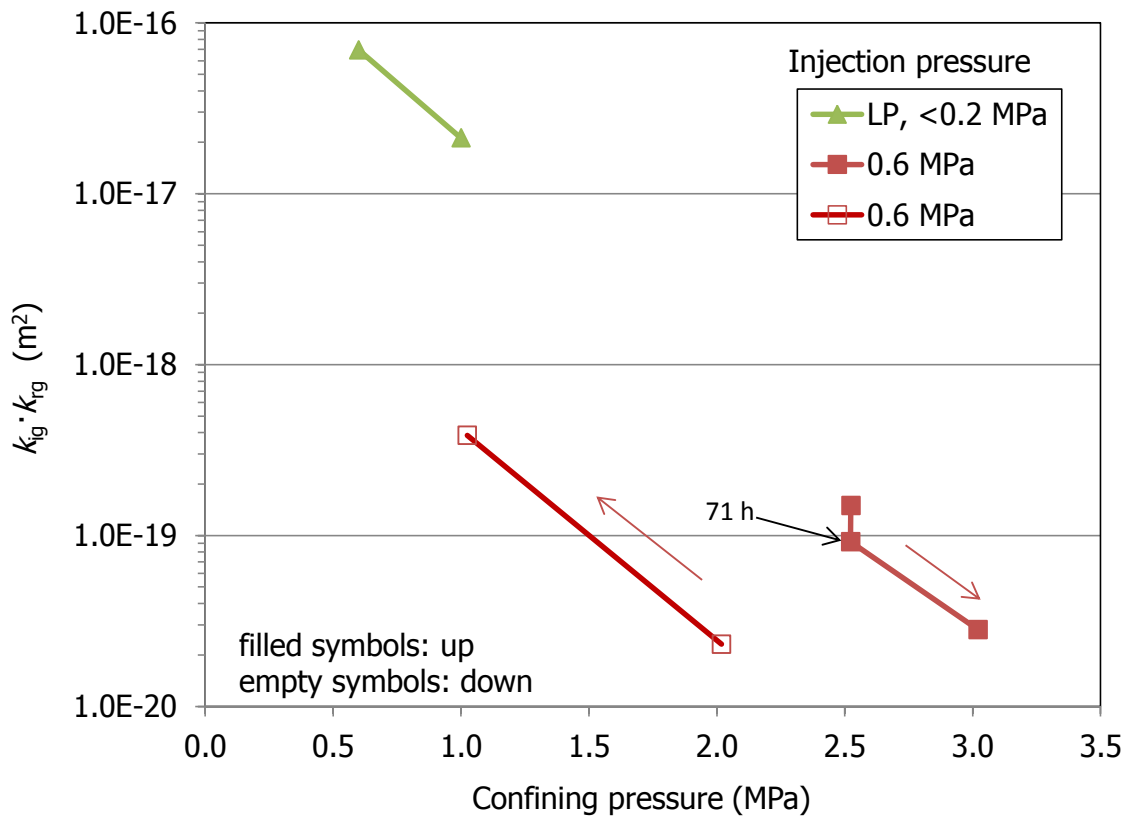
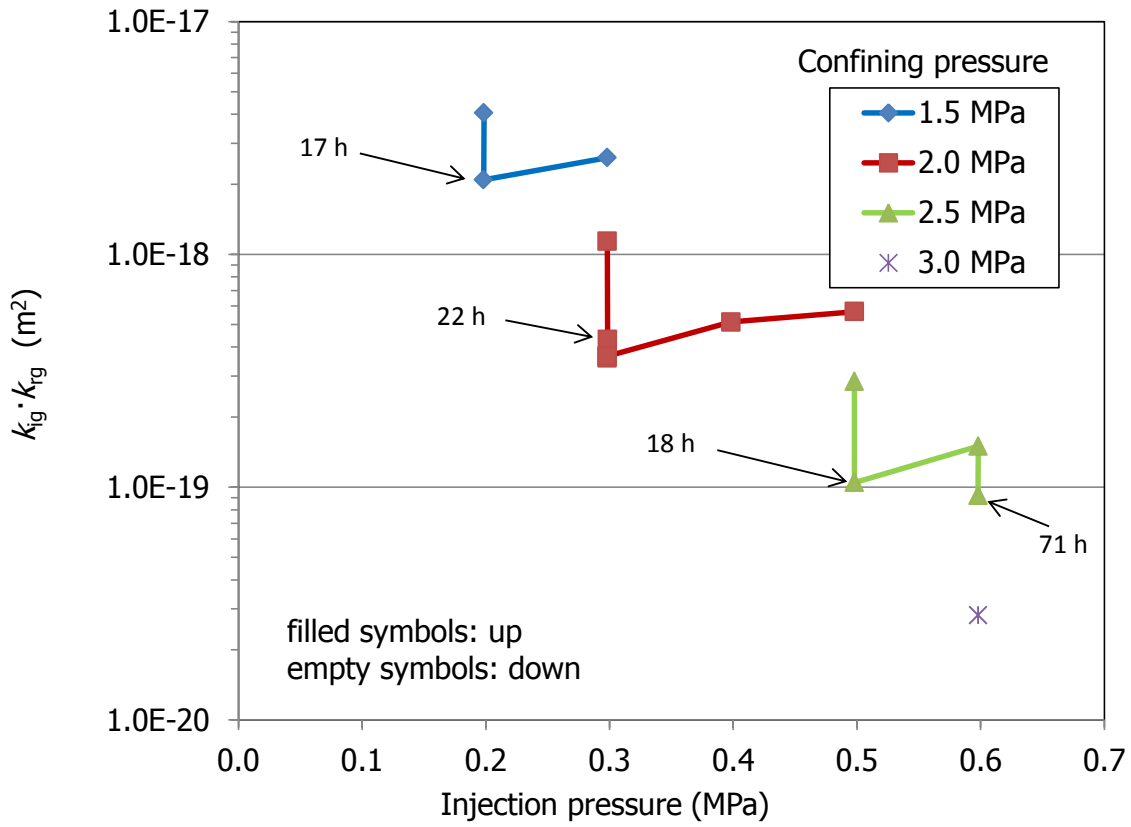
GAS CHARACTERISTICS	
viscosity N ₂ :	1.78E-05 Pa·s (at 20°C)
density N ₂ :	1.12 kg/m ³
g:	9.80665 m/s ²

SAMPLE CHARACTERISTICS				
Interface between blocks			Initial	Final
Specific weight (g/cm ³)	2.70	ρ _d (g/cm ³)	1.51	1.53
Initial weight (g)	103.90	h (cm)	3.90	3.89
Final weight (g)	103.37	φ (cm)	4.18	4.16
Dry weight (g)	80.90	Area (cm ²)	13.73	13.62
		w (%)	28.4	26.7
		S _r (%)	97	94

Stage	Hours	Confining P (MPa)	Injection P (MPa)	Back P (MPa)	Flow (mL/min)	k _{ig} ·k _{rg} (m ²)	k _g (m/s)	T (°C)	P _{medium} (MPa)	P _{c-P_{medium}} (MPa)
1	4.2	1.02	0.21	0.09	0.201	1.0E-17	5.9E-12	22.5	0.15	0.87
2	5.5	1.52	0.20	0.09	0.073	4.1E-18	2.3E-12	23.2	0.15	1.37
3	22.2	1.52	0.20	0.09	0.037	2.1E-18	1.2E-12	22.4	0.15	1.37
4	28.2	1.52	0.30	0.09	0.122	2.6E-18	1.5E-12	22.6	0.20	1.32
5	29.2	2.01	0.30	0.09	0.053	1.1E-18	6.6E-13	23.3	0.20	1.82
6	30.6	2.02	0.30	0.09	0.020	4.3E-19	2.5E-13	23.8	0.20	1.82
7	47.5	2.02	0.30	0.09	0.017	3.6E-19	2.1E-13	22.0	0.20	1.82
8	49.7	2.02	0.30	0.09	0.017	3.6E-19	2.1E-13	22.3	0.20	1.82
9	51.9	2.02	0.40	0.09	0.045	5.1E-19	3.0E-13	22.4	0.25	1.77
10	52.9	2.02	0.50	0.09	0.080	5.7E-19	3.3E-13	22.5	0.30	1.73
11	54.5	2.52	0.50	0.09	0.040	2.9E-19	1.6E-13	22.7	0.30	2.22
12	72.1	2.52	0.50	0.09	0.015	1.0E-19	6.1E-14	22.3	0.30	2.23
13	75.1	2.52	0.60	0.09	0.031	1.5E-19	8.7E-14	22.6	0.35	2.18
14	146.4	2.52	0.60	0.09	0.019	9.2E-20	5.3E-14	20.6	0.35	2.18
15	149.1	3.02	0.60	0.09	0.006	2.8E-20	1.6E-14	21.2	0.35	2.68
16	170.0	3.02	0.60	0.09	0.002			21.9	0.35	2.68
17	172.9	2.52	0.60	0.09	0.001			22.4	0.35	2.18
18	189.6	2.02	0.60	0.10	0.005	2.3E-20	1.4E-14	22.6	0.35	1.67
19	197.1	1.02	0.60	0.10	0.079	3.9E-19	2.3E-13	22.4	0.35	0.68

LP equipment	
Confining P (MPa)	k _{ig} ·k _{rg} (m ²)
0.6	6.9E-17
1.0	2.1E-17





GAS PERMEABILITY

SAMPLE BC-44-7		
START DATE:	08/09/2016	
END DATE:	22/09/2016	
SETUP:	Flow (HCP to LCP)	
CYLINDER	INPUT	1.526E-04
VOLUME (m ³)		
CELL	Steel triaxial	
SAMPLE WRAPPING	Double latex	
FLOWMETER	Range	Turndown
	(mL/min)	(mL/min)
FT1 (a)	2	0.04
FT2 (b)	10	0.2
FT3 (c)	100	2
FT5 (d)	100	2
FT6 (e)	2	0.04

- a) steps 1 and 10
b) steps 2-4 and 6-9
c) step 5
d) steps 17-19
e) steps 11-16 and 20-42

GAS CHARACTERISTICS

viscosity N₂: 1.78E-05 Pa·s (at 20°C)
density N₂: 1.12 kg/m³
g: 9.80665 m/s²

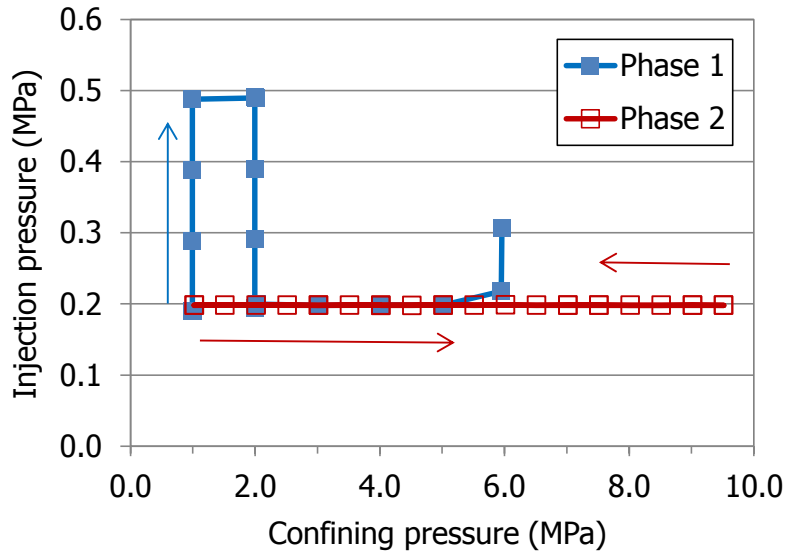
SAMPLE CHARACTERISTICS

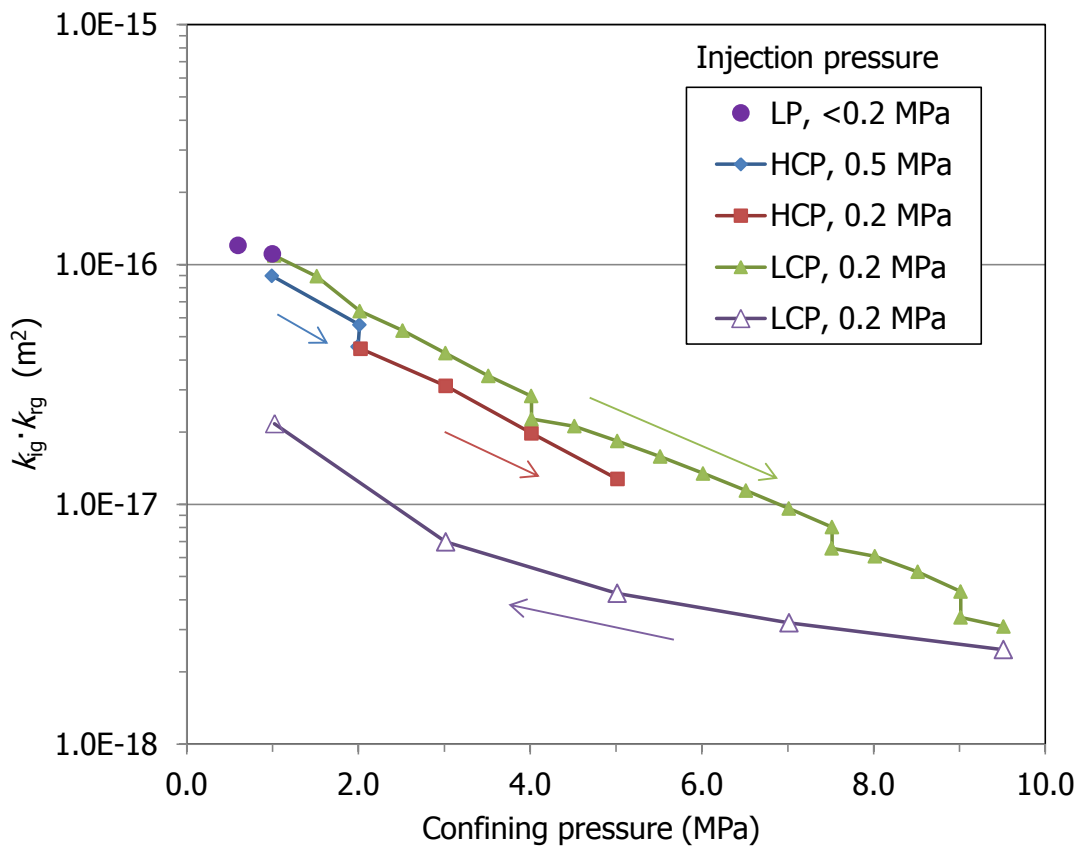
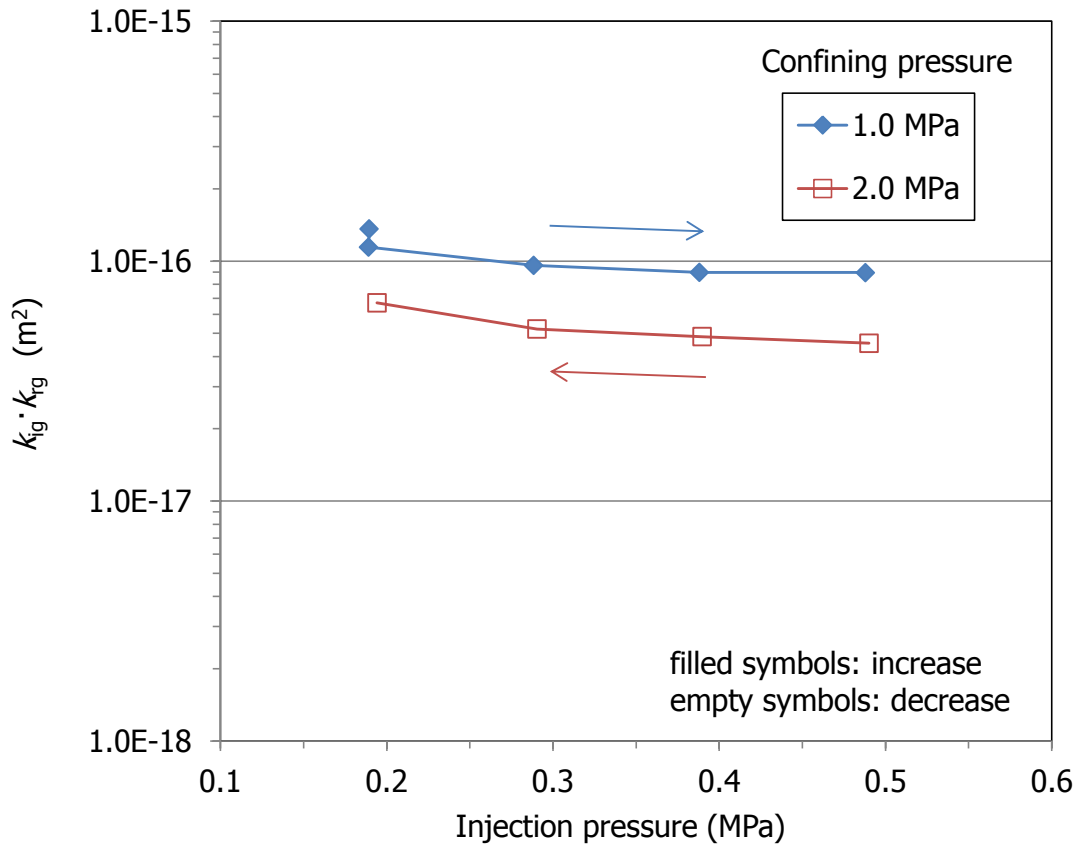
			Initial	Final
Specific weight (g/cm ³)	2.70	ρ _d (g/cm ³)	1.62	
Initial weight (g)	94.80	h (cm)	3.59	
Final weight (g)	94.93	φ (cm)	4.17	
Dry weight (g)	79.31	Area (cm ²)	13.63	
		w (%)	19.5	19.7
		S _r (%)	79	
Modified sample			Initial	Final
Specific weight (g/cm ³)	2.70	ρ _d (g/cm ³)	1.67	1.65
Initial weight (g)	71.73	h (cm)	2.67	2.68
Final weight (g)	71.56	φ (cm)	4.13	4.15
Dry weight (g)	59.70	Area (cm ²)	13.40	13.52
		w (%)		19.9
		S _r (%)		84

Stage	Hours	Confining P (MPa)	Injection P (MPa)	Back P (MPa)	Flow (mL/min)	k _{ig} ·k _{rg} (m ²)	k _g (m/s)	T (°C)	P _{medium} (MPa)	P _c -P _{medium} (MPa)
1	0.6	1.00	0.19	0.12	1.790	1.4E-16	1.0E-10	25.2	0.16	0.84
2	22.3	0.99	0.19	0.09	1.933	1.1E-16	6.7E-11	24.1	0.14	0.85
3	22.5	0.99	0.29	0.10	4.502	9.6E-17	5.6E-11	24.1	0.19	0.80
4	22.7	0.99	0.39	0.10	8.027	9.0E-17	5.3E-11	24.2	0.24	0.75
5	23.3	0.99	0.49	0.09	12.978	9.0E-17	5.2E-11	24.1	0.29	0.70
6	24.8	2.01	0.49	0.10	8.160	5.6E-17	3.3E-11	24.3	0.29	1.72
7	120.5	1.99	0.49	0.10	6.642	4.5E-17	2.7E-11	24.2	0.29	1.70
8	120.6	1.99	0.39	0.09	4.380	4.8E-17	2.8E-11	24.2	0.24	1.75
9	120.8	1.99	0.29	0.09	2.484	5.2E-17	3.0E-11	24.2	0.19	1.80
10	121.1	1.99	0.19	0.09	1.216	6.7E-17	3.9E-11	24.1	0.14	1.85
11	145.3	2.03	0.20	0.10	0.868	4.4E-17	2.6E-11	24.2	0.15	1.88
12	145.8	3.02	0.20	0.10	0.595	3.1E-17	1.8E-11	24.1	0.15	2.87
13	146.5	4.02	0.20	0.09	0.378	2.0E-17	1.2E-11	24.1	0.15	3.87
14	163.9	5.02	0.20	0.09	0.245	1.3E-17	7.5E-12	24.1	0.15	4.87
15	164.9	5.95	0.22	0.09				23.9	0.16	5.79
16	166.0	5.96	0.31	0.09				24.0	0.20	5.76
17	188.8	1.02	0.20	0.10	2.076	1.1E-16	6.4E-11	24.5	0.15	0.87
18	189.4	1.52	0.20	0.10	1.710	8.9E-17	5.2E-11	24.0	0.15	1.37
19	190.2	2.02	0.20	0.10	1.217	6.4E-17	3.8E-11	24.0	0.15	1.87
20	191.0	2.52	0.20	0.10	1.010	5.3E-17	3.1E-11	24.2	0.15	2.37
21	191.7	3.02	0.20	0.10	0.812	4.3E-17	2.5E-11	24.4	0.15	2.87
22	192.6	3.52	0.20	0.10	0.654	3.4E-17	2.0E-11	24.5	0.15	3.37
23	193.3	4.01	0.20	0.10	0.540	2.8E-17	1.7E-11	24.2	0.15	3.87
24	260.3	4.02	0.20	0.10	0.432	2.3E-17	1.3E-11	23.9	0.15	3.87
25	261.1	4.52	0.20	0.10	0.403	2.1E-17	1.2E-11	23.9	0.15	4.37
26	262.2	5.02	0.20	0.10	0.352	1.8E-17	1.1E-11	23.9	0.15	4.87
27	263.3	5.52	0.20	0.10	0.302	1.6E-17	9.3E-12	23.9	0.15	5.37
28	264.3	6.02	0.20	0.10	0.258	1.3E-17	7.9E-12	23.9	0.15	5.87
29	265.7	6.51	0.20	0.10	0.218	1.1E-17	6.7E-12	23.9	0.15	6.37
30	266.9	7.01	0.20	0.09	0.184	9.6E-18	5.6E-12	24.0	0.15	6.87
31	268.6	7.51	0.20	0.09	0.154	8.0E-18	4.7E-12	23.9	0.15	7.37
32	285.1	7.51	0.20	0.09	0.126	6.6E-18	3.8E-12	24.0	0.15	7.37
33	287.2	8.01	0.20	0.09	0.116	6.1E-18	3.5E-12	24.0	0.15	7.87
34	289.8	8.51	0.20	0.09	0.100	5.2E-18	3.0E-12	24.1	0.15	8.37
35	292.3	9.01	0.20	0.09	0.083	4.3E-18	2.5E-12	24.1	0.15	8.87

36	312.1	9.01	0.20	0.09	0.065	3.4E-18	2.0E-12	24.0	0.15	8.87
37	315.6	9.51	0.20	0.09	0.059	3.1E-18	1.8E-12	24.1	0.15	9.37
38	332.6	9.51	0.20	0.09	0.047	2.5E-18	1.4E-12	23.9	0.15	9.37
39	334.2	7.02	0.20	0.09	0.061	3.2E-18	1.9E-12	24.2	0.15	6.87
40	335.3	5.02	0.20	0.09	0.082	4.3E-18	2.5E-12	24.1	0.15	4.87
41	336.0	3.02	0.20	0.09	0.133	7.0E-18	4.1E-12	24.1	0.15	2.87
42	336.2	1.02	0.20	0.10	0.415	2.2E-17	1.3E-11	24.1	0.15	0.88

LP equipment	
Confining P (MPa)	$k_{ig} \cdot k_{rg}$ (m ²)
0.6	1.2E-16
1.0	1.1E-16





GAS PERMEABILITY

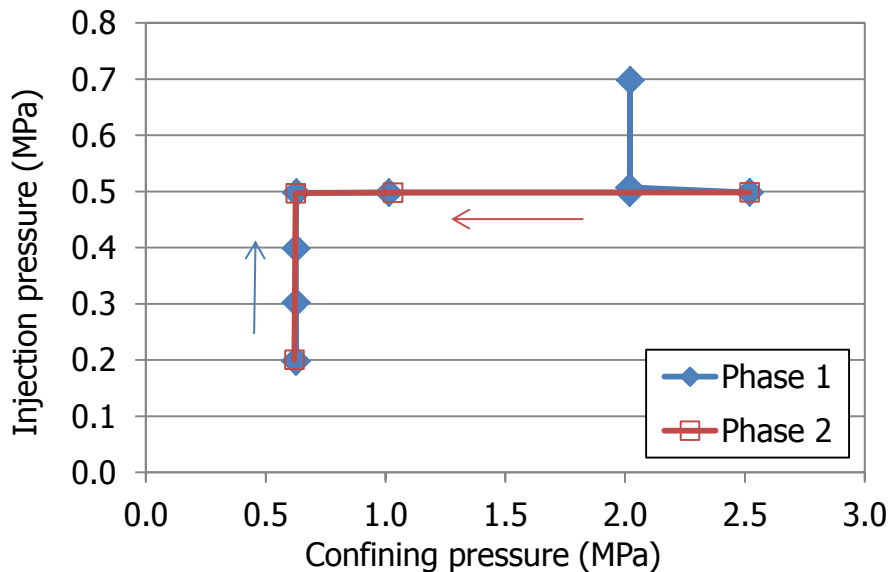
SAMPLE	BC-47-1	
START DATE:	02/08/2016	
END DATE:	11/08/2016	
SETUP:	Flow (LCP)	
CYLINDER VOLUME (m ³)	INPUT	1.526E-04
CELL	Steel triaxial	
SAMPLE WRAPPING	Double latex	
FLOWMETER	Range (mL/min)	Turndown (mL/min)
FT6	2	0.004

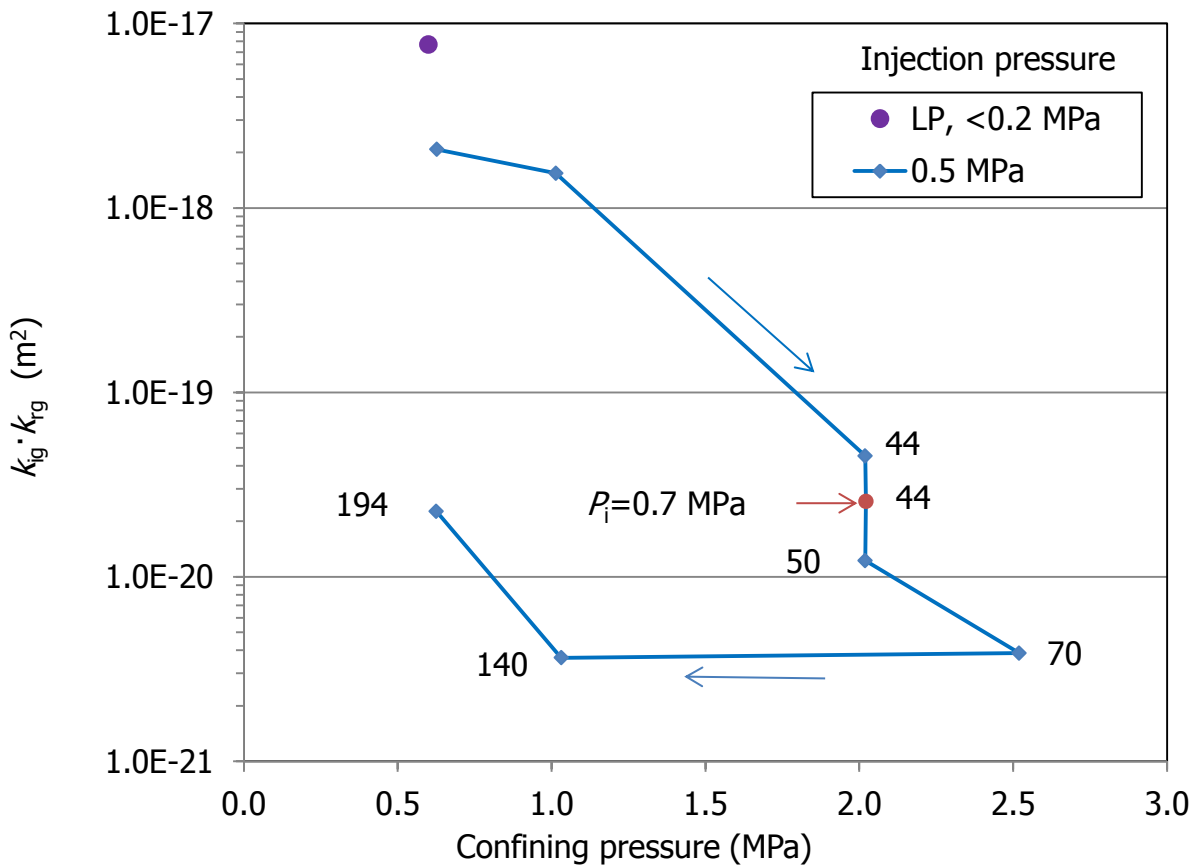
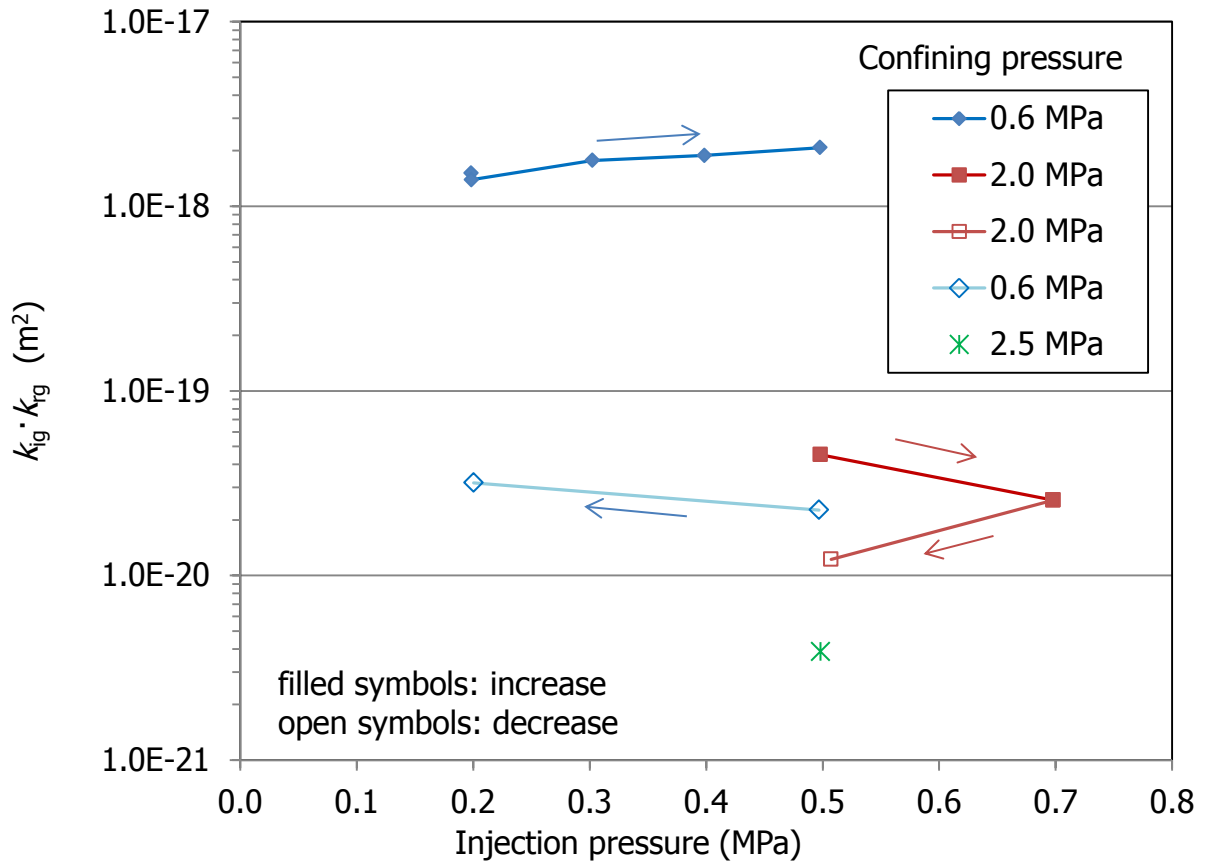
GAS CHARACTERISTICS
 viscosity N₂: 1.78E-05 Pa·s (at 20°C)
 density N₂: 1.12 kg/m³
 g: 9.80665 m/s²

SAMPLE CHARACTERISTICS				
			Initial	Final
Specific weight (g/cm ³)	2.70	ρ _d (g/cm ³)	1.55	1.55
Initial weight (g)	100.75	h (cm)	3.86	3.87
Final weight (g)	100.64	φ (cm)	4.12	4.11
Dry weight (g)	79.70	Area (cm ²)	13.33	13.29
		w (%)	26.4	26.3
		S _r (%)	96	95

Stage	Time elapsed (h)	Confining P (MPa)	Injection P (MPa)	Back P (MPa)	Flow (mL/min)	k _{ig} ·k _{rg} (m ²)	k _g (m/s)	T (°C)	P _{medium} (MPa)	P _{c-medium} (MPa)
1	2	0.62	0.20	0.09	0.026	1.5E-18	8.9E-13	25.0	0.15	0.48
2	22	0.63	0.20	0.09	0.024	1.4E-18	8.1E-13	24.2	0.15	0.48
3	23	0.63	0.30	0.09	0.084	1.8E-18	1.0E-12	24.3	0.20	0.43
4	24	0.63	0.40	0.09	0.162	1.9E-18	1.1E-12	24.1	0.25	0.38
5	25	0.63	0.50	0.09	0.285	2.1E-18	1.2E-12	24.0	0.30	0.33
6	26	1.01	0.50	0.09	0.211	1.5E-18	9.0E-13	24.0	0.30	0.72
7	44	2.02	0.50	0.09	0.006	4.5E-20	2.6E-14	24.1	0.30	1.72
8	44	2.02	0.70	0.09	0.007	2.6E-20	1.5E-14	24.2	0.40	1.63
9	50	2.02	0.51	0.09	0.002	1.2E-20	7.1E-15	24.1	0.30	1.72
10	70	2.52	0.50	0.09	0.001	3.9E-21	2.3E-15	24.0	0.30	2.22
11	140	1.03	0.50	0.10	0.001	3.6E-21	2.1E-15	24.1	0.30	0.73
12	194	0.63	0.50	0.09	0.003	2.3E-20	1.3E-14	24.1	0.30	0.33
13	213	0.62	0.20	0.09	0.001	3.2E-20	1.9E-14	24.1	0.15	0.47

LP equipment	
Confining P (MPa)	k _{ig} ·k _{rg} (m ²)
0.6	7.7E-18





GAS PERMEABILITY

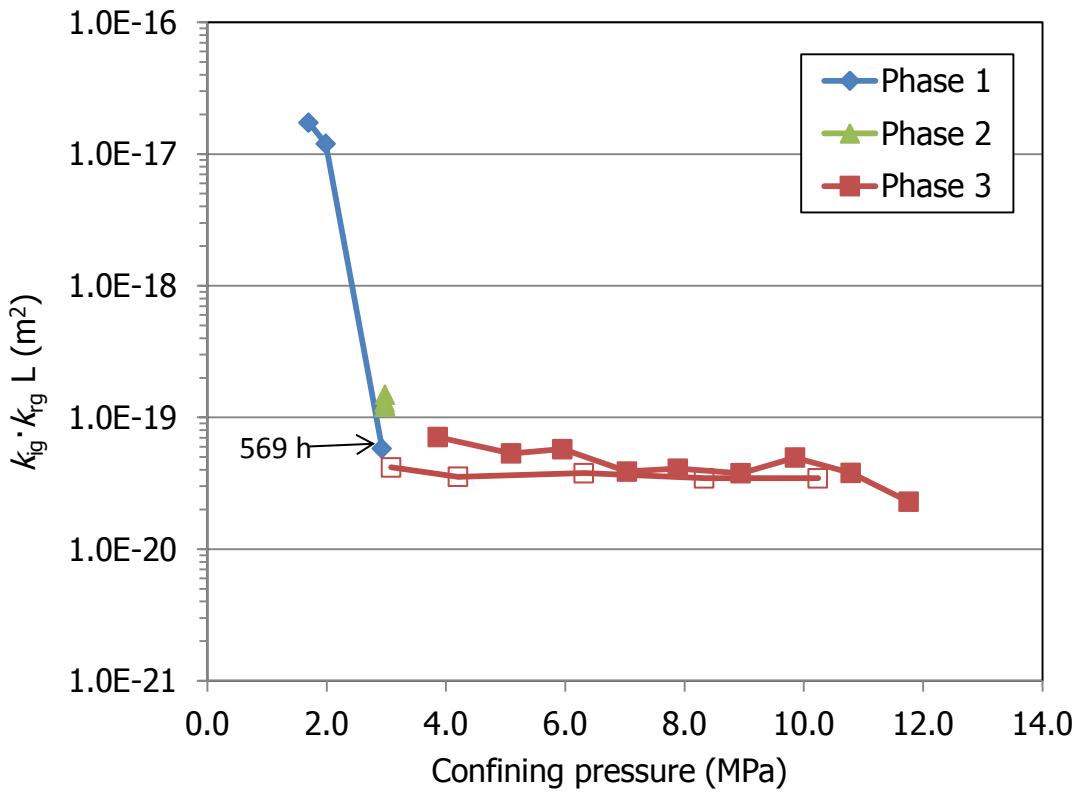
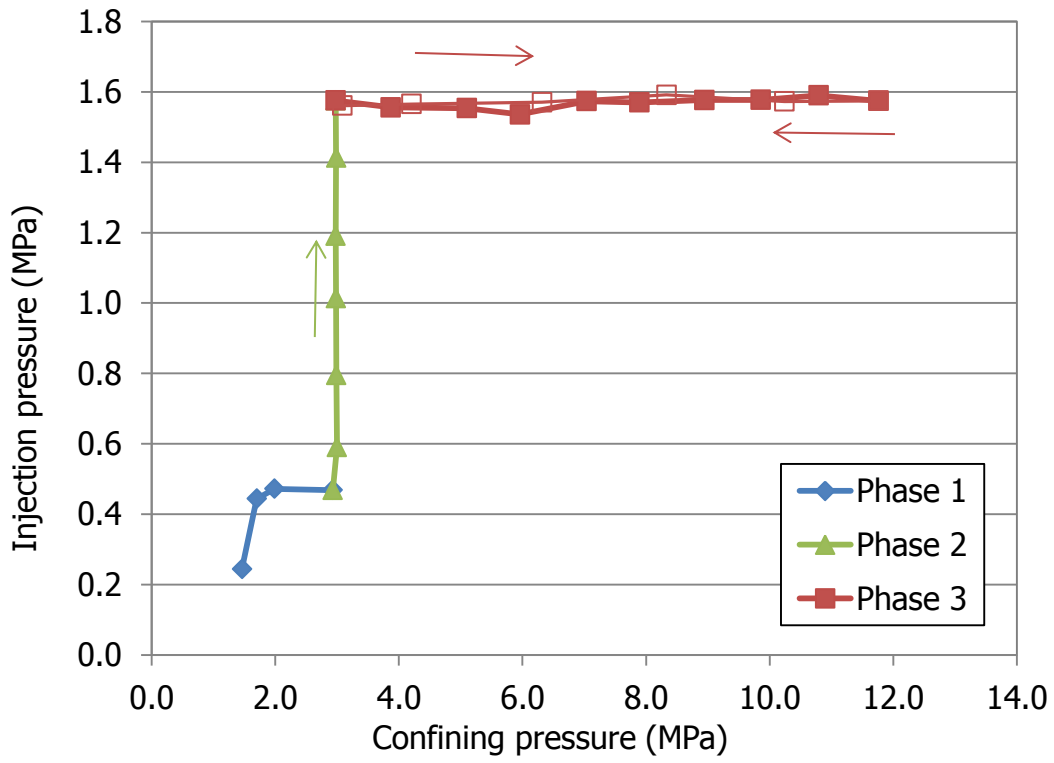
SAMPLE	BC-47-2	
START DATE:	15/12/2015	
END DATE:	19/05/2016	
SETUP:	HP-US	

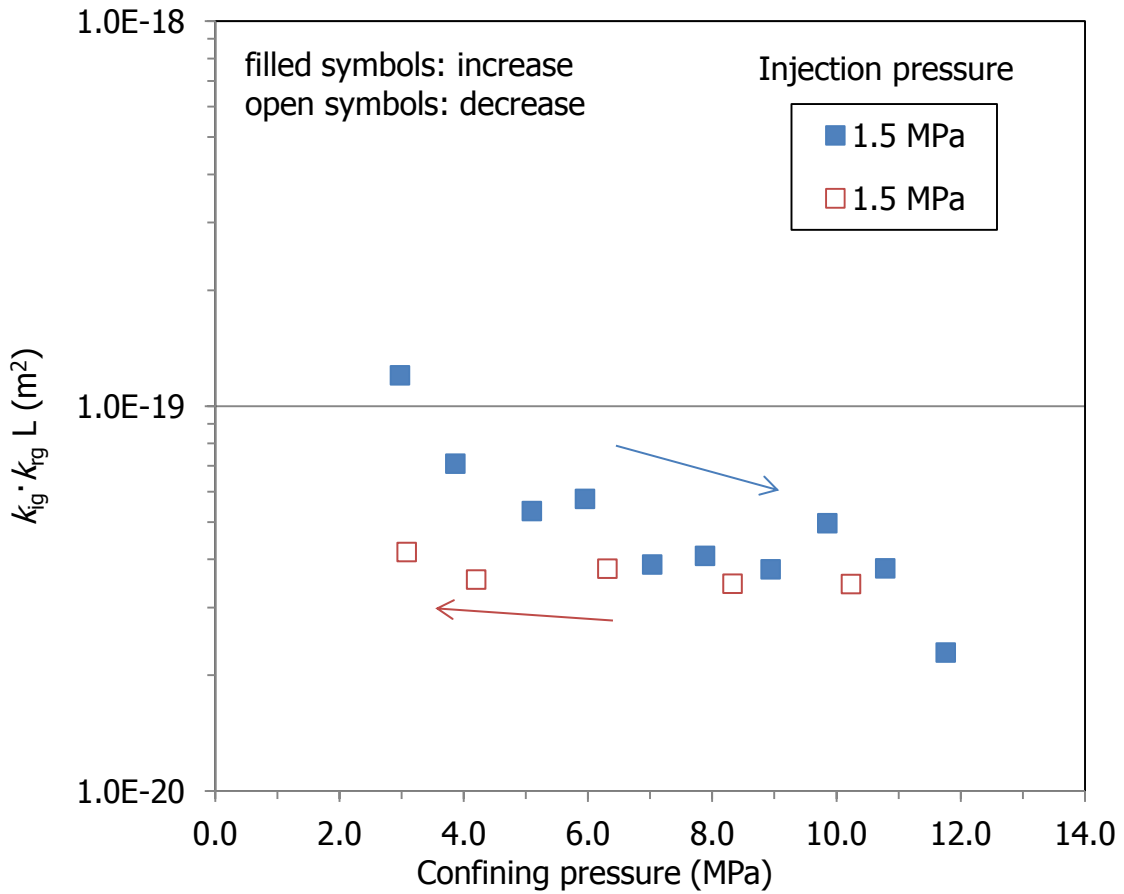
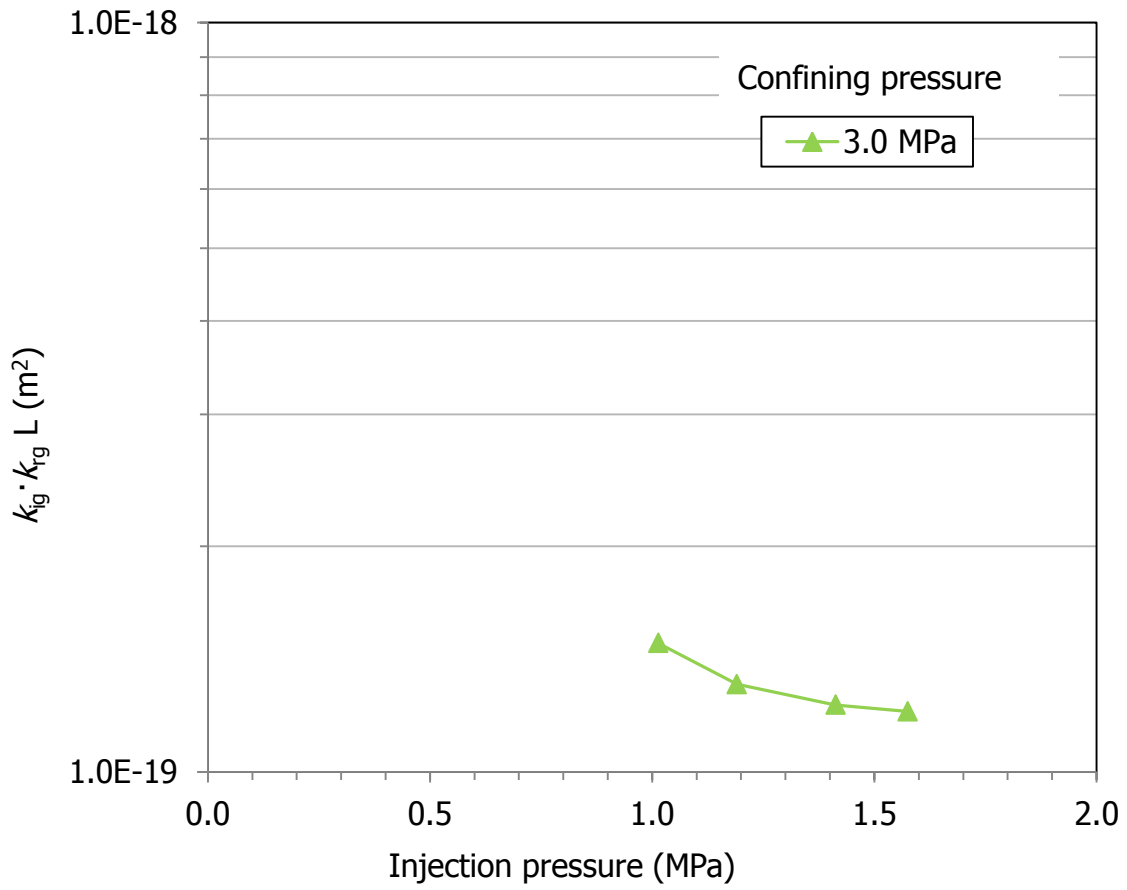
GAS CHARACTERISTICS	
viscosity N ₂ :	1.78E-05 Pa·s (at 20°C)
density N ₂ :	1.12 kg/m ³
<i>g</i> :	9.80665 m/s ²

CYLINDER	INPUT	1.526E-04
VOLUME (m ³)	OUTPUT	1.482E-04
CELL	Steel triaxial	
SAMPLE WRAPPING	latex + neoprene	

SAMPLE CHARACTERISTICS				
			Initial	Final
Specific weight (g/cm ³)	2.70	ρ _d (g/cm ³)	1.54	1.55
Initial weight (g)	87.41	<i>h</i> (cm)	3.98	4.02
Final weight (g)	87.08	φ (cm)	3.80	3.76
Dry weight (g)	69.17	Area (cm ²)	11.32	11.10
		<i>w</i> (%)	26.4	25.9
		<i>S_r</i> (%)	94	94

Stage	Time elapsed (h)	Confining <i>P</i> (MPa)	Injection <i>P</i> (MPa)	Back <i>P</i> (MPa)	<i>k_{ig}·k_{rg}</i> H (m ²)	<i>k_{ig}·k_{rg}</i> L (m ²)	<i>k_g</i> H (m/s)	<i>k_g</i> L (m/s)	<i>T</i> (°C)	<i>P_{medium}</i> (MPa)	<i>P_c</i> <i>P_{medium}</i> (MPa)
1	27	1.46	0.24	0.03	6.6E-17		1.0E-10		21.8	0.14	1.32
2	72	1.70	0.44	0.06	3.1E-17	1.7E-17	9.1E-11	4.9E-12	21.6	0.25	1.45
3	149	1.99	0.47	0.11	1.1E-17	1.2E-17	3.4E-11	6.3E-12	20.8	0.29	1.70
4	718	2.93	0.47	0.11	3.5E-19	5.8E-20	1.0E-12	3.8E-14	20.5	0.29	2.64
5	846	3.00	0.59	0.03	1.1E-18		4.0E-12		21.3	0.31	2.69
6	1152	2.99	0.80	0.01	1.8E-19		9.1E-13		21.6	0.40	2.59
7	1320	2.98	1.01	0.01		1.5E-19		9.9E-15	20.5	0.51	2.47
8	1536	2.98	1.19	0.02	3.4E-19	1.3E-19	2.5E-12	1.4E-14	21.2	0.61	2.37
9	1686	2.98	1.41	0.03	1.3E-19	1.2E-19	1.1E-12	1.9E-14	22.1	0.72	2.26
10	2046	2.98	1.58	0.05	2.0E-19	1.2E-19	2.0E-12	2.9E-14	23.0	0.81	2.16
11	2736	3.87	1.56	0.08	6.8E-20	7.1E-20	6.6E-13	2.9E-14	23.7	0.82	3.05
12	2834	5.10	1.55	0.08	2.2E-20	5.3E-20	2.1E-13	2.5E-14	24.1	0.82	4.28
13	2904	5.96	1.54	0.08	5.5E-19	5.7E-20	5.2E-12	2.8E-14	23.6	0.81	5.15
14	3002	7.04	1.57	0.08		3.9E-20		1.9E-14	23.4	0.83	6.21
15	3074	7.89	1.57	0.08	4.2E-19	4.1E-20	4.1E-12	2.1E-14	22.9	0.83	7.06
16	3168	8.94	1.58	0.08	9.7E-21	3.8E-20	9.4E-14	1.9E-14	23.0	0.83	8.11
17	3224	9.85	1.58	0.09	1.4E-19	5.0E-20	1.4E-12	2.6E-14	23.8	0.83	9.02
18	3360	10.79	1.59	0.09		3.8E-20		2.0E-14	22.9	0.84	9.95
19	3528	11.76	1.57	0.09	2.1E-19	2.3E-20	2.0E-12	1.3E-14	21.3	0.83	10.93
20	3576	10.24	1.57	0.09	5.9E-19	3.5E-20	5.8E-12	1.9E-14	22.3	0.83	9.41
21	3694	8.33	1.59	0.09		3.5E-20		2.0E-14	22.8	0.84	7.49
22	3744	6.32	1.57	0.09	4.1E-19	3.8E-20	4.0E-12	2.2E-14	23.0	0.83	5.48
23	3862	4.20	1.57	0.10	2.2E-19	3.5E-20	2.1E-12	2.1E-14	22.8	0.83	3.37
24	4010	3.08	1.56	0.10	6.1E-21	4.2E-20	5.9E-14	2.5E-14	22.9	0.83	2.25





GAS PERMEABILITY

SAMPLE	BC-47-3	
START DATE:	23/06/2016	
END DATE:	06/07/2016	
SETUP:	LCP	
CYLINDER VOLUME (m ³)	INPUT	1.526E-04
CELL	Steel triaxial	
SAMPLE WRAPPING	Double latex	
FLOWMETER	Range (mL/min)	Turndown (mL/min)
FT4 (a)	10	0.2
FT5 (b)	100	2
FT6 (c)	2	0.04

GAS CHARACTERISTICS

viscosity N₂: 1.78E-05 Pa·s (at 20°C)density N₂: 1.12 kg/m³g: 9.80665 m/s²

SAMPLE CHARACTERISTICS

			Initial	Final
Specific weight (g/cm ³)	2.70	ρ _d (g/cm ³)	1.61	1.57
Initial weight (g)	102.33	h (cm)	3.79	3.81
Final weight (g)	102.49	φ (cm)	4.15	4.20
Dry weight (g)	82.70	Area (cm ²)	13.55	13.83
		w (%)	23.7	23.9
		S _r (%)	95	90

The sample got accidentally wet during dismantling

a) steps 23-35; 56-61; 64-72

b) steps 62-63

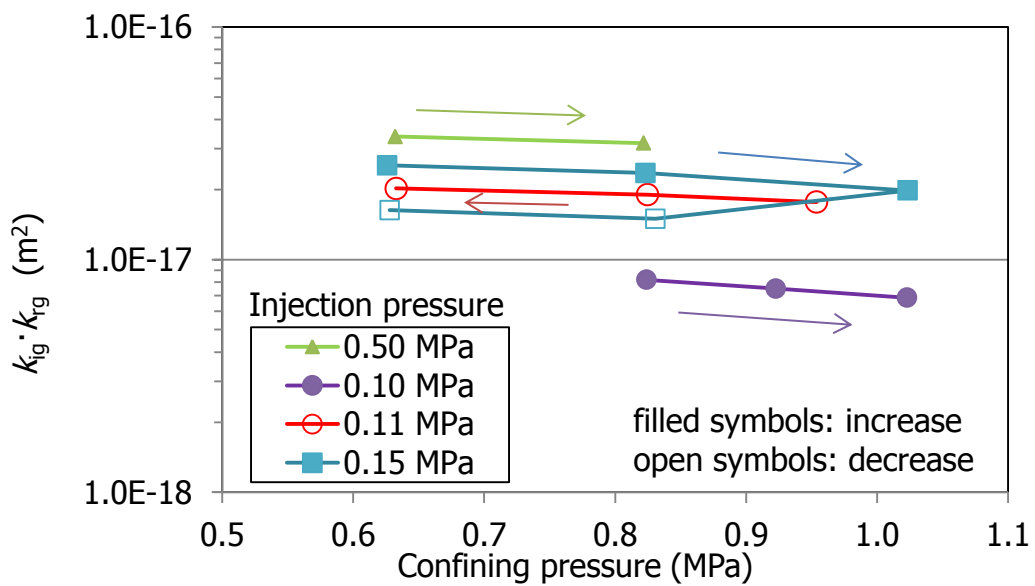
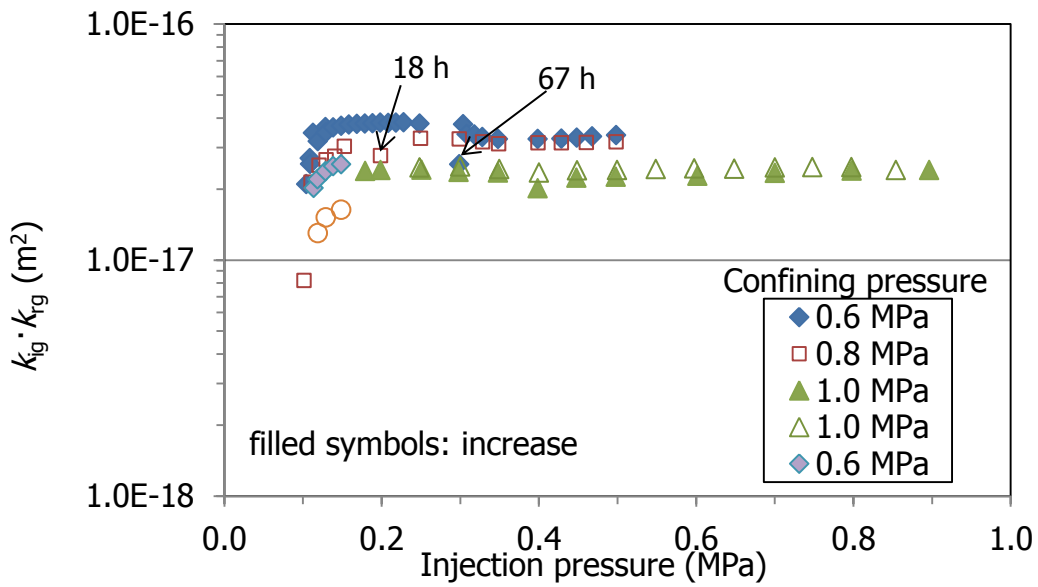
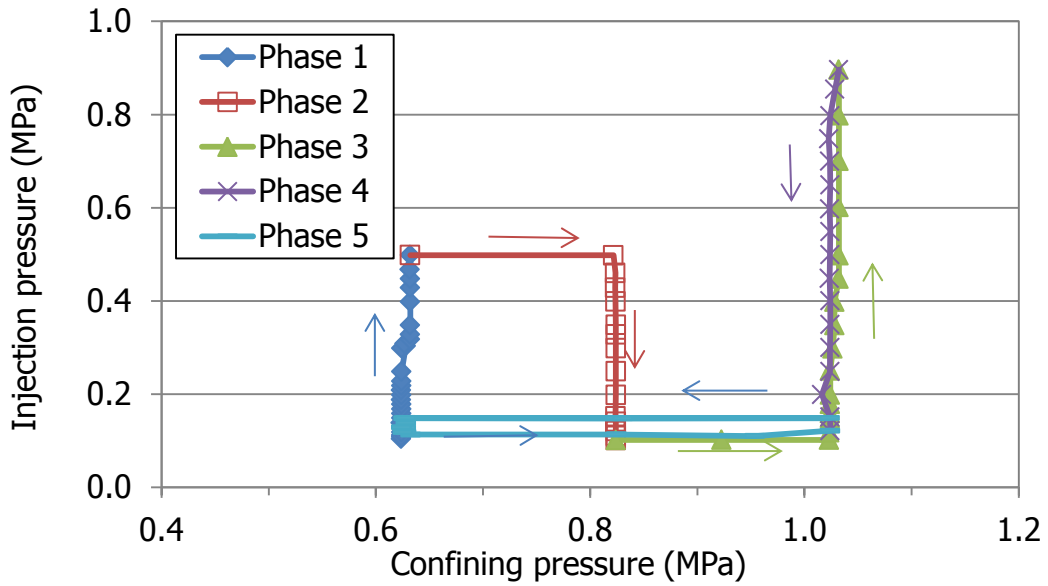
c) steps 1-23; 35-55; 73-91

Stage	Time elapsed (h)	Confining P (MPa)	Injection P (MPa)	Back P (MPa)	Flow (mL/min)	k _{ig} ·k _{rg} (m ²)	k _g (m/s)	T (°C)	P _{medium} (MPa)	P _c -P _{medium} (MPa)
1	1	0.62	0.13	0.10	0.163	3.7E-17	2.1E-11	23.8	0.11	0.51
2	2	0.62	0.11	0.10	0.074	3.5E-17	2.0E-11	23.9	0.10	0.52
3	3	0.62	0.10	0.10	0.023	2.1E-17	1.2E-11	23.5	0.10	0.52
4	4	0.62	0.11	0.09	0.045	2.7E-17	1.6E-11	23.9	0.10	0.52
5	22	0.62	0.11	0.09	0.044	2.6E-17	1.5E-11	23.4	0.10	0.52
6	23	0.62	0.12	0.09	0.096	3.2E-17	1.9E-11	23.5	0.11	0.52
7	23	0.62	0.13	0.10	0.156	3.5E-17	2.0E-11	23.5	0.11	0.51
8	23	0.62	0.14	0.10	0.219	3.6E-17	2.1E-11	23.6	0.12	0.51
9	23	0.62	0.15	0.10	0.287	3.7E-17	2.2E-11	23.6	0.12	0.50
10	24	0.62	0.16	0.10	0.356	3.7E-17	2.2E-11	23.6	0.13	0.50
11	24	0.62	0.17	0.10	0.432	3.8E-17	2.2E-11	23.5	0.13	0.49
12	25	0.62	0.18	0.10	0.513	3.8E-17	2.2E-11	23.5	0.14	0.49
13	25	0.62	0.19	0.10	0.597	3.8E-17	2.2E-11	23.3	0.14	0.48
14	26	0.62	0.20	0.10	0.686	3.8E-17	2.2E-11	23.2	0.15	0.48
15	26	0.62	0.21	0.10	0.778	3.8E-17	2.2E-11	23.1	0.15	0.47
16	27	0.62	0.22	0.10	0.875	3.8E-17	2.2E-11	23.1	0.16	0.47
17	27	0.62	0.23	0.10	0.977	3.8E-17	2.3E-11	23.7	0.16	0.46
18	27	0.62	0.25	0.10	1.185	3.8E-17	2.2E-11	23.9	0.17	0.45
19	28	0.63	0.30	0.10	1.859	3.8E-17	2.2E-11	24.0	0.20	0.43
20	95	0.62	0.30	0.10	1.210	2.5E-17	1.5E-11	23.4	0.20	0.43
21	95	0.63	0.31	0.10	1.744	3.4E-17	2.0E-11	23.6	0.20	0.42
22	95	0.63	0.32	0.10	1.859	3.4E-17	2.0E-11	23.6	0.21	0.42
23	95	0.63	0.33	0.10	1.945	3.3E-17	2.0E-11	23.4	0.21	0.42
24	96	0.63	0.35	0.10	2.170	3.3E-17	1.9E-11	23.7	0.22	0.41
25	96	0.63	0.40	0.10	2.902	3.3E-17	1.9E-11	23.7	0.25	0.39
26	96	0.63	0.43	0.10	3.399	3.3E-17	1.9E-11	23.6	0.26	0.37
27	96	0.63	0.45	0.10	3.761	3.3E-17	1.9E-11	23.6	0.27	0.36
28	96	0.63	0.47	0.10	4.171	3.3E-17	2.0E-11	23.7	0.28	0.35
29	97	0.63	0.50	0.10	4.810	3.4E-17	2.0E-11	23.8	0.30	0.33
30	97	0.82	0.50	0.10	4.502	3.2E-17	1.9E-11	23.9	0.30	0.52
31	98	0.82	0.46	0.10	3.810	3.2E-17	1.9E-11	23.9	0.28	0.55
32	99	0.82	0.43	0.10	3.258	3.1E-17	1.8E-11	23.6	0.26	0.56
33	99	0.82	0.40	0.10	2.798	3.1E-17	1.8E-11	23.8	0.25	0.58
34	100	0.82	0.35	0.10	2.080	3.1E-17	1.8E-11	24.2	0.22	0.60
35	100	0.82	0.33	0.10	1.861	3.2E-17	1.9E-11	24.3	0.21	0.61
36	100	0.82	0.30	0.10	1.550	3.3E-17	1.9E-11	24.3	0.20	0.63

GAS PERMEABILITY

BC-47-3

37	101	0.82	0.25	0.10	1.034	3.3E-17	1.9E-11	24.5	0.17	0.65
38	119	0.82	0.20	0.10	0.500	2.8E-17	1.6E-11	23.7	0.15	0.68
39	119	0.82	0.15	0.10	0.258	3.0E-17	1.8E-11	23.7	0.12	0.70
40	119	0.82	0.14	0.09	0.176	2.7E-17	1.6E-11	23.7	0.12	0.71
41	120	0.82	0.13	0.09	0.122	2.7E-17	1.6E-11	23.6	0.11	0.71
42	120	0.82	0.12	0.09	0.083	2.5E-17	1.5E-11	23.7	0.11	0.72
43	121	0.82	0.11	0.09	0.040	2.1E-17	1.2E-11	24.1	0.10	0.72
44	121	0.82	0.10	0.09	0.006	8.2E-18	4.8E-12	24.4	0.10	0.73
45	121	0.92	0.10	0.09	0.006	7.5E-18	4.4E-12	24.6	0.10	0.82
46	121	1.02	0.10	0.09	0.006	6.9E-18	4.0E-12	24.6	0.10	0.92
47	121	1.02	0.12	0.09	0.051	1.7E-17	1.0E-11	24.7	0.11	0.92
48	121	1.02	0.14	0.09	0.133	2.1E-17	1.3E-11	24.7	0.12	0.91
49	122	1.02	0.15	0.09	0.186	2.4E-17	1.4E-11	24.8	0.12	0.90
50	122	1.02	0.16	0.09	0.230	2.4E-17	1.4E-11	24.8	0.13	0.90
51	122	1.02	0.18	0.10	0.326	2.4E-17	1.4E-11	24.8	0.14	0.89
52	122	1.02	0.20	0.10	0.436	2.4E-17	1.4E-11	24.9	0.15	0.88
53	122	1.02	0.25	0.10	0.774	2.4E-17	1.4E-11	25.0	0.17	0.85
54	122	1.03	0.30	0.10	1.118	2.4E-17	1.4E-11	25.0	0.20	0.83
55	122	1.03	0.35	0.10	1.562	2.3E-17	1.4E-11	25.0	0.22	0.81
56	122	1.03	0.40	0.10	1.793	2.0E-17	1.2E-11	25.1	0.25	0.78
57	122	1.03	0.45	0.10	2.545	2.2E-17	1.3E-11	25.1	0.27	0.76
58	122	1.03	0.50	0.10	3.202	2.3E-17	1.3E-11	25.2	0.30	0.74
59	122	1.03	0.60	0.10	4.780	2.3E-17	1.3E-11	25.2	0.35	0.68
60	122	1.03	0.70	0.10	6.704	2.3E-17	1.4E-11	25.3	0.40	0.63
61	122	1.03	0.80	0.10	8.925	2.4E-17	1.4E-11	25.3	0.45	0.58
62	123	1.03	0.90	0.10	11.418	2.4E-17	1.4E-11	24.9	0.50	0.54
63	123	1.03	0.85	0.10	10.313	2.4E-17	1.4E-11	24.1	0.47	0.55
64	123	1.02	0.80	0.10	9.366	2.5E-17	1.5E-11	24.1	0.45	0.58
65	123	1.02	0.75	0.10	8.087	2.5E-17	1.5E-11	24.1	0.42	0.60
66	123	1.02	0.70	0.10	7.060	2.5E-17	1.5E-11	24.2	0.40	0.63
67	123	1.02	0.65	0.10	5.970	2.4E-17	1.4E-11	24.2	0.37	0.65
68	123	1.02	0.60	0.10	5.066	2.4E-17	1.4E-11	24.3	0.35	0.68
69	123	1.02	0.55	0.10	4.232	2.4E-17	1.4E-11	24.3	0.32	0.70
70	123	1.02	0.50	0.10	3.441	2.4E-17	1.4E-11	24.3	0.30	0.73
71	123	1.02	0.45	0.10	2.742	2.4E-17	1.4E-11	24.4	0.27	0.75
72	124	1.02	0.40	0.10	2.110	2.3E-17	1.4E-11	24.4	0.25	0.78
73	124	1.02	0.35	0.10	1.635	2.4E-17	1.4E-11	24.5	0.22	0.80
74	124	1.02	0.30	0.10	1.199	2.5E-17	1.5E-11	24.6	0.20	0.83
75	125	1.02	0.25	0.10	0.771	2.5E-17	1.4E-11	24.6	0.17	0.85
76	125	1.02	0.20	0.09	0.442	2.4E-17	1.4E-11	24.6	0.15	0.87
77	126	1.02	0.15	0.09	0.201	2.4E-17	1.4E-11	24.6	0.12	0.90
78	126	1.02	0.12	0.09	0.082	2.4E-17	1.4E-11	24.7	0.11	0.92
79	127	0.95	0.11	0.09	0.034	1.8E-17	1.0E-11	24.8	0.10	0.85
80	143	0.82	0.11	0.09	0.045	1.9E-17	1.1E-11	23.7	0.10	0.72
81	145	0.63	0.11	0.09	0.047	2.0E-17	1.2E-11	23.1	0.10	0.53
82	146	0.63	0.12	0.09	0.067	2.2E-17	1.3E-11	23.2	0.11	0.52
83	147	0.63	0.13	0.09	0.107	2.4E-17	1.4E-11	23.2	0.11	0.52
84	148	0.63	0.14	0.09	0.152	2.5E-17	1.5E-11	23.3	0.12	0.51
85	166	0.63	0.15	0.09	0.198	2.5E-17	1.5E-11	23.3	0.12	0.50
86	167	0.82	0.15	0.09	0.184	2.4E-17	1.4E-11	23.2	0.12	0.70
87	263	1.02	0.15	0.09	0.154	2.0E-17	1.2E-11	23.0	0.12	0.90
88	267	0.83	0.15	0.09	0.115	1.5E-17	8.8E-12	23.1	0.12	0.71
89	286	0.63	0.15	0.09	0.127	1.6E-17	9.5E-12	23.2	0.12	0.51
90	291	0.62	0.13	0.09	0.069	1.5E-17	8.9E-12	23.1	0.11	0.51
91	316	0.63	0.12	0.09	0.039	1.3E-17	7.6E-12	23.2	0.11	0.52



GAS PERMEABILITY

SAMPLE	BC-47-4	
START DATE:	10/12/2015	
END DATE:	19/05/2016	
SETUP:	HP-US	
CYLINDER	INPUT	2.950E-04
VOLUME (m ³)	OUTPUT	2.936E-04
CELL	Steel triaxial	
SAMPLE WRAPPING	duct tape + neoprene	

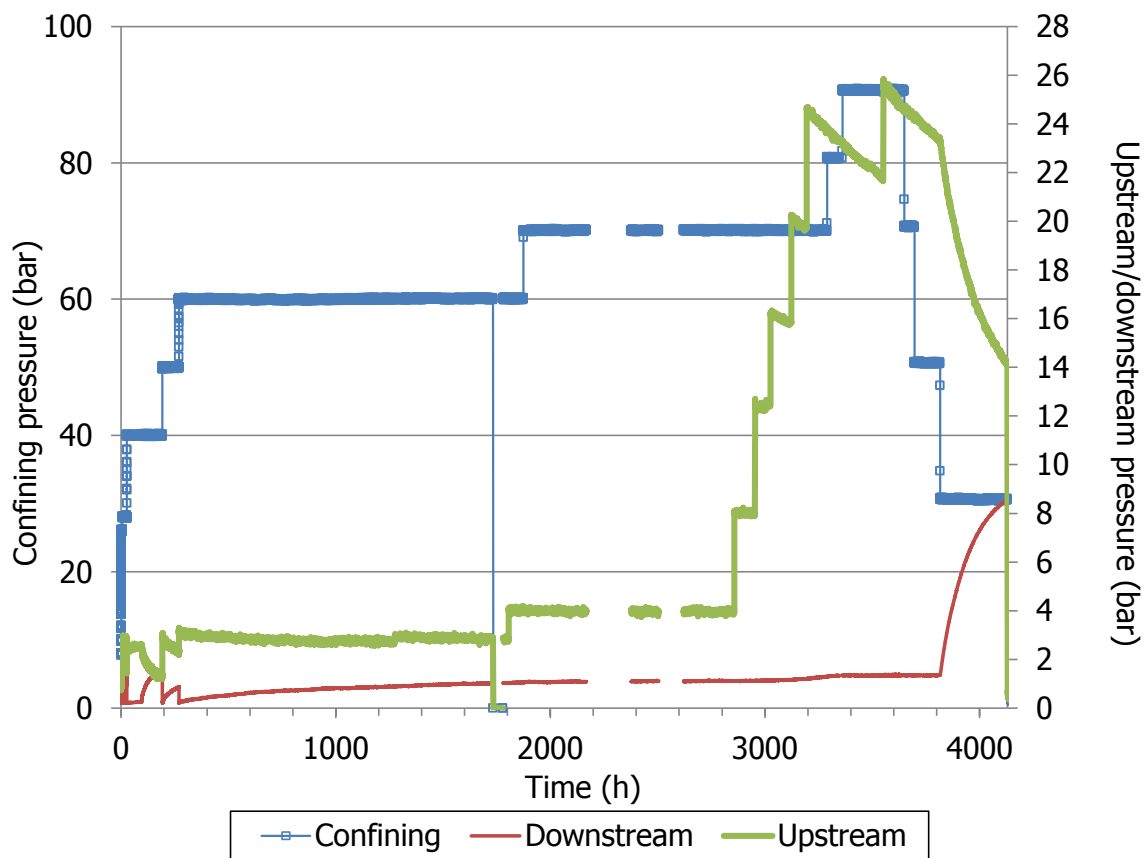
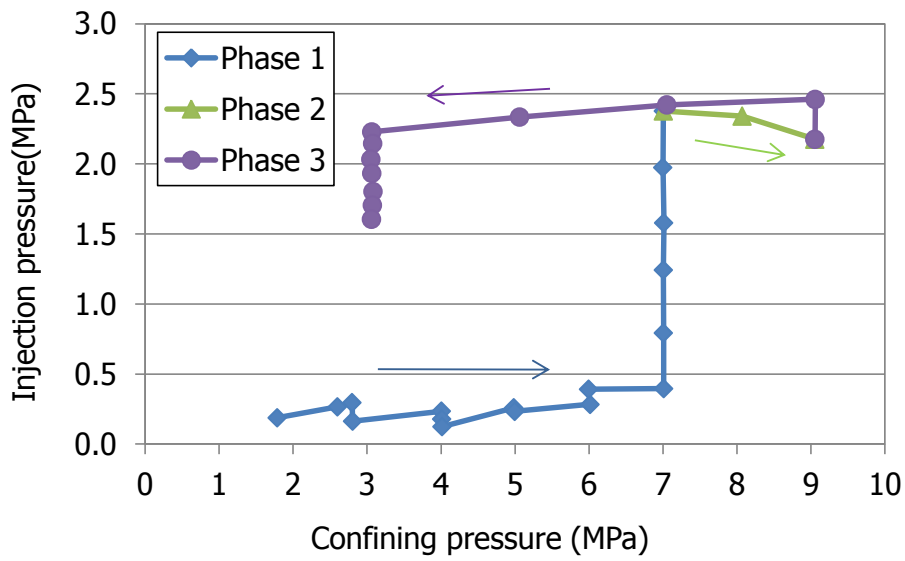
GAS CHARACTERISTICS

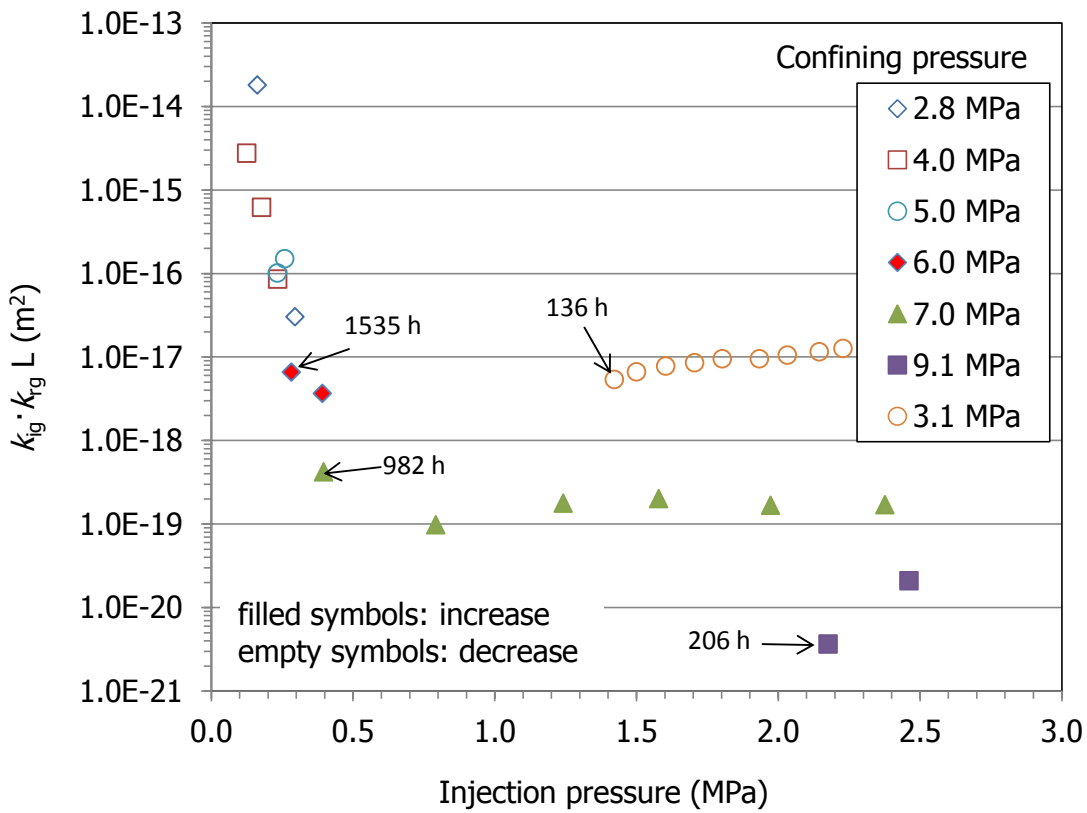
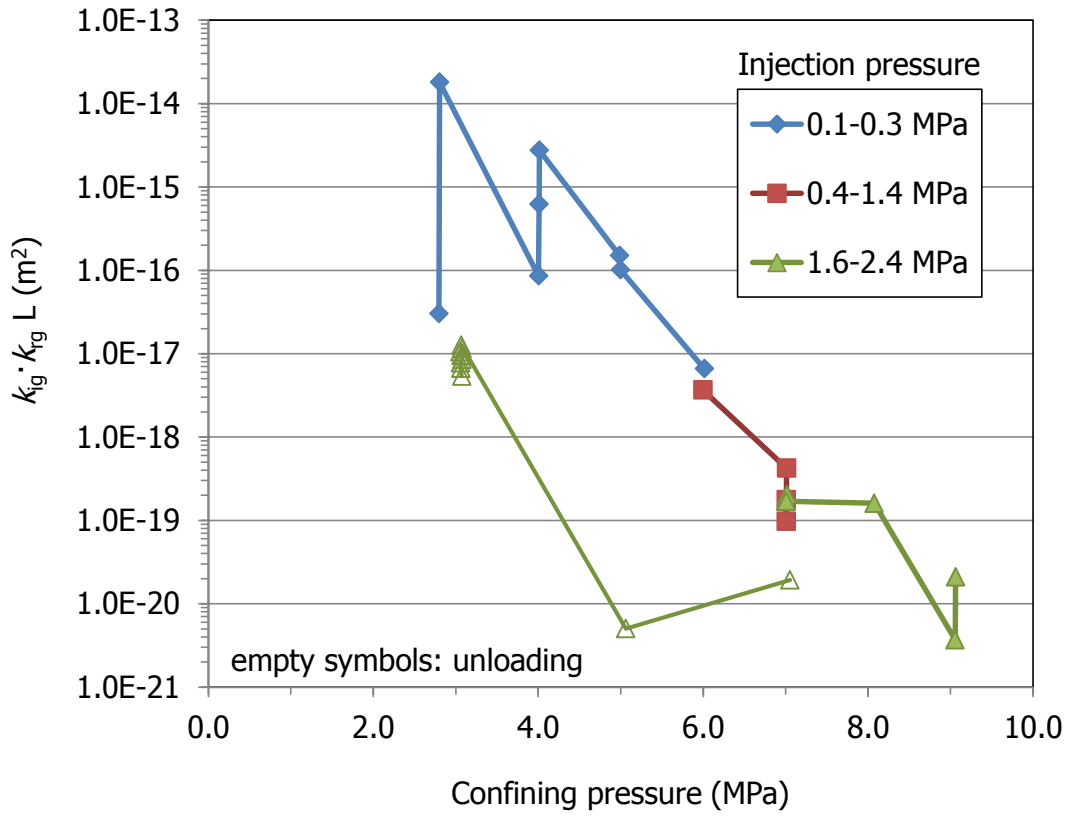
viscosity N₂ 1.78E-05 Pa·s (at 20°C)
density N₂: 1.12 kg/m³
 g : 9.80665 m/s²

SAMPLE CHARACTERISTICS

Interface between blocks			Initial	Final
Specific weight (g/cm ³)	2.70	ρ_a (g/cm ³)	1.59	1.61
Initial weight (g)		h (cm)	3.70	3.72
Final weight (g)	73.89	ϕ (cm)	3.60	3.57
Dry weight (g)	60.03	Area (cm ²)	10.17	10.03
		w (%)	24.8	23.1
		S_r (%)	97	91

Stage	Time elapsed (h)	Confining P (MPa)	Injection P (MPa)	Back P (MPa)	$k_{ig} \cdot k_{rg} H$ (m ²)	$k_{ig} \cdot k_{rg} L$ (m ²)	$k_g H$ (m/s)	$k_g L$ (m/s)	T (°C)	P_{medium} (MPa)	$P_{c-P_{medium}}$ (MPa)
1	1	1.79	0.19	0.13	4.7E-13	1.6E-13	3.9E-07	1.5E-07	22.0	0.16	1.63
2	5	2.60	0.27	0.02	1.9E-16		3.2E-10		22.3	0.14	2.46
3	23	2.80	0.30	0.02		3.0E-17		4.0E-12	22.2	0.16	2.64
4	26	2.80	0.16	0.16	1.4E-14	1.8E-14	1.7E-08	1.4E-08	22.2	0.16	2.64
5	100	4.00	0.23	0.05	5.5E-17	8.6E-17	8.3E-11	2.0E-11	22.3	0.14	3.86
6	129	4.01	0.18	0.11	5.2E-16	6.2E-16	6.3E-10	3.4E-10	22.3	0.15	3.86
7	192	4.01	0.12	0.15	2.6E-15	2.8E-15	2.3E-09	2.3E-09	21.9	0.14	3.87
8	220	4.99	0.26	0.06	1.9E-16	1.5E-16	3.3E-10	4.1E-11	21.4	0.16	4.83
9	269	5.00	0.23	0.09	1.1E-16	1.0E-16	1.6E-10	4.6E-11	21.0	0.16	4.84
10	1804	6.01	0.28	0.10	1.8E-18	6.6E-18	3.3E-12	2.6E-12	22.1	0.19	5.82
11	1874	6.00	0.39	0.11	7.5E-18	3.7E-18	1.8E-11	2.4E-12	23.3	0.25	5.75
12	2856	7.01	0.40	0.11	5.4E-19	4.2E-19	1.3E-12	2.9E-13	24.0	0.25	6.76
13	2952	7.01	0.79	0.11	2.7E-19	9.8E-20	1.3E-12	6.8E-14	24.5	0.45	6.56
14	3024	7.01	1.24	0.11	1.6E-19	1.8E-19	1.2E-12	1.2E-13	23.8	0.68	6.33
15	3122	7.01	1.58	0.12	2.1E-18	2.0E-19	2.0E-11	1.4E-13	23.6	0.85	6.17
16	3194	7.00	1.97	0.12	1.6E-18	1.7E-19	2.0E-11	1.2E-13	23.2	1.05	5.95
17	3288	7.01	2.38	0.13	1.8E-18	1.7E-19	2.8E-11	1.3E-13	23.4	1.25	5.75
18	3344	8.07	2.34	0.13	1.1E-18	1.6E-19	1.5E-11	1.3E-13	24.0	1.24	6.84
19	3550	9.06	2.18	0.13	1.6E-18	3.7E-21	2.3E-11	3.1E-15	23.0	1.16	7.90
20	3648	9.06	2.46	0.14	1.9E-18	2.1E-20	3.0E-11	1.7E-14	21.6	1.30	7.76
21	3696	7.05	2.42	0.13	1.5E-18	1.9E-20	2.2E-11	1.6E-14	22.7	1.28	5.77
22	3814	5.06	2.34	0.13	1.4E-18	5.0E-21	2.0E-11	4.2E-15	23.2	1.24	3.83
23	3832	3.07	2.23	0.23	1.5E-17	1.3E-17	2.1E-10	1.5E-11	23.1	1.23	1.84
24	3848	3.08	2.15	0.31	9.3E-18	1.2E-17	1.2E-10	2.0E-11	23.1	1.23	1.85
25	3870	3.05	2.03	0.40	1.1E-17	1.1E-17	1.5E-10	2.4E-11	23.5	1.22	1.83
26	3894	3.07	1.93	0.48	1.4E-17	9.5E-18	1.8E-10	2.7E-11	23.6	1.21	1.86
27	3932	3.08	1.80	0.60	1.2E-17	9.5E-18	1.4E-10	3.2E-11	23.3	1.20	1.88
28	3968	3.08	1.71	0.67	1.1E-17	8.5E-18	1.2E-10	3.4E-11	23.2	1.19	1.88
29	4010	3.06	1.60	0.74	1.1E-17	7.8E-18	1.1E-10	3.4E-11	23.0	1.17	1.89
30	4068	3.06	1.50	0.81	9.8E-18	6.7E-18	9.3E-11	3.2E-11	23.0	1.16	1.90
31	4130	3.07	1.42	0.86	9.5E-18	5.4E-18	8.5E-11	2.8E-11	23.2	1.14	1.93





GAS PERMEABILITY

SAMPLE	BC-47-6	
START DATE:	10/08/2016	
END DATE:	12/08/2016	
SETUP:	HCP	
CYLINDER VOLUME (m ³)	INPUT	1.526E-04
CELL	Steel triaxial	
SAMPLE WRAPPING	Double latex	
FLOWMETER	Range (mL/min)	Turndown (mL/min)
FT2 (b)	10	0.2
FT3 (a)	100	2

GAS CHARACTERISTICS	
viscosity N ₂ :	1.78E-05 Pa·s (at 20°C)
density N ₂ :	1.12 kg/m ³
g:	9.80665 m/s ²

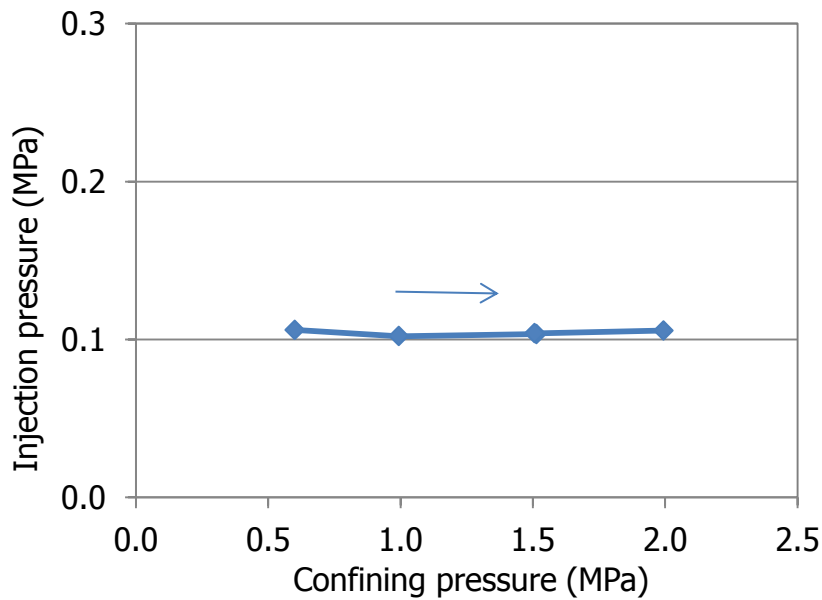
SAMPLE CHARACTERISTICS				
Interface between blocks			Initial	Final
Specific weight (g/cm ³)	2.70	ρ _d (g/cm ³)	1.64	
Initial weight (g)	102.49	h (cm)	3.92	
Final weight (g)		φ (cm)	4.12	
Dry weight (g)	85.69	Area (cm ²)	13.35	
		w (%)	19.6	
		S _r (%)	82	

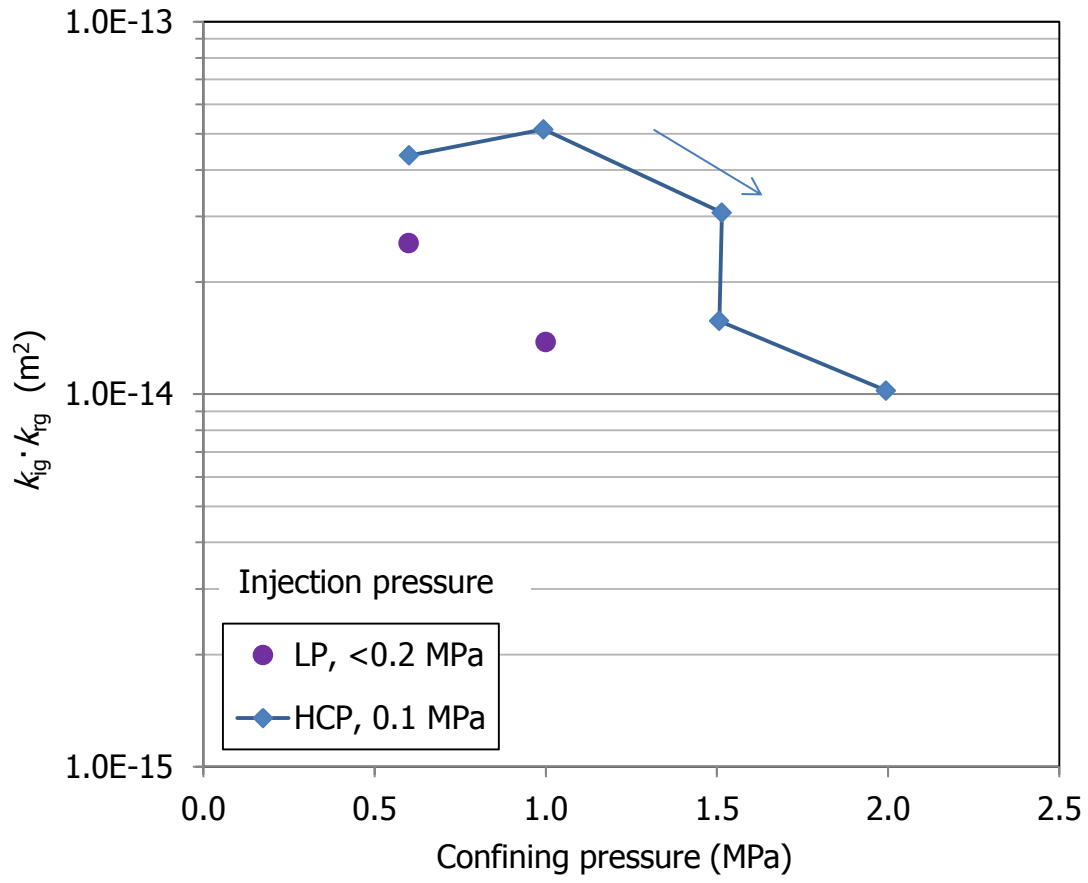
a) steps 1-5
b) step 5

the sample was wetted and damaged because of a failure

Stage	Time elapsed (h)	Confining P (MPa)	Injection P (MPa)	Back P (MPa)	Flow (mL/min)	k _{ig} ·k _{rg} (m ²)	k _g (m/s)	T (°C)	P _{medium} (MPa)	P _c ⁻ P _{medium} (MPa)
1	2.2	0.60	0.11	0.10	39.33	4.4E-14	2.6E-08	24.2	0.10	0.50
2	2.3	0.99	0.10	0.10	28.56	5.1E-14	3.1E-08	24.2	0.10	0.89
3	2.4	1.51	0.10	0.10	21.96	3.1E-14	1.8E-08	24.2	0.10	1.41
4	5.0	1.51	0.10	0.10	14.11	1.6E-14	9.3E-09	24.5	0.10	1.41
5	5.6	1.99	0.11	0.10	10.83	1.0E-14	6.0E-09	24.4	0.10	1.89

LP equipment	
Confining P (MPa)	k _{ig} ·k _{rg} (m ²)
0.6	2.5E-14
1.0	1.4E-14





GAS PERMEABILITY

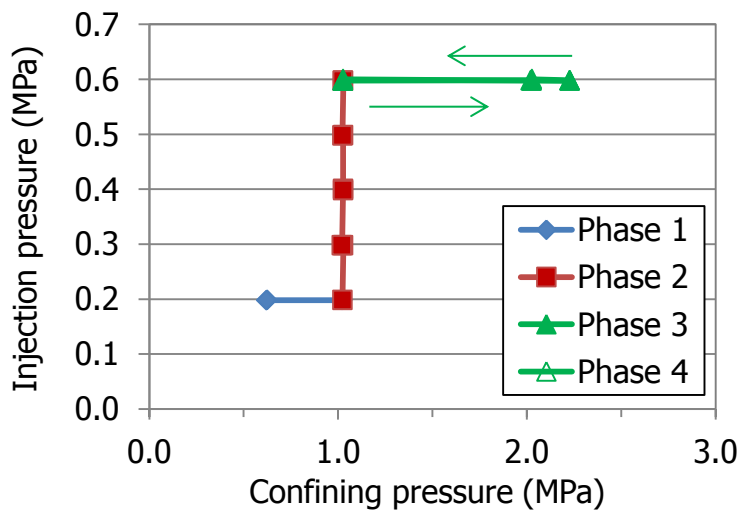
SAMPLE	BC-53-1	
START DATE:	26/06/2017	
END DATE:	10/07/2017	
SETUP:	LCP	
CYLINDER VOLUME (m ³)	INPUT	1.526E-04
CELL	Steel triaxial	
SAMPLE WRAPPING	Duct tape + Double latex	
FLOWMETER	Range (mL/min)	Turndown (mL/min)
FT6	2	0.04

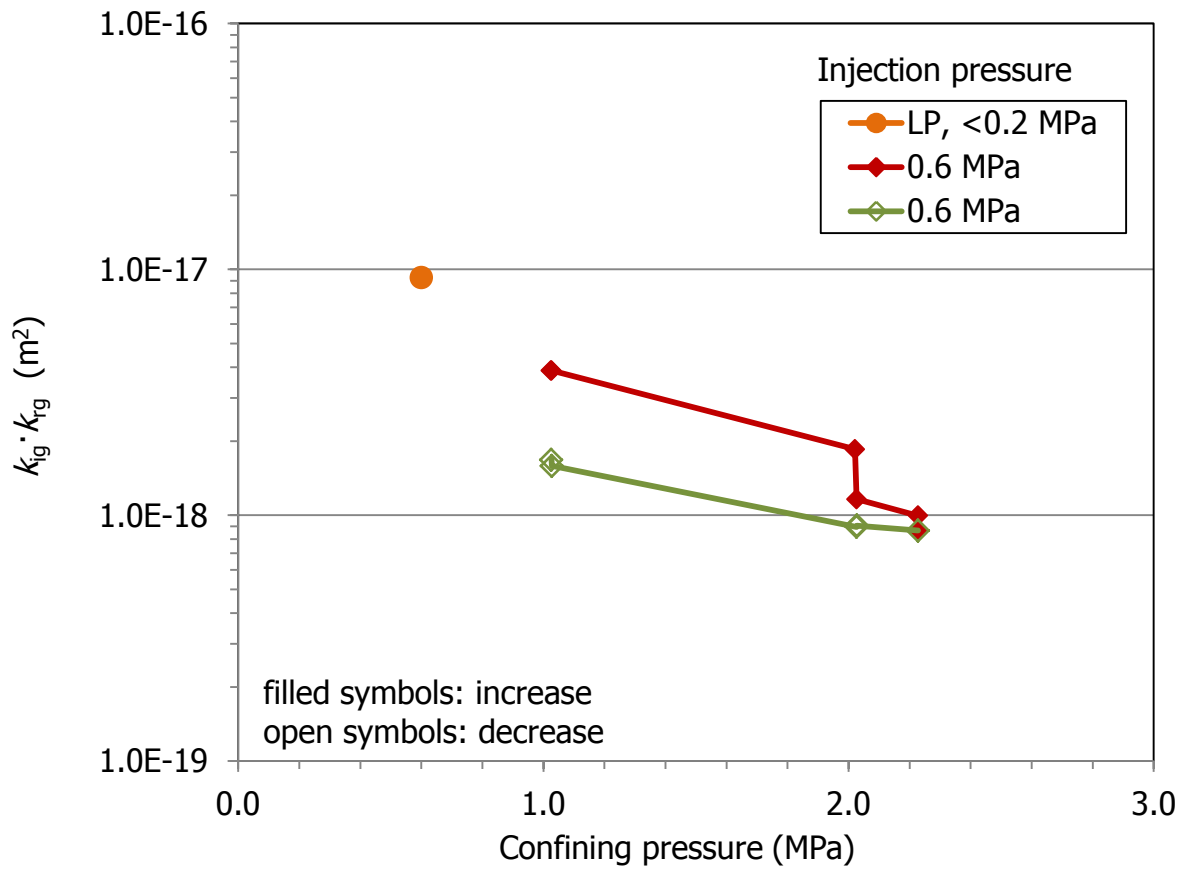
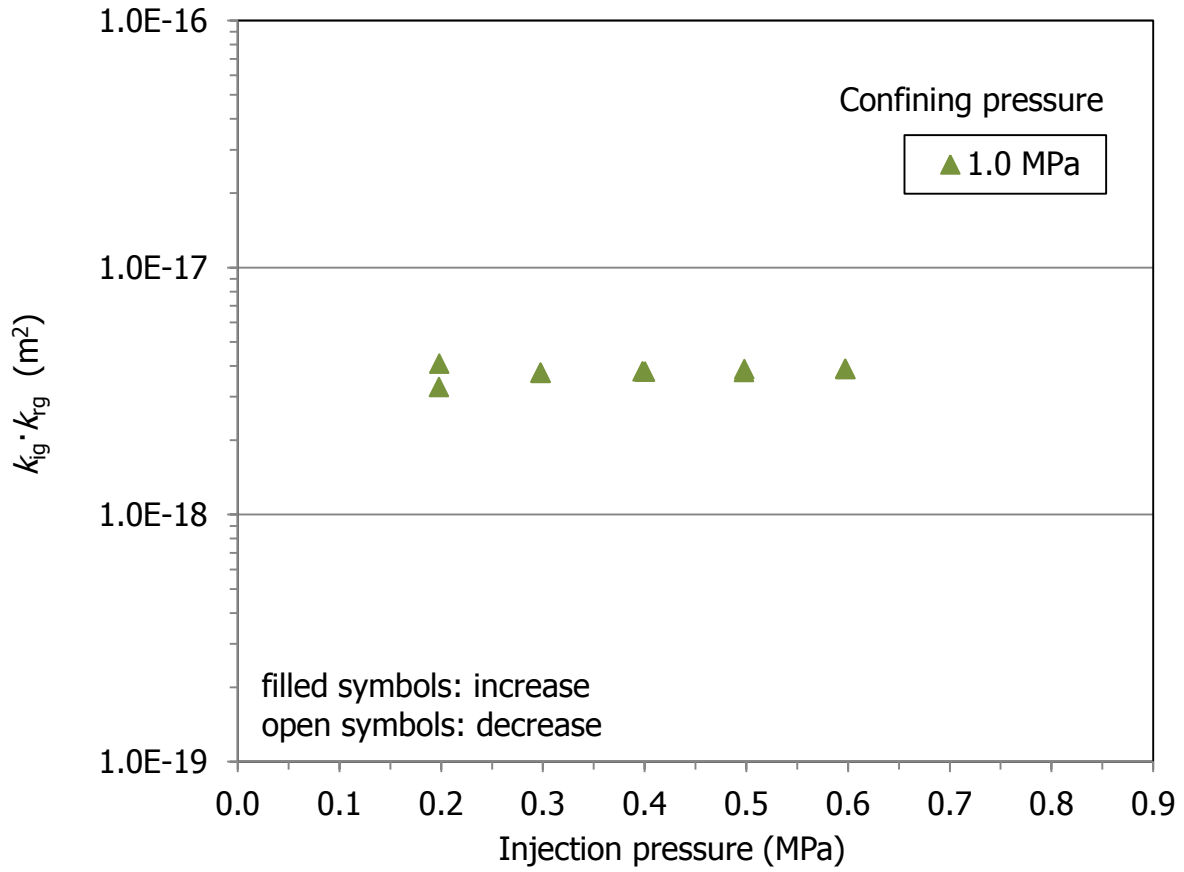
GAS CHARACTERISTICS		
viscosity N ₂ :	1.78E-05 Pa·s (at 20°C)	
density N ₂ :	1.12	kg/m ³
g:	9.80665	m/s ²

SAMPLE CHARACTERISTICS				
			Initial	Final
Specific weight (g/cm ³)	2.70	ρ _d (g/cm ³)	1.59	1.61
Initial weight (g)	100.54	h (cm)	4.08	4.06
Final weight (g)	100.20	φ (cm)	4.00	3.97
Dry weight (g)	81.28	Area (cm ²)	12.54	12.40
		w (%)	23.7	22.3
		S _r (%)	91	90

Stage	Time elapsed (h)	Confining P (MPa)	Injection P (MPa)	Back P (MPa)	Flow (mL/min)	k _{ig} ·k _{rg} (m ²)	k _g (m/s)	T (°C)	P _{medium} (MPa)	P _c - P _{medium} (MPa)
1	3.0	0.63	0.20	0.09	0.10	6.22E-18	3.62E-12	23.5	0.15	0.48
2	24.1	0.62	0.20	0.09	0.10	6.22E-18	3.61E-12	21.5	0.15	0.47
3	27.2	1.02	0.20	0.09	0.06	4.07E-18	2.37E-12	21.5	0.15	0.87
4	47.9	1.02	0.20	0.09	0.05	3.27E-18	1.90E-12	21.2	0.15	0.88
5	51.1	1.03	0.30	0.09	0.15	3.75E-18	2.18E-12	21.8	0.20	0.83
6	71.9	1.02	0.30	0.09	0.15	3.74E-18	2.17E-12	21.9	0.20	0.83
7	75.4	1.03	0.40	0.09	0.29	3.78E-18	2.21E-12	22.0	0.25	0.78
8	96.8	1.03	0.40	0.09	0.29	3.80E-18	2.22E-12	21.8	0.25	0.78
9	99.2	1.03	0.50	0.10	0.47	3.87E-18	2.27E-12	22.0	0.30	0.73
10	167.9	1.02	0.50	0.10	0.46	3.78E-18	2.23E-12	22.0	0.30	0.73
11	171.1	1.03	0.60	0.10	0.69	3.88E-18	2.29E-12	22.1	0.35	0.68
12	192.0	1.03	0.60	0.10	0.69	3.88E-18	2.28E-12	22.3	0.35	0.68
13	195.0	2.02	0.60	0.10	0.33	1.85E-18	1.09E-12	22.6	0.35	1.67
14	216.1	2.03	0.60	0.09	0.21	1.16E-18	6.79E-13	23.1	0.35	1.68
15	219.6	2.23	0.60	0.09	0.18	9.95E-19	5.81E-13	24.0	0.35	1.88
16	240.5	2.23	0.60	0.09	0.15	8.66E-19	5.06E-13	23.6	0.35	1.88
17	242.8	2.03	0.60	0.09	0.16	9.08E-19	5.32E-13	23.8	0.35	1.68
18	264.6	2.03	0.60	0.09	0.16	8.97E-19	5.24E-13	21.9	0.35	1.68
19	267.3	1.03	0.60	0.09	0.28	1.59E-18	9.28E-13	22.2	0.35	0.68
20	338.5	1.03	0.60	0.09	0.30	1.68E-18	9.80E-13	23.0	0.35	0.68

LP equipment	
Confining P (MPa)	k _{ig} ·k _{rg} (m ²)
0.6	9.3E-18





GAS PERMEABILITY

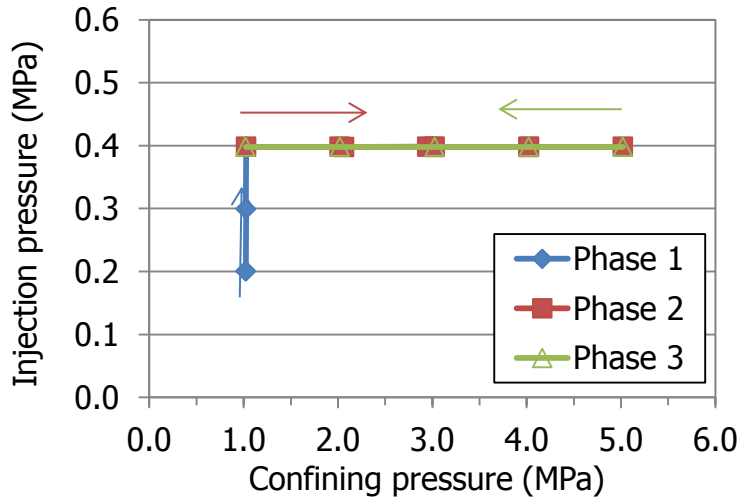
SAMPLE	BC-53-2	
START DATE:	23/10/2017	
END DATE:	16/11/2017	
SETUP:	LCP	
CYLINDER VOLUME (m ³)	INPUT	1.526E-04
CELL	Steel triaxial	
SAMPLE WRAPPING	Duct tape + Double latex	
FLOWMETER	Range (mL/min)	Turndown (mL/min)
FT6	2	0.04

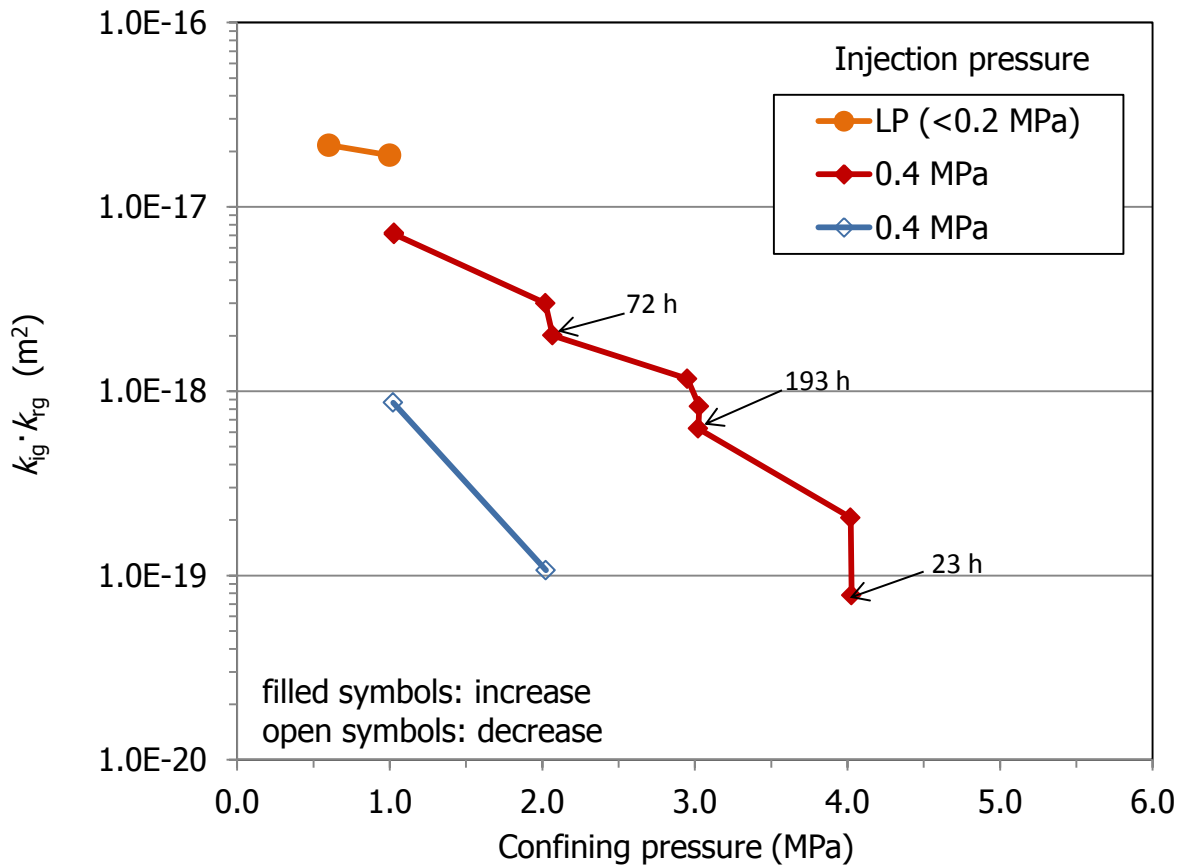
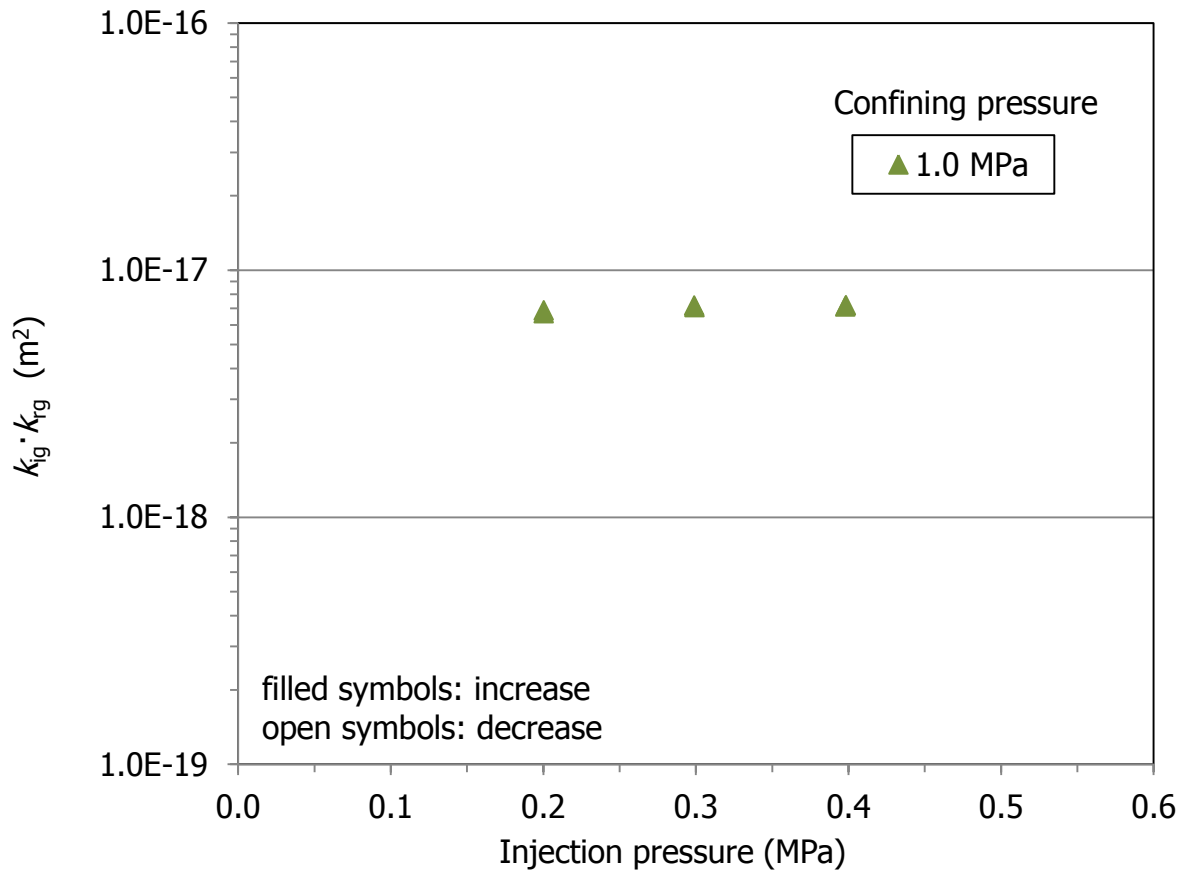
GAS CHARACTERISTICS	
viscosity N ₂ :	1.78E-05 Pa·s (at 20°C)
density N ₂ :	1.12 kg/m ³
g:	9.80665 m/s ²

SAMPLE CHARACTERISTICS				
			Initial	Final
Specific weight (g/cm ³)	2.70	ρ _d (g/cm ³)	1.63	1.64
Initial weight (g)	102.75	h (cm)	4.10	4.09
Final weight (g)	102.40	φ (cm)	3.99	3.99
Dry weight (g)	83.88	Area (cm ²)	12.51	12.50
		w (%)	22.5	23.3
		S _r (%)	93	97

Stage	Time elapsed (h)	Confining P (MPa)	Injection P (MPa)	Back P (MPa)	Flow (mL/min)	k _{ig} ·k _{rg} (m ²)	k _g (m/s)	T (°C)	P _{medium} (MPa)	P _c -P _{medium} (MPa)
1	5.6	1.03	0.20	0.10	0.11	6.87E-18	4.05E-12	20.9	0.15	0.88
2	24.4	1.02	0.20	0.10	0.11	6.68E-18	3.94E-12	22.2	0.15	0.87
3	29.6	1.03	0.30	0.10	0.29	7.19E-18	4.24E-12	22.4	0.20	0.83
4	48.4	1.02	0.30	0.10	0.29	7.07E-18	4.17E-12	22.6	0.20	0.83
5	50.3	1.03	0.40	0.10	0.55	7.21E-18	4.26E-12	22.8	0.25	0.78
6	96.1	1.03	0.40	0.10	0.54	7.12E-18	4.23E-12	23.1	0.25	0.78
7	98.8	2.02	0.40	0.10	0.23	3.00E-18	1.78E-12	23.2	0.25	1.77
8	168.2	2.07	0.40	0.09	0.15	2.01E-18	1.17E-12	21.8	0.25	1.82
9	168.5	2.95	0.40	0.09	0.09	1.17E-18	6.84E-13	21.8	0.25	2.70
10	341.3	3.03	0.40	0.10	0.06	8.27E-19	4.86E-13	19.8	0.25	2.78
11	361.9	3.02	0.40	0.09	0.05	6.27E-19	3.67E-13	20.4	0.25	2.78
12	365.0	4.02	0.40	0.09	0.02	2.06E-19	1.20E-13	20.6	0.25	3.77
13	385.3	4.03	0.40	0.10	0.01	7.81E-20	4.58E-14	20.8	0.25	3.78
14	429.3	5.02	0.40	0.10				20.5	0.25	4.77
15	501.6	4.02	0.40	0.10				19.7	0.25	3.78
16	525.6	3.03	0.40	0.09				19.8	0.25	2.78
17	549.6	2.02	0.40	0.09	0.01	1.07E-19	6.24E-14	20.6	0.25	1.78
18	575.9	1.02	0.40	0.09	0.07	8.66E-19	5.07E-13	20.9	0.25	0.78

LP equipment	
Confining P (MPa)	k _{ig} ·k _{rg} (m ²)
0.6	2.2E-17
1.0	1.9E-17





GAS PERMEABILITY

SAMPLE	BC-53-3	
START DATE:	27/03/2017	
END DATE:	11/04/2017	
SETUP:	LCP	
CYLINDER VOLUME (m ³)	INPUT	1.526E-04
CELL	Steel triaxial	
SAMPLE WRAPPING	Duct tape + Double latex	
FLOWMETER	Range (mL/min)	Turndown (mL/min)
FT6 a) and c)	2	0.04
FT4 d)	10	0.2
FT5 b)	100	2

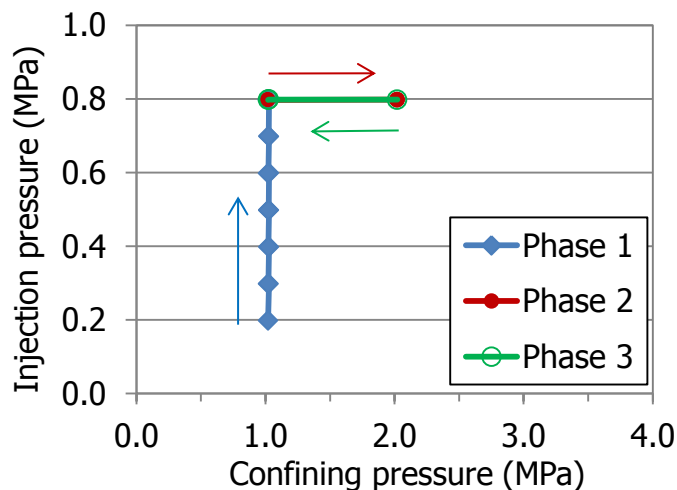
GAS CHARACTERISTICS		
viscosity N ₂ :	1.78E-05 Pa·s (at 20°C)	
density N ₂ :	1.12	kg/m ³
g:	9.80665	m/s ²

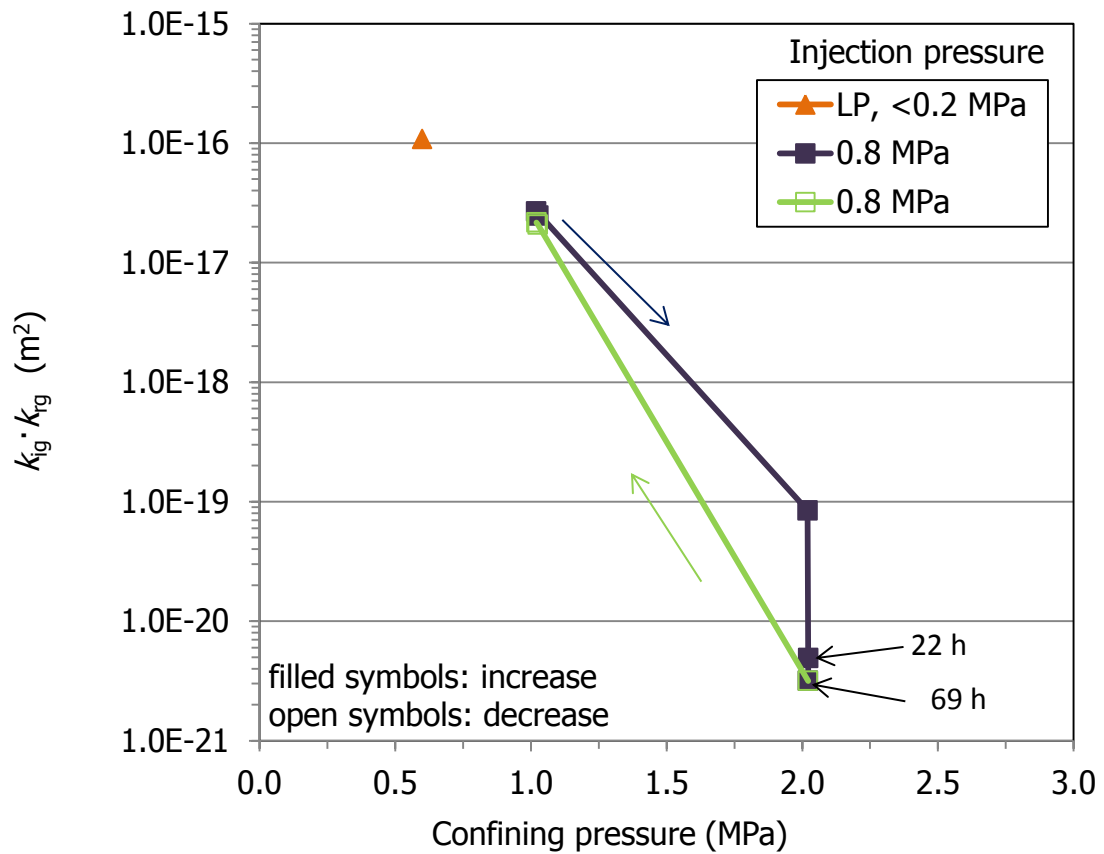
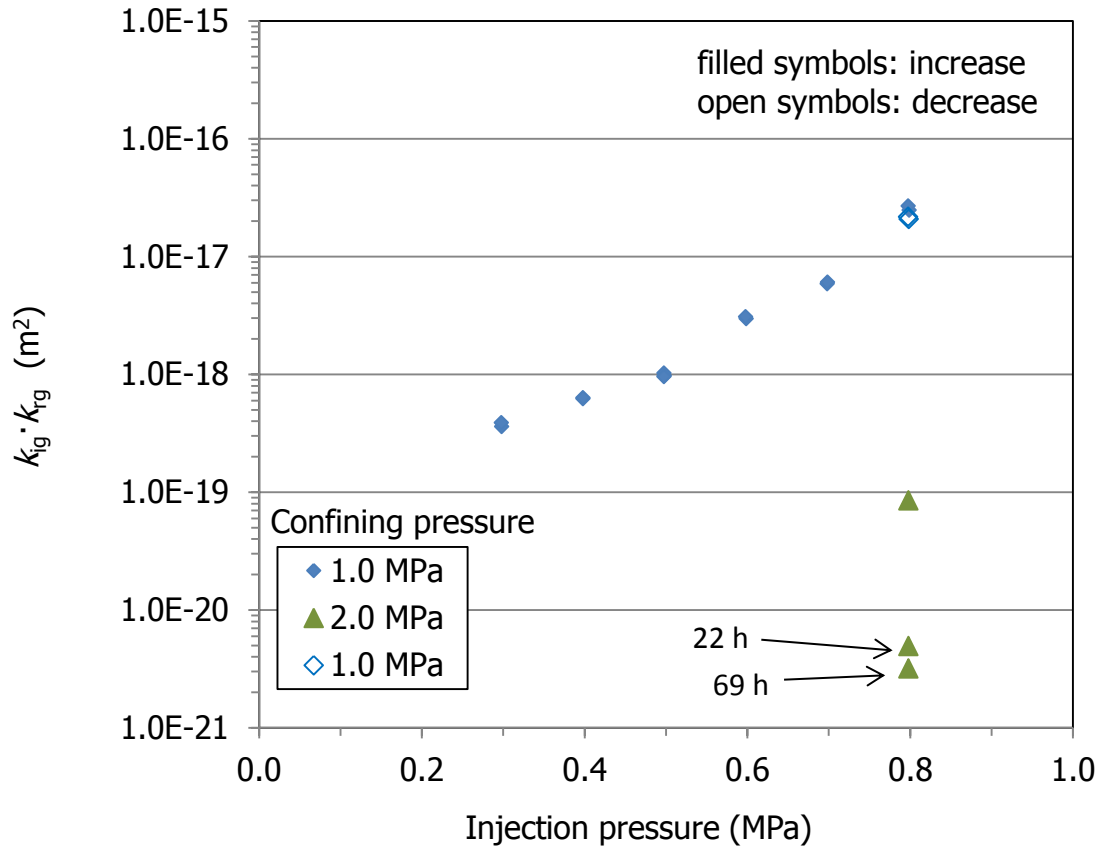
SAMPLE CHARACTERISTICS				
			Initial	Final
Specific weight (g/cm ³)	2.70	ρ _d (g/cm ³)	1.54	1.56
Initial weight (g)	81.95	h (cm)	3.30	3.29
Final weight (g)	81.41	φ (cm)	3.99	3.96
Dry weight (g)	63.53	Area (cm ²)	12.50	12.34
		w (%)	29.0	25.7
		S _r (%)	104	95

a) steps 1-12 c) steps 15-17
 b) steps 13-14 d) steps 18-19

Stage	Time elapsed (h)	Confining P (MPa)	Injection P (MPa)	Back P (MPa)	Flow (mL/min)	k _{ig} ·k _{rg} (m ²)	k _g (m/s)	T (°C)	P _{medium} (MPa)	P _c -P _{medium} (MPa)
1	23.8	1.02	0.20	0.10	0.001			23.5	0.15	0.87
2	25.2	1.03	0.30	0.10	0.018	3.60E-19	2.12E-13	24.2	0.20	0.83
3	47.6	1.02	0.30	0.10	0.019	3.86E-19	2.28E-13	23.9	0.20	0.83
4	48.7	1.03	0.40	0.10	0.058	6.18E-19	3.64E-13	24.3	0.25	0.78
5	71.5	1.02	0.40	0.10	0.059	6.32E-19	3.72E-13	23.7	0.25	0.78
6	72.9	1.03	0.50	0.10	0.146	9.69E-19	5.69E-13	24.2	0.30	0.73
7	94.7	1.02	0.50	0.10	0.153	1.02E-18	5.99E-13	24.3	0.30	0.73
8	164.8	1.02	0.50	0.10	0.143	9.51E-19	5.59E-13	22.1	0.30	0.73
9	169.0	1.03	0.60	0.10	0.649	2.96E-18	1.74E-12	22.5	0.35	0.68
10	189.0	1.02	0.60	0.10	0.671	3.06E-18	1.81E-12	23.2	0.35	0.67
11	192.7	1.03	0.70	0.10	1.761	5.85E-18	3.48E-12	23.1	0.40	0.63
12	213.9	1.02	0.70	0.10	1.818	6.04E-18	3.59E-12	24.3	0.40	0.63
13	216.9	1.03	0.80	0.10	9.783	2.47E-17	1.47E-11	24.4	0.45	0.58
14	237.8	1.02	0.80	0.10	10.594	2.68E-17	1.58E-11	24.5	0.45	0.57
15	240.7	2.02	0.80	0.09	0.033	8.45E-20	4.95E-14	24.5	0.45	1.57
16	262.2	2.02	0.80	0.09	0.002	4.92E-21	2.88E-15	24.9	0.45	1.58
17	331.0	2.02	0.80	0.10	0.001	3.17E-21	1.86E-15	24.6	0.45	1.57
18	336.6	1.03	0.80	0.10	8.196	2.07E-17	1.24E-11	24.5	0.45	0.58
19	356.1	1.02	0.80	0.10	8.540	2.16E-17	1.29E-11	25.1	0.45	0.57

LP equipment	
Confining P (MPa)	k _{ig} ·k _{rg} (m ²)
0.6	1.1E-16
1.0	4.1E-18





GAS PERMEABILITY

SAMPLE	BC-53-4	
START DATE:	24/04/2017	
END DATE:	11/05/2017	
SETUP:	LCP	
CYLINDER	INPUT	1.526E-04
VOLUME (m ³)		
CELL	Steel triaxial	
SAMPLE WRAPPING	Duct tape + Double latex	
FLOWMETER	Range (mL/min)	Turndown (mL/min)
FT6 c)	2	0.04
FT4 b)	10	0.2
FT5 a)	100	2

GAS CHARACTERISTICS

viscosity N₂: 1.78E-05 Pa·s (at 20°C)
 density N₂: 1.12 kg/m³
 g: 9.80665 m/s²

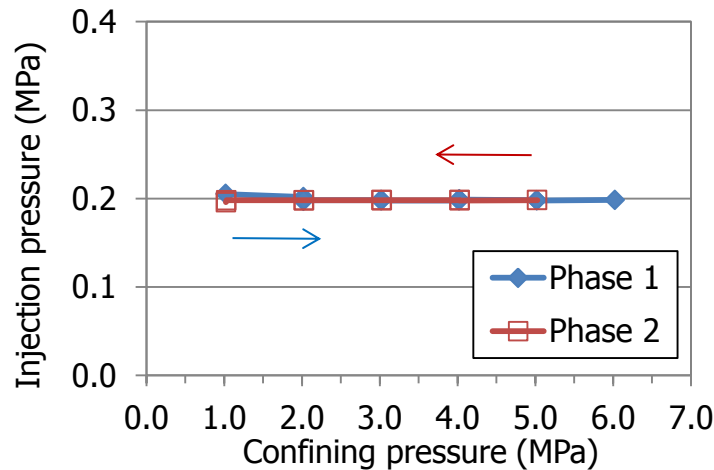
SAMPLE CHARACTERISTICS

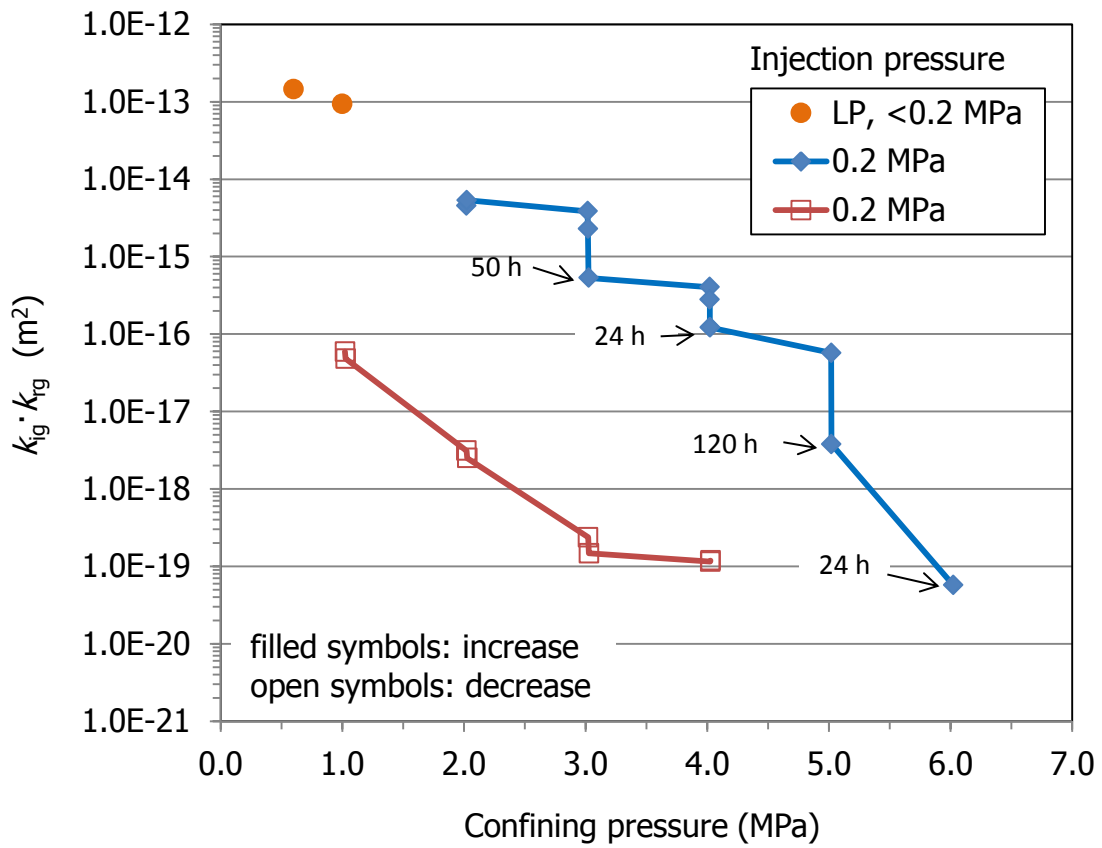
Interface between blocks			Initial	Final
Specific weight (g/cm ³)	2.70	ρ _d (g/cm ³)	1.53	1.60
Initial weight (g)	89.80	h (cm)	3.68	3.65
Final weight (g)	88.40	φ (cm)	4.00	3.93
Dry weight (g)	70.65	Area (cm ²)	12.55	12.12
		w (%)	27.1	25.1
		S _r (%)	96	98

a) steps 3-6 b) steps 7-11 c) steps 12-23

Stage	Time elapsed (h)	Confining P (MPa)	Injection P (MPa)	Back P (MPa)	Flow (mL/min)	k _{ig} ·k _{rg} (m ²)	k _g (m/s)	T (°C)	P _{medium} (MPa)	P _c -P _{medium} (MPa)
1	0.0	1.02	0.21	0.09	<100			22.20	0.15	0.87
2	21.4	2.02	0.20	0.10	<100			21.95	0.15	1.87
3	22.9	2.02	0.20	0.10	75.792	4.5E-15	2.7E-09	21.97	0.15	1.87
4	24.2	2.02	0.20	0.10	90.475	5.4E-15	3.2E-09	22.25	0.15	1.87
5	25.4	3.02	0.20	0.10	65.567	3.9E-15	2.3E-09	22.13	0.15	2.87
6	29.0	3.02	0.20	0.10	39.230	2.3E-15	1.3E-09	22.07	0.15	2.87
7	73.6	3.02	0.20	0.09	9.097	5.3E-16	3.1E-10	21.85	0.15	2.88
8	74.3	4.02	0.20	0.10	6.863	4.0E-16	2.4E-10	21.97	0.15	3.87
9	77.3	4.02	0.20	0.10	4.769	2.8E-16	1.6E-10	21.95	0.15	3.87
10	94.8	4.02	0.20	0.09	2.088	1.2E-16	7.1E-11	21.91	0.15	3.88
11	97.2	4.02	0.20	0.09	2.115	1.2E-16	7.1E-11	22.02	0.15	3.88
12	98.9	5.02	0.20	0.10	0.976	5.7E-17	3.3E-11	22.09	0.15	4.87
13	216.9	5.02	0.20	0.09	0.065	3.8E-18	2.2E-12	21.97	0.15	4.87
14	241.2	6.02	0.20	0.09	0.001	5.7E-20	3.3E-14	22.03	0.15	5.87
15	264.9	5.02	0.20	0.09	0.000			22.08	0.15	4.88
16	266.4	4.03	0.20	0.09	0.002	1.2E-19	4.0E-15	22.11	0.15	3.88
17	335.3	4.03	0.20	0.09	0.002	1.1E-19	6.7E-14	21.85	0.15	3.88
18	341.2	3.03	0.20	0.09	0.003	1.5E-19	8.6E-14	22.03	0.15	2.88
19	359.3	3.02	0.20	0.09	0.004	2.4E-19	1.4E-13	22.02	0.15	2.88
20	364.6	2.03	0.20	0.09	0.043	2.5E-18	1.4E-12	22.22	0.15	1.88
21	385.3	2.02	0.20	0.09	0.054	3.1E-18	1.8E-12	21.95	0.15	1.88
22	391.2	1.03	0.20	0.09	0.828	4.8E-17	2.8E-11	21.96	0.15	0.88
23	408.8	1.02	0.20	0.09	0.994	5.9E-17	3.4E-11	21.773	0.14	0.88

LP equipment	
Confining P (MPa)	k _{ig} ·k _{rg} (m ²)
0.6	1.5E-13
1.0	9.4E-14





GAS PERMEABILITY

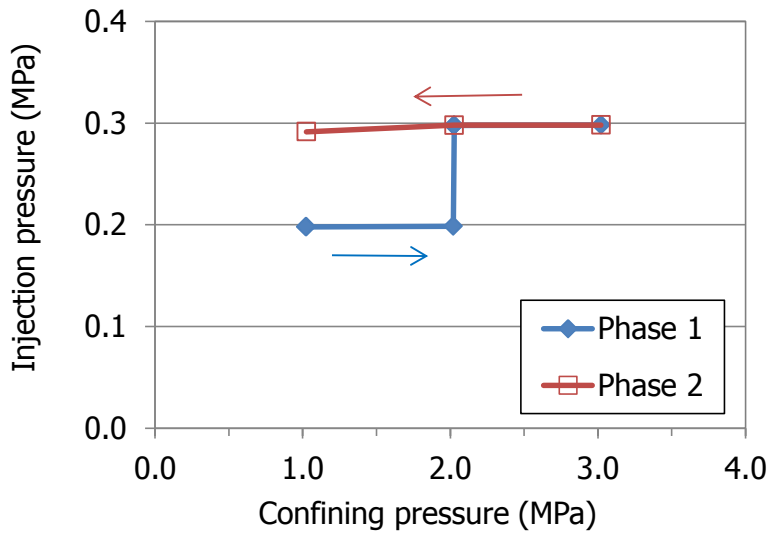
SAMPLE	BC-53-5	
START DATE:	17/05/2017	
END DATE:	25/05/2017	
SETUP:	LCP	
CYLINDER	INPUT	1.526E-04
VOLUME (m ³)		
CELL	Steel triaxial	
SAMPLE WRAPPING	Duct tape + Double latex	
FLOWMETER	Range (mL/min)	Turndown (mL/min)
FT6	2	0.04

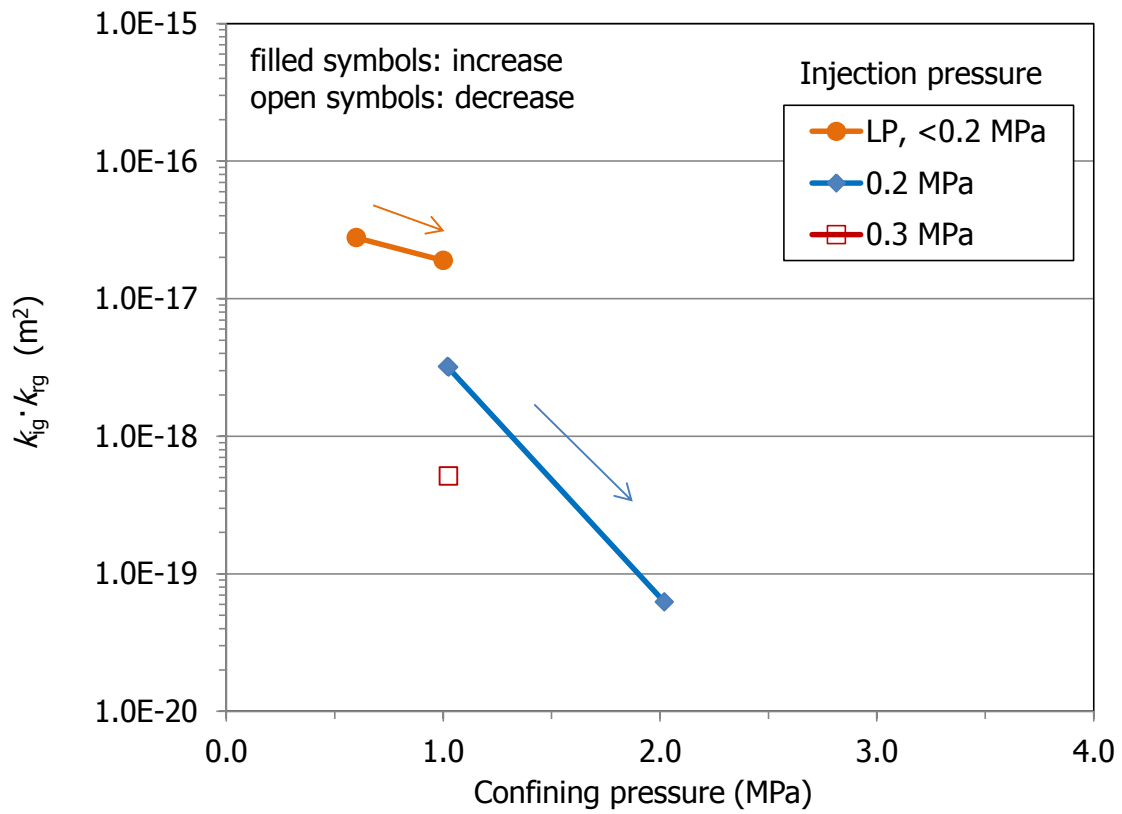
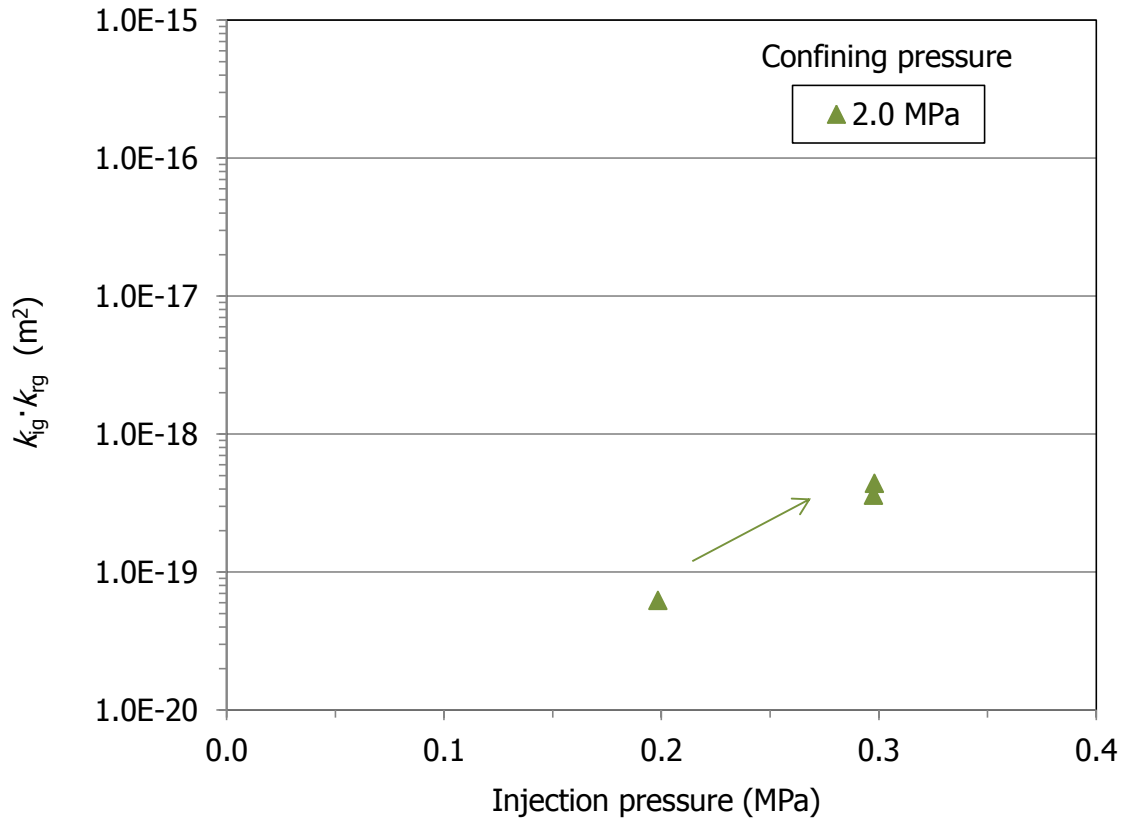
GAS CHARACTERISTICS
viscosity N ₂ : 1.78E-05 Pa·s (at 20°C)
density N ₂ : 1.12 kg/m ³
g: 9.80665 m/s ²

SAMPLE CHARACTERISTICS				
Interface between blocks			Initial	Final
Specific weight (g/cm ³)	2.70	ρ _d (g/cm ³)	1.58	1.59
Initial weight (g)	96.81	h (cm)	3.90	3.89
Final weight (g)	96.42	φ (cm)	4.00	3.99
Dry weight (g)	77.60	Area (cm ²)	12.56	12.53
		w (%)	24.8	24.4
		S _r (%)	95	95

Stage	Time elapsed (h)	Confining P (MPa)	Injection P (MPa)	Back P (MPa)	Flow (mL/min)	k _{ig} ·k _{rg} (m ²)	k _g (m/s)	T (°C)	P _{medium} (MPa)	P _c -P _{medium} (MPa)
1	3.8	1.03	0.20	0.09	0.051	3.2E-18	1.9E-12	22.0	0.15	0.88
2	25.0	1.02	0.20	0.09	0.052	3.2E-18	1.9E-12	22.0	0.15	0.87
3	49.1	2.02	0.20	0.09	0.001	6.2E-20	3.6E-14	21.9	0.15	1.87
4	52.4	2.03	0.30	0.09	0.019	4.4E-19	2.6E-13	21.9	0.20	1.83
5	121.6	2.02	0.30	0.09	0.015	3.6E-19	2.1E-13	21.8	0.20	1.83
6	145.5	3.02	0.30	0.09				22.0	0.20	2.82
7	169.5	2.03	0.30	0.09				22.2	0.20	1.83
8	193.6	1.02	0.29	0.09	0.021	5.1E-19	3.0E-13	22.2	0.19	0.83

LP equipment	
Confining P (MPa)	k _{ig} ·k _{rg} (m ²)
0.6	2.8E-17
1.0	1.9E-17





GAS PERMEABILITY

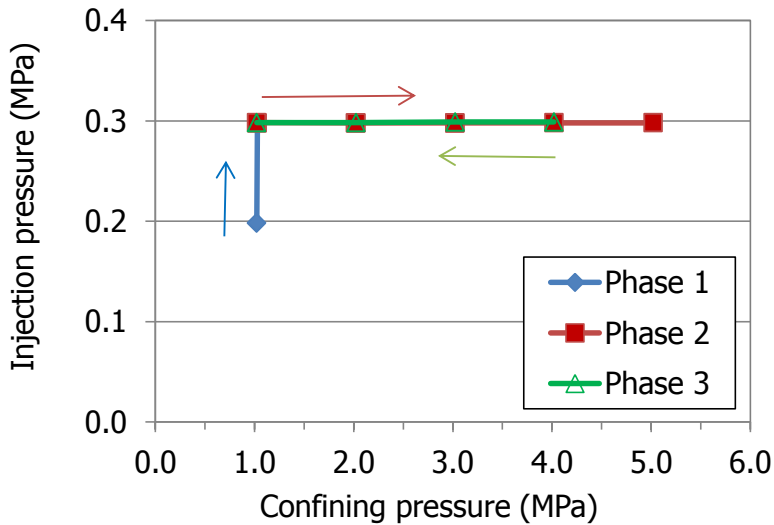
SAMPLE	BC-53-6	
START DATE:	07/06/2017	
END DATE:	21/06/2017	
SETUP:	LCP	
CYLINDER	INPUT	1.526E-04
VOLUME (m ³)		
CELL	Steel triaxial	
SAMPLE WRAPPING	Duct tape + Double latex	
FLOWMETER	Range (mL/min)	Turndown (mL/min)
FT6	2	0.04

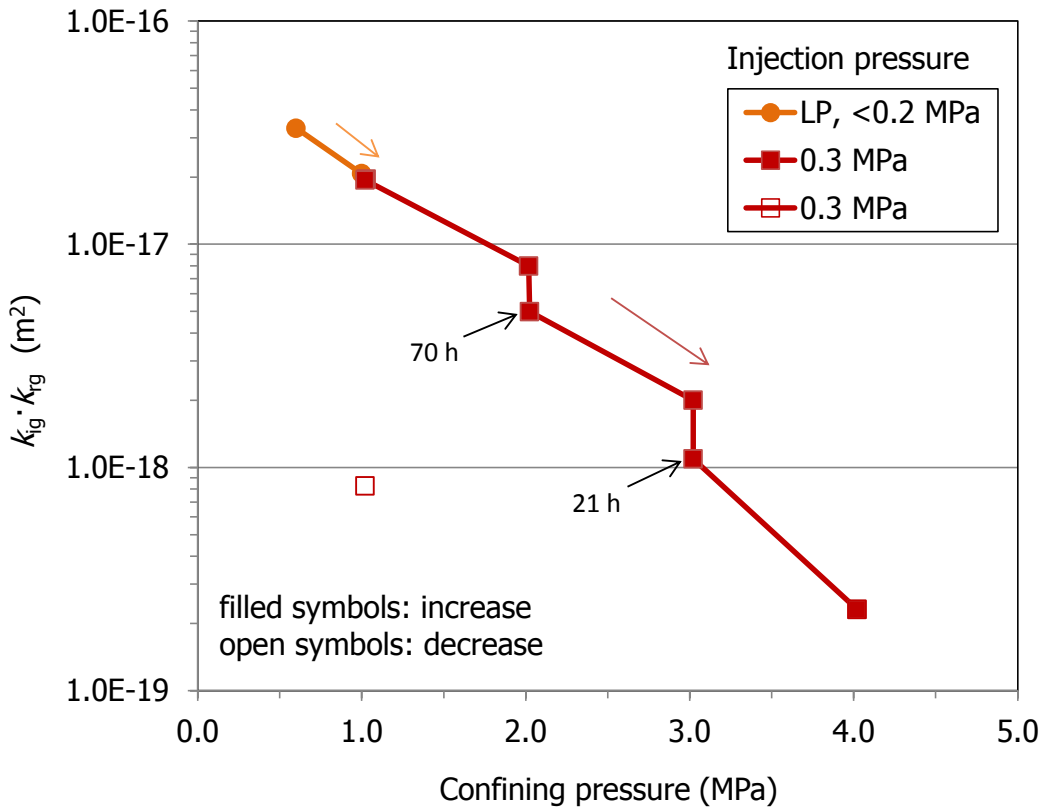
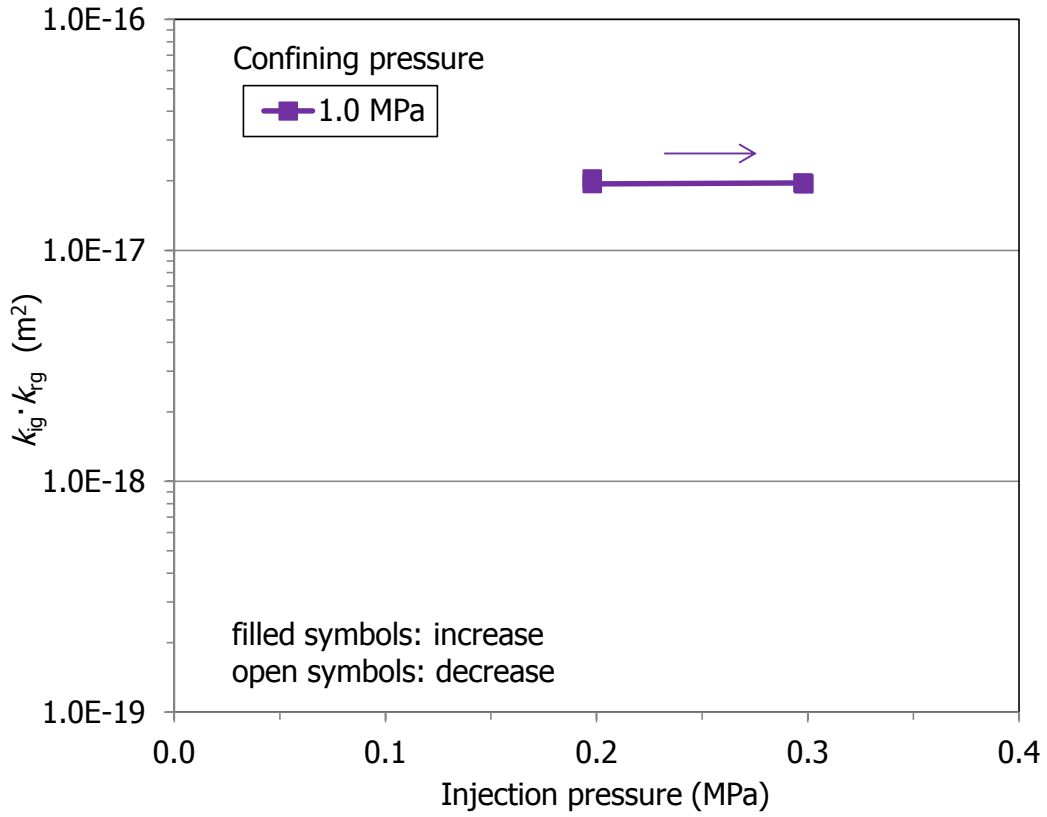
GAS CHARACTERISTICS	
viscosity N ₂ :	1.78E-05 Pa·s (at 20°C)
density N ₂ :	1.12 kg/m ³
g:	9.80665 m/s ²

SAMPLE CHARACTERISTICS			
		Initial	Final
Specific weight (g/cm ³)	2.70	ρ _d (g/cm ³)	1.55
Initial weight (g)	82.98	h (cm)	3.45
Final weight (g)	82.54	φ (cm)	3.97
Dry weight (g)	66.38	Area (cm ²)	12.42
		w (%)	25.0
		S _r (%)	91

Stage	Time elapsed (h)	Confining P (MPa)	Injection P (MPa)	Back P (MPa)	Flow (mL/min)	k _{ig} ·k _{rg} (m ²)	k _g (m/s)	T (°C)	P _{medium} (MPa)	P _c -P _{medium} (MPa)
1	5.0	1.02	0.20	0.10	0.368	2.0E-17	1.2E-11	22.6	0.15	0.88
2	24.0	1.02	0.20	0.09	0.352	1.9E-17	1.1E-11	23.7	0.15	0.87
3	29.8	1.03	0.30	0.10	0.934	2.0E-17	1.1E-11	24.0	0.20	0.83
4	48.0	1.02	0.30	0.10	0.928	1.9E-17	1.1E-11	23.9	0.20	0.82
5	50.4	2.02	0.30	0.09	0.382	8.0E-18	4.7E-12	24.2	0.20	1.82
6	120.0	2.02	0.30	0.09	0.238	5.0E-18	2.9E-12	24.6	0.20	1.83
7	122.9	3.02	0.30	0.09	0.096	2.0E-18	1.2E-12	24.8	0.20	2.82
8	144.0	3.02	0.30	0.09	0.052	1.1E-18	6.4E-13	24.6	0.20	2.83
9	168.2	4.02	0.30	0.09	0.011	2.3E-19	1.3E-13	24.7	0.20	3.83
10	191.8	5.02	0.30	0.09				24.8	0.20	4.82
11	216.3	4.02	0.30	0.09				25.3	0.20	3.82
12	284.6	3.02	0.30	0.14				25.8	0.22	2.80
13	312.1	2.02	0.30	0.09				25.0	0.20	1.83
14	335.8	1.02	0.30	0.09	0.040	8.3E-19	4.8E-13	24.5	0.20	0.82

LP equipment	
Confining P (MPa)	k _{ig} ·k _{rg} (m ²)
0.6	3.3E-17
1.0	2.1E-17





GAS PERMEABILITY

SAMPLE	BB-53-5-1	
START DATE:	19/05/2016	
END DATE:	15/06/2016	
SETUP:	LCP	

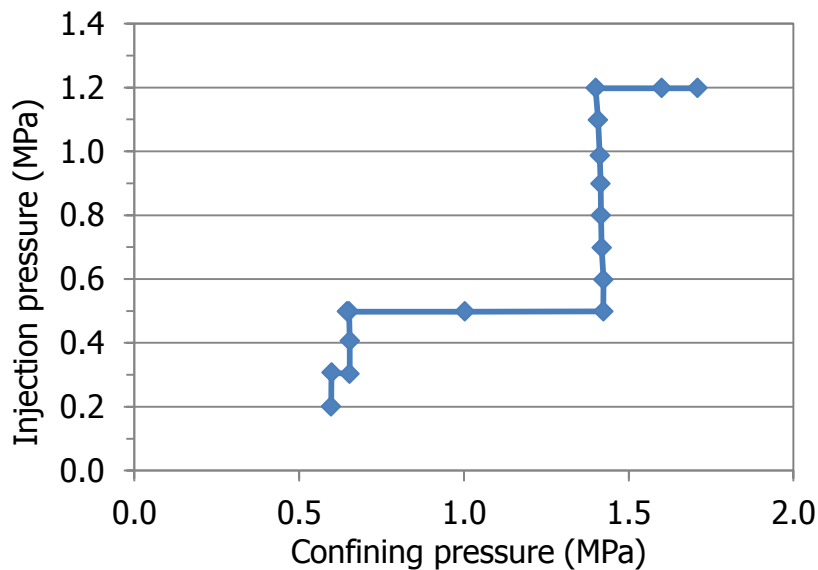
GAS CHARACTERISTICS	
viscosity N ₂ :	1.78E-05 Pa·s (at 20°C)
density N ₂ :	1.12 kg/m ³
g:	9.80665 m/s ²

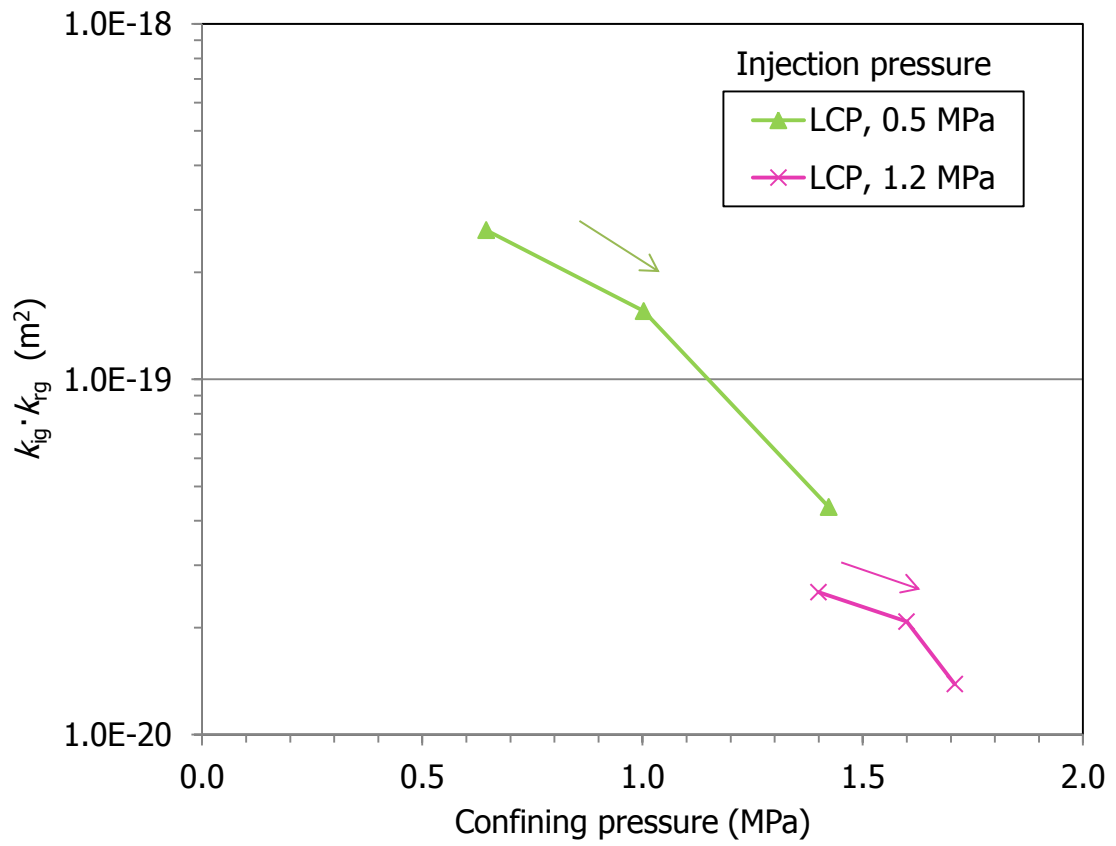
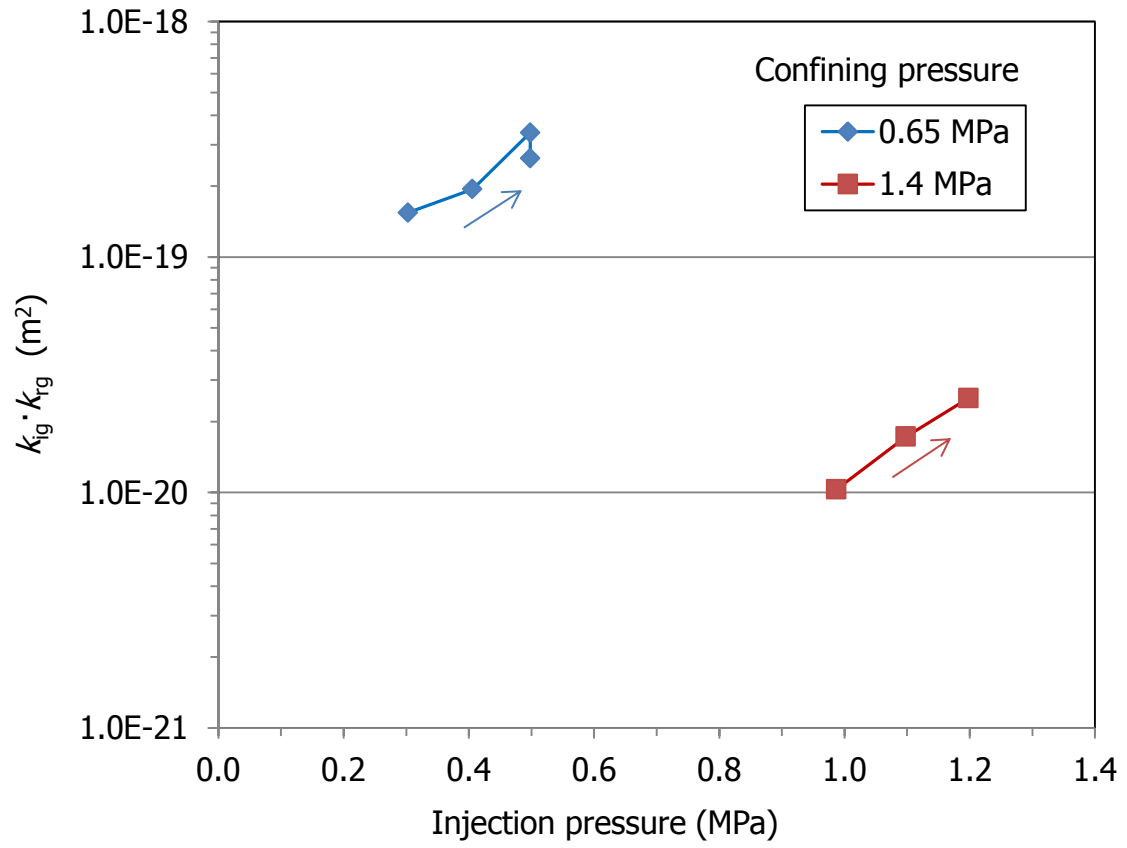
CYLINDER VOLUME (m ³)	INPUT	1.526E-04
CELL	Steel triaxial	
SAMPLE WRAPPING	Double latex	
FLOWMETER	Range (mL/min)	Turndown (mL/min)
FT6	2	0.04

SAMPLE CHARACTERISTICS				
			Initial	Final
Specific weight (g/cm ³)	2.70	ρ _d (g/cm ³)	1.63	1.60
Initial weight (g)	187.88	h (cm)	4.85	4.88
Final weight (g)	189.83	φ (cm)	4.95	4.98
Dry weight (g)	152.35	Area (cm ²)	19.22	19.49
		w (%)	23.3	24.6
		S _r (%)	97	92

the sample was accidentally wetted during dismantling

Stage	Time elapsed (h)	Confining P (MPa)	Injection P (MPa)	Outflow P (MPa)	Flow (mL/min)	k _{ig} ·k _{rg} (m ²)	k _g (m/s)	T (°C)	P _{medium} (MPa)	P _c ⁻ P _{medium} (MPa)
1	190	0.60	0.20	0.09	0.000			23.0	0.15	0.45
2	195	0.60	0.31	0.09	0.001			22.9	0.20	0.40
3	268	0.65	0.30	0.09	0.008	1.5E-19	6.6E-13	24.2	0.20	0.45
4	270	0.65	0.41	0.09	0.020	1.9E-19	1.4E-13	24.1	0.25	0.40
5	271	0.65	0.50	0.09	0.053	3.4E-19	2.4E-13	24.0	0.30	0.35
6	288	0.65	0.50	0.09	0.041	2.6E-19	1.9E-13	23.6	0.30	0.35
7	291	1.00	0.50	0.09	0.025	1.6E-19	1.1E-13	23.6	0.30	0.71
8	293	1.42	0.50	0.09	0.005	4.4E-20	2.4E-14	23.6	0.30	1.13
9	294	1.42	0.60	0.09	0.000			22.8	0.35	1.08
11	315	1.42	0.70	0.09	0.000			23.2	0.40	1.02
12	318	1.42	0.80	0.09	0.001			23.0	0.45	0.97
13	319	1.41	0.90	0.09	0.002			23.0	0.50	0.92
14	339	1.41	0.99	0.09	0.007	1.0E-20	7.3E-15	23.0	0.54	0.87
15	359	1.41	1.10	0.09	0.014	1.7E-20	1.2E-14	23.0	0.60	0.81
16	436	1.40	1.20	0.09	0.024	2.5E-20	1.8E-14	23.0	0.65	0.75
17	465	1.60	1.20	0.09	0.020	2.1E-20	1.5E-14	23.1	0.65	0.95
18	561	1.71	1.20	0.09	0.013	1.4E-20	9.9E-15	23.0	0.65	1.06





GAS PERMEABILITY

SAMPLE	BB-53-5-2	
START DATE:	19/05/2016	
END DATE:	15/06/2016	
SETUP:	HCP	

GAS CHARACTERISTICS		
viscosity N ₂ : 1.78E-05 Pa·s (at 20°C)		
density N ₂ :	1.12	kg/m ³
<i>g</i> :	9.80665	m/s ²

CYLINDER	INPUT	1.526E-04
VOLUME (m ³)		
CELL	Steel triaxial	
SAMPLE WRAPPING	Double latex	
FLOWMETER	Range	Turndown
	(mL/min)	(mL/min)
FT1	2	0.04

SAMPLE CHARACTERISTICS				
			Initial	Final
Specific weight (g/cm ³)	2.70	ρ _d (g/cm ³)	1.63	1.59
Initial weight (g)	195.23	<i>h</i> (cm)	4.99	5.04
Final weight (g)	197.52	φ (cm)	5.00	5.03
Dry weight (g)	158.86	Area (cm ²)	19.60	19.89
		<i>w</i> (%)	22.9	24.3
		<i>S_r</i> (%)	94	94

Stage	Time elapsed (h)	Confining <i>P</i> (MPa)	Injection <i>P</i> (MPa)	Back <i>P</i> (MPa)	Flow (mL/min)	<i>k_{ig}·k_{rg}</i> (m ²)	<i>k_g</i> (m/s)	<i>T</i> (°C)	<i>P_{medium}</i> (MPa)	<i>P_c-P_{medium}</i> (MPa)
1	268	0.65	0.20	0.10	0.041	1.5E-19	9.3E-14	23.2	0.15	0.50
2	270	0.65	0.30	0.10	0.075	2.8E-19	1.6E-13	22.7	0.20	0.45
3	272	0.65	0.39	0.09	0.153	5.6E-19	3.3E-13	22.6	0.24	0.41
4	289	0.65	0.39	0.09	0.148	5.5E-19	3.2E-13	22.6	0.24	0.40
5	292	1.00	0.39	0.09	0.131	2.0E-19	1.2E-13	22.4	0.24	0.76
6	294	1.42	0.39	0.09	0.089	6.7E-20	3.9E-14	22.4	0.24	1.18
7	295	1.42	0.49	0.09	0.120	9.1E-20	5.3E-14	22.5	0.29	1.13
8	315	1.42	0.49	0.09	0.087	6.7E-20	3.9E-14	22.9	0.29	1.12
9	318	1.42	0.59	0.09	0.148	1.1E-19	6.6E-14	22.7	0.34	1.07
10	341	1.41	0.59	0.09	0.112	8.6E-20	5.0E-14	22.8	0.34	1.07
11	365	1.41	0.49	0.09	0.083	6.5E-20	3.7E-14	22.8	0.29	1.11
12	431	1.40	0.39	0.09	0.066	5.2E-20	3.0E-14	22.9	0.24	1.15
13	436	1.40	0.30	0.09	0.043	3.4E-20	2.0E-14	22.8	0.20	1.20
14	623	1.67	0.29	0.09	0.026	1.4E-20	8.3E-15	23.1	0.19	1.48

